# Human-machine cooperative control : transition management between manual/auto mode for the semi-autonomous vehicle

Alex Hamdan

Par **Alex HAMDAN**

# *Human-machine cooperative control: transition management between manual/auto mode for the semi-autonomous vehicle*

Thèse présentée
pour l'obtention du grade
de Docteur de l'UTC

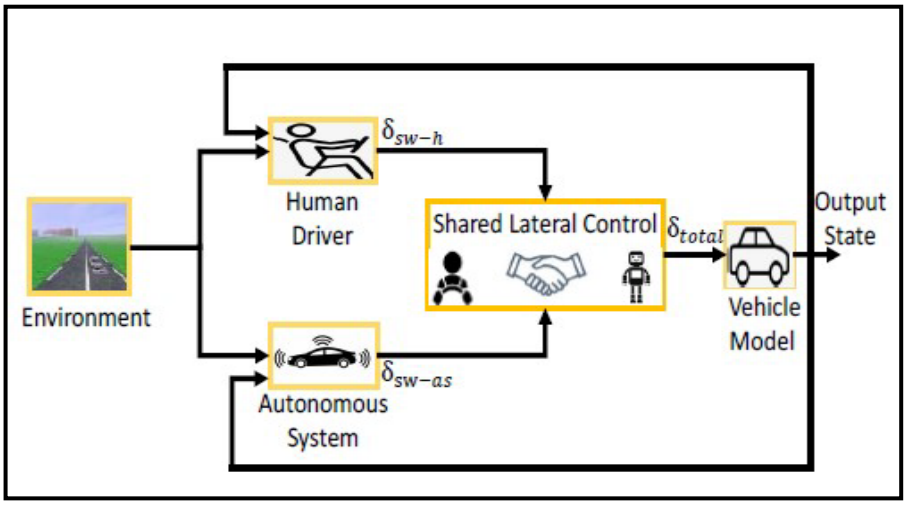


Soutenue le 14 décembre 2022
**Spécialité :** Automatique et Robotique : Unité de recherche Heudyasic (UMR-7253)
D2712

# Human-machine cooperative control: transition management between manual/auto mode for the semi-autonomous vehicle


## HAMDAN Alex


**Spécialité : Automatique et Robotique**

Thesis defended on 14 December, 2022 in front of the jury composed of:

**Reporters:**

| | |
|---|---|
| *POPIEUL Jean-Christophe* | *SENAME Olivier* |
| Full Professor | Full Professor |
| Univ. Polytechnique Hauts-de-France | Univ. Grenoble Alpes |

**Examiners:**

| | | |
|---|---|---|
| *BASSET Michel* | *CORREA VICTORINO Alessandro* | *SENTOUH Chouki* |
| Full Professor | Associate-professor, HDR | Associate-professor, HDR |
| Univ. Haute-Alsace | Univ. de Technologie de Compiègne | Univ. Polytechnique Hauts-de-France |

**Thesis co-directors/co-supervisors:**

| | |
|---|---|
| *TALJ Reine* | *CHERFAOUI Véronique* |
| CNRS researcher, HDR | Full professor |
| Univ. de Technologie de Compiègne | Univ. de Technologie de Compiègne |


Université de technologie de Compiègne

Heudiasyc Laboratory UMR CNRS 7253


14 - 12 - 2022


**Thesis funding**

Doctoral contract/Ministry allocation

... to my parents, my family, my sisters and friends...

# *Contents*

# *List of Figures*

# *List of Tables*

# *Notations*

Table 1 – Notations

| Symbol | Description | Unit |
|---|---|---|
| $i$ | $i = \{f : front, r : rear\}$ | $[-]$ |
| $j$ | $j = \{r : right, l : left\}$ | $[-]$ |
| $z_{s,ij}$ | Sprung mass bounce at the corner $ij$ | $[m]$ |
| $z_{us,ij}$ | Unsprung mass bounce at the corner $ij$ | $[m]$ |
| $z_{r,ij}$ | Road vertical profile at the corner $ij$ | $[m]$ |
| $z_s$ | $CG$ vertical displacement (bounce/heave) | $[m]$ |
| $F_{s,ij}$ | Suspension total force (corner $ij$) | $[N]$ |
| $U_{ij}$ | Active suspension force (corner $ij$) | $[N]$ |
| $F_{z,ij}$ | Tire $ij$ vertical force | $[N]$ |
| $F_{x,ij}$ | Tire $ij$ longitudinal force | $[N]$ |
| $F_{y,ij}$ | Tire $ij$ lateral force | $[N]$ |
| $F_{yi}$ | Lateral forces at the $i$ axle (bicycle model) | $[N]$ |
| $a_x$ | Longitudinal acceleration at the $CG$ | $[m/s^2]$ |
| $a_y$ | Lateral acceleration at the $CG$ | $[m/s^2]$ |
| $x$ | Vehicle longitudinal displacement (body frame) | $[m]$ |
| $y$ | Vehicle lateral displacement (body frame) | $[m]$ |
| $\theta$ | Sprung mass roll angle | $[rad]$ |
| $\phi$ | Sprung mass pitch angle | $[rad]$ |
| | Vehicle yaw angle | $[rad]$ |
| $\delta_{fj}$ | Front j (left or right) steering angle | $[rad]$ |
| $\delta_f$ | front steering wheel angle (bicycle model) | $[rad]$ |
| $V$ | Vehicle speed | $[m/s]$ |
| $\Omega_{ij}$ | Wheel $ij$ angular velocity | $[rad/s]$ |
| $\beta$ | Vehicle side-slip angle at $CG$ | $[rad]$ |
| $\alpha_{ij}$ | Side-slip angle of the tire $ij$ | $[rad]$ |
| $C_{m,ij},\ C_{f,ij}$ | Motor, braking torques at the wheel $ij$ | $[N.m]$ |
| $\sigma_{x,ij}$ | Longitudinal tire slipping | $[-]$ |

Table 2 – Complete Vehicle Model parameters

| Symbol | Description | Value |
|---|---|---|
| $m_{s,ij}$ | Sprung mass mass at the corner $ij$ | 281.6 $[kg]$ |
| $m_{us,ij}$ | Unsprung mass mass at the corner $ij$ | 40 $[kg]$ |
| $K_{s,fr},\ K_{s,fl}$ | Suspension stiffness coefficient (front tires) | 20000 $[N/m]$ |
| $K_{s,rr},\ K_{s,rl}$ | Suspension stiffness coefficient (rear tires) | 13000 $[N/m]$ |
| $C_{s,fr},\ C_{s,fl}$ | Suspension damping coefficient (front tires) | 9830 $[N.s/m]$ |
| $C_{s,rr},\ C_{s,rl}$ | Suspension damping coefficient (rear tires) | 3000 $[N.s/m]$ |
| $K_t$ | Tire stiffness coefficient | 467000 $[N/m]$ |
| $C_t$ | Tire damping coefficient | 500 $[N.s/m]$ |
| $t_f$ | Half front track | 0.75 $[m]$ |
| $t_r$ | Half rear track | 0.75 $[m]$ |
| $l_f$ | Wheelbase to the front | 1.13 $[m]$ |
| $l_r$ | Wheelbase to the rear | 1.48 $[m]$ |
| $h$ | Height of the vehicle CG | 0.58 $[m]$ |
| $h_\theta$ | Sprung mass roll arm | 0.42 $[m]$ |
| $h_\phi$ | Sprung mass pitch arm | 0.42 $[m]$ |
| $M$ | Total vehicle mass | 1286.4 $[kg]$ |
| $M_s$ | Sprung mass | 1126.4 $[kg]$ |
| $m$ | Total vehicle mass (bicycle model) | 1286.4 $[kg]$ |
| $I_x$ | Roll moment of inertia of sprung mass | 534 $[kg.m^2]$ |
| $I_y$ | Pitch moment of inertia of sprung mass | 1860 $[kg.m^2]$ |
| $I_z$ | Vehicle yaw moment of inertia | 1970 $[kg.m^2]$ |
| $g$ | Gravity constant | 9.81 $[m/s^2]$ |
| $C_{\sigma,ij}$ | Longitudinal tire stiffness | 18700 $[N/m]$ |
| $C_{\alpha,ij}$ | Lateral (cornering) tire stiffness | 38388 $[N/rad]$ |
| $\mu$ | Road adherence coefficient | dry surface= 1 $[-]$ |
| $r_{ij}$ | Effective wheel radius | 0.3 $[m]$ |
| $I_r$ | Tire moment of inertia around rotational axis | 0.85 $[kg.m^2]$ |
| $C_f,\ C_r$ | Front, rear tire cornering stiffness (bicycle model) | 76776 $[N/rad]$ |

Table 3 – Zoe Vehicle parameters

| Symbol | Description | Value |
|---|---|---|
| $m_{s,ij}$ | Sprung mass mass at the corner $ij$ | 417.5 $[kg]$ |
| $m_{us,ij}$ | Unsprung mass mass at the corner $ij$ | 53.4 $[kg]$ |
| $K_{s,fr},\ K_{s,fl}$ | Suspension stiffness coefficient (front tires) | 20000 $[N/m]$ |
| $K_{s,rr},\ K_{s,rl}$ | Suspension stiffness coefficient (rear tires) | 13000 $[N/m]$ |
| $C_{s,fr},\ C_{s,fl}$ | Suspension damping coefficient (front tires) | 9830 $[N.s/m]$ |
| $C_{s,rr},\ C_{s,rl}$ | Suspension damping coefficient (rear tires) | 3000 $[N.s/m]$ |
| $K_t$ | Tire stiffness coefficient | 467000 $[N/m]$ |
| $C_t$ | Tire damping coefficient | 500 $[N.s/m]$ |
| $t_f$ | Half front track | 0.77 $[m]$ |
| $t_r$ | Half rear track | 0.77 $[m]$ |
| $l_f$ | Wheelbase to the front | 1.08 $[m]$ |
| $l_r$ | Wheelbase to the rear | 1.55 $[m]$ |
| $h$ | Height of the vehicle CG | 0.57 $[m]$ |
| $M$ | Total vehicle mass | 1456.4 $[kg]$ |
| $M_s$ | Sprung mass | 1670 $[kg]$ |
| $m$ | Total vehicle mass (bicycle model) | 1456.4 $[kg]$ |
| $I_x$ | Roll moment of inertia of sprung mass | 600 $[kg.m^2]$ |
| $I_y$ | Pitch moment of inertia of sprung mass | 100 $[kg.m^2]$ |
| $I_z$ | Vehicle yaw moment of inertia | 2400 $[kg.m^2]$ |
| $g$ | Gravity constant | 9.81 $[m/s^2]$ |
| $C_{\sigma,ij}$ | Longitudinal tire stiffness | 19000 $[N/m]$ |
| $C_{\alpha,ij}$ | Lateral (cornering) tire stiffness | 77349 $[N/rad]$ |
| $\mu$ | Road adherence coefficient | dry surface= 1 $[-]$ |
| $r_{ij}$ | Effective wheel radius | 0.31 $[m]$ |
| $I_r$ | Tire moment of inertia around rotational axis | 1.83 $[kg.m^2]$ |
| $C_f,\ C_r$ | Front, rear tire cornering stiffness (bicycle model) | 77349 $[N/rad]$ |

# *Acronyms*

| | |
|---|---|
| $ACC$ | Active Cruise Control |
| $ADAS$ | Advanced Driving Assistance Systems |
| $AFS$ | Active Front Steering |
| $AS$ | Active Suspension |
| $APC$ | Adaptive Predictive Control |
| $BRL$ | Bounded Real Lemma |
| $CG$ | Center of Gravity |
| $DA$ | Driver's Availability |
| $DS$ | Driving Safety |
| $DYC$ | Direct Yaw Control |
| $EM$ | Emergency Mode |
| $EMB$ | Electro-Mechanical Brakes |
| $ESP$ | Electronic Stability Program |
| $FLC$ | Fuzzy Logic Controller |
| $\mathcal{H}_\infty$ | H infinity |
| $HLC$ | High Level of Cooperation |
| $HMI$ | Human-Machine Interface |
| $HSC$ | Haptic Shared Control |
| $LDR$ | Lane Departure Risk |
| $LKAS$ | Lane Keeping Assist System |
| $LLC$ | Low Level of Cooperation |
| $LMI$ | Linear Matrix Inequality |
| $LPV$ | Linear Parameter Varying |
| $LQR$ | Linear Quadratic Regulator |
| $LTI$ | Linear Time Invariant |
| $LTV$ | Linear Time Varying |
| $MIMO$ | Multi-Input-Multi-Output |

| | |
|---|---|
| $NDST$ | Non-Driving Secondary Task |
| $NDRA$ | Non-Driving Related Activities |
| $NHTSA$ | National Highway Traffic Safety Administration |
| $NMS$ | Neuromuscular System |
| $PEM$ | Prediction Error Method |
| $RT$ | Reaction Time |
| $SA$ | Situation Awareness |
| $SDP$ | Semi-Definite Program |
| $SI$ | Stability Index |
| $SISO$ | Single-Input-Single-Output |
| $STSM$ | Super-Twisting Sliding Mode |
| $TLC$ | Time to Lane Crossing |
| $TS$ | Takagi-Sugeno |
| $TOR$ | Takeover Request |
| $TTC$ | Time to Collision |

# *Publications*

**The contributions related to the thesis were the subject of some published papers and other submitted ones.**

- Conference articles (Accepted/published):
  - ◇ Hamdan Ali, Talj Reine, and Cherfaoui Véronique. "A Fuzzy Logic Shared Steering Control Approach For Semi-Autonomous Vehicle." 2021 20th International Conference on Advanced Robotics (ICAR). IEEE, 2021.
  - ◇ Hamdan Ali, Talj Reine, and Cherfaoui Véronique. "Transition Management Between an Autonomous Vehicle and a Real Human Driver, in a Context of Take-Over Request." IFAC-PapersOnLine 55.14 (2022): 65-70.
- Conference articles (To be submitted):
  - ◇ Hamdan Ali, Talj Reine, and Cherfaoui Véronique. "Design of an Advanced Driving Assistance Controllers for lane keeping in semi-autonomous vehicles, based on $LPV/\mathcal{H}_\infty$ and Super-Twisting Sliding Mode control techniques."
  - ◇ Hamdan Ali, Talj Reine, and Cherfaoui Véronique. "A centralized multilayer $LPV/\mathcal{H}_\infty$ ADAS system control architecture for the lane keeping maneuver, and comparison with a decentralized architecture."

**The contributions related to my master 2 internship in Heudiasyc laboratory, on ADAS systems for vehicle stabilization, published during the first year of my thesis**

- Conference articles (Accepted/published):
  - ◇ Hamdan Ali, Chokor Abbas, Talj Reine and Doumiati Moustapha. "A centralized multilayer LPV/H-infinity control architecture for vehicle's global chassis control, and comparison with a decentralized architecture." 21st International Federation of Automatic Control World Congress (IFAC WC 2020). 2020.
  - ◇ Hamdan Ali, Chokor Abbas, Talj Reine and Doumiati Moustapha. "A decentralized multilayer sliding mode control architecture for vehicle's global chassis control, and comparison with a centralized architecture."

International Conference on Electronic Engineering and Renewable Energy. Springer, Singapore, 2020.

- Journal articles (accepted/published):
  - ◇ Chokor, A., Talj, R., Doumiati, M., Hamdan, A., & Charara, A. (2022). A comparison between a centralised multilayer $LPV/\mathcal{H}_\infty$ and a decentralised multilayer sliding mode control architectures for vehicle's global chassis control. International Journal of Control, 95(2), 303-318.

# *Résumé*

La conduite autonome est devenue un objectif primordial pour les industries automobiles ainsi que pour les recherches académiques ces dernières années. De nombreuses études avancées ont été réalisées dans ce domaine afin de rendre cette technologie accessible au public. Selon le département des transports aux États-Unis “National Highway Traffic Safety Administration NHTSA”, il existe 6 niveaux d'autonomie : de 0 à 5. Cependant, le remplacement de la conduite traditionnelle par un système autonome reste une question ouverte et les véhicules entièrement autonomes ont besoin de plus de temps pour être réalisés afin de surmonter toutes les situations de conduite. Ainsi, afin de préparer l'environnement pour les véhicules autonomes, un contrôle latéral partagé pour le maintien de la voie sera traité dans cette thèse, pour gérer la transition entre le mode manuel/auto pour le véhicule semi-autonome (niveau 2 et 3). Ce contrôle partagé assure la sécurité sur la route et le confort du conducteur lorsque les deux agents agissent sur le contrôle du véhicule. La transition fait partie de l'interaction homme-machine ($IHM$), ce qui signifie que l'interaction de l'homme avec le système est importante pour que l'homme comprenne le comportement du système et agisse avec lui pour atteindre un objectif commun. Dans ce contexte, l'objectif de cette thèse est de développer un contrôle latéral partagé pour maintenir la voie en utilisant un système de direction steer-by-wire. L'objectif de ce contrôle partagé est de gérer l'autorité de contrôle entre le conducteur et le système autonome afin d'assurer la sécurité routière, d'améliorer les performances de conduite et de réaliser une transition lisse et sûre entre les deux agents. L'autorité de contrôle est réalisée en utilisant le contrôle partagé mixte qui permet la fusion de deux entrées de commande : l'angle de braquage du conducteur humain sur le volant et l'angle de braquage calculé par le système autonome, via un paramètre de fusion. Pour cela, un modèle de conducteur est développé dans ce travail, pour représenter l'humain dans la boucle. Les mouvements longitudinaux et latéraux du véhicule sont effectués par un système autonome développé en utilisant l'approche de contrôle par mode glissant "Super-Twisting", afin de suivre une trajectoire de référence. Ensuite, un algorithme de prise de décision est développé pour le contrôle latéral partagé afin de gérer l'autorité entre le conducteur et le système autonome et de calculer le paramètre de la fusion. Différents critères sont pris en compte et intégrés dans les algorithmes de décision, tels que : le degré de confiance de chaque entrée (conducteur humain et système autonome), l'erreur latérale, le comportement et l'intention du conducteur, la demande de prise de contrôle, etc. Enfin, l'implémentation et la validation du contrôle partagé proposé est effectuée sous Matlab/Simulink et sous le simulateur de véhicules "SCANeR Studio" (OKTAL) en interaction avec l'humain dans la boucle à travers le volant "Logitech G29" pour les différents scénarios de

conduite.
La dernière partie de la thèse porte sur le développement d'un système avancé d'aide à la conduite ($ADAS$) (niveau 2), comportant une direction avant active ($AFS$) et un contrôle direct du lacet ($DYC$). Les approches du contrôle partagé centralisée et décentralisée sont développées en se basant sur les techniques de commande : $LPV/\mathcal{H}_\infty$ et mode glissant "Super-Twisting", afin d'aider le conducteur dans la manoeuvre de maintien de la voie, tout en garantissant la stabilité latérale du véhicule. Enfin, la validation des différentes approches est effectuée sous Matlab/Simulink pour les différentes études de cas avec un modèle non linéaire complet du véhicule validé sous le simulateur professionnel "SCANeR Studio".

**Mots clés :** *Véhicule semi-autonome, Conduite coopérative, Contrôle latéral partagé, Prise de décison, Conduite autonome, Gestion de transition, Approche centralisée, Approche décentralisée, $LPV/\mathcal{H}_\infty$, Mode glissant "Super-Twisting".*

# *Abstract*

The development of the autonomous vehicles has become a purposeful target for automotive industries as well as for the academic researches in the recent years. Many advanced studies have been done in this field to make this technology accessible for the public. According to the US Department of Transportation "National Highway Traffic Safety Administration NHTSA", there are 6 levels of automation: from 0 to 5. However, the act of replacing the traditional driven by an autonomous system is still an open question and the full autonomous vehicle needs more time to be realized in order to overcome all the possible driving situations. So, in order to prepare the environment for the autonomous vehicles, a shared lateral control for the lane keeping purpose will be treated in this thesis, to manage the transition between manual/auto mode for the semi-autonomous vehicle (level 2 and 3). This shared control ensures driving safety on the road and the driver's comfort when the two agents act on the vehicle's control. The transition shifting is a part of human machine interaction ($HMI$) which means that the interaction of human with the system is important for the human to understand the system's behavior and act with him to accomplish a shared goal. In this context, the objective of this thesis is to develop a shared lateral control for the lane keeping objective using steer-by-wire system. The objective of this shared control is to manage the control authority between driver and autonomous system in order to ensure road safety, enhance driving performance and realize a smooth and safe switching between the two agents. The control authority is realized using the blended shared control that permits the fusion of the two agents inputs on the steering wheels: the steering wheel angle of the human driver and the steering wheel angle of the autonomous system, via a fusion parameter. To do that, a driver model is developed in this work, to represent the human in the loop. The vehicle longitudinal and lateral movements are performed by an autonomous system developed using the Super-Twisting Sliding Mode ($STSM$) control approach, in order to follow a reference trajectory. Then, decision-making algorithms are developed for the shared lateral control to manage authority between the driver and the autonomous system and calculate the fusion parameter. Different criteria are considered and integrated in the decision algorithms, such as: the degree of confidence of each input (human driver and autonomous system), the lateral error, driver's behavior and intention, take over request, etc. Finally, validation and implementation of the proposed shared control is done on Matlab/Simulink and on "*SCANeR Studio*" vehicle's simulator (OKTAL) interacting with the human in-the-loop through the "*Logitech G29*" steering wheel for the different driving scenarios. The last part of the thesis deals with the development of Advanced Driving Assistance System ($ADAS$) (level 2), involving Active Front Steering ($AFS$) and Direct

Yaw Control ($DYC$). The proposed centralized and decentralized shared control approaches are developed based on: the $LPV/\mathcal{H}_\infty$ and Super-Twisting Sliding Mode ($STSM$) control techniques, to help the driver in the lane keeping maneuver, while guaranteeing vehicle's lateral stability. Finally, validation of the different approaches is done on Matlab/Simulink for the different case studies with a complete nonlinear model of the vehicle validated on "*SCANeR Studio*" professional simulator.

**Keywords**: *Semi-autonomous vehicle, Human-machine cooperative control, Cooperative driving, Shared lateral control, Decision-making, Autonomous driving, Transition management, Centralized Approach, Decentralized Approach, $LPV/\mathcal{H}_\infty$, Super-Twisting Sliding Mode.*

# *Introduction*

Safety is an important issue that should be realized while driving on the road. Road accidents are caused by the human's errors in most cases. According to National Highway Traffic Safety Administration ($NHTSA$) statistics, human leads to 90% of road accidents [Rajamani, 2012]. In such situation, when the driver is tired or distracted, he can be assisted by an Advanced Driving Assistance System ($ADAS$) to prevent a critical situation. There are many examples of $ADAS$ systems, like Electronic Stability Program $ESP$, Anti-lock Braking System $ABS$ that stabilize the vehicle in slipping situations. Systems like audible or visual alert, alarm the driver in case of hazardous situation. Other systems assist the driver in the longitudinal control, for example: the Active Cruise Control ($ACC$) regulates the speed of the car. Finally the Lane Keeping Assist System ($LKAS$) can help him to stay within the lane and warn him when he is crossing the boundaries. These systems reduce traffic accidents and facilitate the driver's task. However, these systems are dedicated for specific tasks, in some precise driving situations, and their functionalities are limited. This new technology of automated system starts to emerge progressively in order to automate the driving activities and realize a full autonomous vehicle.

## 0.1 Motivation

The development of the autonomous vehicles is an important subject for the automotive industries and the academic researches. Many advanced studies have been done in this field to make this technology accessible for the public. However, the act of replacing the traditional driven by an autonomous system is still an open question and the full autonomous vehicles need more time to be realized in order to cover all the possible driving situations. So, in order to prepare the environment for the autonomous vehicles, we treat the shared lateral control for the lane keeping purpose in this thesis, to manage the transition between manual/auto modes for the semi-autonomous vehicle (level 3). This shared control ensures driving safety on the road and the driver's comfort when the two agents act on the vehicle's control. A degree of confidence for each agent is considered depending on many factors: driver's state of attention, driver's behavior and intention, driving situation, and limitation of automated system, etc. The transition shifting is a part of human machine interaction ($HMI$) which means that the interaction of human with the system is important for the human to understand the system's behavior and act with him to accomplish a shared goal. For that, the human driver still in the loop monitors the driving situations and takes the action of control if necessary. For example, if the autonomous system reaches the limitation performance or an inappropriate decision

is taken by the system and leads to fatal problems, the human takes the control to prevent an undesirable situation and vice-versa. The intervention of the human driver is urgent or optional depending on the driving situations and on the overall behavior's system. In this context, the objective of this thesis is to develop a shared lateral control for the lane keeping objective using steer-by-wire system. However, this method can be adapted to consider the tracking of a local trajectory with more complex maneuvers (overtaking, collision avoidance...). The objectives of this shared control is to manage the control authority between driver and autonomous system in order to ensure road safety, enhance driving performance and realize a smooth and safe switching between the two agents. This shared control ensures the fusion of the two agents inputs on the steering wheels: the steering wheels angle of the human driver and the steering wheels angle of the autonomous system calculated in order to follow a reference trajectory. Then, the proposed shared control will be validated for specific driving scenarios and cases. A degree of confidence for each input is calculated depending on different criteria discussed later and integrated in the decision algorithm. The autonomous vehicles also are equipped with the necessary algorithm for the planning trajectory and control, and provided by the data to ensure the vehicle's autonomy. Finally, the thesis deals also with the development of Advanced Driving Assistance System ($ADAS$) (level 2), involving Active Front Steering ($AFS$) and Direct Yaw Control ($DYC$) to help and assist the driver in the lane keeping maneuver.

To manage this shared mode, many steps are required:

- Define the limitations of each system (human driver and autonomous system) and its capacity.
- Define the conditions of shifting process between the two agents.
- Develop the calculation methods for the degree of confidence of each input (human driver and autonomous system).
- Define the criteria that influence the transition mode: driver's behavior, driver's status, driving situation and safety.
- Determine the way of how the human driver takes the control of steering wheels to get smooth changes on the vehicle's state and to guarantee driver's comfort.

## 0.2 State of the Art

### 0.2.1 Automation Driving

The automation driving is a process that aims to automate the driving activities in order to realize a full autonomous vehicle on the road. The German Federal Highway Research Institute (Bundesanstalt für Straßenwesen-BASt) [Gasser et al., 2012], the National Highway Traffic Safety Administration ($NHTSA$) [Administration et al., 2013], and the $SAE$ International (Society of Automotive Engineers) [SAE, 2016]

classified automation driving to many levels. According to the *SAE* International [SAE, 2016], there are 6 levels of automation (see Figure. 1). These levels are defined as:

- Level 0 ($L_0$): no automation. The driver realizes all driving tasks: the longitudinal and the lateral control.
- Level 1 ($L_1$): driving assistance. The driver acts on the longitudinal control while an assistance system accomplishes the lateral control or vice-versa.
- Level 2 ($L_2$): partial automation. On the level 2, some driving tasks are accomplished by the system in a specific use case (acceleration/braking, etc.), while the driver supervises and monitors the system with the surrounding environment at all times.
- Level 3 ($L_3$): conditional automation. The human is the main responsible of driving tasks, that means even if he does not have to supervise and monitor the scene at all time, but the driver should be able to retain control and reacts if the automated system reaches his limits for many reasons: sensor's failures, lack of localization information, bad weather, etc.
- Level 4 ($L_4$): high automation. The system accomplishes all driving tasks without driver's intervention. The driver can retain the control action if he is available and when needed.
- Level 5 ($L_5$): full automation. The driver is eliminated from the control loop. The system navigates on the road by achieving the totality of driving tasks without driver's intervention.

Nowadays, full autonomous vehicles (level 5) [Favarò et al., 2017] are taking an important attention in the researches and automotive industry where several tasks of driving are done by an autonomous system itself. The challenge now is to realize a full autonomous vehicle (level 5) where the driver is eliminated from the control loop (see Figure. 1). However, replacing the traditional vehicle by the autonomous one needs more time to be reached. The realization of full autonomous vehicles should be evaluated step by step considering many criteria: system's robustness, road safety, ethics rules, the high cost of hardware and software, and test and validation of the system for any possible scenario on the public road, etc. The autonomous driving system is the result of different tasks: environment perception, motion planning and vehicle control. However, many problems are caused by these modules, and will need more time to be fixed. Thus, a shared cooperative control is necessary to compensate the gap between the manual driving (level 0/1 and 2) and full autonomous driving (level 5) [Favarò et al., 2017].

### 0.2.2 Shared Control

The intelligent vehicles are defined to realize different tasks: obstacle avoidance, lane changing, lane keeping. These vehicles are equipped with *ADAS* system ($L_2$

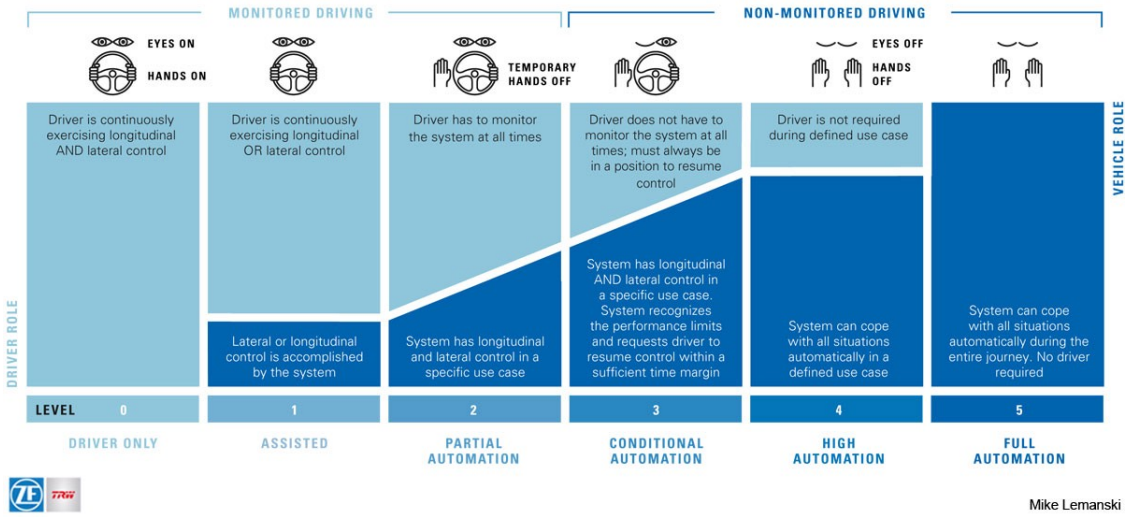


Figure 1 – The 6 levels of automation [SAE, 2016]

and $L_3$) to ensure safety and enhance performance. The integration of the $ADAS$ system helps the driver in dangerous situation. The problem until now is that the application of autonomous vehicles brings risks, so it's important to investigate the idea of shared control. The shared control is a new aspect of control in the automotive field that ensures road's safety and enhances driving performance. It aims to reduce the workload of the driver, help and assist him to prevent a critical situation when he is distracted or tired. It depends on the driver's intentions and behaviors to assist him in case of hazardous situation. During this collaborative control, the human and the autonomous controller cooperate together to accomplish a common goal simultaneously. In addition, interaction between the human and the autonomous system that keeps the driver in the loop, should compensate the limits and problems of autonomous systems and improve driving safety. The driver should be able to take the action of control if the autonomous system is not able to realize the driving task, for example obstacle detection and avoidance. Therefore, if a conflict occurs between the two agents during driving and they do not have the same objective, the shared strategy of control will be the solution of this conflict in order to enhance the performance of driving tasks. Many important modules are integrated in the context of the shared control, such as: the Human Machine Interaction $HMI$, the Driver Monitoring System $DMS$ and the Shared Lateral Control $SLC$ in order to address the issues of driver's interaction with the system. These modules aims: to treat the authority between both agent, to manage the levels of automation and to prioritize the information during $HMI$.

#### 0.2.2.1 Human Machine Interaction $HMI$

In our days, machine plays a good role in many fields such as medicine, industry, space exploration, etc, where it performs many tasks [Chandrasekaran and Conrad, 2015]. It collaborates with human in the framework of human-machine interaction ($HMI$) to realize a shared goal. Each agent has some skills adopted to a situation

where the other agent has not. So, it is very useful to talk about a Human Machine Interaction in order to have a stable system with a good performance enhancement. In the automotive field, the Human Machine Interaction $HMI$ interface has a very important role in the exchange of information and sharing of intentions between the human driver and the system (trajectory, perception of the environment, action, etc.).

- Optional: each agent has its own goal and it can cooperate with the other agent to realize another goal.

- Required: the aim of this interference is to manage and facilitate the role and activity for each one and realize a common task.

However, each agent has errors and limitations in his functionality. So, in order to compensate these errors and made the Human machine Interaction effective and useful, a human centered design [Miyata and Norman, 1986] is applied in the shared control where the controller depends on the human intention and behavior. This approach assumes being able to know at all times the driver's state, the driving situation and the limitations of the automated system in order to take a decision about the driving strategies [Benloucif et al., 2017]. The human driver is configured in the loop. The act of keeping the driver in the loop leads to a good understanding of the first agent to the other one and ensures the overall system's stability and safety. Moreover, the human gives trust to the automated system in specific driving situations.

#### 0.2.2.2 Driver Monitoring System $DMS$

The driver's inattention is a major cause of road accidents. For that, a Driver Monitoring System $DMS$ is needed to supervise the driver's attention and the fatigue's levels in order to evaluate his state. The driver's abilities strongly depend on his physiological and psychological states. Many studies are presented in the literature to deal with the estimation of the driver's state and the development of the alert systems [Blaschke et al., 2009], [Popieul et al., 2002]. This state is usually determined through the detection of the level of the drowsiness and distraction [Muzet, 2006]. The lack of driver's attention is caused by an internal distraction like: the using of a smart phone or using a GPS application, traffic [Markkula et al., 2005], [Regan et al., 2011] and the mental efforts of driver [Schaap et al., 2017]. There are many methods have been used to identify the driver's state. The direct methods are related to the driver's eyes observation, the driver's head position and the level of driver's sleepiness, etc, using Driver Monitoring System $DMS$. The indirect methods are based on the analyzing of the vehicle's states like the steering angle, the vehicle lateral position on the road, etc. However, the determination of the driver's state is not the scope of this work and it is assumed as a known input determined by a diagnosis module.

#### 0.2.2.3 Shared Lateral Control

The shared lateral control is the aspect of the control where the driver is presented in the control loop. The relation between the driver and the autonomous system resembles to the "$H-metaphor$" [Flemisch et al., 2003] concept, applicable in some assistance cases.

***"$H-metaphor$" concept:***
The authority control of the horse depends on the rider's decision. He tights the reins to enforce the horse executes his intentions, or he leaves the reins to give the authority of control to the horse. The reins is identical to the haptic shared control between the driver and the automation. This comparison proves the importance of keeping the driver in the loop to make the system more reliable and reduce the driver's workload. Moreover, the authors in [Flemisch et al., 2010] demonstrate the necessity of assistance in case of driver under-load and over-load (see Figure 2). Well, in case of overload and underload the driver can be in relax, and the autonomous system take the action of driving. In addition, an assessment module was developed to test and supervise the system, and to take action in case of system's limits and failure.

Some studies deals with machine learning and Deep learning for the shared control. It builds the environment perception, decision making and vehicle control. Decision making is an algorithm that constructs the trajectory and driving commands according to the environment perception (Neural networks). In [Jugade, 2019] a fusion of driving inputs represented by the vehicle speed and steering wheel angle has been done. The human and autonomous system provide their driving inputs to the fusion system for the calculation of the final driving inputs. This fusion is done by all these tasks: a computation of admissibility for the two driving inputs using Belief function theory in order to add uncertainty to the output. A model predictive control is used to predict the driving inputs trajectory, looking in some future horizon, using neural network. The final input is computed completely by using the game theory where the conflict is solved by the Nash equilibrium. The final control inputs have the form of vehicle speed and steering wheel angle. Other studies in the shared lateral control focus on the evaluation of the driver's skills. These studies treat the driver's tasks change with long term in the shared control. The authors in [de Winter and Dodou, 2011] have explored the topic of shared control in terms of its advantages and drawbacks on the driving tasks. They presented the risks that can occur during this shared control, the conflict for example, and the influence of this control strategy on the driver's skills.

In shared control, the driver and the system act simultaneously through an interface (process) or an actuator (like steer-by-wire system). Note that the traditional steering system (mechanical or assisted steering) are not efficient with the shared control because the mechanical connection does not allow a real sharing between the driver and the autonomous system. For that, the automotive companies decide to decouple the steering wheel from the wheels by developing a steer-by-wire system.

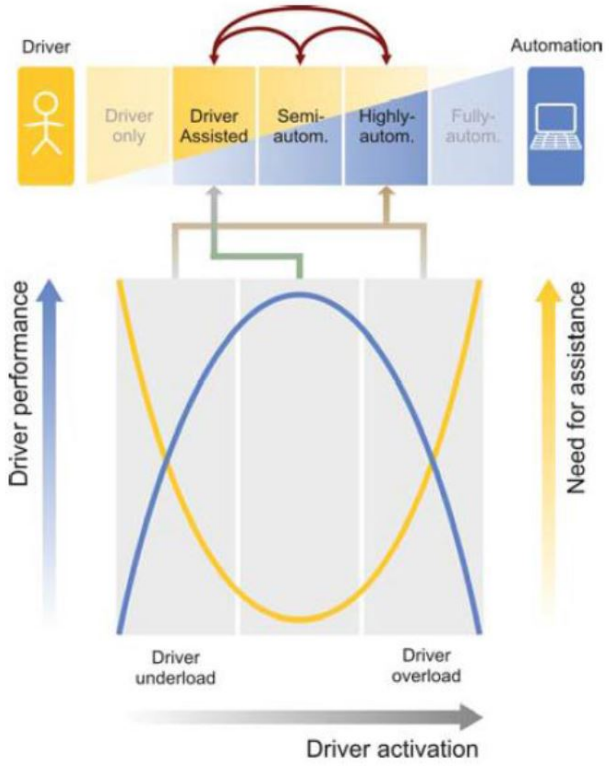


Figure 2 – Dynamic task repartition of assistance and automation system [Flemisch et al., 2010]

The steering wheel will be an interface that permits to the driver to execute his actions through an electronic actuator to follow the trajectory. A haptic feed-back is generated to inform the driver about the driving situation. Refer to [Abbink and Mulder, 2010], [Guo, 2017], the shared control is divided into two types: the shared control where the driver is represented in the loop (blended and haptic shared control) and human supervisory control when the driver gives commands to control the automated system.

#### 0.2.2.3.1 Blended vs Haptic shared control

***Blended shared control:***
This type is used for the system where there is no mechanical connection. An example of this type is the system by wire like the steer-by-wire. The human's input is an electronic signal increased or decreased depending on the behaviors of automation. The familiar form of blending shared control is the blending using weights parameter. The total blending control input is given as:

$$u_{total} = (1 - \gamma) * u_h + \gamma * u_a, \tag{1}$$

where $u_{total}$, $u_h$ and $u_a$ are the total control input, input of human operator and automated system respectively. $\gamma$ is the weighting factor that represents the percentage of influence of each agent on the total input. The blending shared control permits the direct interaction of human driver, but the last is not aware about the behaviors of the system because there is no mechanical link between the agents and the controlled device. The haptic feedback control solves this drawback.

The literature is rich in the Blended shared control. A shared lateral control is presented in [Sentouh et al., 2010] to illustrate the authority of driving between the driver and the automatic system. A linear quadratic regulator ($LQR$) method is used to develop the steering assist system. The sharing of the authority of driving is determined using a decision making process. The decision making process uses a weighting function to manage the sharing authority. This process is also used in [Soualmi et al., 2011], where a fuzzi-TS-logic method is applied in the development of controller. A new method for the decision making algorithm is given in [Sentouh et al., 2013], depending on the coordination variable $\Omega$ (see [Sentouh et al., 2013] for more details). The development of the assistance torque is done by using the $H_2$ approach. The authors in [Nguyen et al., 2015], [Nguyen et al., 2016] developed a shared lateral control to help the driver and assist him in different driving situations. The novelty in this work compared to the previous works is the integration of the driver model in the development of the control law. This integration allows the prediction of driver's behaviors and activity that permits the management of the conflict between the two agents. An assistance steer-by-wire system is presented in [Perozzi et al., 2020], where the fusion of two steering inputs is performed considering the availability of the driver via monitoring system. Finally, many factors related to safety and driver's behavior (avoidance of lane departure, prevention of high acceleration and excessive steering) are taken into account when calculating the fusion parameter to deal with the tire blowout on the road [Li et al., 2020].
A similar approach of the work of LAMIH laboratory is presented in [Borroni and Tanelli, 2018], where a shared lateral control authority is done. The controller is developed based on $H_\infty$ technique. The control authority is given by this equation:

$$T_{tot} = (1 - \alpha) * T_a + \alpha * T_d, \tag{2}$$

where $T_{tot}$, $T_a$ and $T_d$ are the total torque, the assistance torque and the driver torque respectively. $\alpha$ is adjusted manually or automatically between [0;1] depending on the driver attention or driver situation.

The control inputs for the steering system are: the steering angle and the steering torque. The authors in [Iwano et al., 2014] suppose that the steering systems based on the steering torque is more reliable than the steering angle since the steering torque provides the driver some degree of freedom to control the vehicle. For that, a shared control based on the steering torque is developed for the emergency obstacle avoidance. The assistance torque is calculated based on the desired yaw rate delivered by a yaw rate command generator. The shared control is done by multiplying the assistance steering torque with a weight coefficient $w$ varying between 0 and 1. The total steering torque is the resultant of the driver torque and

the weighted assistance torque (see Figure 3). The problem of this shared control is when an important difference between the two torques is detected. This difference increases as the weighting parameter increases. This means a conflict exists between the two agents and the assistance system behaves against the driver's intentions.

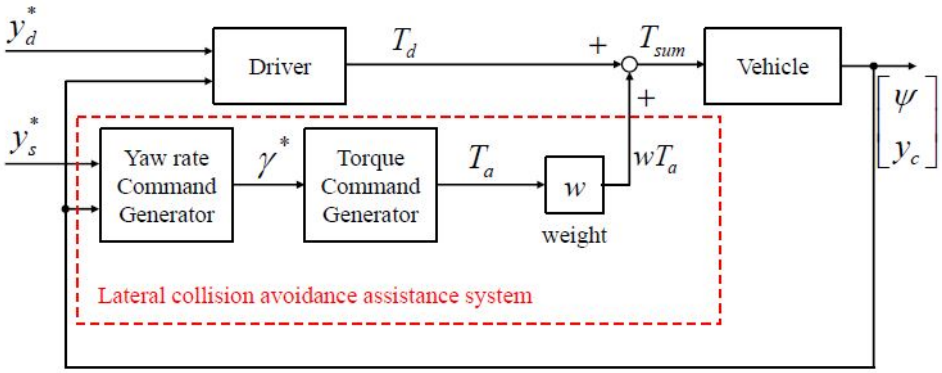


Figure 3 – The Block diagram of the steering assistance system for the obstacle avoidance purpose [Iwano et al., 2014].

Another approach of shared control is the integration of the driver's state in the cooperation process. In [Benloucif et al., 2016a], a lane keeping assistance system is developed taking into account the driver's state. If the driver is very distracted, a high authority is given to the assistance system to keep the vehicle on the desired lane. However, if the driver is very awarded about the driving supervision, he can take the task of driving vehicle. They use the fatigue and distraction criteria to determine the driver's state, that depends on eyes analysis for fatigue, and the head orientation and position for distraction.
According to the Michon's hierarchical levels [Benloucif et al., 2016c] (Figure 4), there are three levels of cooperation between the driver and the automated system: the strategic level, the tactical level and the operational level. The authors in [Benloucif et al., 2016b], [Benloucif et al., 2016c] propose a multi-level cooperation of driving based on the Michon's model to handle the interferences and manage the decision authority between the two agents. A shared control of multi- level based on the active system is developed to change the lane when the driver tends to do that. Two algorithms are developed at the operational and tactical level to determine the authority management that reduces the negative interferences. Finally, the multi-level cooperation is done by coupling the authority management of two levels. Another new scheme for the haptic shared lateral control on the highway including the trajectory planning is developed in [Benloucif et al., 2017]. The conflict is solved by considering the steering of the driver in the planning trajectory where the desired trajectory of the system is adjusted in order to deal with the driver's intention. The proposed shared lateral control is presented in the Figure 5. The primitives polynomial path methods were used in this work to generate the planned trajectories concerning the lateral and longitudinal movements. In [Rath et al., 2018], a shared

control approach was developed based on nonlinear vehicle-road-driver model for the lane keeping purpose. A sharing parameter was integrated in the shared design to consider the conflict between the two agents. Then, the shared lateral control is done using the U-shape based on the driver's activity determined by the driver's state and involvement of driver torque.

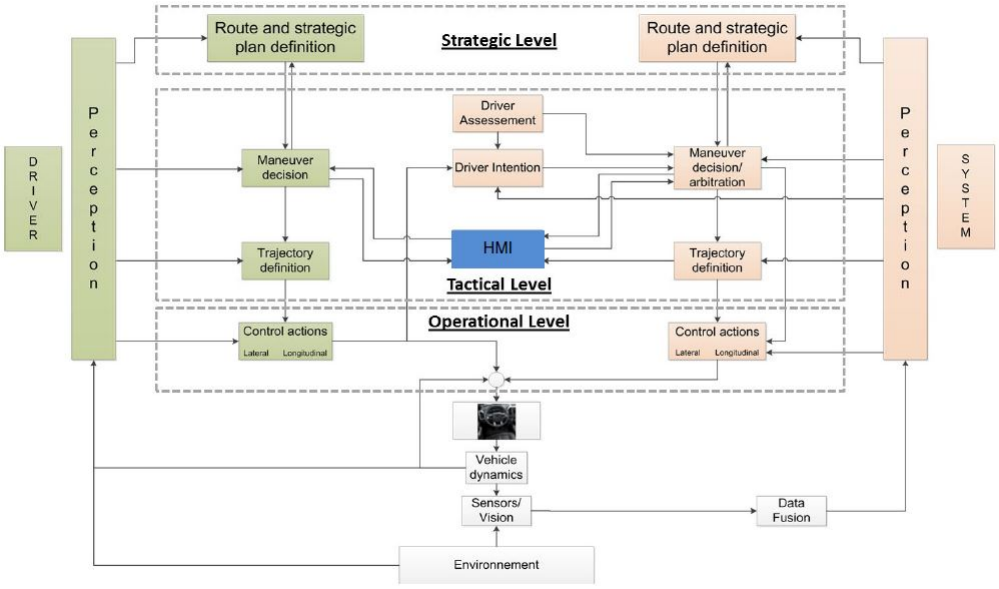


Figure 4 – The Michon's hierarchical levels for the multi-level cooperation [Benloucif et al., 2016c]

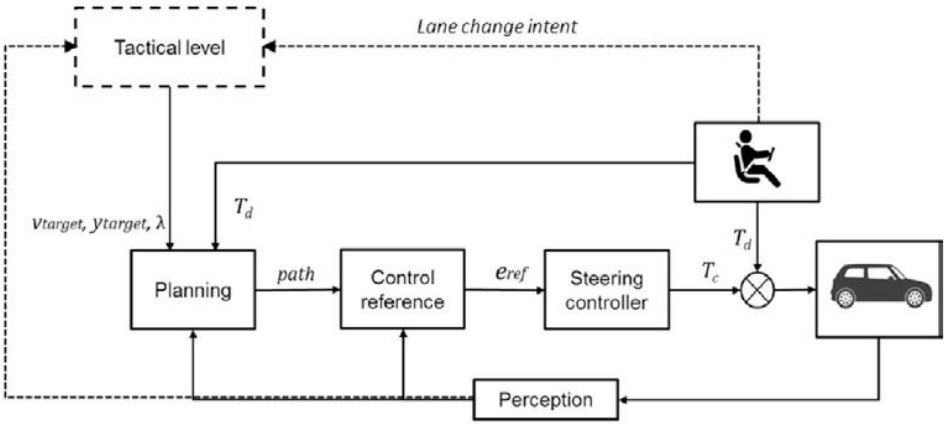


Figure 5 – The proposed shared lateral control presented in [Benloucif et al., 2017].

The vehicle's accident can by caused by a lane departure when the driver is inattentive, drowsy and tired. To prevent these accidents, the authors in [Saleh et al., 2013] have developed an active system which is applied to the vehicle and improves the driving safety and vehicle's performance. A cybernetic driver's model presented

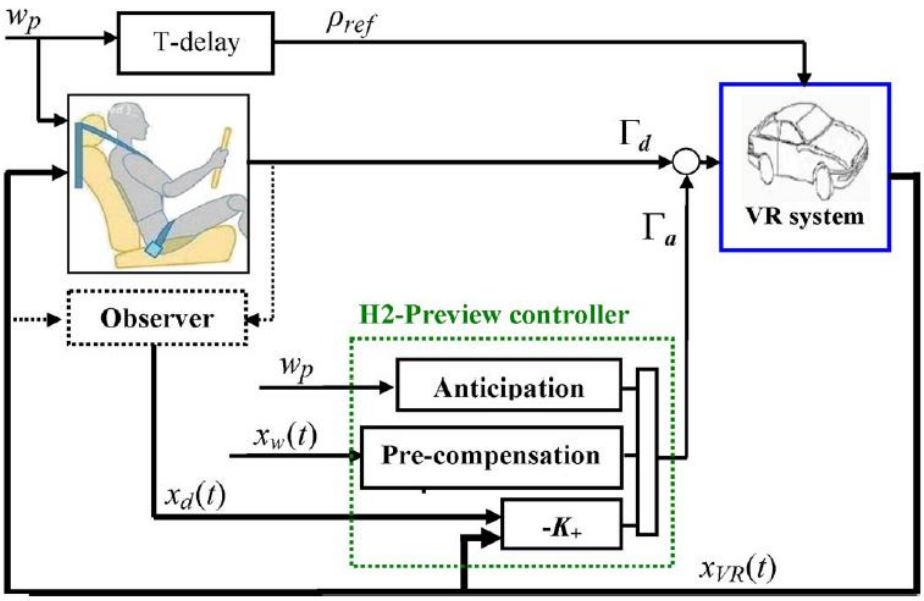


Figure 6 – The shared lateral scheme [Saleh et al., 2013].

in [Saleh et al., 2011] is used to consider the variation of driver's behaviors. Then, an advanced driving assistance system ($ADAS$) for the lane keeping is developed using the $H_2$ control theory. Many criteria are presented to evaluate the lateral shared control where the assistance system assists the driver to keep the lane and cooperate with him to avoid any conflict. Examples of these criteria: lateral deviation error, time to lane crossing ($TLC$) that indicates lane departure risk ($LDR$), etc. Finally, the proposed shared control can be realized by a simple summation of the driver's torque delivered from the cybernetic driver model and the assistance system (see Figure 6).

***Haptic shared control:***
The basic idea of the haptic shared control is that the two agents interact and respond in a common physical interaction block. The identification of the haptic shared control leads to two designs. The first design consists to compute a feedback force, and, feed it back to the human operator in order to predict the surrounding environment. The impedance control [Hogan, 1985] is used to compute the feedback force. It is given as:

$$F_{impedance} = K^d(x^d - x) + C^d(\dot{x}^d - \dot{x}), \tag{3}$$

$F_{impedance}$ represents the human's resistance force to the external disturbance. The desired state (position and velocity) is given by $x^d$ and $\dot{x}^d$. $x$ and $\dot{x}$ are the actual position and velocity. $k^d$ and $C^d$ are the stiffness and viscosity impedance. The second design is based on the human-centered automation, where a shared control authority is formed between the two operators to gain or release the right to control the system. To conclude, the advantage of the shared control is that human driver knows about

the driving situation and automation system through the haptic feedback. It also leads to the conflict resolution and attenuation.

The haptic shared control ($HSC$) is the configuration where the driver feels the inputs of automated system and there is a possibility to override or correct his input. The challenges of haptic shared control is related to different terms: Adaptation of force, appropriate trust, understanding driver responses and adaptive shared control. A haptic shared control was presented in [Soualmi, 2014]. The cooperation is made on two levels:

- Low level of cooperation ($LLC$): is carried out at the level of driver's actions. $ADAS$ systems use the steering wheel system (haptic interface) because it is the fast way of acting if there is risk detected.
- High level of cooperation ($HLC$): depends on different criteria: the driver's state, the environment, the possible trajectories, to properly take the decisional aspects, navigation and control.

Then a Takagi-Sugeno ($TS$) fuzzy logic method is introduced for the development of lane keeping controller. This controller interacts with the driver for the lane-keeping purpose. The results show that the two agents have the same decision in case of lane-keeping while a conflict appears in case of obstacle avoidance. To resolve this conflict problem, two architectures of haptic shared control are exposed in this work as:

- Sharing control by weighting: The idea of weighting is based on a Gaussian function which guarantees smooth weighting without discontinuity. This approach is validated in numerical simulations. The results are good since it degrades the performance of the controller depending on the driving situation and the steering torque rate.
- The sharing is considered as one of the objectives of the controller. In this approach the driver is modulated in the design of control command. There is another sharing of driving containing a feed-back on the High level of cooperation ($HLC$). This sharing allows to modify the target trajectory using the planning module. Once the target trajectory is given by the trajectory module, the difference criterion between driver and controller torque is used to determine the direction of deviation (right/left).

There are many haptic methods presented in the literature that use the vehicle components like the vehicle seat, steering wheel, foot pedals and gear selector and provide interface between human and machine. The research studies ensure that the visual feedback is the most feasible operation to inform the driver. However, this operation needs a high attention of the driver who uses his eyes to analyze the environment and driving conditions. In addition, an auditory feedback is used to aware the driver face to hazardous situation but it can lead to a confusion when combining with the road noise. A haptic feedback based on the steering wheels is presented in [Jensen et al., 2011] to inform the driver about the roadway information

and improve the overall driving performance. This haptic feedback ensures the earlier enabling avoidance obstacle. The authors in [Johns et al., 2016] proposed a haptic-feedback shared control between the driver and the automated system using the torque on the steering wheel. The study shows that the haptic feedback torque on steering wheel is unsufficient to predict the driver's intention in the future. A two-phase haptic interface based on the human-machine interaction is developed in [Lv et al., 2021] to manage the authority shift from autonomous to manual mode. This haptic torque on the steering wheel aims to guide and assist the human while he is engaged in the control loop, depending on his ability. However, the shared control can cause a conflict in dangerous situations. A haptic guidance torque calculated with respect to the driver's behavior is presented in [Boink et al., 2014] to mitigate the conflict between both agents.

#### 0.2.2.3.2 Human supervisory control

In the human supervisory control, the human monitors the tasks of the automated system. He doesn't participate in the control activities, but he chooses a goal achieved by the autonomous system. The role of the human is included in a supervision process to verify if the automated system acts in the best way. A commercial application of this feature is the "active lane change assist" where the driver chooses a lane and drives within it. This type of shared control offers a simple way of interaction with the automated system without direct participation of the driver in the control system. However, through the human supervisory control, the driver can express his intention using signal commands without having potential acts to change the vehicle trajectory like the case of manual driving. From the other hand, many studies have been developed in the literature to treat the shared control as a transition management between the human driver and the autonomous system especially in the level 3 and 4 of autonomy.

### 0.2.2.4 Transition Management:

***Why a Transition is needed?***
As said before, the presence of human driver is essential to navigate safely on the road in many levels of autonomy ($SAE$ level 3). In level 3, the human is the main responsible of driving tasks. He supervises the scene not at all times, monitors the vehicle's control and reacts if the automated system reaches his limits. In addition, in the higher level of automation (level 4), the system acts on vehicle's control alone without any help from the driver. The driver can retain control if he is available. In addition, even if the driver is trusted during autonomous mode (auto mode), a smooth transition from auto to manual mode is needed to ensure this switching. Moreover, according to the $NHTSA$ [Ayoub et al., 2019], the autonomous system should inform the driver about its status: (1) normal/abnormal functioning, (2) Available/not available for autonomous driving mode and (3) On/Off transition request from automated system to the driver. Thus, the transition between the manual driving and autonomous driving modes creates a new challenge for the automotive industry and researches in the framework of shred control. This

transition can be from autonomous to manual driving mode and vice-versa. For that, two types of transitions are defined:

- Takeover: Control is shifted from the system to the human driver.
- Handover: Control is switched from the human driver to the system.

Depending on the initiation of transition, the transition can be a driver-initiated or system-initiated transitions. When the driver demands a takeover request ($TOR$), that means he is ready to take the control, while a transition is initiated by the system, the driver needs more time to be engaged in the loop. In addition, considering the driver involvement, the transitions are defined as 3 types:

- Active transitions: the system allows to the driver to initiate a transition (Takeover or Handover) by pressing a bottom, additive steering or pedals, or other inputs. This transition is managed by the driver.
- Semi-active transitions: A transition initiated by the system where the driver can accept or deny this transition.
- Passive transitions: A transition implicitly signaled by the driver. An example is the Lane keeping system ($LKS$) system. The driver can switch-On/Off this option. This transition can be Takeover or Handover.

The literature is rich in the works related to the transition management topic. In [Kim et al., 2018], the authors presented a driver's cognitive model to analyze the influence of driver's experience and workload on the transition between the two agents. A planned control transition was applied in [Holländer and Pfleging, 2018] to switch from automated system to the driver by using the auditory and visual information systems. These systems help and prepare the human who is engaged in non driving related activities to be ready for regaining control. Moreover, an overview for the last ten years was done in [Ayoub et al., 2019] that summarizes the different works related to the shifting from manual to autonomous driving. An overview of the different systems for transition between the human and the autonomous system is done in [Mirnig et al., 2017]. The different works related to the transition management developed in the literature, and the interaction technologies of the industry are discussed. This overview aims to show the results and the lack of attention in order to move forward in the transition control management. The authors in [Stevens et al., 2019] have presented an overview of research methods related to driving simulation, the survey, etc, to address the human's factors of autonomous driving. They have defined the impact of autonomous system driving on the different levels: the individual, social interaction and societal level.

- At the individual level: how we can ensure a good understanding between the human driver and the autonomous system to realize a takeover, handover, etc. For example, the communication of user's with auto taxi is not very easy in order to determine the destination and the stop. Moreover, the human can take control from the autonomous vehicle when he was engaged in the non-driving secondary tasks, like: writing emails, using phone, playing games, etc. Different methods are presented to help him to be out of the loop.

- At the social level: how we can assure the communication with the autonomous-car face to road user's, cyclists and pedestrians, etc.
- At the societal level: involves the impact of autonomous system cars on the society. The question is if the people accept the autonomous cars on the road. Many points should be clarified: the confidence of autonomous system, safety on the road, what happened in case of failure (blackout of the internet), losing the job by replacing the human and the losing of pleasure to drive, etc.

In the highly automated system (level 3 and 4), the driver intention is not required. However, the latter is able to override the autonomous system at any time. This override can be at the system or driver initiation. During this transition, the driver should be provided by a sufficient time to be totally engaged in the control loop. The time is essential to realize the takeover. The authors in [Melcher et al., 2015] have developed a transition strategy from automated to the manual driving to deal with the Takeover request ($TOR$) and the reaction time of the driver. The study of the $TOR$ is done considering many conditions: integration/no integration of mobile phone and with/without additional brake, to show the influence of variation conditions on the driver's reaction time. 10 seconds are considered to realize a $TOR$. The results show that the $10s$ are sufficient to attempt a comfortable $TOR$ where the driver can override the system in marge $1.4s$ to $6.7s$ without any problems. According to the $SAE$, retain control from autonomous system is required especially in the level 2 and 3 where the $ADAS$ system reaches its limits. For that, a transition from autonomous to manual mode is needed to compensate the $ADAS$ system's limitation or failures. When the driver realizes that the autonomous system is not working properly, he demands to take vehicle's control. To have a smooth shifting, four required steps are reported by the $SAE$, given as:

- Display the $TOR$ from the system to the human driver.
- Prepare the driver quickly. He is ready to take control.
- Communicate the driver's readiness to ensure control to the autonomous system.
- Realize a smooth transition authority of the steering operation control to the human driver.

A smooth method is proposed in [Wada et al., 2016] to shift control from autonomous mode to human driver via haptic shared control ($HSC$) based on the cooperative state. The cooperative state is determined according to the initiative holder and the intent consistency. The driver's takeover intention is detected via the steering actions on the steering wheel. However, this study did not cover the case where a control shifting is initiated by the system. The authors in [Miller et al., 2014] presented an experimental study to treat the importance of situation awareness ($SA$) in the different levels of automation on the driver's behaviors and performances. The situation awareness is essential especially when switching from auto to manual mode in order to transmit the information to the driver and realize a comfort and safe

driving. The study shows that the driver's performance is affected by the level of automation. There are many studies presented in the literature to deal with the situation awareness of the driver, and how to alert him to take control when he was distracted with non-driving activities. A high level of autonomy leads to a high trust and comfort on the system. An enhancement of the level of situation awareness ($SA$) and the driving safety ($DS$) for the partially automated system is done in [Wulf et al., 2014] by developing a human-machine interface ($HMI$) mechanism. The level of situation awareness is affected by two factors: Out of the loop of the driver in partially automated driving mode, and the non-driving secondary task ($NDST$); while the driving safety ($DS$) is related to: the reaction time, the minimum time to line crossing, etc. The $DS$ is increased in partially automated driving compared to a manual driving. The results demonstrate that the mechanism is able to improve driver's $SA$ and $DS$ in a partially automated system.

In a self-driving car, the driver's distraction is increased. The challenge now is how to manage the driver's distraction. The authors in [van der Heiden et al., 2017] have studied the impact of an auditory pre-alert on the handover in case when the driver is engaged in a non-driving secondary task ($NDST$). The driver will be more attentive about the driving situation after a pulse pre-alert. The pre-alert is provided before a few seconds of handover. The research is based on: effect of this pre-alert on the eye-gaze on the road, the driving performance and if this pre-alert attracts the driver's attention to be ready to take control. A user study of 24 drivers is done in order to show the effect of the pre-alert on the handover in term of reaction time, stress level, speed reduction, eye-gaze and unsafe incidents. The results show that the pre-alert gives the driver enough time to take control and will be less stressed to be engaged in the driving activity. The driver is less stressful and responds faster during the driving with a pre-alert configuration. He can responds faster to steer or brake to prevent a dangerous situation. However, there are implications for this theory and design, like if the $20s$ are enough to make a pre-alert on the road regarding the complexity of the road's traffic. Modifications occur in terms of: alert's length, modality of the reasons of the pre-alert, solutions proposed by the system and dynamic time, to deal with each situation on the road.

The authors in [Reimer et al., 2016] treated the impact of automation driving levels on the driver's behaviors during his engagement in secondary tasks (non-driving tasks activities). The change of autonomous levels affects the engagement of the driver in a secondary task. The impact of the level distraction on the 3 levels of driving: manual, semi-autonomous and autonomous, is presented. The difference between the semi-auto and the auto mode is that in the first mode the driver can lunch a lane change realized by the system while in the second mode he can't. The semi-automated technologies like $ACC$, $LKS$ have a limited functionality for many reasons: sensor's failures, environment conditions, miss understanding for the surrounding conditions by the system. In this case, the driver's supervision is necessary to take control's responsibility. The role of the driver is transformed from controller to a supervisor. For this reason, in semi-autonomous vehicle, the driver is less probably engaged in non-driving related activities ($NDRA$) than in

the fully autonomous vehicle. The results show that the driver is less distracted in the manual mode. This distraction increases with the augmentation of automation levels. In addition, the driver will be more in hand-off situation where the automation level is higher, and the face detection is more complicated in the full autonomous system.

Moreover, in takeover request ($TOR$) process, it's important to understand the driver's performance to deal with road safety. In the level 2 and 3, the driver is able to retain control at any time and monitor the environment. The driver will demand a $TOR$ when the system does not operate properly. With the increasing of automation level, the driver will be engaged in the secondary task and then reduce the situation awareness and increase the reaction time. The study in [van der Meulen et al., 2016] focus on the driving performance when switching from auto to manual mode for two cases: after an autonomous driving and after a period of stationary. The difference of take over request in these two cases is figured in: the amount of gaze, the time looking at the road and the distraction before and after the Takeover request ($TOR$). The research question in this study is if the driver's distraction is caused by the autonomous system itself or because the driver is distracted from a stationary and non-autonomous activity. The results show that no difference in gaze behavior and driving performance (driving distraction) when starting to switch manually from an autonomous driving, before and after a period of stationary. An ambient interface design is developed in [Borojeni et al., 2016] to perform a takeover request while the driver is engaged in a secondary task. In this case, the transition from auto mode to the driver who is engaged in a secondary task is essential to ensure this switching. The fact that the driver is engaged in a secondary task, can cause a delay or an error on his behavior. For that, an ambient visual display is used to support the $TOR$. An interface formed from light display and auditory cue is developed to realize the $TOR$. The question is if conveying contextual information can affect the driver's behaviors. Then, the baseline light and other types like static and moving light are used in this study to show the consequence of this display on the $TOR$ action. The results show that the conveying information can increase the situation awareness ($SA$) that means decrease the reaction time ($RT$) and increase the time to collision ($TTC$). However, depending on the qualitative feedback, the users prefer to use the static light more than the moving light because the static light can help them to know the direction to steer without any stress. The limitation of this study is that the developed interface was tested on driving simulator with a specific scenario. In a real and complex scenario, many factors can affect the interface and should be taken into consideration, like: type of road, driving conditions, weather, etc. The authors in [Walch et al., 2015] designed a generic handover process to realize the transition from the self-autonomous to the manual driving. This process uses the visual and auditory cues to assist the driver taking handover in three driving conditions: No hazard, car hazard and curve hazard situations. The study aims to prove if the driver is able to take the handover request and if he feels like comfortable and less stressed by using this process. 30 participants participate to this study and all quantitative and qualitative data are collected and analyzed ($TOR$, braking behavior, comfort of $TOR$, performance of $TOR$, etc.). The participants prefer the alert followed by a

take over request where the $TOR$ is easy and not stressing. The results show that handover conveying a combination of visual and auditory cues covers the critical situations when the driver is distracted and the autonomous system reaches its limits.

The work presented in [Politis et al., 2015] aims to develop a multimodal language-based for the handover from auto to manual mode and vice-versa in an urgent driving situation. The motivation of this work is to integrate the multimodal cues (tactical, visual and audio) in a handover situation where the driver is busy. Then an experimental study is done to address the handover topic in a warning situation. The analysis of driver's performance, subjective and objective results are presented for the unimodal and multimodal cues. Three levels of urgency are discussed later. The results show that the multimodal warnings are more efficient in term of urgency to takeover control from the car to the driver. However, the unimodal signal is not sufficient to treat the urgent situation. The limitation of this study is that the game is visual based concept.

The cooperative control is a black-and-white approach where both agents cooperate together to realize a common driving task. For that, authors in [Walch et al., 2016] have designed a cooperative control interaction between the driver and the autonomous system to deal with the handovers situation. This cooperation aims to compensate the system's limitations (overtaking obstacle, pass road works, lane change etc.) and avoid handovers by the driver. In such situations, the handover is needed to avoid a critical situation. The driver who is out of-the-loop and distracted by other activities should be able to take control. The new challenge now is to prepare the system asking the driver to perform some driving task and propose him many solutions. To do that, the authors have developed a generic interaction based on the visual and auditory cues alerting the driver, where the autonomous system proposes several solutions to prevent such dangerous situations. Then, the driver should choose the suitable one. So, no need to the handover in this case. Finally, the autonomous system operates safely. The feedback from the participants assessed that the cooperative approach is easy and not stressful. However, its drawback is that the users are less confident in the speech system when talking with the autonomous system. An open question resulted from this study is: if the cooperative control is more feasible in all driving situations in order to avoid handovers, despite the driving situations.

A geometrical transformation steering wheel is addressed in [Kerschbaum et al., 2015], for two issues: avoiding the detrimental effect of automation and providing an interface to the driver to give him time and feel comfortable while driving in highly automated system. The main idea of the transformation steering wheel is when the system is in automated configuration, the steering wheel is moved out of the sight, giving the information to the driver that no need to be controlled. However, when the system reaches his boundary, the steering wheel adopts his original shape and there is a need to be controlled by the driver. Then, the study aims later to prove if there is an influence of this transformation on the transition from auto to manual

and how the driver evaluates this transformation of steering wheel. The results show that the steering wheel influences the gaze behavior. However, the takeover time will be longer with no errors in case of lane change. In addition, the transformation of the steering wheel has no negative effects on the takeover performance and can improve the takeover quality.

The authors in [Kim and Yang, 2017] have adopted a methodology to determine the takeover request time in the level 3 autonomous driving. This methodology takes into account the driver characteristics to calculate the $TOR$ time. Then, the performance-based method is used to identify the optimal $TOR$ value. The proposed methodology is tested experimentally for 4 different scenarios. The quantitative and qualitative results show that the performance of $TOR$ is improved considering human's factors. In [Bueno et al., 2016], the authors have studied the impact of mental workload levels on the takeover request after an autonomous driving. The mental workload is caused by a non-driving task before a takeover request demanded by the autonomous system. The analysis of driver during a transition from autonomous to manual mode in case of low and high mental workload is presented in this paper. The driver performs a non driving-task represented by finding a word related to three images during an autonomous mode. Then, the driver is notified by a visual and auditory alert to take control and avoid an obstacle appeared on the lane. The results show that the driver's mental workload decreases the situation awareness ($SA$) and influences negatively the takeover performance. The drawback of this study is that the results show the effect of driving mode and not the effect of the mental workload on the takeover driver performance. To a good understanding of the effect of mental workload on the transition and takeover process, information about driver's environment and state should be provided to the system via a human machine interface ($HMI$).

Based on the literature review, many advanced studies have been presented to investigate the shared control between the driver and the autonomous system in different contexts, including the transition and control authority management and shifting between both agents and the fusion methods of both agent's inputs. All these interesting studies have motivated us to develop a shared lateral control for the lane keeping objective to manage the control authority and the transition between manual/auto mode for the semi-autonomous vehicle (level 3, ($L_3$)) by using steer-by-wire system. Firstly, in the present work, we are interested to develop a shared lateral control approach to manage the control authority between the driver and the autonomous system in case of autonomous system's failure while the human driver can be available or not. Secondly, we are investigated the shared lateral control in the context of a Take Over Request ($TOR$) to deal with the transition management. The driver can retain control if he is available. Otherwise the autonomous system intervenes to interrupt the driver's input and take vehicle's control. Note that the autonomous system operates correctly without failures in this new shared lateral approach. The control authority in both shared control approaches is done using the blended shared control given in the Section 0.2.2.3.1.

Moreover, a development of Advanced Driving Assistance Systems ($ADASs$) (level 2, ($L_2$)), involving Active Front Steering ($AFS$) and Direct Yaw Control ($DYC$) integrated to the vehicle during lane keeping maneuver is done in this thesis. These systems help and assist the driver to keep the lane and to enhance the vehicle's lateral stability.

## 0.3 Thesis Contribution

The main contributions of this thesis are listed in the following:

- A shared lateral control architecture for the lane keeping purpose including the human driver and the autonomous system, based on the blended shared control, which permits the fusion of the two inputs, is developed in this work.

- A decision-making algorithm for the shared lateral control to manage authority between the driver and the autonomous system is also developed (level 3, ($L_3$)), based on many criteria, such as: the degree of confidence of each input, the lateral error, etc. A Fuzzy Logic Controller ($FLC$) and a situation-based analysis block are developed for decision-making. This shared control treats the case where a failure occurs on the autonomous system while the human driver can be available or not.

- A transition management between the human driven and the autonomous system in the Take Over Request ($TOR$) context is also done (level 3, ($L_3$)), to deal with the retain control from autonomous to manual driving and vice-versa.. The human demand a Take Over Request in many cases. A decision algorithm is developed to evaluate the driver's status and generate the switching between both agents based on different criteria: the driver's behavior and availability, the vehicle's state and the take over request ($TOR$).

- Driving case studies and scenarios on the road are defined to test and validate the different shared control approaches given above.

- A validation and implementation of algorithms on Matlab/Simulink and on the "*SCANeR Studio*" vehicle's simulator (OKTAL) interacted with the human in-the-loop through the "*Logitech G29*" steering wheel for the different driving scenarios are presented later.

- A development of advanced Driving Assistance Systems ($ADASs$) (level 2, ($L_2$)) for the lane keeping maneuver and the vehicle's lateral stability enhancement is presented. The developed architectures are based on the $LPV/\mathcal{H}_\infty$ and the Super-Twisting Sliding Mode $STSM$ control approach. Validation and implementation of these systems on Matlab/Simulink with a complete nonlinear vehicle model validated on the "*SCANeR Studio*" simulator are also done.

## 0.4 Thesis Outline

The thesis is organized in 4 chapters, see Figure 7:

- **Chapter 1**: deals with the global architecture of the shared lateral control. The different tools used in this framework are evoked in this chapter.
- **Chapter 2**: provides a full description of a proposed shared lateral control to manage control authority between both agents (level 3, ($L_3$)) in case of autonomous system failure. A Fuzzy Logic Controller ($FLC$) and a situation-based analysis block are developed for decision-making process, to determine the fusion parameter.
- **Chapter 3**: investigates a new shared lateral control approach to deal with the transition management between the human driver and the autonomous system in the Take Over Request ($TOR$) context (level 3, ($L_3$)). A coordinator based on a decision algorithm is developed for the driving modes and the fusion parameter determination.
- **Chapter 4**: develops an Advanced Driving Assistance Systems ($ADASs$) involving Active Front Steering ($AFS$) and Direct Yaw Control ($DYC$) (level 2, ($L_2$)) for the lane keeping maneuver while guaranteeing vehicle's lateral stability. The $LPV/\mathcal{H}_\infty$ (respectively the Super-Twisting Sliding Mode $STSM$) control technique is applied to develop the control layer of the centralized (respectively decentralized) architecture, while weighting parameters are calculated in the decision layer of both architectures to coordinate different controllers and objectives. Finally, a comparison is done between the centralized and decentralized control architectures.

Finally, the thesis concludes with a summary about the obtained results and an outlook about future work.

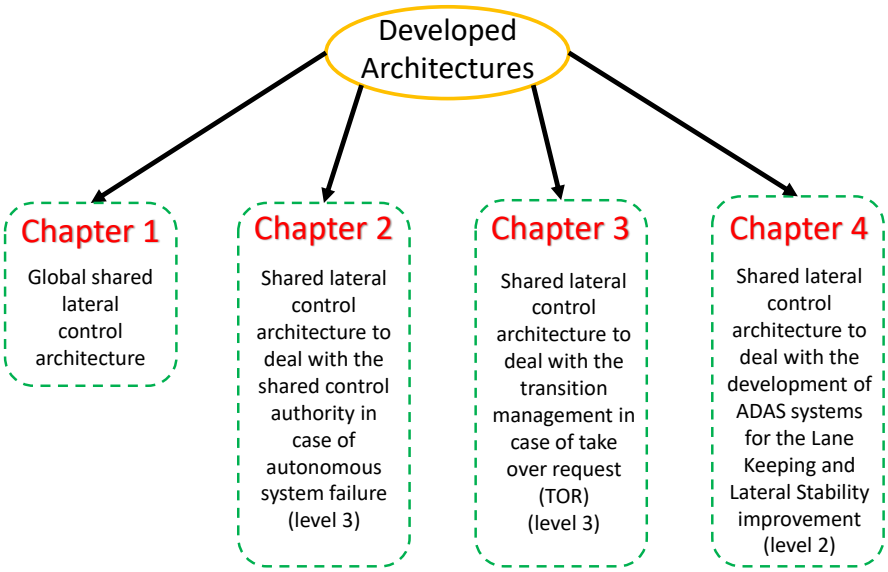


Figure 7 – Block Diagram of the Developed Architectures of the present work

## 0.5 Conclusion

In this chapter, the motivation of this work and a state of the art on the automation driving, the shared control and the transition management are exposed. Next chapter presents the global proposed architecture of the shared lateral control including the vehicle model, human Driver and the Autonomous System to prepare the environment work.

*Part I*

# Shared Lateral Control

# Architecture

This chapter presents the global architecture of the shared lateral control. The different components are detailed later to deal with this topic.

## 1.1 Introduction

This chapter introduces the different tools used in the framework of the shared lateral control. The global shared lateral control architecture is given in the Figure 1.1. Its main components are: the Vehicle Model, the Human Driver and the Autonomous system (detailed in this chapter); and the shared lateral control (detailed in chapter 2 and 3). A vehicle model representing the vertical, longitudinal and lateral dynamics, is given. The human driver can be presented in-the-loop by two ways: through a driver model or a steering wheel (human in-the-loop). Finally, an autonomous system controller is developed to realize a path following for a desired trajectory.

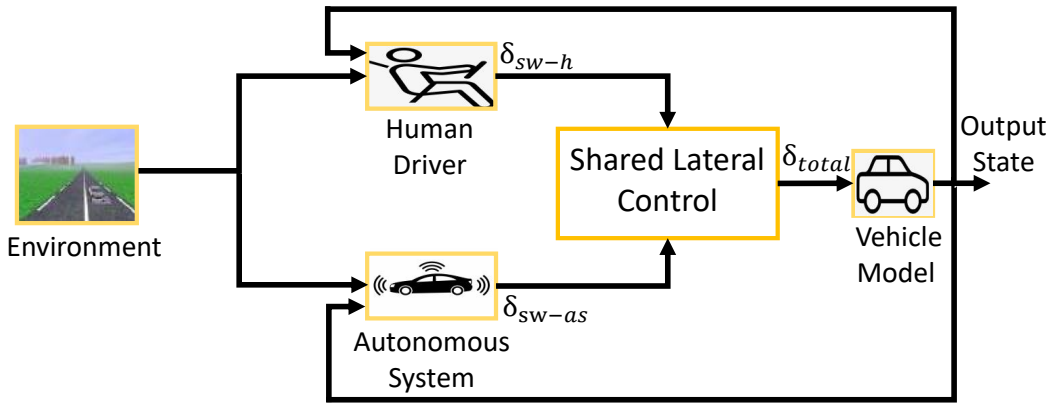


Figure 1.1 – The global shared lateral control architecture.

## 1.2 Vehicle Model

The vehicle is a group of interconnected mechanical and electrical systems and subsystems. The global vehicle's dynamics are influenced by these systems. Modeling and simulating vehicle dynamics are essential for a good understanding of the vehicle's behavior. Several methods have been developed in the literature to model the vehicle kinematics and dynamics. Some models depend on the physical laws

called the closed-form models. For example, authors in [Villagra et al., 2007], [Rajamani, 2012] have developed the vehicle planner dynamics in the longitudinal and lateral directions using the Newton's laws. Vertical dynamics are presented in [Kiencke and Nielsen, 2000], [Rajamani, 2012] by developing vertical models to deal with automotive suspensions, tires/road friction, etc. On the other hand, the multi-body models have been developed to model the vehicle. These models are more accurate with respect to the closed-form models. Several approaches are used to develop a multi-body model ([Khalil and Kleinfinger, 1986]), such as Newton-Euler ([Khalil and Kleinfinger, 1987]), Lagrange, Appell's method, etc. Moreover, the literature is rich in vehicle models, less or more complex depending on the use objective. A full vehicle model is used for the validation purpose while a vehicle bicycle model is dedicated for the control synthesis.
In this section, we will present briefly the vehicle's dynamics based on the closed-form models. A complete vehicle model is developed, including vehicle vertical model. Then, the longitudinal and lateral motion planner are given in the following. Finally, a simplified bicycle model is presented.

### 1.2.1 Complete Vehicle Model

From our point of view, the vehicle model could be presented as four sub-models combined together to develop a full vehicle model. These sub-models are:

- the vehicle vertical model which describes the suspension deflection, the tire deflection, and the sprung mass roll, pitch and heave motions;
- the vehicle longitudinal and lateral model (in the horizontal plan) which describes the longitudinal acceleration, the lateral acceleration and the vehicle yaw rate;
- the tire/road contact model;
- the wheels dynamics model.

#### 1.2.1.1 Vehicle Vertical Model

The vehicle vertical model is a part of the vehicle dynamics. Therefore, to better understand and analyze vehicle's behavior, the modeling and the representation of the vertical model is important. This model describes the automotive suspension deflection, the tire deflections, and the sprung mass roll, pitch and heave motions. The automotive suspension system is composed of a spring and a damper that rely the sprung masses (chassis) to the unsprung masses (wheels). The aim of the suspension system is to improve passenger's comfort by isolating the vehicle chassis from an irregular ground. In addition, the suspension system ensures passenger's safety by providing a good-holding properties. Indeed, the suspensions help the wheels to maintain a sufficient contact with the road in presence of irregularities of the road and load transfer. Many types of suspension systems have been developed, like the passive suspension system model, the semi-active and the active suspension ($ASus$) systems [Rajamani, 2012]. A quarter vehicle vertical model is represented

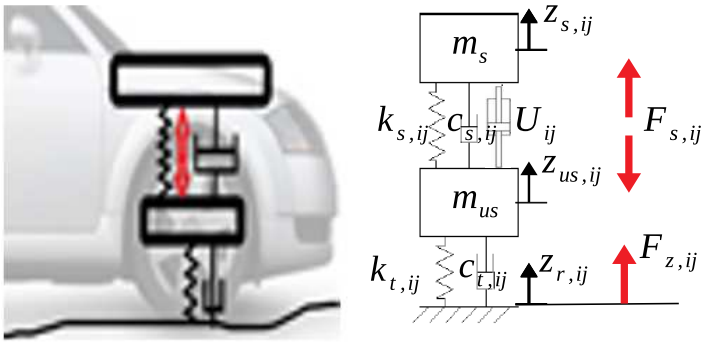


Figure 1.2 – Quarter vehicle vertical model [Chokor, 2019]

in this section, which is a combination between the active suspension model and the vertical tire model.

### Quarter Vehicle Vertical Model

The quarter vehicle vertical model is given in the Figure 1.2. It represents the motion of the axle and of the vehicle body at each wheel. The suspension system and the tire are subjected to a dynamical motions/vibrations, while the vehicle moves. The equations that describe the system dynamics at the $ij$ ($i = \{f : front, r : rear\}$ and $j = \{r : right, l : left\}$) corner of the vehicle are:

$$F_{s,ij} = -K_{s,ij}(z_{s,ij} - z_{us,ij}) - C_{s,ij}(\dot{z}_{s,ij} - \dot{z}_{us,ij}) + U_{ij}, \tag{1.1}$$

$$\ddot{z}_{us,ij} = \frac{1}{m_{us,ij}}(F_{z,ij} - F_{s,ij}), \tag{1.2}$$

$$F_{z,ij} = -K_{t,ij}(z_{us,ij} - z_{r,ij}) - C_{t,ij}(\dot{z}_{us,ij} - \dot{z}_{r,ij}), \tag{1.3}$$

where $m_s$, $m_{us}$, $K_{t,ij}$, $C_{t,ij}$, $K_{s,ij}$, $C_{s,ij}$, $U_{ij}$, $F_{s,ij}$, and $F_{z,ij}$, are respectively, the quarter vehicle suspended mass, unsuspended mass, the tire stiffness coefficient, the tire damping coefficient, the suspension stiffness coefficient, the suspension damping coefficient, the actuator force of the $ASus$ system (active force), the total (passive+active) suspension force, and the vertical force on the tire of the $ij$ corner. $z_{s,ij}$ and $z_{us,ij}$ are respectively the vertical displacement of the sprung mass and the unsprung mass (wheel bounce). $z_{r,ij}$ and $g$ are respectively the vertical profile of the road and the gravitational constant.

### Full Vehicle Vertical Model

In order to express the vertical displacement of each corner, and the roll, pitch and heave motions of the sprung mass at the center of gravity, the full vehicle vertical model is developed (see Figure 1.3).
Let $\theta$, $\phi$ and $z_s$ be respectively the roll, pitch and heave of the sprung mass. Geometrically, the vertical displacements of the vehicle corners $z_{s,ij}$ can be approximated

by:

$$z_{s,fr} = z_s - t_f sin\theta - l_f sin\phi, \tag{1.4}$$
$$z_{s,fl} = z_s + t_f sin\theta - l_f sin\phi, \tag{1.5}$$
$$z_{s,rr} = z_s - t_r sin\theta + l_r sin\phi, \tag{1.6}$$
$$z_{s,rl} = z_s + t_r sin\theta + l_r sin\phi, \tag{1.7}$$

where $t_f$, $t_r$, $l_f$ and $l_r$ are respectively half front track, half rear track, wheelbase to the front and wheelbase to the rear.
The vertical velocities of the vehicle corners $\dot{z}_{s,ij}$ are the time derivatives of the four above equations, such that:

$$\dot{z}_{s,fr} = \dot{z}_s - t_f \dot{\theta} cos\theta - l_f \dot{\phi} cos\phi, \tag{1.8}$$
$$\dot{z}_{s,fl} = \dot{z}_s + t_f \dot{\theta} cos\theta - l_f \dot{\phi} cos\phi, \tag{1.9}$$
$$\dot{z}_{s,rr} = \dot{z}_s - t_r \dot{\theta} cos\theta + l_r \dot{\phi} cos\phi, \tag{1.10}$$
$$\dot{z}_{s,rl} = \dot{z}_s + t_r \dot{\theta} cos\theta + l_r \dot{\phi} cos\phi. \tag{1.11}$$

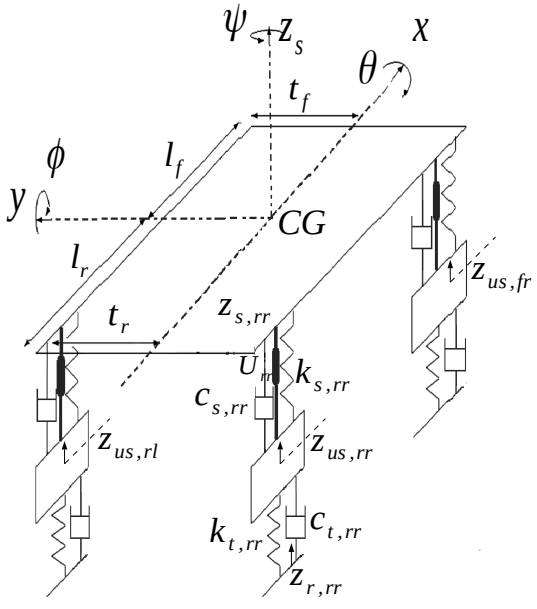


Figure 1.3 – Full vehicle vertical model [Chokor, 2019]

The dynamic equations of the sprung mass i.e. the roll, pitch and heave (angular) accelerations ($\ddot{\theta}$, $\ddot{\phi}$, and $\ddot{z}_s$) can be modeled as:

$$\begin{aligned}\ddot{\theta} = \frac{1}{I_x + M_s h_\theta^2}[&(-F_{s,fr} + F_{s,fl})\, t_f + (-F_{s,rr} + F_{s,rl})\, t_r \\ &+ M_s\,(h_\theta\ cos\,(\theta) + z_s)\, a_y + M_s\,(h_\theta\ sin\,(\theta) + z_s)\, g],\end{aligned} \tag{1.12}$$

$$\begin{aligned}\ddot{\phi} = \frac{1}{I_y + M_s h_\phi^2}[&-(F_{s,fr} + F_{s,fl})\, l_f + (F_{s,rr} + F_{s,rl})\, l_r \\ &+ M_s\,(h_\phi\ cos\,(\phi) + z_s)\, a_x + M_s\,(h_\phi\ sin\,(\phi) + z_s)\, g],\end{aligned} \tag{1.13}$$

$$\ddot{z}_s = \frac{1}{M_s}(F_{s,fr} + F_{s,fl} + F_{s,rr} + F_{s,rl}), \tag{1.14}$$

where, $M_s$, $h_\theta$ and $h_\phi$ are respectively the mass of the sprung mass, the distance between the center of gravity of the sprung mass and the roll rotation center, and the distance between the center of gravity of the sprung mass and the pitch rotation center. $I_x$ and $I_y$ are respectively the moment of inertia of the sprung mass around $x$ axis and $y$ axis. $a_x$ and $a_y$ are considered as exogenous inputs to this model, they are calculated in the lateral and longitudinal vehicle model. They represent the longitudinal and lateral accelerations respectively.

#### 1.2.1.2 Longitudinal-Lateral Model

To develop the longitudinal and lateral vehicle models, the second Newton law is applied to the horizontal vehicle scheme shown in Figure 1.4. The governed equations are given by:

$$Ma_x = (F_{x,fl}\cos\delta_{fl} + F_{x,fr}\cos\delta_{fr} - F_{y,fl}\sin\delta_{fl} - F_{y,fr}\sin\delta_{fr} + F_{x,rl} + F_{x,rr}), \tag{1.15}$$

$$Ma_y = (F_{x,fl}\sin\delta_{fl} + F_{x,fr}\sin\delta_{fr} - F_{y,fl}\cos\delta_{fl} + F_{y,fr}\cos\delta_{fr} + F_{y,rl} + F_{y,rr}), \tag{1.16}$$

$$\begin{aligned}I_z\ddot{\psi} = &-t_f(F_{x,fl}\cos\delta_{fl} - F_{x,fr}\cos\delta_{fr} - F_{y-fl}\sin\delta_{fl} + F_{y,fr}\sin\delta_{fr}) \\ &+ l_f(F_{x,fl}\sin\delta_{fl} + F_{x,fr}\sin\delta_{fr} + F_{y,fl}\cos\delta_{fl} + F_{y,fr}\cos\delta_{fr}) \\ &- l_r(F_{y,rl} + F_{y,rr})) - t_r(F_{x,rl} + F_{x,rr})),\end{aligned} \tag{1.17}$$

where $a_x$, $a_y$, and $\ddot{\psi}$ are respectively the longitudinal acceleration, the lateral acceleration, and the yaw acceleration. $M$ is the total vehicle mass and $I_z$ is the moment of inertia of the vehicle around $z_s$ axis. $F_{x,ij}$ and $F_{y,ij}$ are respectively the longitudinal and lateral forces applied to the tire $ij$ as shown in Figure 1.5. These forces are determined (in the next sub-section) based on the tire/road contact properties and the vertical force $F_{z,ij}$ applied to the tire.

#### 1.2.1.3 Tire/Road Contact Model

In order to enhance vehicle's control, a Tire/Road contact model is needed. The interaction between the vehicle and the road is determined by the tire. It has

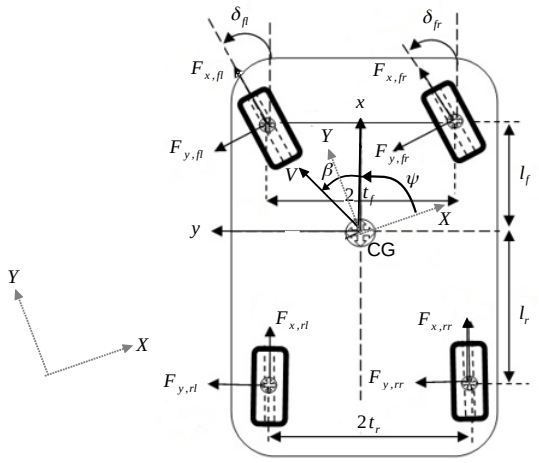


Figure 1.4 – Vehicle lateral/longitudinal model [Chokor, 2019]


Figure 1.5 – Tire forces [Chokor, 2019]

an important role in the vehicle's movement determination through the lateral and longitudinal forces generated with the road. In addition, the tire can handle the vehicle mass taking into account the vehicle vertical dynamics and road perturbations. These two aspects can be described by the tire vertical model and tire/road contact model.

In literature, there are many different tire vertical models. Some researchers present the tire as a spring and a damper with constant stiffness and damper coefficients, while others neglect the damping coefficients. Automotive industry and vehicle dynamics simulators as "*SCANeR Studio*" (OKtal) model the tire as a spring and a damper with passive variable stiffness and damping coefficients, depending on the suspension deflection and its velocity. In this thesis, the tire is supposed a punctual mass at its center of gravity and modeled as a spring and a damper with constant stiffness and damping coefficients (see Figure 1.6).

On the same time, the literature is rich in tire/road contact forces models which aim at describing the lateral and longitudinal tire forces as nonlinear functions of the vertical load, tire properties, and road properties. Here, we cite the well-known

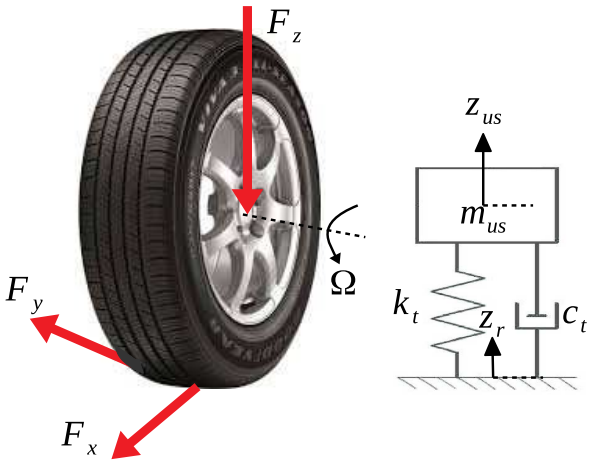


Figure 1.6 – Tire vertical model [Chokor, 2019]

models:

- analytical models which are developed from the basic theory of sliding and adherence constraints, taking into account tire parameters (material, pressure, rigidity) and the environment (temperature, road nature);
- Pacejka-Baker model known by the magic formula [Pacejka and Besselink, 1997];
- LuGrue model or Carlos Canudas-de-Wit model [Canudas-de Wit et al., 2003];
- DUGOFF model [Dugoff et al., 1970];
- Burckhardt/Kiencke model [Kiencke, 1993];

In this thesis, the DUGOFF's model is presented because of its simplicity and computational implementation. The tire longitudinal and lateral forces can be given as:

$$F_{x,ij} = C_\sigma \frac{\sigma_{x,ij}}{1-\sigma_{x,ij}} f(\lambda_{ij}), \tag{1.18}$$

$$F_{y,ij} = C_\alpha \frac{\tan(\alpha_{ij})}{1-\sigma_{x,ij}} f(\lambda_{ij}), \tag{1.19}$$

$$f(\lambda_{ij}) = \begin{cases} (2-\lambda_{ij})\lambda_{ij} & for \quad \lambda_{ij} < 1 \\ 1 & for \quad \lambda_{ij} > 1, \end{cases} \tag{1.20}$$

$$\lambda_{ij} = \frac{\mu F_{z,ij}(1-\sigma_{x,ij})}{2 \times \sqrt{(C_\sigma \sigma_{x,ij})^2 + (C_\alpha \tan(\alpha_{ij}))^2}}. \tag{1.21}$$

As these equations show, the lateral and longitudinal tire forces ($F_{y,ij}$ and $F_{x,ij}$) only depend on three parameters i.e. the longitudinal tire stiffness $C_\sigma$, the lateral tire stiffness (cornering stiffness) $C_\alpha$, and the road adherence $\mu$. From DUGOFF model, $F_{y,ij}$ and $F_{x,ij}$ are nonlinear functions of the tire variables i.e. the longitudinal tire slipping $\sigma_{x,ij}$, the side slip angle of the tire $\alpha_{ij}$, and the vertical load applied on the tire $F_{z,ij}$. $\sigma_{x,ij}$ and $\alpha_{ij}$ are calculated in the wheels dynamics model.

#### 1.2.1.4 Wheels Dynamics Model

The wheel side slip angle $\alpha_{ij}$ represents the deviated angle between the wheel speed vector and the wheel orientation as shown in Figure 1.7. $\alpha_{ij}$ of each wheel can be obtained based on the speed vector of the vehicle at its center of gravity and the vehicle geometry, as given in the following equations:

$$\alpha_{fr} = \delta_{fr} - \arctan\left(\frac{V_y + l_f\dot{\psi}}{V_x + t_f\dot{\psi}}\right), \tag{1.22}$$

$$\alpha_{fl} = \delta_{fl} - \arctan\left(\frac{V_y + l_f\dot{\psi}}{V_x - t_f\dot{\psi}}\right), \tag{1.23}$$

$$\alpha_{rr} = -\arctan\left(\frac{V_y - l_r\dot{\psi}}{(V_x + t_r\dot{\psi}}\right), \tag{1.24}$$

$$\alpha_{rl} = -\arctan\left(\frac{V_y - l_r\dot{\psi}}{V_x - t_r\dot{\psi}}\right). \tag{1.25}$$

The longitudinal tire slipping represents the difference between the actual linear

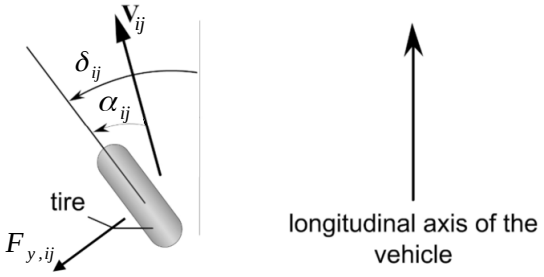


Figure 1.7 – Tire side-slip [Chokor, 2019]

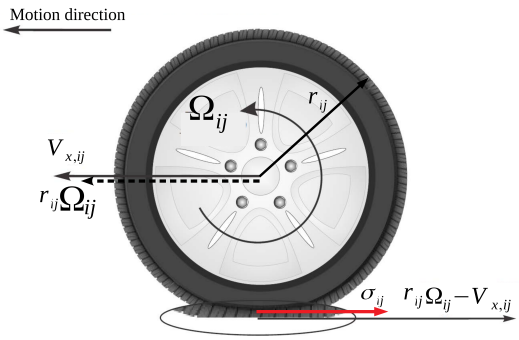


Figure 1.8 – Actual vs expected wheel speed [Chokor, 2019]

wheel speed in the longitudinal direction $V_{x,ij}$ at its center of gravity and the expected one $r_{ij}\Omega_{ij}$ due to its rotation (see Figure 1.8). The longitudinal tire slipping

of the tire $ij$ is given by the following equation:

$$\sigma_{x,ij} = \begin{cases} \frac{r_{ij}\Omega_{ij} - V_{x,ij}}{r\Omega_{ij}} & acceleration \\ \frac{r_{ij}\Omega_{ij} - V_{x,ij}}{V_{x,ij}} & braking \end{cases} \tag{1.26}$$

where $r_{ij}$ is the effective tire radius and $\Omega_{ij}$ is its angular velocity. $\Omega_{ij}$ has the dynamics given in the following equation:

$$I_r\dot{\Omega}_{ij} = -r_{ij}F_{x,ij} + C_{m,ij} - C_{f,ij}, \tag{1.27}$$

where $I_r$ is the moment of inertia around the wheel axis of rotation. $C_{m,ij}$ and $C_{f,ij}$ are respectively the motor and braking torques applied to the wheel as shown in Figure 1.9. $C_{m,ij}$ is transmitted from the motor to the wheels through the power transmission system, and $C_{f,ij}$ is generated by the braking system.

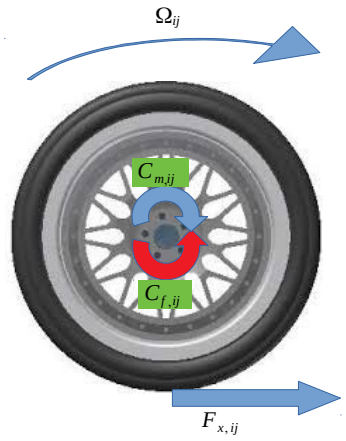


Figure 1.9 – Wheel dynamics [Chokor, 2019]

## 1.2.2 Bicycle Model

The vehicle bicycle model is a simplified version of the full vehicle model. It is usually used as a reference model to represent the lateral vehicle's behavior. As shown in the Figure 1.10, the bicycle model consists of merging each two wheels of the same axle at the center of the axle. The bicycle model expresses the lateral acceleration and the yaw rate of the vehicle at its center of gravity as the following [Rajamani, 2011],[Ackermann et al., 1995]:

$$\begin{aligned} \ddot{y} &= -\tfrac{\mu(C_f+C_r)}{mV_x}\dot{y} - (\tfrac{\mu(l_fC_f-l_rC_r)}{mV_x} + V_x)\dot{\psi} \\ &\quad + \tfrac{C_f\mu}{m}\delta_f, \\ \ddot{\psi} &= -\tfrac{\mu(l_fC_f-l_rC_r)}{I_zV_x}\dot{y} - (\tfrac{\mu(l_f^2C_f+l_r^2C_r)}{I_zV_x})\dot{\psi} \\ &\quad + \tfrac{l_fC_f\mu}{I_z}\delta_f, \end{aligned} \tag{1.28}$$

where $y$ and $\psi$ are respectively the lateral position and the yaw angle of the vehicle; $V_x$ is the vehicle longitudinal speed at the center of gravity $CG$; $\delta_f$ is the steering

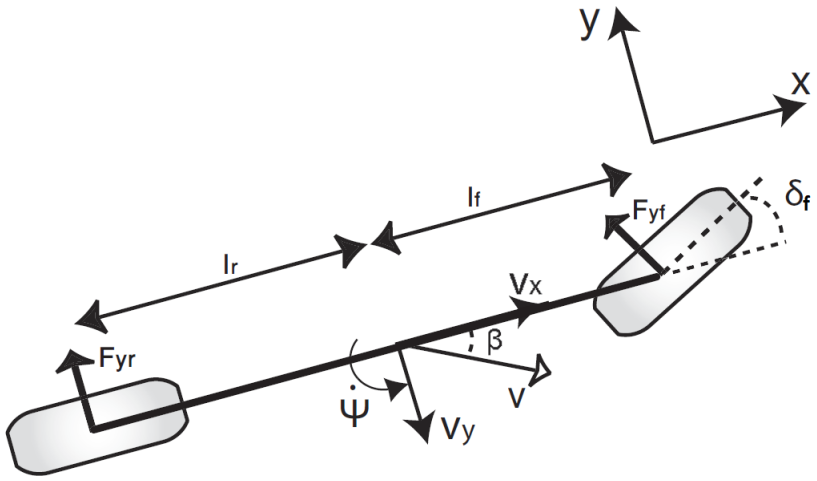


Figure 1.10 – Bicycle model [Chokor, 2019]

wheel angle. The remaining notations of these equations are given in Tables 1 3. This model is widely used considering a satisfied behavior of the vehicle in normal driving situations. Note that this bicycle model does not consider any of the vehicle roll and pitch motion, and is valid only for small angles of $\delta_f$ and $\beta$. Moreover, this model considers linear tire forces. It is usually used for model-based control synthesis.

## 1.3 Human Driver

The human driver is presented in-the-loop through:

- A steering wheel "*Logitech G29*", given as in Figure 1.11, connected to the simulator "*SCANeR Studio*" (Human-in-the-loop).
- A driver model, given as in Figure 1.16.

### 1.3.1 The Steering Wheel "*Logitech G29*"

A real human driver acts on the vehicle's lateral control through a steering wheel. The "*Logitech G29*" (Figure 1.11) is the steering wheel that permits the interaction between a real driver and the vehicle's simulator ("*SCANeR Studio*" for example). The wheel can rotate up to 900°, corresponding to 60° on the wheels. It has three pedals and a dual motor force feedback with a overheat safe guard. All these features make the driving more realistic for the users.

### 1.3.2 Driver Model

A state of art on the driver model is done. Then, the proposed driver model is developed to represent the driver's behavior in the loop. Validation of the developed model is done in Matlab/Simulink.

Figure 1.11 – The steering wheel hardware, Logitech *G*29.

#### 1.3.2.1 State of Art on Driver Model

The way to compensate the errors and failures of automated systems is to keep the driver in the loop. The shared control between human and autonomous system has many advantages:

- interaction between the driver and the automated system.
- supervision of the driving situation by the driver when he intervenes if necessary.
- enhancement of the overall performance of the driving tasks.
- reducing the workload of human driver.
- cooperation of two agents to realize a shared goal and understand the driver's behaviors and intentions by the automated systems.

The driver model is important in the autonomous driving system. It expresses the description, evaluation, understanding and prediction of the driver. This model allows the prediction of driver's intention in order to enhance the cooperation tasks between the two systems. In addition, the driver's model detects the inappropriate driving behaviors, and it can precise the action of the driver on the vehicle: steering, accelerate/decelerate. Tasks needed by the diver are the situation awareness and workload [Zou et al., 2018]. Many driver's models have been presented in the literature that module the driver in the loop. In [Salvucci and Gray, 2004], a steering model is developed based on the definition of the near and far point. The aim of the near point is to maintain a lane centerline while the far point is to anticipate the upcoming roadway. This model is based on the perceptual features of the near and far points using the visual features. The near point is fixed on the center of the road at a distance in front of the vehicle. The far point is situated at a distance of the vehicle and it depends on the nature of the road. Then a PI controller feeds

the steering angle to handle the curve negotiation, corrective steering after a lateral drift, lane changing, and individual differences. For the validation of this model, the data in [Land and Horwood, 1995] is used in order to test the proposed model for the fourth cases study. The authors in [Ungoren and Peng, 2005] have developed an adaptive lateral human driver model to predict the driver's behavior. An adaptive predictive control ($APC$) is used to develop this model which aims to minimize a cost function depending on the lateral position and yaw errors. This model has a similar cost function as McAdam's driver model [MacAdam, 1980] with different assumptions related to the cost function that makes the proposed driver model a generalized version of McAdam's driver model. In [Edelmann et al., 2007], a driver model for higher lateral accelerations is developed based on analytical method. The driver's steering angle depends on the demanded trajectory, where the driver's action is composed of two-layers: leading and compensation action. For the leading control, an anticipatory feedforward control is derived to cover the previewed curvature and its changes. The second layer is predictive closed-loop control to compensate the shifting of the vehicle from the desired trajectory. An estimation module is needed in this layer to calculate the deviation error between the previous and estimated positions. In addition, the use of assistance system for the vehicle to realize a driving task needs to modulate the driver's behavior. According to [Rajamani, 2011] the steering assistance control systems are divided into two categories: lane keeping and lane departure warning, where a driver model is developed to take into account the driver's cognitive and intention about the driver situation. All models presented in the literature have the same idea presented in the Figure 1.12:

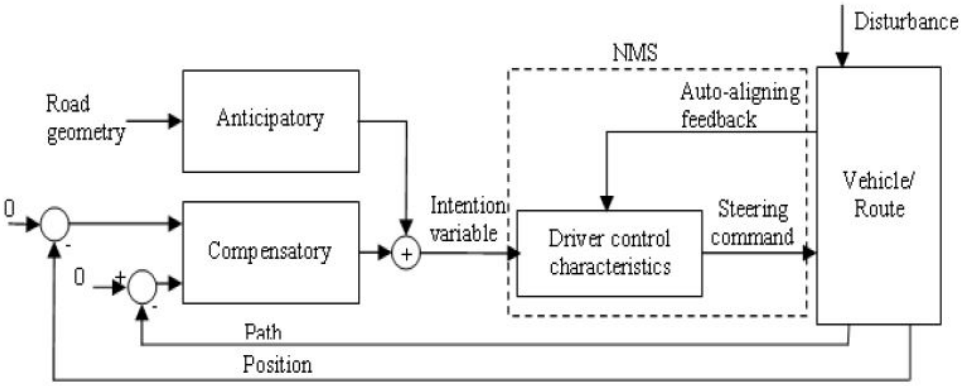


Figure 1.12 – General structure of driver steering model [Saleh et al., 2011].

However, these models differ in the way of how to define mathematically the sub-models of driver's action presented in 1.12. A driver's model is presented in [Saleh et al., 2011] for the steering assistance system purpose (Lane keeping). This model is characterized by its simplicity in the framework of automation for shared lateral control. The architecture of the model is given in the Figure 1.13. According to the Figure 1.13, the driver uses the visual information to anticipate with the upcoming road changing, and the state's information (velocity, position, heading, etc.) about

the positioning of the vehicle on the road. Then, the desired steering angle feeds the Neuromuscular system (NMS) that gives the steering torque. The concept of the $\theta_{near}$ and $\theta_{far}$ illustrated in the Figure 1.14 is used to maintain a centerline position of the vehicle and to compensate the lateral positioning errors through $\theta_{near}$, where $\theta_{far}$ takes into account the changing of the upcoming road curvature.

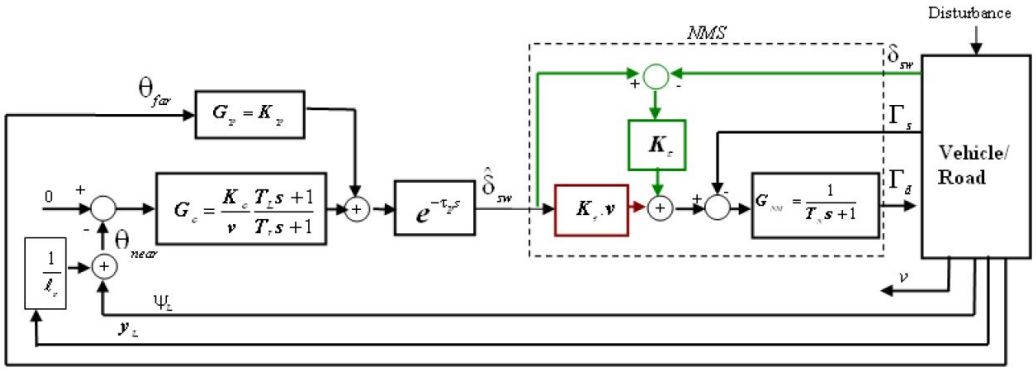


Figure 1.13 – Proposed cybernetic driver model for lane keeping maneuver [Saleh et al., 2011].

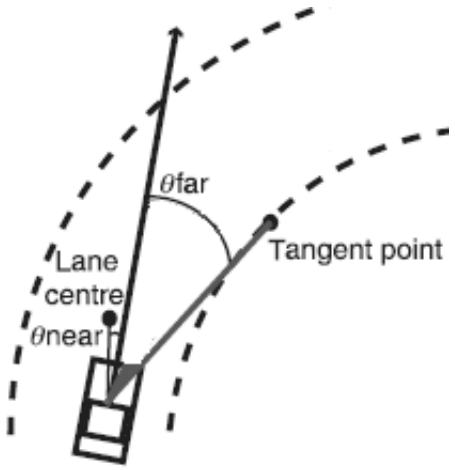


Figure 1.14 – $\theta_{near}$ and $\theta_{far}$ angles [Mars et al., 2011].

The near angle represents the vehicle's position with respect to the road, and the far angle is the difference between the vehicle's heading and the tangent point. The time delay of the driver's reaction is figured $\tau_p$. A neuromuscular module system ($NMS$) inspired from [Hoult and Cole, 2008] is incorporated in this model to represent the internal steering system compliance muscle co-activation by $\alpha$ and $\gamma$ signals and the stretch reflex. Finally, the transfer function $G_{NM}$ reflects the dynamics of the neuromuscular system including the passive damping and stiffness of neuromuscular driver's arm. Then, a Prediction Error Method ($PEM$) is used to identify the different parameters of the model. To conclude, this model will be used to illustrate the driver's behaviors in the simulation based on the visual and

haptic aspect of the driver. This model is simple to use for the intelligent steering assistance system and can be adapted to capture various characteristics of the driver (driver's state, attention, etc.). In [Sentouh et al., 2009], the authors have developed a new driver model that generates the driver's steering torque applied to the vehicle by taking into account the interaction between the driver and the vehicle. The new structure of this model is given in the Figure 1.15. The different parameters and gains of model are determined using the Prediction Error Method ($PEM$). The visual and the kinesthetic perception are taken into account by the integration of anticipatory and compensatory process in this model.

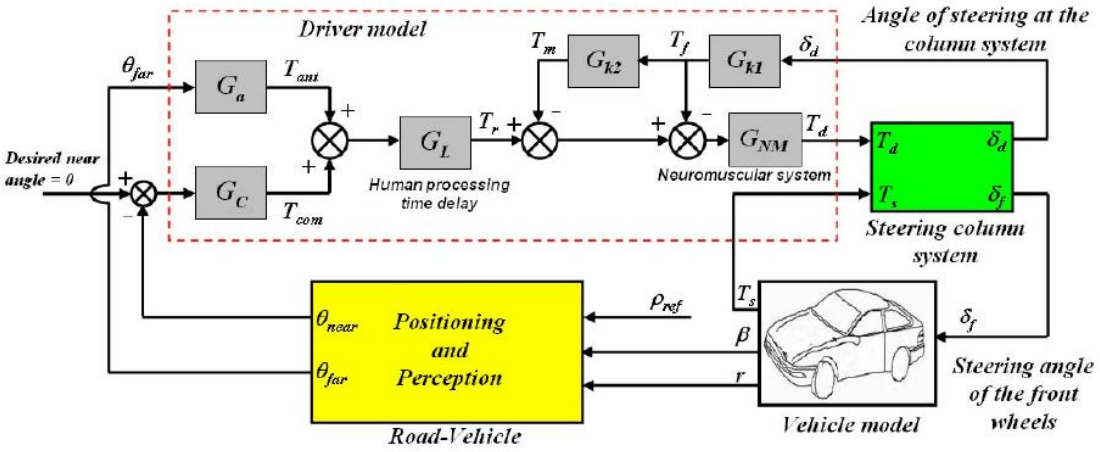


Figure 1.15 – The new structure of the driver model [Sentouh et al., 2009].

### 1.3.2.2 Driver Model-1 Reformulation [Saleh et al., 2011]

The proposed human driver model for the lane keeping purpose in [Saleh et al., 2011], [Mars et al., 2011] is used to represent the human's behavior in the loop. This model is based on the hypothesis that the driver uses the visual information to anticipate with the upcoming road changing, and the vehicle state's information (velocity, position, heading, etc.) to position the vehicle on the road (Anticipatory and Compensatory action). The structure of the adopted driver model, used in this work, is given in Figure 1.16. The calculation of angles' block that gives $\theta_{near}$ and $\theta_{far}$ angles is based on the definition in [Mars et al., 2011]. $\theta_{near}$ is calculated at a distance $l_p$ in front of the vehicle to maintain the vehicle's lateral position. It is function of the vehicle's heading error $e_\psi$ ($e_\psi$= $\psi$-$\psi^*$) and the lateral error $e_y$ ($e_y$= $y$-$y^*$), where $\psi^*$ and $y^*$ are the desired heading angle and the lateral coordinate of the road respectively. The errors $e_\psi$ and $e_y$ are calculated by a Map Matching block (see Figure 2.1) that aims to localize the vehicle on the reference map extracted from a "*SCANeR Studio*" scenario. $\theta_{far}$ is calculated as a tangent point (Figure 1.14) at a far distance $D_{far}$ that depends on the curvature of the road. The far distance becomes constant when the driver drives on a curve road (usually between 10 and 20m according to the radius of the road curvature). It depends on the vehicle's

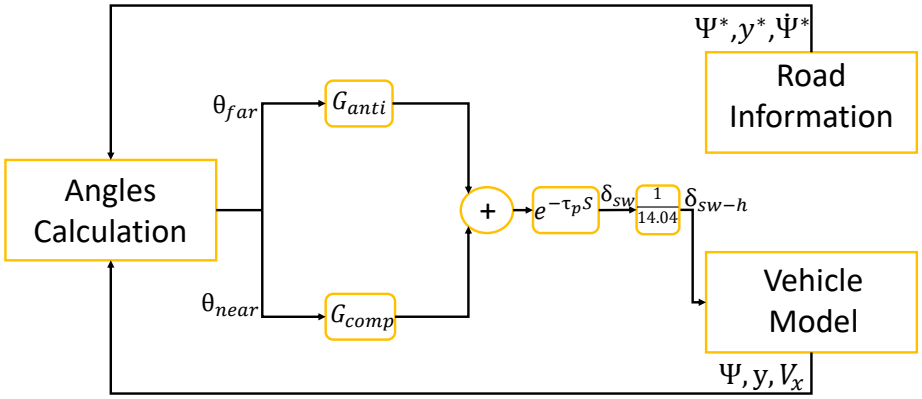


Figure 1.16 – Structure of the driver steering model.

velocity $V_x$ and the heading velocity of the road $\dot{\psi}^*$. $\theta_{near}$ and $\theta_{far}$ (see Figure 1.14) are given as:

$$\theta_{near} = \frac{e_y}{l_p} - e_\psi, \tag{1.29}$$

$$\theta_{far} = \frac{D_{far}}{V_x} * \dot{\psi}^*. \tag{1.30}$$

$D_{far}$ is function of $V_x$, given as:

$$D_{far} = \begin{cases} D_{far,min} & for \quad V_x < 20 \\ a * V_x + b & for \quad 20 < V_x < 50, \\ D_{far,max} & for \quad V_x > 50 \end{cases} \tag{1.31}$$

$$\tag{1.32}$$

where $a$ and $b$ are two constants calculated depending on $V_x$, and on the minimum and the maximum value of $D_{far}$. The driver reaction is composed of two parts: A compensatory part $G_{comp}$ that depends on $\theta_{near}$ to maintain a centerline position of the vehicle, and anticipatory part $G_{anti}$ which acts upon $\theta_{far}$ to consider the upcoming road curvature. $G_{anti}$ and $G_{comp}$ are given as:

$$G_{anti} = k_p, \tag{1.33}$$

$$G_{comp} = \frac{k_c}{V_x} \frac{T_L s + 1}{T_I s + 1}, \tag{1.34}$$

where $k_p$ is a positive constant parameter and $k_c$ represents the driver's cautiousness when he drives close to the lanes markers. $T_L$ and $T_I$ define the compensation frequency band and the compensation rate respectively. $s$ is the Laplace transformation variable. Finally, the visual processing delay module is represented by $e^{-\tau_p s}$. An approximation of the visual processing delay is given as:

$$e^{-\tau_p s} = \frac{1 - 0.5\tau_p s}{1 + 0.5\tau_p s}, \tag{1.35}$$

where $\tau_p$ represents the time delay. Thus, the output of the adopted driver model is the steering wheel angle $\delta_{sw}$. Noting that the relation between the steering wheel

angle $\delta_{sw}$ and the real angle of rotation of the front wheels $\delta_{sw-h}$ (for Zoe vehicle) is given as a proportional function:

$$\delta_{sw-h} = \frac{\delta_{sw}}{14.04} \tag{1.36}$$

The values of the different parameters are given in Table 1.1 [Saleh et al., 2011].

Table 1.1 – Driver Model-1 Parameters

| Parameters | Values |
|---|---|
| $l_p; D_{far,min}; D_{far,max}$ | $2; 15; 20$ |
| $k_c; k_p$ | $20; 2.5$ |
| $T_L : T_I$ | $2; 0.5$ |
| $\tau_p$ | $0.04$ |

#### 1.3.2.3 Driver Model-2 Reformulation

Another driver model given in Figure 1.17 is developed in this section by adding an integral term for $\delta_2$ component. This model is similar to the proposed driver model-1 given in 1.3.2.2. It is based on the same hypothesis, that the driver uses the visual system for the positioning of the vehicle on the road. $\theta_{near}$ and $\theta_{far}$ angles are calculated in the same way presented in 1.3.2.2. The total steering angle $\delta_{sw}$ is given as:

$$\delta_{sw} = (\delta_1 + \delta_2) * e^{-\tau_p s}, \tag{1.37}$$

where the visual processing delay $e^{-\tau_p s}$ is similar to the one presented in (1.35). A simple constant gain $b_1$ is used to generate the $\delta_1$ component of $\delta_{sw}$. $\delta_1$ is given as:

$$\delta_1 = b_1 * \theta_{far}, \tag{1.38}$$

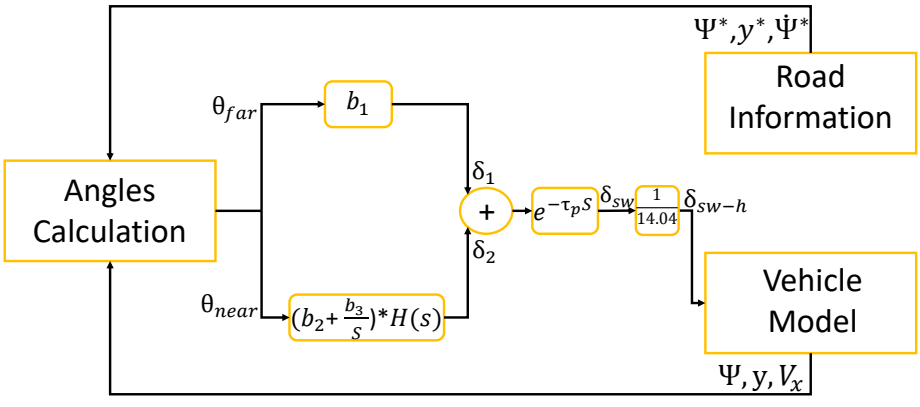


Figure 1.17 – Structure of the second driver model.

A Proportional-integral controller with $\theta_{near}$ as input, is used to generate the $\delta_2$ component. $\delta_2$ is given as:

$$\delta_2 = ((b_2 + \frac{b_3}{s}) * H(s)) * \theta_{near}, \tag{1.39}$$

where $b_2$ and $b_3$ are the proportional and integral gains respectively. And finally, $H(s)$ is a transfer function related to the compensation part of the driver model, given by:

$$H(s) = \frac{T_h s + 1}{T_n s + 1}, \tag{1.40}$$

where $T_h$ and $T_n$ define the compensation frequency band and the compensation rate respectively. For the following of this thesis, the proposed driver model-1 given in 1.3.2.2 is validated on Matlab/Simulink and "*SCANeR Studio*" simulator. This model will be used to represent the human driver in-the-loop.

#### 1.3.2.4 Validation of the Driver Model-1 on Matlab/Simulink

The proposed driver model-1 given in 1.3.2.2 is validated on Matlab/Simulink. The test track represented in the Figure 1.18 is used in the validation simulation. The driver is asked to take in charge the vehicle's lateral control, while the longitudinal control of the vehicle is provided by a super-twisting sliding mode ($STSM$) algorithm detailed in 1.4.2. As shown in the Figure 1.18, the driver is able to drive the vehicle in order to follow the desired trajectory.

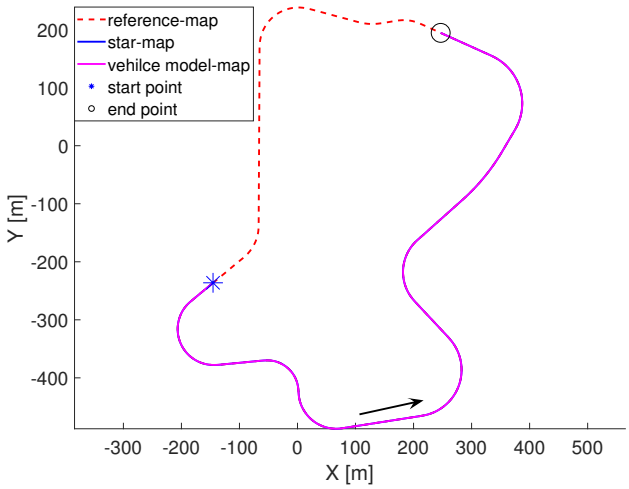


Figure 1.18 – The trajectory on the map

The lateral error is given in the Figure 1.19. It shows that the lateral error is bounded between $10cm$ as minimum and $30cm$ as maximum. This lateral error is small for a manual driving when the driver aims to keep the vehicle on the center line and to anticipate with the changing of the road curvature. Figure 1.20 and Figure 1.21 show the driving/braking torque generated by the $STSM$ controller and the driver steering wheel angle given by the driver model, as control inputs applied to the vehicle. The longitudinal speed in the Figure 1.22 converges to the desired one through the $STSM$ controller with a good tracking performance. Figure 1.22 shows also the road curvature of the desired track and the longitudinal and lateral accelerations. The driving is comfortable, because the lateral acceleration does

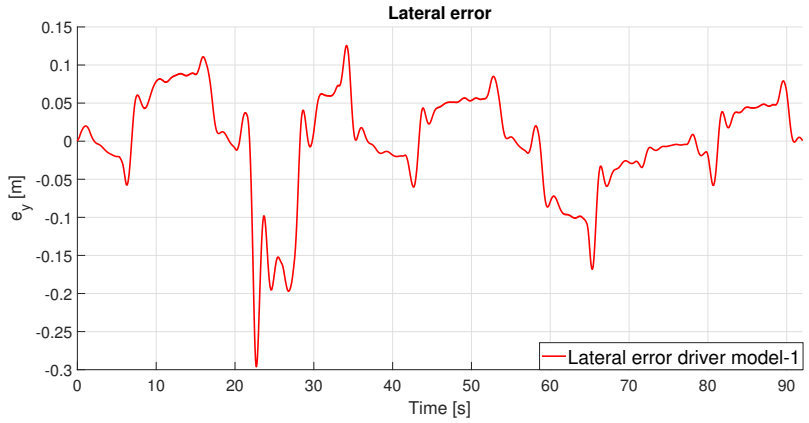


Figure 1.19 – Driver model lateral error

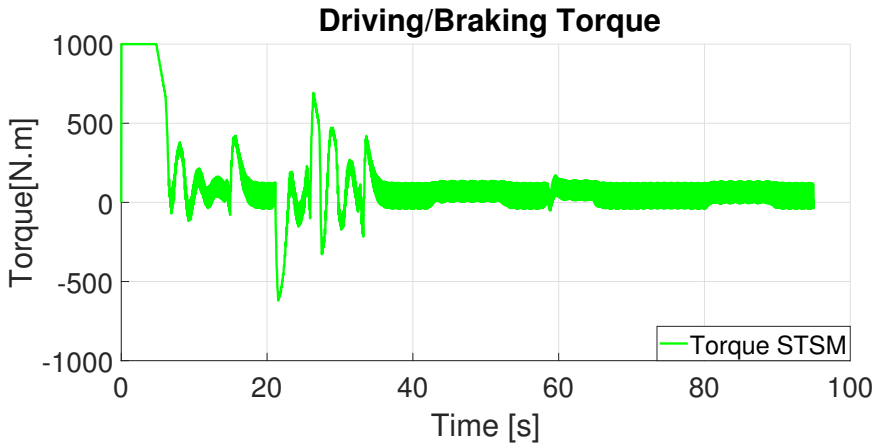


Figure 1.20 – The driving/braking torque

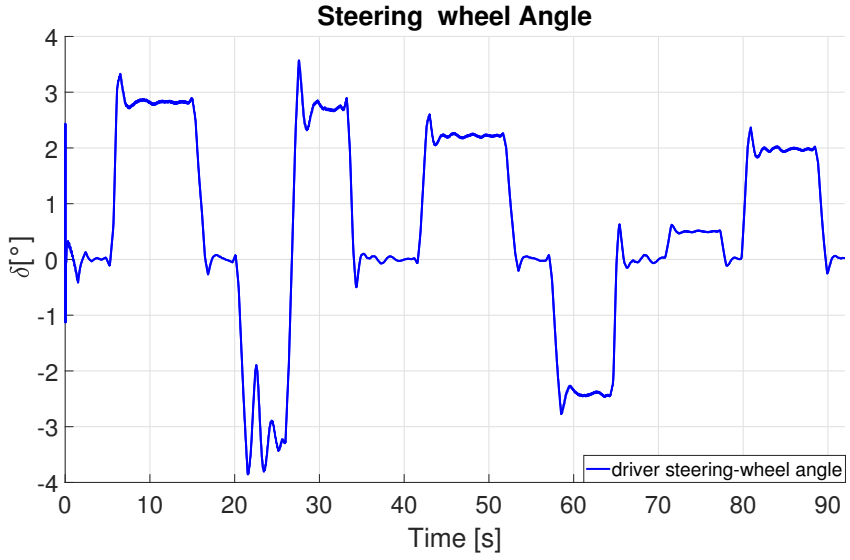


Figure 1.21 – The driver steering wheel angle

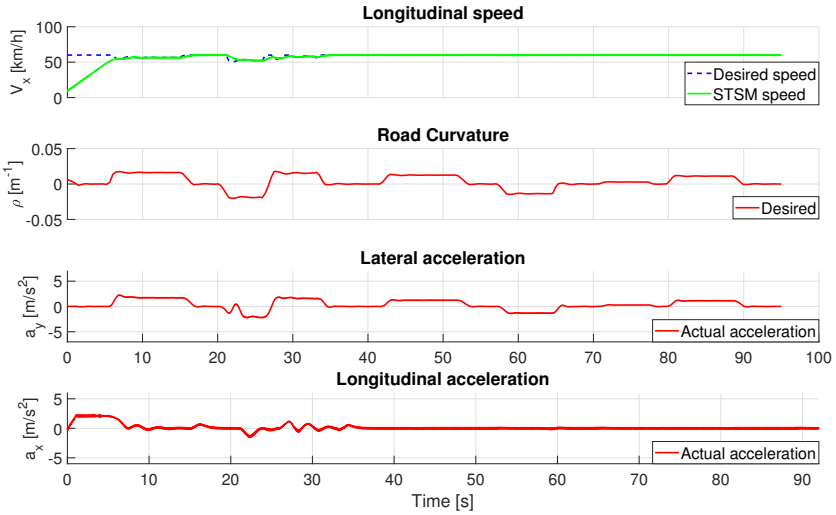


Figure 1.22 – Vehicle dynamic variables

not exceed $\pm 3m/s^2$. In addition, the longitudinal acceleration is limited between $\pm 3m/s^2$, which confirm the passenger's comfort.
To conclude, the driver model-1 is simple to apply. It is valid for the prediction of the driver's behaviors and intentions. It will be used in the framework of the shared lateral control to represent the human driver in-the-loop, cooperating with an autonomous system.

## 1.4 Autonomous System Control

Several control techniques are presented in the literature to deal with the longitudinal and the lateral control of the vehicle. Some techniques are developed independently to control the longitudinal and lateral vehicle dynamics. Others are designed based on the coupled control notion. The longitudinal control aims to provide the desired velocity profile. An example of the longitudinal controller is the active cruise control ($ACC$). The lateral control is used to realize a lane keeping and lane changing maneuvers, by acting on the steering wheel system.

### 1.4.1 State of Art on the Longitudinal and Lateral Controllers for Autonomous System

The vehicle is a non-linear system subjected to disturbances and uncertainties (variation of road, effect of wind, etc). This non-linearity creates a new challenge in the vehicle's control field, in order to develop robust and optimal controllers taking into account these uncertainties and perturbations. To design these controllers, a vehicle model is represented to express the vehicle dynamics. The dynamic bicycle model is the most commonly used model in the literature [Li and Wang, 2007]. It is formed with simple equations representing the behavior of the vehicle. Other

models are developed by linearizing the vehicle model to reduce its complexity. Some examples of linear models are: the Linear time Invariant ($LTI$) model, the Linear Parameter Varying ($LPV$) model and the Linear Time Varying($LTV$) model [White et al., 2013].
For the lateral control, there are many control techniques to guide the vehicle on a desired trajectory. A Proportional ($P$), Integral ($I$) and Derivative ($D$) controllers or a combination between the three controllers are widely used in the literature [Marino et al., 2011]. A path tracking system is presented in [Zhao et al., 2012] using the adaptive $PID$ controller. In [Rajamani, 2011], a state feedback has been developed to steer the vehicle keeping a lane. An optimal model predictive control has been designed in [Falcone et al., 2008] to select the control inputs by optimizing a cost function related to the lateral and heading errors. Authors in [Lin et al., 2021] have proposed a model predictive controller to track the desired trajectory regarding the roll stability using a Fuzzy $PID$ controller. A combined model predictive with a $PID$ feedback controllers are developed in [Chu et al., 2022] to track a planned trajectory. In [Hingwe and Tomizuka, 1997], a robust controller based on the sliding mode approach is developed to deal with the lateral vehicle control, etc.
Considering the longitudinal control, several control laws have been developed in the literature, to deal with the speed tracking control objective. The most widely used is the $PID$ controllers [Hima et al., 2011]. Another example is a second order sliding mode controller given in [Ferrara and Vecchio, 2009].
Finally, there are many approaches that treat the longitudinal and the lateral control as coupled control problem. In [Lim, 1998], a coupled longitudinal and lateral control based on the sliding mode technique is presented. Another approach based on the backstepping technique is developed in [Nehaoua and Nouvelière, 2012].
In the following, we will present the designing of the longitudinal and lateral controllers for autonomous system based on the super-twisting sliding mode ($STSM$) control technique.

### 1.4.2 Design of Longitudinal and Lateral Controllers for Autonomous System

The autonomous system consists of longitudinal and lateral controllers based on the super-twisting sliding mode ($STSM$) algorithm [Shtessel et al., 2014], to realize a trajectory following at the desired velocity. The main idea of the $STSM$ is to define a sliding surface, representing the desired behavior of the system, where the dynamic states are forced to reach this surface during a finite time and remain on it. Consider the second order system given as:

$$\dot{X} = f(X,t) + g(X,t)u(t) \tag{1.41}$$

where $X = [x, \dot{x}]^T \in \Re^2$ is the state vector, $u$ is the control input, and $f$, $g$ are continuous non-linear functions. $X^*$ is the desired state of $X$ with $X^* = [x^*, \dot{x}^*]^T \in \Re^2$. The error vector is given by $E = X - X^* = [e, \dot{e}]^T \in \Re^2$ where $e = x - x^*$ and $\dot{e} = \dot{x} - \dot{x}^*$. Therefore, a sliding variable $s$ with relative degree $r = 1$ w.r.t the control input, is defined as:

$$s = \dot{e} + \lambda\, e. \tag{1.42}$$

The second order derivative of $s$ can be written in the form:

$$\ddot{s}(s,t) = \Phi(s,t) + \xi(s,t)\dot{u}(t) \tag{1.43}$$

where $\Phi(s,t)$ and $\xi(s,t)$ are unknown bounded functions.
The goal of the Super-Twisting algorithm is to enforce the sliding variable $s$ to converge to zero ($s = 0$) in finite time. Assume that there exist positive constants $S_0$, $b_{min}$, $b_{max}$, $C_0$, $U_{max}$ verifying for all $X \in \Re^n$ and $|s(X,t)| < S_0$:

$$\begin{cases} |u(t)| \leq U_{max} \\ |\Phi(s,t)| < C_0 \\ 0 < b_{min} \leq |\xi(s,t)| \leq b_{max} \end{cases} \tag{1.44}$$

Thus, the control input based on the Super-Twisting Sliding Mode algorithm [Rivera et al., 2011], is given as:

$$u(t) = u_1 + u_2 \begin{cases} u_1 = -\alpha_1 |s|^{\tau} \text{sign}(s), & \tau \in ]0,\ 0.5] \\ \dot{u}_2 = -\alpha_2 \text{sign}(s) \end{cases} \tag{1.45}$$

$\alpha_1$ and $\alpha_2$ are positive gains. The following conditions guarantee the finite time convergence:

$$\begin{cases} \alpha_1 \geq \sqrt{\frac{4C_0(b_{max}\alpha_2 + C_0)}{b_{min}^2(b_{min}\alpha_2 - C_0)}} \\ \alpha_2 > \frac{C_0}{b_{min}} \end{cases} \tag{1.46}$$

The convergence analysis is shown in [Utkin, 2013].
The controller synthesis is based on a robotic formalism model presented in [Chebly et al., 2019], [Chebly, 2017] (more details in Appendix .1), that represents the coupling between the longitudinal and lateral dynamics. Based on this model, we choose the two sliding variables for the longitudinal and lateral controllers as follows:

$$\begin{array}{ll} s_1 = e_{Vx} + \lambda_x \int e_{Vx}, & \lambda_x > 0 \\ s_2 = \dot{e_y} + \lambda_y e_y, & \lambda_y > 0 \end{array} \tag{1.47}$$

where $\lambda_x$ and $\lambda_y$ are positive constants, and, $e_{Vx}$ ($e_{Vx}$= $V_x$-$V_x^*$) and $e_y$ are the vehicle longitudinal speed error and the lateral error respectively. The sliding variables $s_1$ and $s_2$ have a relative degree equal to one w.r.t the inputs respectively, the driving/braking torque $\Gamma_c$ for the longitudinal dynamics and the steering angle $\delta_{sw-as}$ for the lateral dynamics. Thus, in order to converge these variables to zero and the controlled states follow the desired ones, and based on the above discussion, the torque and the steering angle control applied to the vehicle, are given by:

$$\begin{array}{l} \Gamma_c = -\alpha_{\Gamma_c,1} |s_1|^{\tau_{\Gamma_c}} sign(s_1) - \alpha_{\Gamma_c,2} \int_0^t sign(s_1) d\tau, \\ \delta_{sw-as} = u_1 + u_2 + \delta^* \quad \begin{cases} u_1 = -\alpha_{\delta,1} |s_2|^{\tau_\delta} sign(s_2), \\ u_2 = -\alpha_{\delta,2} \int_0^t sign(s_2) d\tau, \\ \delta^* \text{ is the equivalent control input,} \end{cases} \end{array} \tag{1.48}$$

where $\alpha_{\delta,i}$ and $\alpha_{\Gamma_c,i}$ with $i = [1, 2]$, are positive constants satisfying the conditions in (1.46). $\tau_{\Gamma_c}$ and $\tau_\delta$ are constants in $]0, 0.5]$. The function $sign$ is smoothed by the approximation $sign(s_1) = \frac{s}{|s|+\varepsilon_x}$ and $sign(s_2) = \frac{s}{|s|+\varepsilon_y}$, where $\varepsilon_x$ and $\varepsilon_y$ are positive small values. Finally, $\delta^*$ is the equivalent control input, corresponding to the steering wheels angle at the equilibrium when $\dot{s_2} = 0$.

#### 1.4.2.1 Validation of $STSM$ controller on Matlab/Simulink

The developed longitudinal and lateral super-twisting sliding mode ($STSM$) controllers are validated on Matlab/Simulink for the test track given in the Figure 1.18. Then, a comparison is done between the $STSM$ controller and a $PID$ controller in order to show the effectiveness of the developed controller in terms of performance. Numerical values of the controller parameters used in the simulation are given in Table 1.2.

Table 1.2 – Controllers' Parameters for Simulation

| Parameters | Values |
|---|---|
| $\lambda_x; \lambda_y$ | 0.01; 8 |
| $\alpha_{\delta,1}; \tau_\delta; \alpha_{\delta,2}$ | 0.1;0.5;0.01 |
| $\alpha_{\Gamma_c,1}; \tau_{\Gamma_c}; \alpha_{\Gamma_c,2}$ | 500;0.5;5 |
| $\varepsilon_x; \varepsilon_y$ | 0.1; 1 |

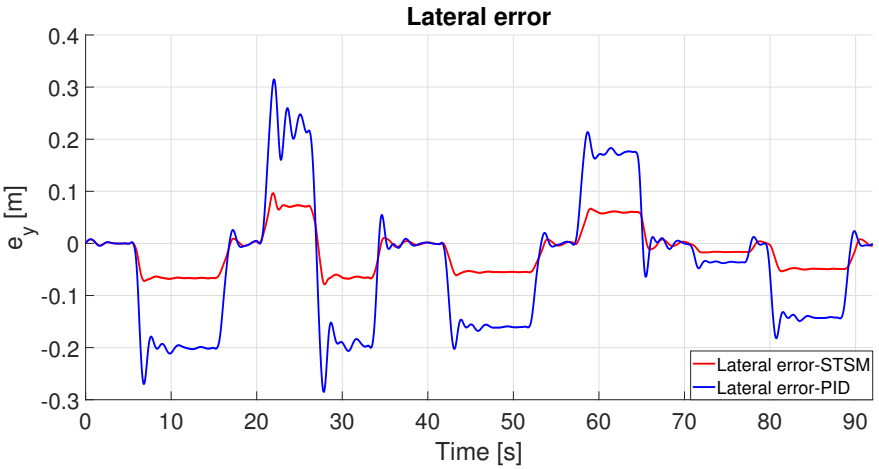


Figure 1.23 – The lateral error

The Figure 1.23 shows the $STSM$ and $PID$ lateral error. As we can see in the Figure 1.23 the lateral error is bounded between $-10cm$ and $+10cm$ for the $STSM$ controller, while $-30cm$ and $+30cm$ for the $PID$ controller. The $STSM$ controller is capable to reduce more the lateral error to zero compared to the $PID$ controller that is less performant. The different steering wheel angles are given in the Figure 1.24. For the longitudinal movement, the driving/braking torques are given in the

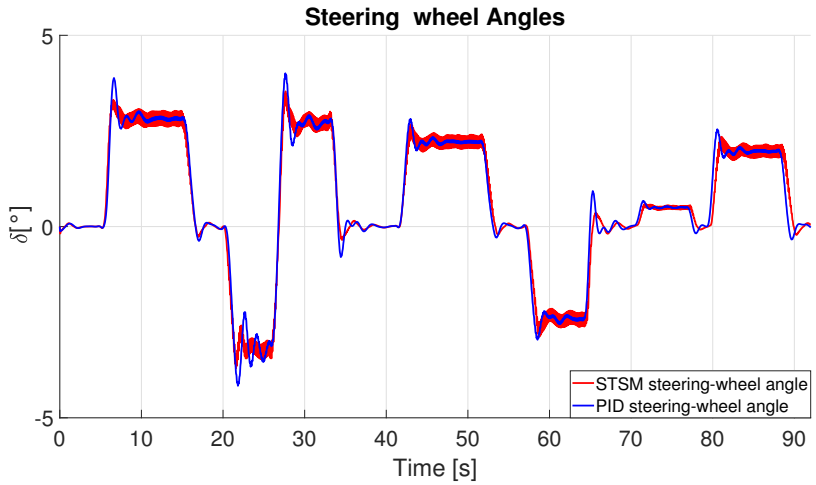


Figure 1.24 – The steering wheel angles

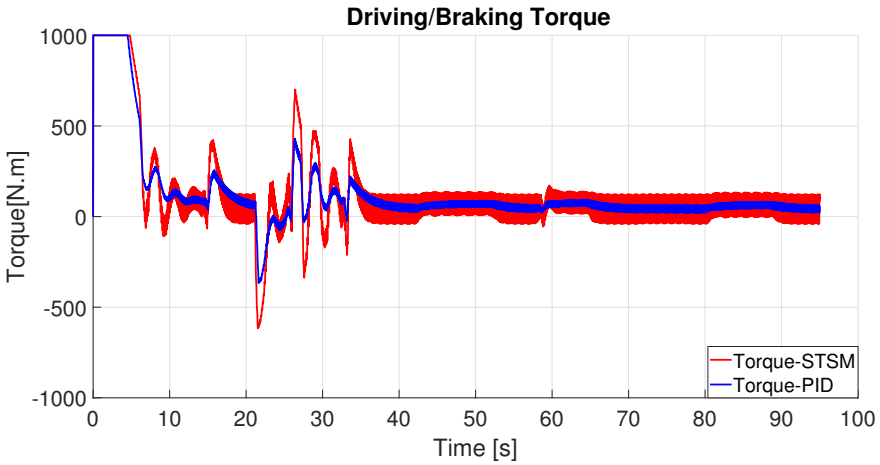


Figure 1.25 – The driving/braking torques

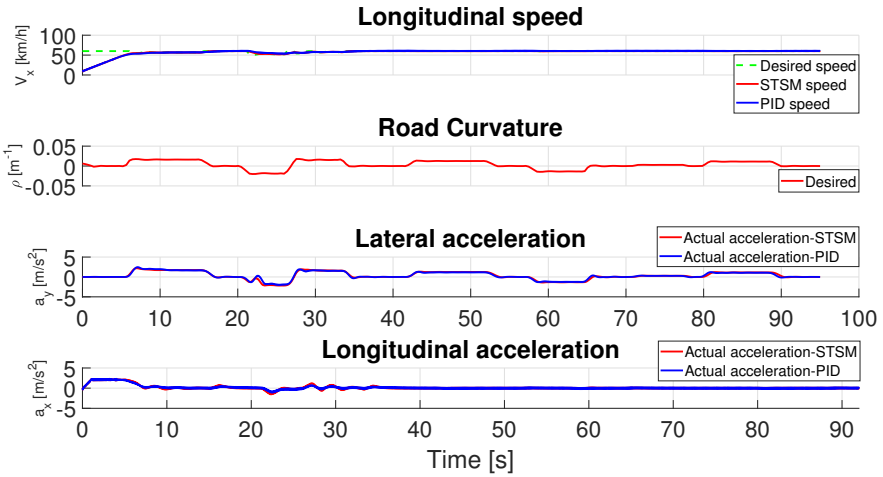


Figure 1.26 – The vehicle dynamic variables

Figure1.25. Finally, the Figure 1.26 shows the different dynamic variables such as the longitudinal speed, the road curvature and the actual lateral and longitudinal accelerations respectively. Figure 1.26 shows that the longitudinal speed tracks the reference speed and both controllers have almost the same behavior. In addition, the road curvature of the desired trajectory is given in this figure. The actual lateral and longitudinal accelerations do not exceed $\pm 2.5 m/s^2$ which correspond to a comfortable driving zone that guarantees the passenger's comfort.

## 1.5 Conclusion

In this chapter, the global architecture of the shared lateral control is presented. The different tools needed to realize a shared lateral control are detailed. The used vehicle models are presented. Then, the human driver in-the-loop is given by developing a driver model or by using a steering wheel. Finally, an autonomous controller based on the super-twisting sliding mode ($STSM$) control technique is developed. The proposed controller is validated by simulation using Matlab/Simulink, and a comparison is done with a $PID$ controller that has been developed in order to show the difference in behavior and performance of both techniques of control. In the next chapter, we will develop the first shared lateral control approach to manage the control authority between the driver and the autonomous system.

# A Fuzzy Logic Shared Steering Control Approach

This chapter provides a full description of the first proposed shared lateral control. The different driving modes are defined. The shared lateral control authority is detailed. Then, the fusion approach based on the Fuzzy Logic Controller ($FLC$) and the situation-based analysis block are developed in the following for decision-making. Finally, the proposed shared control is validated on"*SCANeR Studio*" simulator and on Matlab/Simulink with a complete nonlinear model of the vehicle validated on "*SCANeR Studio*" (OKtal) professional simulator.

## 2.1 Introduction

Driving on the road is the resulting of multi-tasks: perception of surrounding environment, trajectory planning and vehicle control. The challenge now is to realize an autonomous vehicle that imitates the human driver and acts like him to accomplish a driving maneuver: obstacle avoidance, lane keeping, overtaking, etc. By this way, the driver is eliminated from the loop. However, until now the act of replacing the human by an autonomous system is still under study, in order to cover all the possible driving situations. A full autonomous system needs more time to be accessible on the public road for many reasons: high cost, trust of user on this system, security road, etc. Thus, a shared lateral control that keeps the driver in the loop is defined to compensate the gap between the two aspects of driving: Manual and Auto driving. In addition, keeping the driver in loop to supervise the scene, monitor the vehicle's control and react if needed, is necessary to ensure road safety and compensate the limitation and problems of autonomous system. So, this chapter deals with the shared lateral control between the driver and the autonomous system for the lane keeping purpose (see Figure 2.1). The objective of this shared control is to manage the control authority between the driver and the autonomous system in order to prevent a dangerous situation and promote road safety. Adaptation of this shared control is possible to overcome another complex maneuvers. Therefore, in the present work, the autonomous system is in charge of controlling the vehicle while the driver still in the loop, monitors and analyzes the scene. The confidence on the driver is considered as full or low. An error or failure occurs on the autonomous system and the intervention of the driver is needed to take the control action. To do that, many criteria should be taken into consideration before managing the control authority .

Considering this management, many cases are identified based on the driver's status and autonomous system behavior. For example, if the driver's confidence is full, a control authority is given to him to drive the vehicle. Otherwise, an emergency mode is defined in order to stop the vehicle because the driver is not able to be the leader during the autonomous system failures. More information about all cases are given in this chapter. The different driving modes are defined as: 1) The driver model developed in Section 1.3.2.2 is used to represent the human in-the-loop; 2) The vehicle longitudinal and lateral movements are performed by using the autonomous system based on Super-Twisting Sliding Mode ($STSM$) control approach, given in Section 1.4.2. Then, the control authority is realized using the blended shared control that permits the fusion of two inputs via a fusion parameter. The novelty of this work is illustrated in the computation of the fusion parameter. A Fuzzy Logic Controller ($FLC$) associated to a situation-based Analysis Block for the decision-making process are developed to determine the fusion parameter, according to many criteria: the lateral deviation error and the confidence on each agent. Finally, the proposed shared control is validated on "*SCANeR Studio*" and on Matlab/Simulink for two defined case-studies with a complete nonlinear model of the vehicle validated on "*SCANeR Studio*" (OKtal) professional simulator.

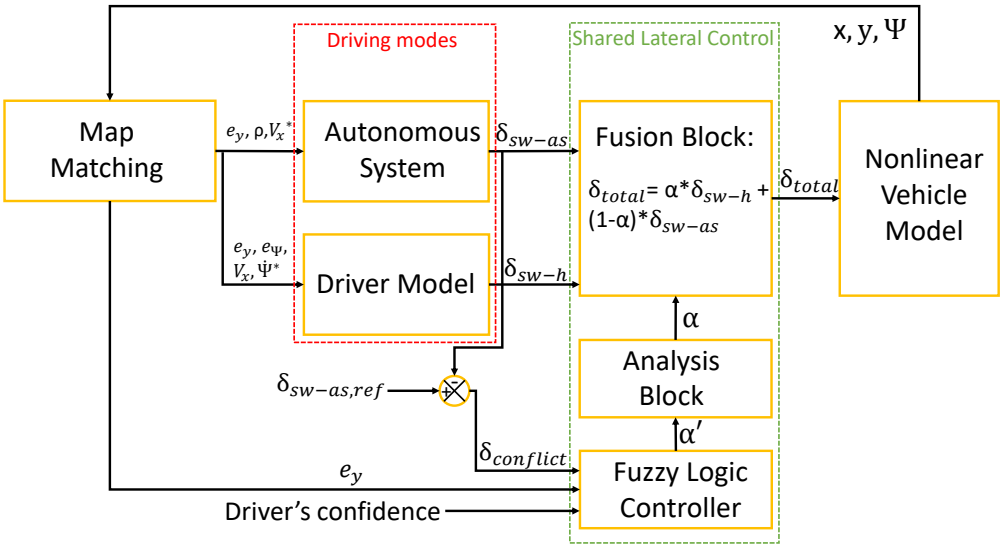


Figure 2.1 – Architecture of the shared lateral control.

## 2.2 DESIGN OF SHARED LATERAL CONTROL

### 2.2.1 Driving Modes

Figure 2.1 shows the global shared lateral control architecture. It is composed of two parts: the driving modes and the shared lateral control. The different driving modes are detailed in the following.

#### 2.2.1.1 Human Driver

The human driver is represented in-the-loop by using the driver model-1 developed in Section 1.3.2.2. His steering input will be noted as $\delta_{sw-h}$.

#### 2.2.1.2 Autonomous System

The autonomous system consists of longitudinal and lateral controllers developed based on Super-Twisting Sliding Mode ($STSM$) control approach given in Section 1.4.2. The control inputs are the driving/braking torque $\Gamma_c$ for the longitudinal dynamics and the steering wheel angle $\delta_{sw-as}$ for the lateral dynamics. Note that the longitudinal control is common for both modes: the Human Driver and the Autonomous System.

### 2.2.2 Shared lateral control

This section details the proposed shared lateral control (see Figure 2.1). The control authority between the two agents is presented. Then, the decision-making process is done through a Fuzzy Logic Controller ($FLC$) followed by a situation-based analysis block are developed to determine the fusion parameter.

#### 2.2.2.1 Shared Lateral Control Authority

The shared control authority between the driver and the autonomous system is performed by using the blended shared control [Borroni and Tanelli, 2018] which allows the fusion of two inputs from each agent. This type of shared control is used for the systems where there is no mechanical connection between both inputs such as the steer-by-wire system. The familiar form of blending shared control is the blending using weight parameters (see. [Li et al., 2020], [Li et al., 2018]). The total blending control input is given as:

$$\delta_{total} = \alpha * \delta_{sw-h} + (1 - \alpha) * \delta_{sw-as}, \tag{2.1}$$

where $\delta_{total}$, $\delta_{sw-h}$ and $\delta_{sw-as}$ are the total control input, inputs of human driver and autonomous system respectively. $\alpha$ is the fusion parameter representing the influence proportion of each agent on the total input. $\alpha$ is bounded in [0,1]. The blending shared control permits a direct interaction between human driver and autonomous system. The fusion parameter $\alpha$ is calculated based on Fuzzy Logic Controller and a situation-based analysis block (Figure 2.1) detailed later.

#### 2.2.2.2 Fuzzy Logic Controller ($FLC$)

An intermediate fusion parameter $\alpha'$ is determined by a Fuzzy Logic Controller ($FLC$) as in Figure 2.1. The situation-based analysis block analyzes the driving situation and gives the final value of fusion parameter $\alpha$ in order to promote driving safety and avoid dangerous situations. The Fuzzy Logic structure is given by the Figure 2.2. The lateral error $e_y$, the conflict of the automated steering angle $\delta_{conflict}$ and the driver's confidence are applied to the Fuzzy Logic Controller ($FLC$) as

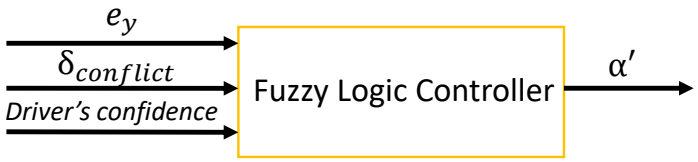


Figure 2.2 – The structure of Fuzzy Logic Controller.

inputs, and the fuzzy parameter $\alpha'$ is the output. Two scenarios are discussed and later addressed to demonstrate the effectiveness of this approach against different driving conditions. Using the $FLC$ for the decision-making process for the cooperative control, makes the determination of the intermediate fusion parameter $\alpha'$ simple, depending on the lateral error, the conflict of the automated steering angle $\delta_{conflict}$ and the driver's confidence. Note that the conflict of the automated steering angle $\delta_{conflict}$ is the difference between the steering wheel angle applied by the autonomous system ($\delta_{sw-as}$) and the reference steering angle ($\delta_{sw-as,ref}$) on the desired trajectory given as:

$$\delta_{conflict} = |\delta_{sw-as,ref} - \delta_{sw-as}|. \tag{2.2}$$

The $\delta_{conflict}$ represents the confidence on the autonomous system that could be given by a diagnosis module. On the other hand, the driver's confidence can be determined in different ways depending on: driver's eyes observation, environment conditions, trajectory prediction, etc. However, the calculation of driver's confidence is not in the scope of this thesis and it is considered as an input to the $FLC$ fusion block. Three fuzzy sets are defined for the lateral error $e_y$: $\{S(Small),\ M(Medium),\ B(Big)\}$. Two fuzzy sets are defined for the conflict automated steering angle $\delta_{conflict}$: $\{S(Small),\ B(Big))\}$. Note that $\delta_{conflict}$ and the autonomous system's confidence are directly dependent. A small $\delta_{conflict}$ corresponds to a high autonomous system's confidence and a big $\delta_{conflict}$ corresponds to a low autonomous system's confidence. Three fuzzy sets are defined for the driver's confidence: $\{S\ (Small),\ M(Medium),\ B(Big)\}$. And finally, three fuzzy sets are defined for the output parameter $\alpha'$: $\{S(Small),\ M(Medium),\ B(Big)\}$. $\alpha'$ is Small corresponds to the autonomous system driving mode, $\alpha'$ is Big corresponds to the human driver and finally $\alpha'$ is Medium corresponds to a shared driving mode (50/50). By default, the driving mode is autonomous.
The normalized Membership Functions (MFs) of fuzzification of the controller inputs and defuzzification of the controller output are respectively given in Figures 2.3, 2.4, 2.5 and 2.6. The values and the types of these fuzzy sets are chosen depending on the feedback and observation of simulation for different scenarios and a lot of experiments.

To determine the fuzzy controller output $\alpha'$ for the given fuzzy controller inputs $e_y$, $\delta_{conflict}$ and the driver's confidence, the decision matrix of the linguistic control rules is used. There are 18 rules (in total) where 15 are determined in the $FLC$ to give the value of $\alpha'$, and the 3 remaining rules are detailed in the analysis block (see Figure 2.1). So, the analysis block receives $\alpha'$ and modifies it if necessary, depending on the driving situation. The final output of the analysis block is $\alpha$. Noting that $\alpha$

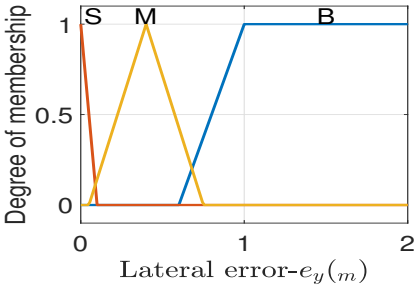


Figure 2.3 – Fuzzy sets - input 1

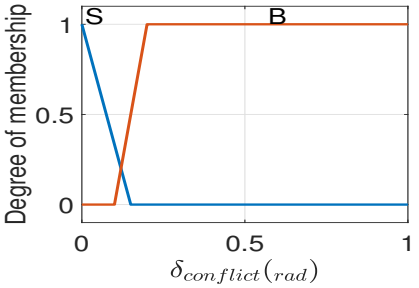


Figure 2.4 – Fuzzy sets - input 2

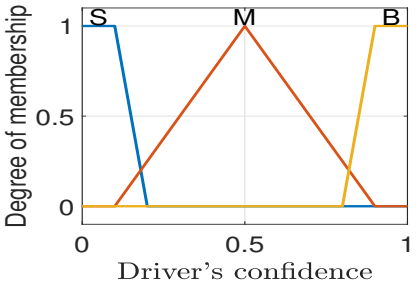


Figure 2.5 – Fuzzy sets - input 3

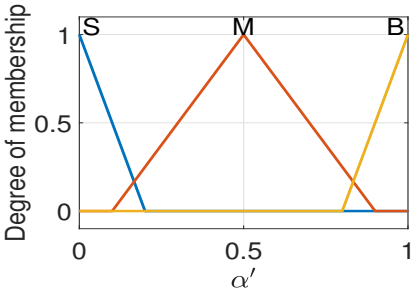


Figure 2.6 – Fuzzy sets - output

is equal to the output of $FLC$, $\alpha'$, if no check needed. The goal of using the analysis block with the $FLC$ is to cover all the possibilities of driving situations that can occur while driving on the road, and that cannot be covered by the $FLC$ alone. The rules of $FLC$ are designed and presented in the Table 2.1 and Table 2.2 for $\delta_{conflict}$ Small or Big respectively. These fuzzy sets, membership functions, and the linguistic rules are usually determined based on an expert knowledge of the system by performing several simulations for different driving conditions. Refer to Table 2.1, the rules of $FLC$ are determined as:

Table 2.1 – Rules of $FLC$ when $\delta_{conflict}$ is S

| $\alpha'$ | | $e_y$ | | |
|---|---|---|---|---|
| | | **S** | **M** | **B** |
| Driver's confidence | **S** | S | S | M |
| | **M** | S | S | M |
| | **B** | S | B | check case |

- If the lateral error is Small (S) and whatever the value of driver's confidence (Small, Medium or Big) and $\delta_{conflict}$ is Small (S), then $\alpha'$ is Small (S). So, the control is given to the autonomous system.
- If the lateral error is Medium (M) and the value of driver's confidence is Small (S) or Medium (M) and $\delta_{conflict}$ is Small (S), then $\alpha'$ is Small (S).
- If the lateral error is Medium (M) and the driver's confidence is Big (B) and $\delta_{conflict}$ is Small (S), then $\alpha'$ is Big (B). So, the control is given to the human.
- If the lateral error is Big (B) and the driver's confidence is Small (S) or Medium (M) and $\delta_{conflict}$ is Small (S), then $\alpha'$ is Medium (M). A shared-control is applied.
- If the lateral error is Big (B) and the driver's confidence is Big (B) and $\delta_{conflict}$ is Small (S), then the case will be checked in the analysis block (detailed in the following).

Table 2.2 – Rules of $FLC$ when $\delta_{conflict}$ is B

| $\alpha'$ | | $e_y$ | | |
|---|---|---|---|---|
| | | **S** | **M** | **B** |
| Driver's confidence | **S** | check case | M | check case |
| | **M** | B | B | B |
| | **B** | B | B | B |

Similar to the Table 2.1, the rules of $FLC$ in the Table 2.2 for the case of $\delta_{conflict}$ is Big (B), are given as:

- If the lateral error is Small (S) and the driver's confidence is Small (S) and $\delta_{conflict}$ is Big (B), then the case will be checked in the analysis block (detailed in the following).

- If the lateral error is Small (S) and the value of driver's confidence is Medium (M) or Big (B) and $\delta_{conflict}$ is Big (B), then $\alpha'$ is Big (B). The human takes the control.

- If the lateral error is Medium (M) and the driver's confidence is Small (S) and $\delta_{conflict}$ is Big (B), then $\alpha'$ is Medium (M).

- If the lateral error is Medium (M) and the driver's confidence is Medium (M) or Big (B) and $\delta_{conflict}$ is Big (B), then $\alpha'$ is Big (B).

- If the lateral error is Big (B) and the driver's confidence is Small (S) and $\delta_{conflict}$ is Big (B), then the case will be checked in the analysis block (detailed in the following).

- If the lateral error is Big (B) and the driver's confidence is Medium (M) or Big (B) and $\delta_{conflict}$ is Big (B), then $\alpha'$ is Big (B).

Finally, to defuzzify the result/output, the "*Mamdani centroid fuzzy inference method*" is used [Reznik, 1997].

#### 2.2.2.3 Situation-Based Analysis Block

In order to check the remaining 3 cases, an algorithm (given below) is developed in the analysis block to cover the possible driving situations that cannot be resolved appropriately by the $FLC$ approach.

**Algorithm 1** checked cases in the analysis block

**if** (lateral error is S) and (driver's confidence is S) and ($\delta_{conflict}$ is B) **then**
  retain the previous input
**else if** (lateral error is B) and (driver's confidence is B) and ($\delta_{conflict}$ is S) **then**
  $\alpha = 1$ (human driver) and brake the vehicle
**else if** (lateral error is B) and (driver's confidence is S) and ($\delta_{conflict}$ is B) **then**
  Emergency mode until driver will be attentive
**else**
  Keep the fusion parameter $\alpha'$ from $FLC$
**end if**

Based on the algorithm, three cases are defined considering all possible driving situations. For example, if the lateral error is Small (S) at the same time where there is no confidence on two agents (driver's confidence is Small (S) and $\delta_{conflict}$ is Big (B), the algorithm retain the previous input that leads to a small lateral error. In addition, for the driving situation where the lateral error is Big (B) and the agent's confidence is Big (B), it will be better to give the authority of control to the driver, decelerate and brake the vehicle. Finally, an emergency mode is defined in the case where the confidence on both agents is Small (S) and the lateral error is Big (B). The vehicle starts to decelerate in order to reduce its velocity to 0.

## 2.3 Validation of the Proposed Approach

In this section, the developed shared lateral control is validated on Matlab/Simulink with a complete nonlinear model of the vehicle, validated on "*SCANeR Studio*" (OKtal) simulator. The vehicle is asked to follow the desired trajectory given in the Figure 2.7, of a track extracted from a "*SCANeR Studio*" scenario. A control authority decision is generated by the $FLC$ and the analysis block in order to determine the fusion parameter and then the leader of the vehicle for each case. The results are presented to show the adaptation and functionality of the $FLC$ and the analysis block in each case.

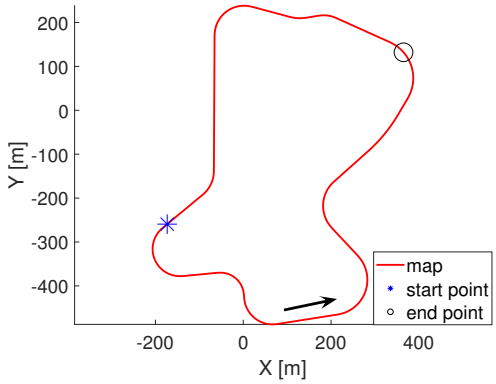


Figure 2.7 – Scaner Studio: Map of the test track

### 2.3.1 Case Study Definition

In this subsection, the case studies are detailed to test and validate the proposed shared lateral control for different driving situations. Indeed, two case studies are presented for the same scenario to show the adaptation and functionality of the proposed approach in each case:

- Case 1: This case is defined to show functionalities managed by the $FLC$. The developed controller aims to follow the desired trajectory by reducing the lateral error, at a desired velocity. It is addressed to assist the driver and help him in a shared control mode (an example of Advanced Driving Assistance System $ADAS$). A human driver (presented by the driver model-1 in the simulation) is kept in the loop to supervise the scene and interact if necessary. Sudden failures occur in the autonomous system's behavior at $9s$ and $40s$ respectively (see Figure 2.9). The vehicle deviates from the centerline of the road and the driving situation is considered dangerous. A driving mode is defined in a way to give the total authority of control to the driver at $9s$ even when the driver's confidence is Medium (0.5)(Figure 2.10). In addition, at $40s$, the driver takes the control action to compensate the second failure of the automated system and retain the driving stability. Noting that the driver is aware and attentive about the scene at $40s$ to the rest of the trajectory (full Driver's confidence=1, see Figure 2.10). The importance of this case is to illustrate the effectiveness of our method in terms of smooth switching

between the two agents and failure's detection on the autonomous system. So, the control authority is determined through the Fuzzy Logic Controller to manage the driving situation.

- Case 2: This case is defined to show the functionality of the analysis block with the $FLC$. Two functionalities of the analysis block are tested in this case: An emergency mode ($EM$) situation where the confidence on the driver is lost (Figure 2.14) and a failure occurs on the autonomous system at a defined time (Figure 2.13). The vehicle decelerates to stop. The ON/OFF conditions of emergency mode are given in the Figure 2.8. The ON/OFF conditions are defined as:

  - ◇ If the lateral error is higher than $e_{y_{min}}$ and the driver's confidence is low and $\delta_{conflict}$ is higher than $\delta_{threshold}$, then the emergency mode is activated.
  - ◇ If the lateral error is lower than $e_{y_{min}}$ and the value of driver's confidence is high, or if longitudinal speed $V_x$ is lower than $V_{x_{min}}$, and the value of driver's confidence is high, then the emergency mode is deactivated.

  Note that $e_{y_{min}}$ and $V_{x_{min}}$ are the lower limits of the lateral error and the longitudinal speed respectively, that define a no critical driving situation. $\delta_{threshold}$ is a threshold from which we consider that there is an error on the autonomous system and the conflict on the automated steering angle is big, that means the autonomous system's confidence is low. The second functionality keeps the previous input that realizes a small lateral error when there is no driver's confidence (driver's confidence=0) at the same time of autonomous system's failure (Figure 2.13). The driver's confidence varies in [0,1] (Figure 2.14).
  Results will be addressed in the next section, including the fusion parameter $\alpha$ to show the shared control authority between the two agents for each case given above.

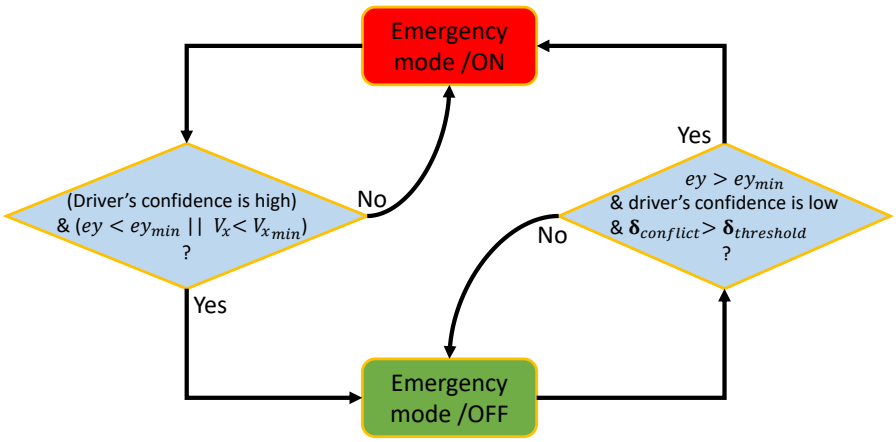


Figure 2.8 – Emergency mode ON/OFF

### 2.3.2 Simulation Results

For the case 1, errors are injected between $9s$ and $23s$ and between $40s$ and $70s$ respectively on the automated system (see Figure 2.9). Remember that the human (presented by the driver model-1) is the supervisor of the scene, who compensates the errors that occurred in the behavior of the autonomous system.
The Figure 2.9 shows the lateral error of: autonomous system with failure, manual driving mode and shared mode. As we can see, the shared mode diminishes the lateral error (1.5 m) caused by the autonomous system failure on the curvy road (see Figure 2.12), by penalizing the last one and giving the authority of control to the driver. So, the driver takes the action of control at the beginning of the failure $9s$, that is the decision of the $FLC$, until $23s$, even though his confidence is medium (Figure 2.10). The curve of the lateral error in the shared mode is the same as the manual curve between $[9s;23s]$ (Figure 2.9). Similar to the second failure, the driver acts on the vehicle at $40s$ to $70s$ in order to diminish the lateral error of the autonomous system. A smooth switching is done between the two agents that makes the system stable. The shared control is done thanks to the fusion parameter $\alpha$ (Figure 2.10) delivered by the $FLC$ and analysis block modules. As shown in the Figure 2.10, the value of $\alpha$ is equal to 0 expect the two intervals of time: $[9s;23s]$ and $[40s;70s]$. For the region where $\alpha = 0$, the autonomous system is able to control the vehicle. However, for the two intervals of time: $[9s;23s]$ and $[40s;70s]$, an unexpected error occurred on the autonomous system, illustrated by a conflict in the Figure 2.11. At this time, the driver interacts by taking the action of driving to reduce the conflict of the autonomous system, and $\alpha$ increases from 0 to 1. The $STSM$ steering angle, the driver steering angle, the shared steering angle calculated by the fusion system and $\delta_{conflict}$ are given in the Figure 2.11. And finally, Figure 2.12 shows the longitudinal speed converging to the desired one through the $STSM$ controller, the road curvature of the desired trajectory and finally, the actual lateral acceleration in the shared mode that shows a stable and comfortable driving.

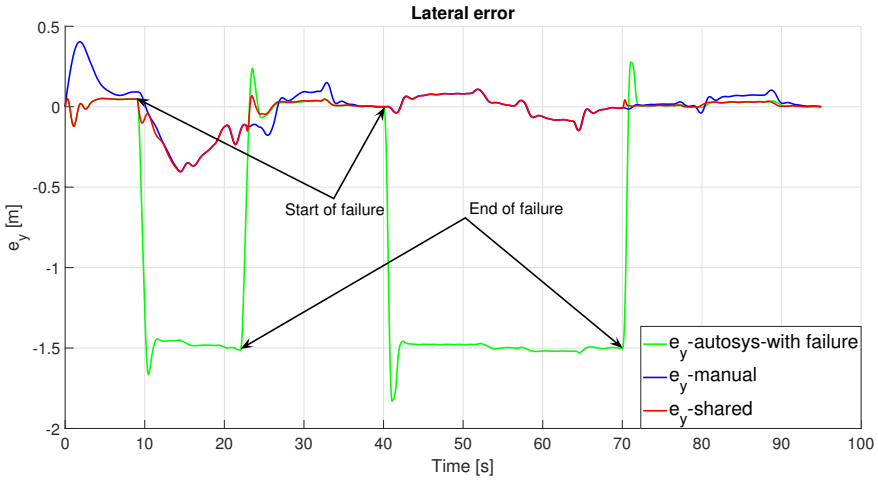


Figure 2.9 – The lateral error - case 1

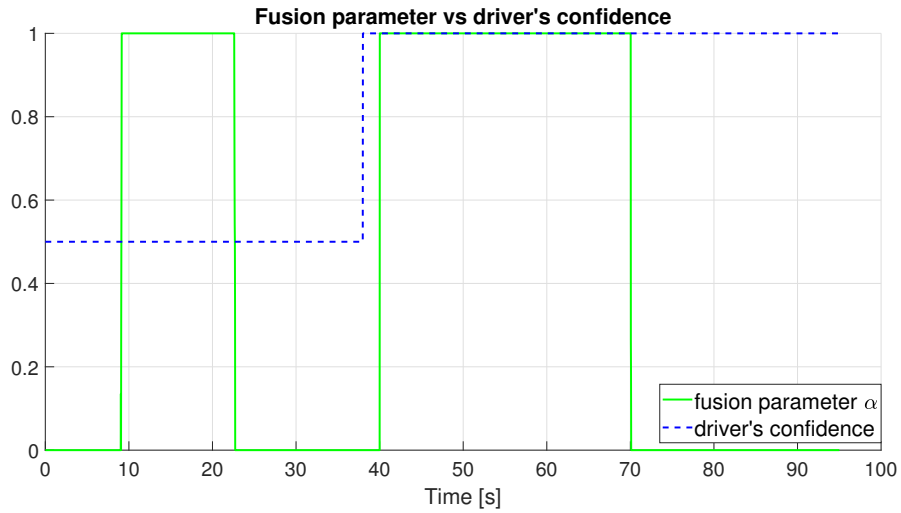


Figure 2.10 – The fusion parameter $\alpha$ - case 1

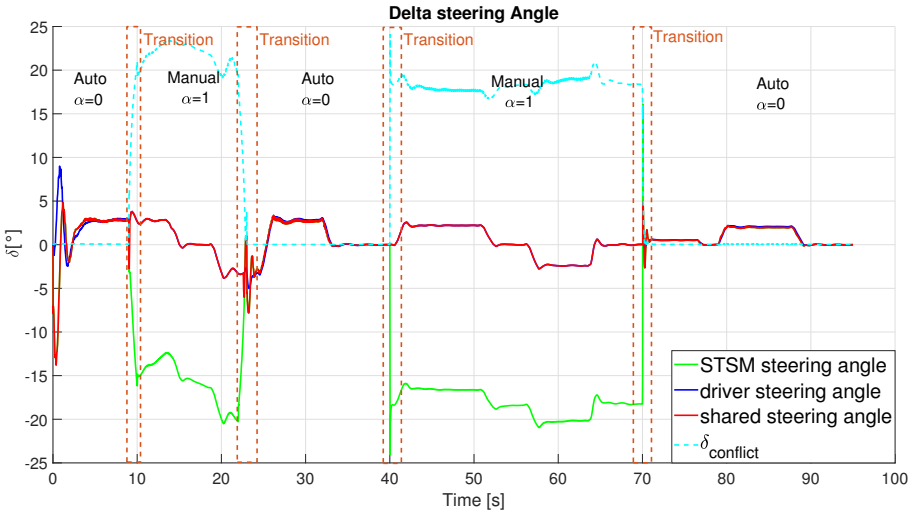


Figure 2.11 – The different steering wheel angles - case 1

Concerning case 2 the failure of the autonomous system is injected at $40s$ until $70s$ (see Figure 2.13) where there is no driver's confidence between $40s$ and $50s$ (driver's confidence= 0; see Figure 2.14). An emergency mode is activated corresponding to $\alpha$=1 (Manual steering mode) while braking the vehicle, that means the driver takes the driving task in the emergency mode situation until the vehicle is stopped or the conditions of deactivation of this mode are realized (Figure 2.14). Then, the driver is more attentive and careful to take the action of control between $50s$ until $60s$ (driver's confidence= 1; see Figure 2.14). He is still acting on the vehicle's control between $60s$ and $70s$ even though his confidence decreased again to 0 (Figure 2.14). Therefore, this mode is defined in the algorithm above which retains the previous input if it leads to a small lateral error, even if the confidence is small on this input. Figure 2.13 shows the different lateral errors. The different values of fusion parameter $\alpha$ are given in Figure 2.14, and Figure 2.15 shows the different steering angles. The

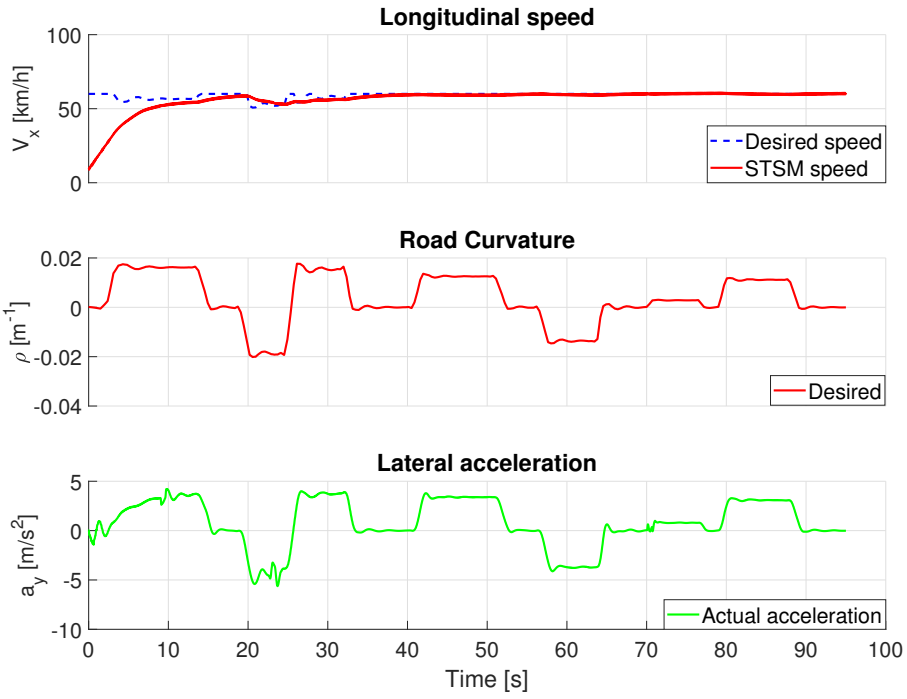


Figure 2.12 – The vehicle dynamic variables - case 1

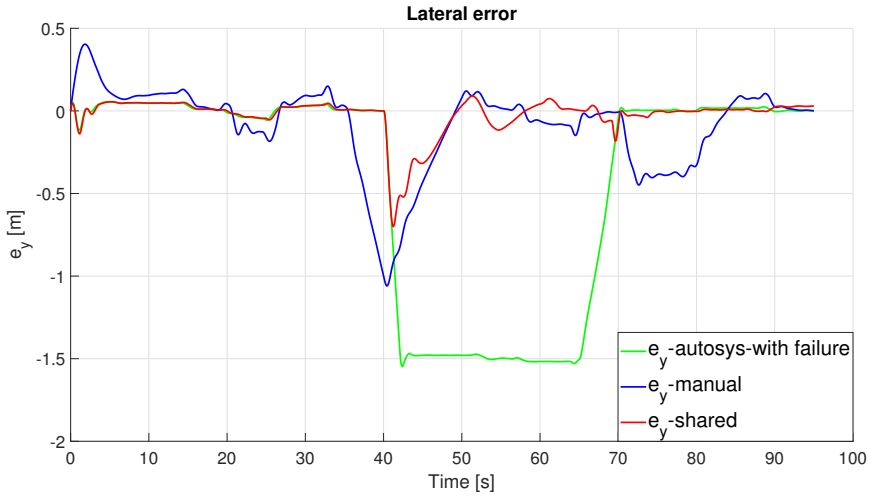


Figure 2.13 – The lateral error - case 2

longitudinal speed, the road curvature of the desired trajectory, the driving/braking torque and the longitudinal and lateral acceleration of the shared mode are given in Figure 2.16. As we can see in Figure 2.16, when the emergency mode is activated, the vehicle starts decreasing its velocity until the driver will be more attentive and will be able to drive the vehicle. And finally, the longitudinal speed starts to increase at $50s$, ending the emergency mode. Noting that driving is comfortable for the overall trajectory including the emergency situation, what ensures a stable driving situation. Moreover, many different tests are done for several driving situations to

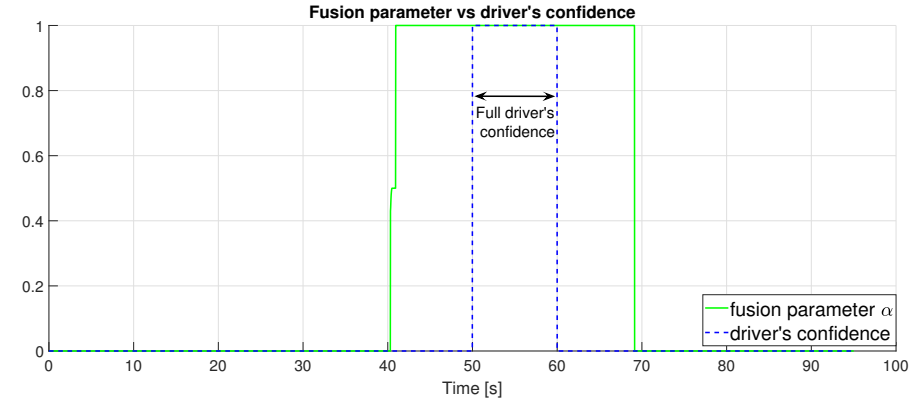


Figure 2.14 – The fusion parameter $\alpha$ - case 2

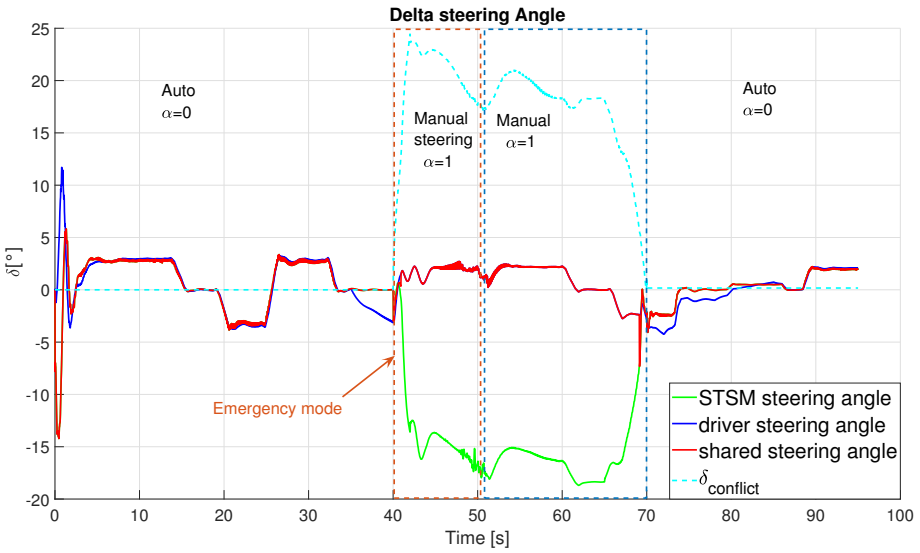


Figure 2.15 – The different steering wheel angles - case 2

validate the proposed approach based on the decision making of the $FLC$ and the different functionalities of the block analysis.

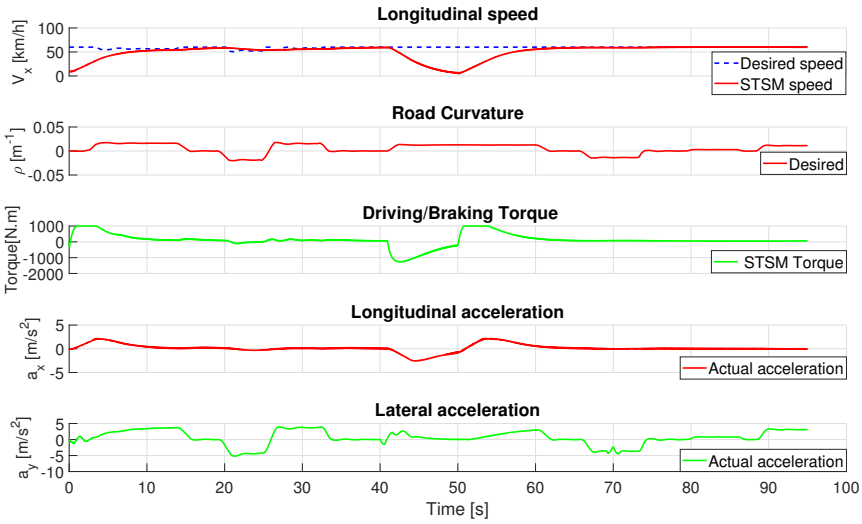


Figure 2.16 – The vehicle dynamic variables - case 2

### 2.3.3 *SCANeR Studio* Simulator Results

In this section, the proposed shared lateral control is validated on the "*SCANeR Studio*" (OKtal) simulator with a co-simulation with Matlab/Simulink, to show the results of the two case studies with a complete nonlinear "*SCANeR*" vehicle model.

#### 2.3.3.1 Case 1:

The lateral errors of the manual, autonomous mode with failures and the shared mode are given in the Figure 2.17. Similar to the simulation results on Matlab 2.3.2, the lateral error had the same behaviors in the Figure 2.9. The shared mode is able to reduce the lateral error caused by the autonomous system and give the right to drive the vehicle to the driver. The driver drives the vehicle from $9s$ to $23s$ where

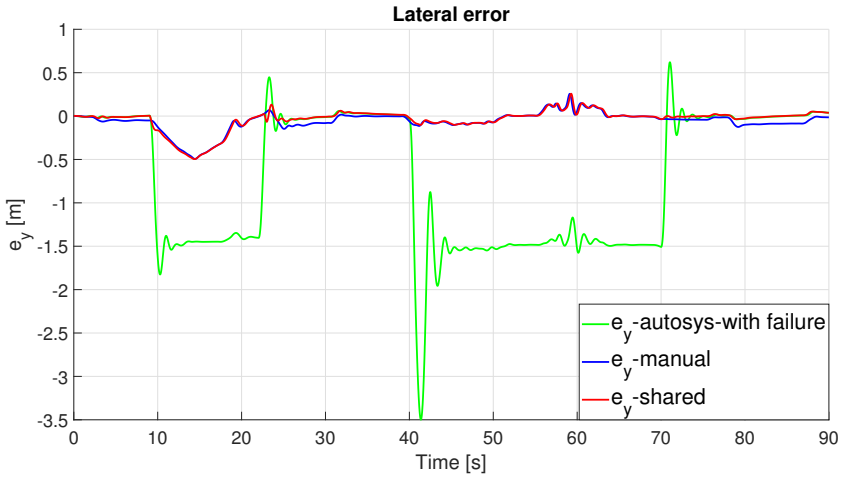


Figure 2.17 – The lateral error - case 1, on *SCANeR Studio* simulator

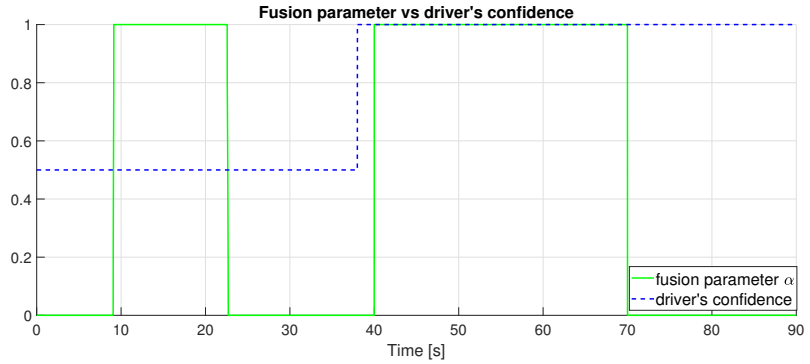


Figure 2.18 – The fusion parameter $\alpha$ - case 1, on *SCANeR Studio* simulator

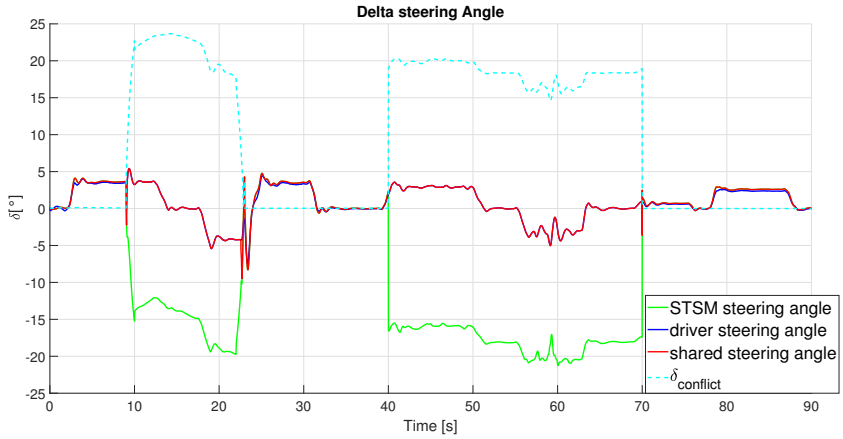


Figure 2.19 – The different steering wheel angles - case 1, on *SCANeR Studio* simulator

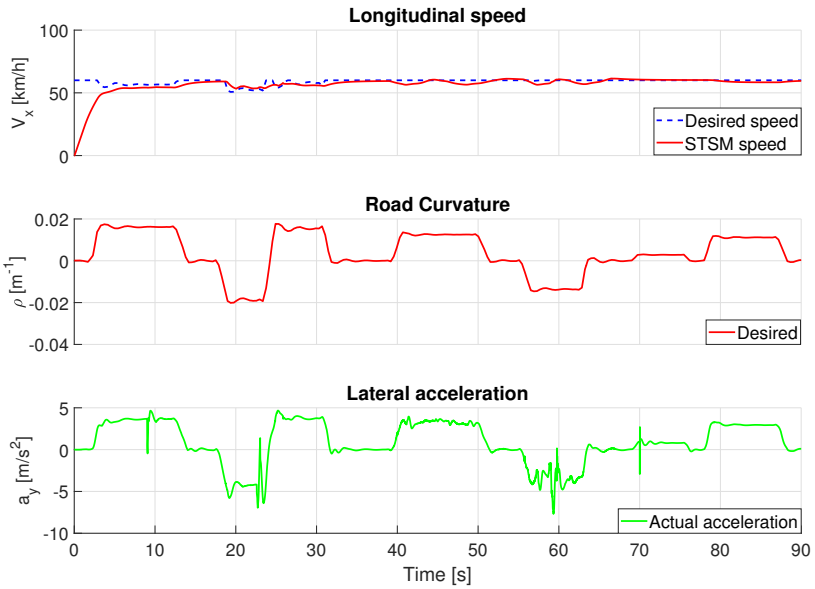


Figure 2.20 – The vehicle dynamic variables - case 1, on *SCANeR Studio* simulator

there is a failure on the autonomous system. Noting that the driver had the right to take vehicle's control in case of autonomous system's failure even though his confidence is medium (see Figure 2.18), that is the decision of the $FLC$ block. In addition, between $40s$ and $70s$, the driving mode is manual and the driving is safe thanks to the $FLC$ block that determines the leader of the vehicle depending on the driving situation. The fusion parameter $\alpha$ is given in the Figure 2.18. Figure 2.19 shows that the switching between the two agents is safe and smooth. The different steering angles are given in Figure 2.19. Finally, the longitudinal tracking speed, road curvature of the desired trajectory and the actual lateral acceleration are given in Figure 2.20. The results show that the driving is comfortable and safe for the overall trajectory regarding the change of driving situation.

#### 2.3.3.2 Case 2:

Similar to case 1, the curves of the case 2 had the same behavior as on Matlab 2.3.2. The lateral error is given in the Figure 2.21. However, there is no driver's confidence

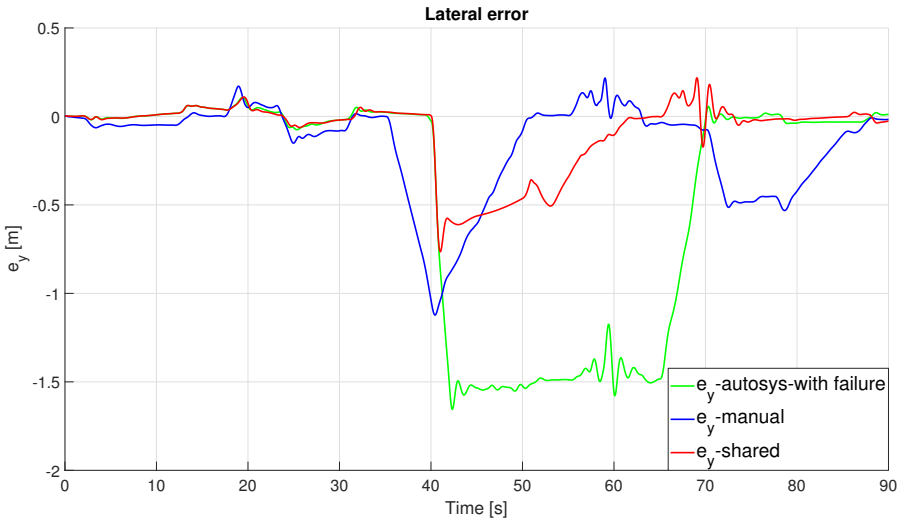


Figure 2.21 – The lateral error - case 2, on *SCANeR Studio* simulator

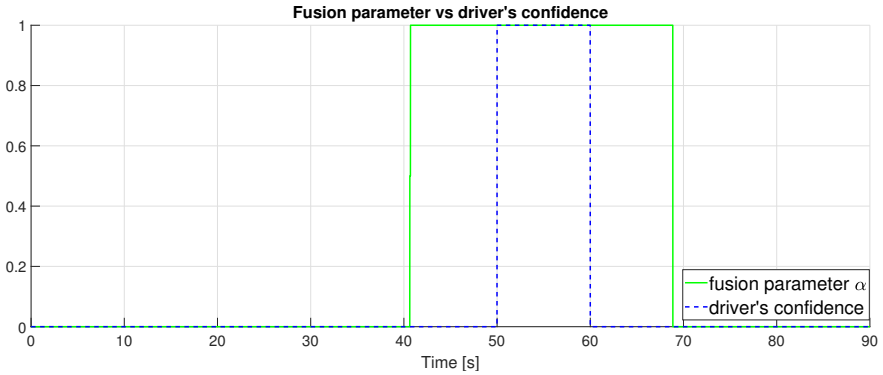


Figure 2.22 – The fusion parameter $\alpha$ - case 2, on *SCANeR Studio* simulator

between $40s$ and $50s$ (driver's confidence= 0; see Figure 2.22) at the same time of autonomous system's failures (see Figure 2.21). An emergency mode is activated corresponding to $\alpha$=1 (Manual steering mode) while braking the vehicle, because the conditions of activation of emergency mode are realized. The driver takes vehicel's control in the emergency mode situation until the conditions of deactivation of this mode are realized (Figure 2.22). Between $50s$ until $60s$, the driver's confidence is equal to 1 (see Figure 2.22) and the driver is able to control his vehicle. He still acting on vehicle's lateral control even though his confidence decreased again to 0 between $60s$ and $70s$ (see Figure 2.22). Moreover, this mode is defined in the analysis block to conserve the previous driving mode that causes a small lateral error even though the agent's confidence is small in this mode. The different values of the fusion parameter $\alpha$ are given in Figure 2.22, and Figure 2.23 shows the different steering angles. Figure 2.24 shows the longitudinal speed, the road curvature of the desired trajectory, the driving/braking torque and the longitudinal and lateral accelerations of the shared mode respectively. As we can see in Figure 2.24, the vehicle decreases its velocity, when the emergency mode is ON, until the driver will be more attentive and will be able to control the vehicle. And finally, the longitudinal speed starts to increase at $50s$ and the emergency mode is switched-off. Noting that driving is comfortable for the overall trajectory including the emergency situation, what ensures a safe driving situation.

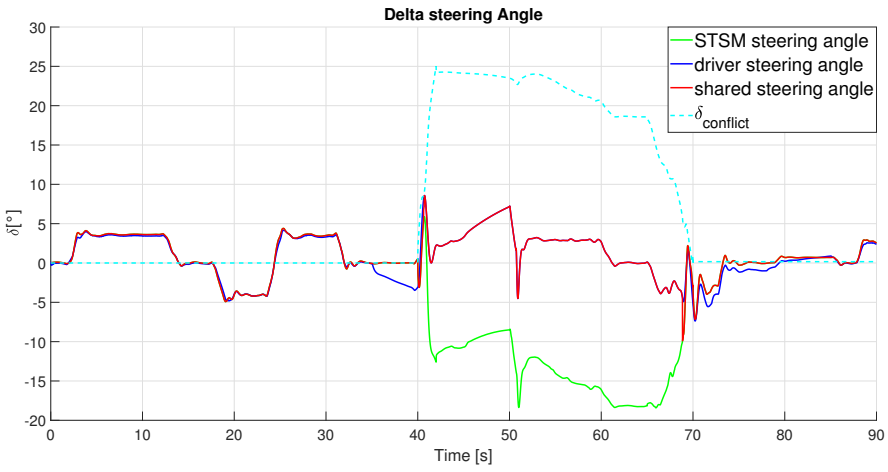


Figure 2.23 – The different steering wheel angles - case 2, on *SCANeR Studio* simulator

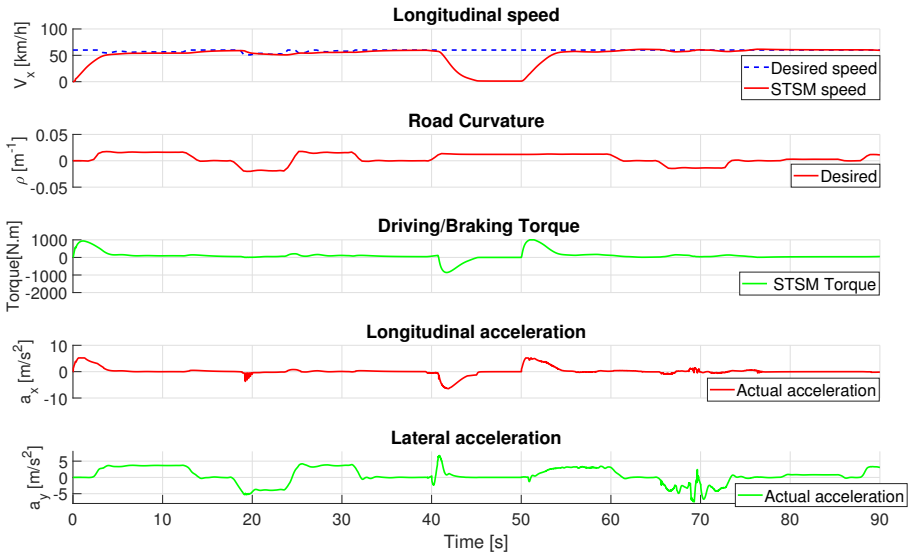


Figure 2.24 – The vehicle dynamic variables - case 2, on *SCANeR Studio* simulator

## 2.4 Conclusion and Perspectives

To conclude, in this chapter a shared lateral control has been developed to improve the system's performance and enhance driving safety, where the different driving modes are detailed. This cooperative control is done by using blended shared control, where a Fuzzy Logic Controller and a situation-based analysis block are presented to determine the decision making authority. The proposed shared control is validated on Matlab/Simulink with a complete nonlinear model of the vehicle, validated on "*SCANeR Studio*" (OKtal) simulator. The validation of this shared control under different possible critical driving situations is done in this work. In addition, the results show the effectiveness of the proposed approach to compensate the errors of autonomous system and prevent an undesirable driving situation. The validation of the proposed shared lateral control on the "*SCANeR Studio*" (OKtal) simulator confirms the validation on Matlab/Simulink where the results have the same behavior. In the next chapter, we will consider another shared lateral control approach to manage the transition between the human driver and the autonomous system.

# *Transition Management Between Autonomous System and Human Driver In a Take Over Request Context (TOR)*

This chapter investigates a new shared lateral control approach to deal with the transition management between the human driver and the autonomous system. The different driving modes are described. Then, the proposed shared lateral control is developed including a coordinator and a fusion block. Finally, the proposed shared lateral control is designed, tested and validated on the "*SCANeR Studio*" (OKtal) professional simulator with the human in-the-loop through the "*Logitech G29*" steering wheel for many different tests and scenarios.

## 3.1 Introduction

This introduction answers the question of why to manage the transition between the human driver and the autonomous system. The answer is simple because there are many driving situations where a transition is required between both agents in order to prevent a critical situation. This transition is needed especially in the level 3 and 4 of automation, where the presence of the driver in the loop interacting with an autonomous system is necessary to ensure road safety. For example, in the level 3, the human may be asked to take the control of the vehicle if a problem occurs on the autonomous system behavior. In addition, in the higher level of automation (level 4), the driver is able to retain vehicle's control if he is available. Moreover, the shared control is the aspect of control where both agents cooperate together to accomplish a common goal. During this collaboration, a smooth switching can occur to realize the goal. To deal with this topic, a new shared lateral control approach is presented in this chapter to address the transition management between the human driver and the autonomous system (see Figure 3.1). The objective of this shared control is to realize a smooth and safe switching between the two agents steering inputs during a lane keeping maneuver. However, this method can be adapted to cover more complex maneuvers. In the present work, the driving is considered as autonomous by default while the driver can demand a take over request anytime to be in charge of vehicle's control. Many conditions and criteria related to the driver are considered

before initiating this transition. If all conditions are satisfied, a switching from Auto to Manual takes place. Otherwise, the autonomous system intervenes to penalize the driver and retake the control, that means a return to Auto mode is realized if an error occurs on the driver's behavior. Thus, our contribution is illustrated in the development of the different driving modes including the transition system. Two transition modes are defined, that ensure the shifting from auto to manual mode and vice-versa, according to many criteria: the Driver's availability, the conflict on the driver's behavior, and the take over request. The human driver acts on the vehicle's lateral control. The autonomous system consists of longitudinal and lateral controller developed based on Super-Twisting Sliding Mode ($STSM$) control approach given in Section 1.4.2. Then, the control authority allocation is performed using the blended shared control that permits the fusion of two inputs via a fusion parameter. To do that, a coordinator based on a decision algorithm is developed for the driving modes and the fusion parameter determination. Finally, validation of the proposed shared control is done on the "*SCANeR Studio*" (OKtal) professional simulator with the human in-the-loop through the "*Logitech G29*" steering wheel for many different scenarios and set of tests. Two scenarios are chosen and integrated in this work to sum up the effectiveness and the performance of the transition system in terms of driving safety enhancing and vehicle's stability keeping.

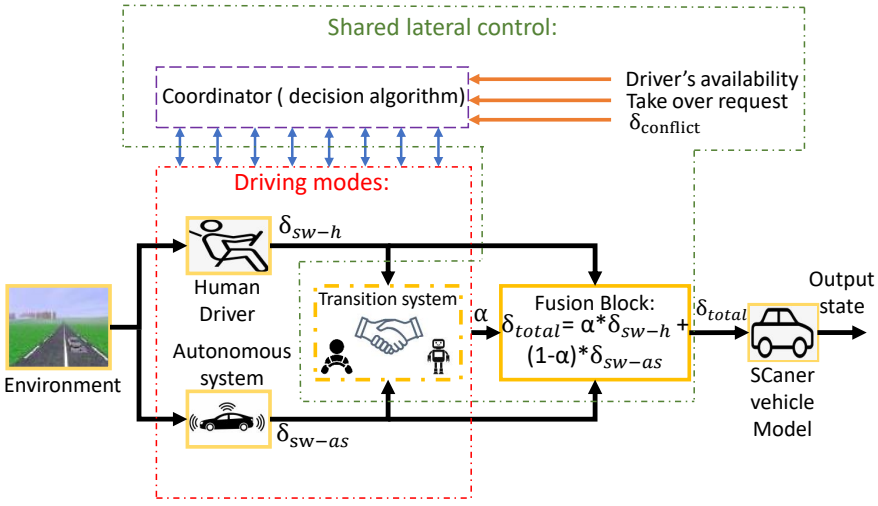


Figure 3.1 – Architecture of the shared lateral control.

## 3.2 DESIGN OF SHARED LATERAL CONTROL

### 3.2.1 Driving Modes

Figure 3.1 shows the global shared lateral control architecture. It is composed of two parts: the Driving modes and the shared lateral control. The different components of the driving modes block (see Figure 3.1) are detailed in the following.

#### 3.2.1.1 Human Driver

A real human driver acts on the vehicle's lateral control through a steering wheel (human in-the-loop). His steering input will be noted as $\delta_{sw-h}$.

#### 3.2.1.2 Autonomous System

The autonomous system consists of longitudinal and lateral controller developed based on Super-Twisting Sliding Mode ($STSM$) control approach given in Section 1.4.2. The control inputs are the driving/braking torque $\Gamma_c$ for the longitudinal dynamics and the steering wheel angle $\delta_{sw-as}$ for the lateral dynamics.

#### 3.2.1.3 Transition System

The transition system defines the way to switch from the auto to manual mode or from manual to auto mode. For that, two modes are defined to realize these transitions. The transition system structure is given in the Figure 3.2(a). The two

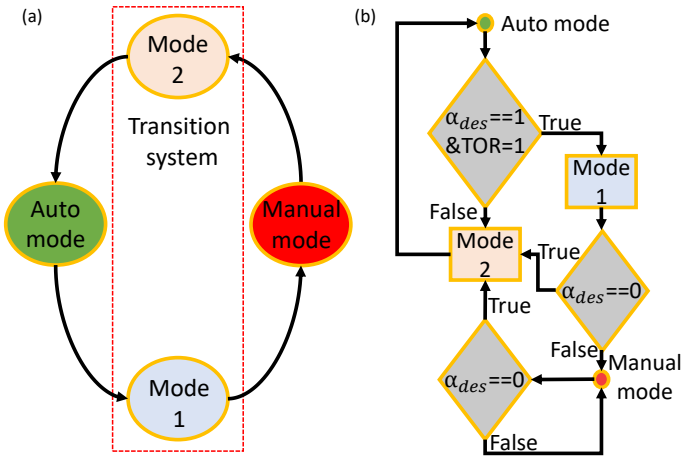


Figure 3.2 – The structure of the transition system

modes are given as:

- Transition mode 1: This mode is defined to switch from the auto mode to the manual mode after a take over request demanded by the driver (Figure 3.2(b)). We define $\alpha_{des}$ function of the driver's availability ($DA$) and the conflict on the driver's behaviors ($\delta_{conflict}$). The role of $\alpha_{des}$ is to determine the direction of transition (from auto to manual mode or vice-versa, auto mode corresponds to $\alpha_{des} = 0$, and manual mode corresponds to $\alpha_{des} = 1$), depending on the driver's availability and behaviors. $\alpha_{des}$ is the desired reference for the fusion parameter $\alpha$, given as:

$$\alpha_{des} = DA * (1 - \delta_{conflict}) \tag{3.1}$$

  The driver's availability ($DA$) is a dynamic variable related to the driver, and can be calculated based on different factors: driver's eyes movement, driver's head position, level of driver's sleepiness, etc. Therefore, the calculation of

diver's availability is not in the scope of this work and it is considered as an input to the transition system.
On the other hand, the conflict on the driver's behaviors $\delta_{conflict}$ is the difference between the steering wheel angle applied by the driver ($\delta_{sw-h}$) and the approximate steering angle ($\delta_{approx}$) on the desired trajectory given as:

$$\delta_{conflict} = B_{\delta_{threshold}}(|\delta_{approx} - \delta_{sw-h}|) \tag{3.2}$$

$$\delta_{approx} = \rho^* * (l_f + l_r) \tag{3.3}$$

with $\rho^*$ the curvature of the desired trajectory, $l_f$ and $l_r$ the distances from the center of the vehicle to the front and rear wheels respectively. The conflict of the driver's behavior, $\delta_{conflict}$ is a Boolean value, equal to 0 or 1 depending on $\delta_{threshold}$ a threshold from which we consider that there is a conflict on the driver's behavior.
This transition is done, if the driver demands a take over request ($TOR = 1$) and $\alpha_{des} = 1$, that means the driver is available to take the action of vehicle's control ($DA = 1$), and there is no conflict on his behavior ($\delta_{conflict} = 0$). So, the transition mode 1 is activated in order to switch to the manual mode and $\alpha$ increases from 0 to 1 in a time $T_{up} = 1.5s$. $\alpha$ is the fusion parameter varying between 0 and 1 to blend the two agents steering inputs. $\alpha$ is equal to 0 in auto mode and to 1 in manual mode.

- Transition mode 2: The aim of this mode is to assure the transition from the manual mode to the auto mode, in the case when the human driver is totally engaged in the driving tasks (manual mode) and suddenly the value of $\alpha_{des}$ is equal to 0 because the driver is no more available to take control ($DA = 0$), or there is a conflict occurs on his behaviors while driving ($\delta_{conflict} = 1$)(Figure 3.2(b)). So, the transition mode 2 is activated to realize the transition from manual mode to auto mode and $\alpha$ decreases from 1 to 0 in a time $T_{down} = 0.2s$. In this case, the transition mode 2 is an example of Advanced Driving Assistance System (*ADAS*) application. In addition, the transition mode 2 is activated if during the transition from auto to manual mode (transition mode 1), suddenly the value of $\alpha_{des}$ returns to 0, that happens if a conflict occurs on the driver's behaviors, or the driver is no more available during this phase (Figure 3.2(b)). Thus, the transition to the auto mode is done and $\alpha$ decreases from $\alpha_0$ ($\alpha_0 < 1$) to 0, respecting the same decrease rate.

### 3.2.2 Shared lateral control

This section details the proposed shared lateral control (see Figure 3.1). The shared control authority allocation between the two agents is presented. Then a coordinator based on a decision algorithm is developed to determine the way of switching between the different driving modes.

#### 3.2.2.1 Shared Lateral Control Authority

The shared control authority allocation between the driver and the autonomous system is performed by using the blended shared control given in Section 2.2.2.1.

The total blending control input is given as:

$$\delta_{total} = \alpha * \delta_{sw-h} + (1 - \alpha) * \delta_{sw-as}, \tag{3.4}$$

where $\delta_{total}$, $\delta_{sw-h}$ and $\delta_{sw-as}$ are the total steering wheel angle, steering wheel angles of human driver and autonomous system respectively. $\alpha$ is the fusion parameter representing the influence proportion of each agent on the total steering angle. $\alpha$ is bounded in [0,1], calculated depending on the decision algorithm in the coordinator.

#### 3.2.2.2 Coordinator

In order to determine the driving mode and the value of the fusion parameter, a coordinator is needed to switch between the different driving modes: Auto mode, Manual mode and finally the modes 1 and 2 of the transition system (see Figure 3.3). These modes are defined as:

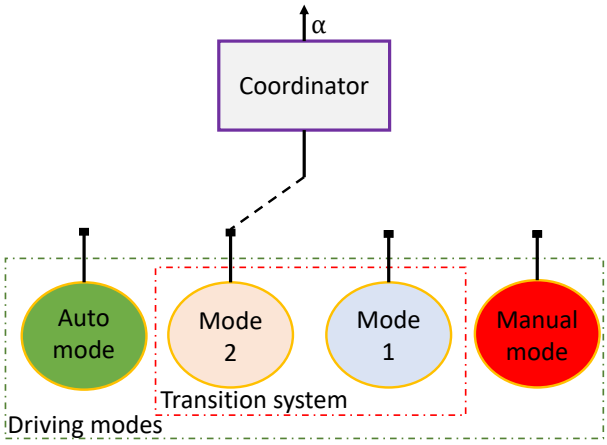


Figure 3.3 – The structure of the coordinator

- Auto mode: an autonomous controller provides the vehicle with the appropriate torque for the longitudinal movement. For the lateral dynamics, a robust controller generates the steering angle to follow the desired trajectory and keep the lane. Noting that, in this mode the steering wheel and the wheels are mechanically disconnected corresponding to a steer-by-wire system.

- Manual mode: the human driver acts on the vehicle's lateral control by using the steering wheel, "*Logitech G29*" (Figure 3.6), while the longitudinal controller is realized by the same autonomous longitudinal controller used in the Auto mode. The driver can demand a take over action by pressing the button $R2$ and he can turn off the manual driving by using the button $L2$ on the "*Logitech G29*" steering wheel (see Figure 3.6(b)).

- Transition system's modes: transition mode 1 and 2 are detailed above to describe the switch from Auto mode to the Manual mode and vice-versa.

Then, a decision algorithm (given below) is developed in this layer for the switching between the different modes, and the determination of the final value of the fusion parameter $\alpha$.

**Algorithm 2** A decision algorithm for the switching purpose (Mode 1 & 2)

```
if (Take over request equal to 0 (TOR=0)) then
  Auto mode is activated (α = 0)
else
  if (α_des = 0) then
    if (α_{t-1} = 0) then
      Auto mode is activated
    else
      Transition mode 2 is activated (Manual to Auto)(Figure. 3.2)
    end if
  else
    if (α_{t-1} < 1) then
      Transition mode 1 is activated (Auto to Manual)(Figure. 3.2)
    else
      Manual mode is activated (α = 1)
    end if
  end if
end if
```

The inputs of the algorithm are: the take over request $TOR$, the desired reference of the fusion parameter $\alpha_{des}$ and the fusion parameter $\alpha_{t-1}$ at $t-1$. The output is the fusion parameter $\alpha$. Based on the algorithm, $\alpha$ is calculated as:

- If there is no take over request demanded by the driver ($TOR = 0$), then keep the Auto mode.
- If there is a take over request demanded by the driver ($TOR = 1$) and $\alpha_{des} = 0$, two cases are defined, depends on $\alpha_{t-1}$, given as:
  - ◇ If the driving was Auto mode ($\alpha_{t-1} = 0$), then keep this previous mode (Auto).
  - ◇ If the driving was not Auto mode ($\alpha_{t-1} \leq 1$): Manual or Transition mode 1, then activate the Transition mode 2 to switch from Manual to Auto mode.
- If there is a take over request demanded by the driver ($TOR = 1$) and $\alpha_{des} = 1$, two cases are defined, depends on $\alpha_{t-1}$, given as:
  - ◇ If the driving was not Manual mode ($\alpha_{t-1} < 1$), then activate the Transition mode 1 to switch from Auto to Manual mode.
  - ◇ If the driving was Manual mode ($\alpha_{t-1} = 1$), then keep the previous mode (Manual).

## 3.3 System's Validation

The simulation tools used in the validation are presented in this section. Validation is done on the "*SCANeR Studio*" (OKtal) simulator by co-simulation between the later and Matlab/Simulink. Then, the simulation results of two chosen scenarios are presented latter to show the effectiveness and performance of the proposed shared lateral control including the transition system.

### 3.3.1 Simulation Tools

#### 3.3.1.1 *SCANeR Studio simulator:*

*"SCANeR Studio*" simulator is a simulation platform answering the demand of researches and engineers. This simulator allows user to create a safe and controllable environment for the validation of different scenarios with the different driving conditions (Figure 3.4). The main modules are: Models (dynamic vehicle, autonomous traffic, pedestrians, etc.), Restitutors (visual, sound, dynamic platform, etc.) and Acquisitions (virtual or real pilot, tracking systems , physiological data, etc.). The idea of this software is to be used around the operational processes of driving simulators, structured of five dedicated modes:

- Terrain mode: Road network creator RoadXML tool allowing the rapid creation of realistic road networks-useable directly in the simulation.
- Vehicle mode: Tool for the vehicle's models preparation and modeling.
- Scenario mode: Driving simulator scenario editing tool.
- Simulation mode: Simulation supervision tool.
- Analysis mode: Detailed graphical and recorded data analysis tool.

The co-simulation between the "*SCANeR Studio*" (OKtal) simulator and Matlab/Simulink is done by using the library Application Programming Interfaces (SCANeR *APIs*). A Simulink S-function developed by OKTAL allows interfacing a Simulink model with SCANeR communication protocols. It is based on the SCANeR *API*. This S-function reads the network and the shared memory, and sends data to the Simulink model. Similarly, it writes on the network and the shared memory data computed by the Simulink model.
A "*SCANeR*" vehicle model is used on this software, with the different driving modes: Autonomous and Manual modes and the 2 modes of transition system. Thus, the "*SCANeR Studio*" simulator is used in this work to validate the proposed shared control that interacts with the human driver through a "*Logitech G29*" steering wheel (see Figure 3.6). Note that, the steering wheel and the wheels are decoupled corresponding to a steer-by-wire system.. There is no haptic feedback torque from the "*SCANeR Studio*" simulator on the steering wheel.

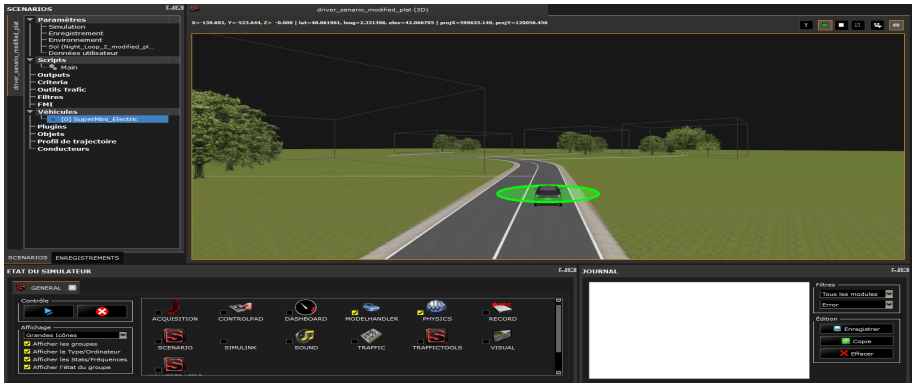

Figure 3.4 – The *SCANeR Studio* environment.

#### 3.3.1.2 *Matlab/Simulink:*

The co-simulation is done on *Matlab/Simulink*, by developing the different Simulink blocks in Figure 3.5. The "*Logitech G29*" (Figure 3.6) is the steering wheel that permits the interaction between the driver input and the "*SCANeR Studio*" simulator. The wheel can rotate up to 900°, corresponding to 60° on the wheels. It has three pedals and a dual motor force feedback with a overheat safe guard. All these features make the driving more realistic for the user. In addition, the different blocks for the autonomous controller, localization, etc., are developed on Matlab/Simulink.

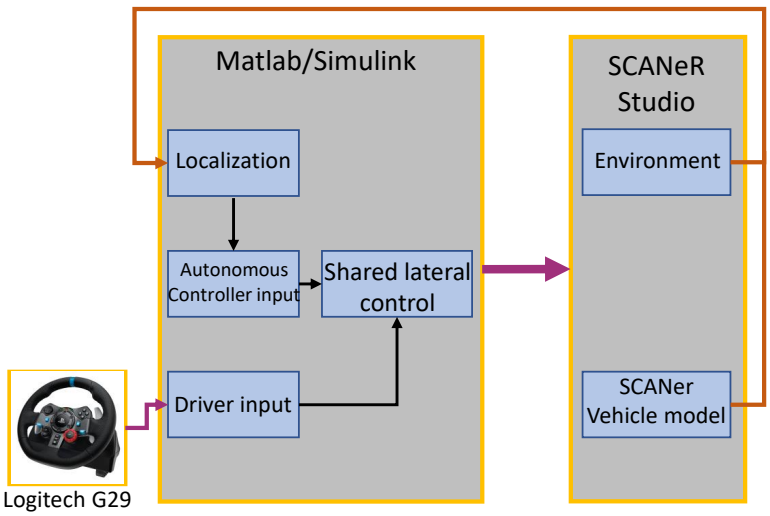


Figure 3.5 – Co-simulation between *Matlab/Simulink* and *SCANeR Studio*.

### 3.3.2 Scenarios Definition

In this subsection, two scenarios are chosen between a set of scenarios to test and validate the proposed shared lateral control for different driving situations. Indeed, two scenarios are detailed to show the effectiveness and the performance of the

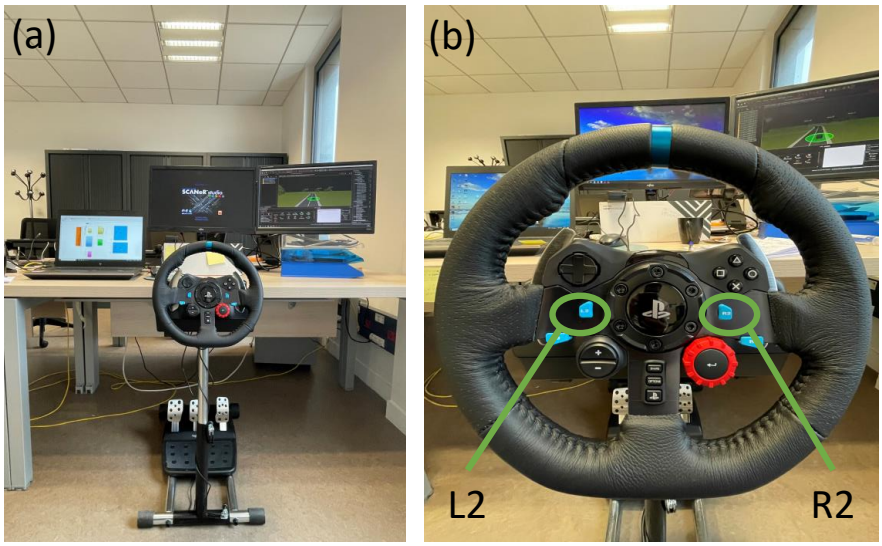


Figure 3.6 – The steering wheel hardware, Logitech $G29$. $R2$: take over ON and $L2$ take over OFF.

developed shared lateral control including the transition system against the variation of different driving conditions.

- Scenario 1: This scenario is defined to show the adaptation and performance of the transition system. This scenario shows the transition between the auto and manual modes depending on the driving situations. For the beginning of scenario, the driving mode is autonomous where the autonomous controller keeps the lane of the test track given in the Figure 3.7, by reducing the lateral error at a desired velocity. The driver who interacts with "*SCANeR Studio*" simulator through a "*Logitech G29*" steering wheel, demands a take over request at t=8.5$s$. The transition system 1 is activated to switch from Auto to Manual mode because all the conditions of activation of this mode are realized. The transition is done by ensuring road safety and enhancing driving performance and the driver controls his vehicle until t=32$s$. The driver's availability is considered full ($DA = 1$) for the overall trajectory (see Figure 3.8). In addition, at t=32$s$, the driver is penalized and the transition mode 2 is activated to switch to the Auto mode. This activation is occurred after a conflict detected on the driver's behaviors caused by the inappropriate steering wheel angle by the driver on the vehicle (see. Figure 3.9). Again the transition mode 1 is switched-on at t=50$s$ to give the authority of driving to the driver after verification of all conditions of activation of this mode. Finally, the driver decides to switch-off the Manual mode at t=70$s$ through the button $L2$ on the "*Logitech G29* steering wheel. The driving will be Auto until the end of the scenario according to the transition mode 2. To conclude, this scenario shows a safe switching between both agents at each phase while ensure road safety.

- Scenario 2: This scenario is defined to deal with the variation of different

variables: $DA$, $\delta_{conflict}$, $\alpha_{des}$, $TOR$. The transition system is adapted against these variations to show the functionalities of this system. The management between the different modes under varying driving conditions is presented here. The driver's availability is considered as variable in this scenario. $DA$ is equal to 1 except the 3 intervals of time: $[0s; 10s]$, $[25s; 40s]$ and $[60s; 70s]$ (see Figure 3.11). Many phases are presented in this scenario to show the adaptation of the transition system against the variation of variables, given as:

- ◇ Phase 1: corresponds to the case where the driver demands a take over request while he is not available at t=$5s$, then the transition system 1 is not activated until t=$10s$ when the driver will be available (see Figure 3.11).
- ◇ Phase 2: represents the case where the driving is Manual (between $10s$ and $25s$) and suddenly the driver is no more available at t=$25s$ that leads to the activation of the transition mode 2 to switch to the Auto mode (see Figure 3.11).
- ◇ Phase 3: illustrates the case where the driver is ready and available to take control. However, during the switching to the Manual mode, a conflict is detected on his behavior caused by an inadequate driver steering angle (see Figure 3.12), then transition mode 2 is switched-on at t=$40s$ and t=$50s$ respectively to switch to the Auto mode.
- ◇ Phase 4: treats the case where the conflict on the driver behavior decreases, but the driver is no more available, so a switching to the Auto mode is required at t=$60s$ (see Figure 3.11).
- ◇ Phase 5: describes the case where the conditions of activation of transition mode 1 are realized to give the control authority to the driver at t=$70s$, while the latter decides to switch-on the Auto mode at t=$83s$.

Simulation results will be addressed in the next section, including the different variables: $DA$, $\delta_{conflict}$, $\alpha$ and $TOR$, to show the performance of the proposed shared lateral control and the transition system.

### 3.3.3 Simulation Results

After preparing the simulation environment to validate the proposed shared control, and after definition of two different scenarios, validation is done on "*SCANeR Studio*" simulator, by using the test track given in the Figure 3.7. The vehicle realizes the path following maneuver while cooperating with the human in 2 scenarios. The simulations results are presented in the following. Note that $\delta_{threshold}$=1.2 $rad$ on the steering wheel for the 2 scenarios, that corresponds to 4.6° on the wheels.

#### 3.3.3.1 Scenario 1:

As said before, this scenario shows the transition between the auto and manual modes depending on the driving situations. Remember that the human driver is available for the overall trajectory (see Figure 3.8). He demands a take over request

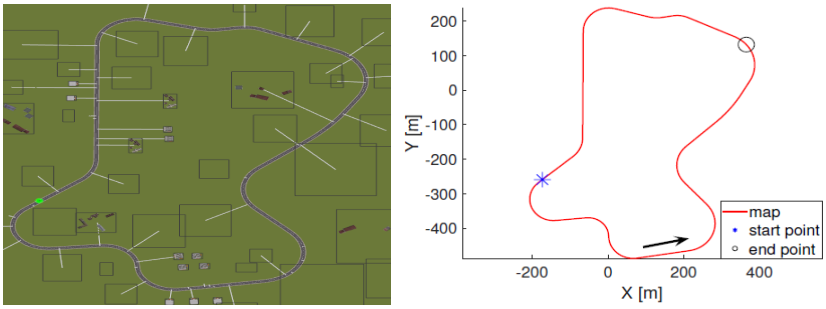


Figure 3.7 – Map of the test track.

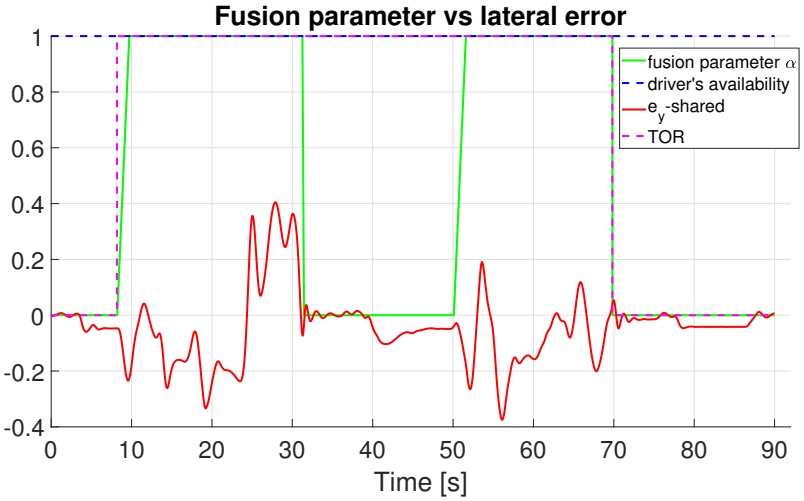


Figure 3.8 – The lateral error - Scenario 1

($TOR = 1$ at t=8.5$s$) by pressing the $R2$ button, so $\alpha_{des} = 1$ (eq.3.1) because the driver's availability is equal to 1, and there is no conflict on the driver's behaviors ($\delta_{conflict} = 0$). For that, $\alpha$ increases from 0 to 1 in 1.5$s$ at t=10$s$ according to the transition mode 1 of transition system. The driver takes the action of vehicle's control until t=32$s$. At t=32$s$, there is a conflict on driver's behaviors ($\delta_{conflict} = 1$) illustrated by a higher human driver steering angle (see. Figure 3.9) and $\alpha_{des}$ becomes 0. For that, $\alpha$ decreases again to 0 in 0.2$s$ to penalize the driver, and the driving will be fully autonomous, according to the transition mode 2. Again at t=50$s$ the driver still asking a take over action ($TOR = 1$) and $\alpha = 1$ because the conditions of activation of transition mode 1 are realized. The driver acts on the vehicle's control until t=70$s$ and finally he decides to switch-off the manual mode by pressing the $L2$ button, so $\alpha$=0 at t=70$s$. The different values of $\alpha$ are given in the Figure 3.8, which shows that the lateral error is between $-40cm$ and $+40cm$, that means the cooperation of the driver with the autonomous system leads to an acceptable and accurate lane keeping with an acceptable lateral error. The steering angles on the wheels of Auto, Manual and shared modes are given in the Figure 3.9. As we can see in Figure 3.9, a smooth switching is done between the two agents to ensure the transition between them and compensate the conflict of

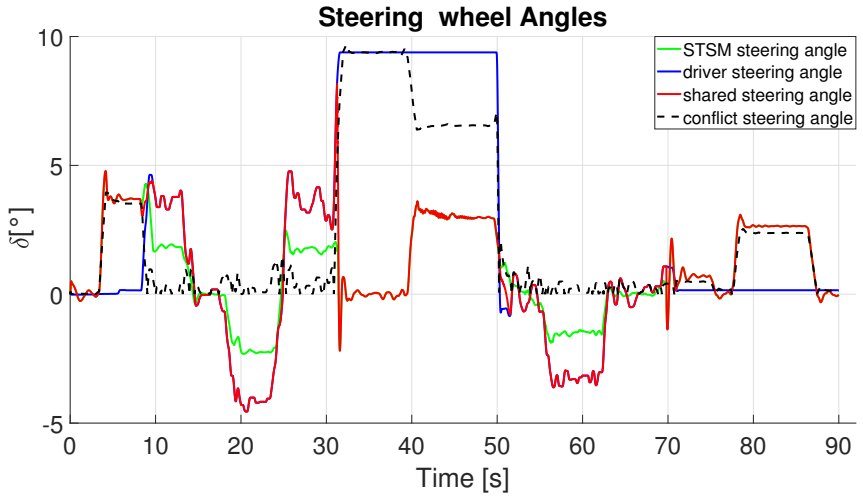


Figure 3.9 – The different steering wheels angles - Scenario 1

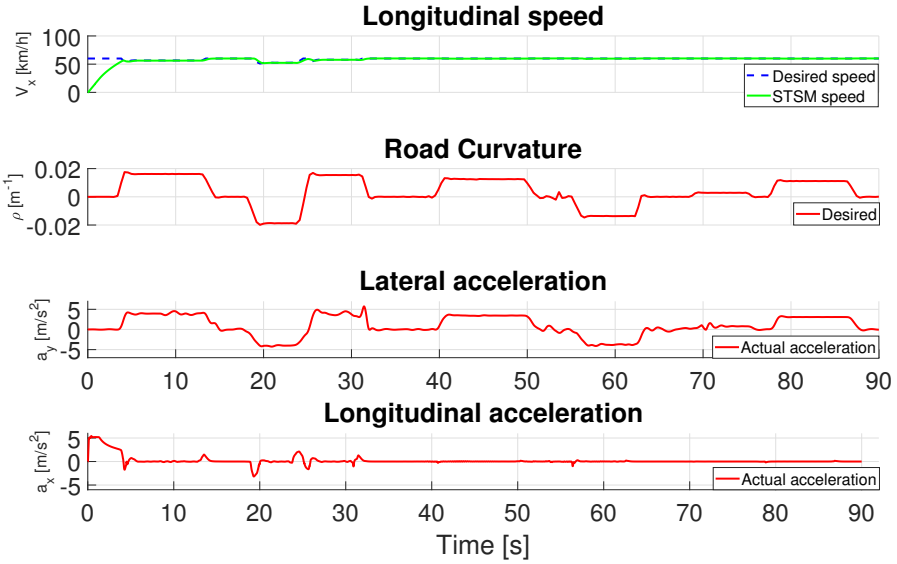


Figure 3.10 – Vehicle dynamic variables - Scenario 1

driver's behaviors, what makes the system stable. Finally, the Figure 3.10 shows the longitudinal speed which tracks the desired one using the $STSM$ controller, the road curvature of the desired track and finally the lateral and longitudinal accelerations. The actual lateral acceleration does not exceed the $\pm 5m/s^2$, which corresponds to a comfortable driving zone. In addition, the actual longitudinal acceleration is pertinent ($< \pm 3m/s^2$) for a comfortable maneuver. To conclude, the Scenario 1 proves that the transition between the two agents is possible while maintaining a comfortable and smooth driving, despite the switching between the different modes, and enhancing safety on the road.

#### 3.3.3.2 Scenario 2:

As said before, this scenario shows the adaptation of the transition system against the variation of different variables ($DA$, $\delta_{conflict}$, $\alpha_{des}$, $TOR$). Refer to Figure 3.11, the driver asks the take over action permission ($TOR = 1$) at t=5$s$, however this action is not approved until t=10$s$ where the driver's availability is full (see Figure 3.11) and $\alpha_{des} = 1$ because $DA = 1$ and $\delta_{conflict} = 0$. $\alpha$ starts to increase and the driver takes totally control at t=11.5$s$, according to the transition mode 1 (phase 1). He is still acting on the vehicle's control until t=25$s$, where the $DA$ is lost ($DA = 0$) and $\alpha_{des} = 0$ (eq.3.1). Thus, the auto mode is switched-on to drive the vehicle until t=40$s$ (phase 2), according to the transition mode 2.
At t=40$s$, the driver retains the vehicle's control because the $DA$ is equal to 1 again, that means $\alpha_{des} = 1$ and $\alpha$ starts to increase. During this phase (phase 3), there is a conflict that occurs on the driver's behavior ($\delta_{conflict} = 1$) and $\alpha_{des}$ returns to 0, then the value 1 for $\alpha$ is not reached. $\alpha$ will decrease again to 0 to give the control authority to the autonomous system in case the driver is not able to drive the vehicle. For the same reasons, $\alpha$ has the same behavior around t=50$s$ and the transition mode 2 is activated to switch to the Auto mode (phase 3).
In addition, $\alpha$=0 at t=60$s$ even though the conflict on the driver's behaviors starts to decrease ($\delta_{conflict} = 0$) (see Figure 3.12), but the driver's availability is equal to 0 again and $\alpha_{des} = 0$ (eq.3.1) at t=60$s$, so the switching-on of the auto mode is done thanks to the transition mode 2 (phase 4).
The increase of $DA$ at t=70$s$ ($DA = 1$) leads to increasing in the $\alpha$ value because the conditions of activation of the transition mode 1 are realized. The driver drives his vehicle from t=70$s$ to t=83$s$ when he decided to switch on the Auto mode ($TOR = 0$) and take his rest (phase 5).
The parameter $\alpha$ is given in the Figure 3.11. As shown in Figure 3.11, the different transitions in each phase lead to a small lateral error that guarantees the driving safety in terms of vehicle's stability during the lane keeping. Figure 3.12 shows the

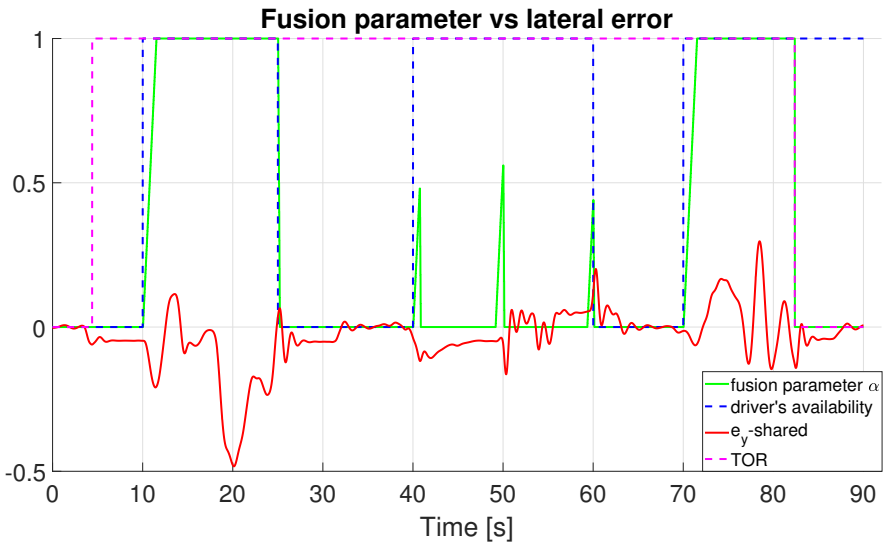


Figure 3.11 – The lateral error - Scenario 2

different steering angles on the wheels. The transition between the manual and auto modes is smooth and safe specially during the switching (at t=25$s$, 40$s$, 70$s$ for example). As we can see in the Figure 3.13, there is a good tracking for the desired longitudinal speed. The actual lateral and longitudinal accelerations are limited between $\pm 5m/s^2$ and $\pm 3m/s^2$ respectively, which confirm the passenger's comfort. Thus, the driving is safe and comfortable despite the variation of driving conditions and the switching between the three modes: Auto, Manual and transition system's modes.

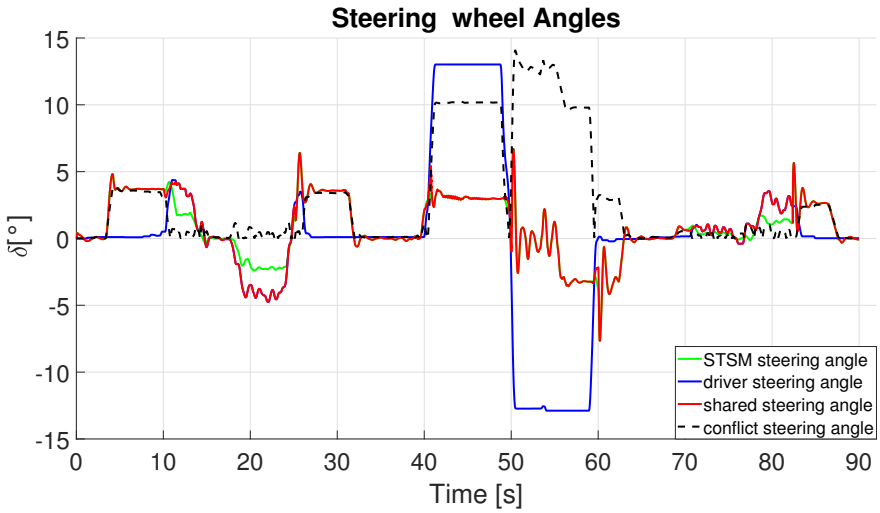


Figure 3.12 – The different steering wheels angles - Scenario 2

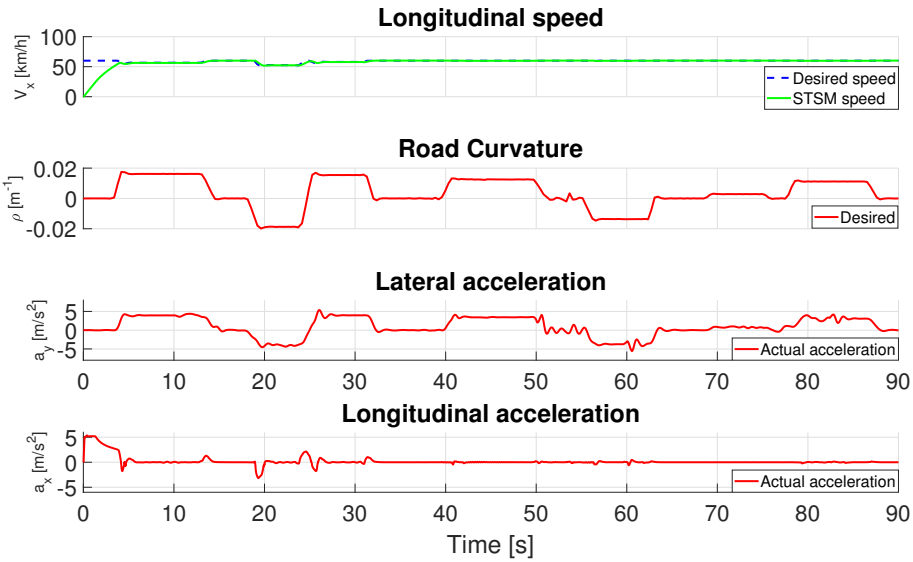


Figure 3.13 – Vehicle dynamic variables - Scenario 2

## 3.4 Conclusion and Perspectives

To conclude, in this chapter a shared lateral control has been developed to ensure the transition between the human driver and the automated system. The different driving modes including the transition system are detailed in this work. Then, the shared lateral control architecture is presented to blend the two control inputs. A decision making algorithm is developed, using a coordinator for the control authority allocation and driving modes determination. The proposed shared control is validated on the "*SCANeR Studio*" (OKtal) professional simulator interacting with human driver through the "*Logitech G29*" steering wheel. The validation is done for two chosen scenarios of lane keeping maneuver. The results show the effectiveness of the proposed approach to ensure a smooth transition and promote road's safety. In the next chapter, we will consider the development of Advanced Driving Assistance Systems (*ADASs*) (level 2) to assist and help the driver during a lane keeping maneuver while guaranteeing vehicle's lateral stability.

*Part II*

# *ADAS* Systems

# Development of Advanced Driving Assistance Systems (ADAS) for Lane Keeping Purpose

In the previous chapters, a shared lateral control between the driver and the automated system for the lane keeping purpose has been treated in order to ensure road's safety (level 3). In this chapter the development of an Advanced Driving Assistance Systems ($ADASs$) (level 2) are detailed to assist and help the driver during a lane keeping maneuver while guaranteeing vehicle's lateral stability.

## 4.1 Introduction

Autonomous driving has become a purposeful target for automotive companies as well as for research institutes in the recent years. For that, in 2013, the US Department of Transportation "National Highway Traffic Safety Administration NHTSA" has classified the autonomy of self-driving vehicles into 5 levels to characterize their capabilities [Favarò et al., 2017]. These levels start at having some assistance features and end at the full-autonomous vehicle passing by the semi-autonomous ones. Level 2 of autonomy consists of assisting the driver by several automated functionalities especially for active safety purpose. These systems are called advanced driving assistance systems ($ADASs$). They are integrated in the vehicle to protect the passengers in case of accident. There are the Passive systems (air bags, seat belts, etc.), and the active systems that help and assist the driver in some driving tasks especially when he is tired or distracted (Lane keeping system, Emergency braking, Lane departure avoidance, etc.). The lane departure avoidance system that warns the driver when he is crossing the lane, the Lane keeping to stay within the lane and the Emergency braking system to stop the vehicle, are integrated in the vehicle to promote road safety. Moreover, the development of electronics and sensors devices (LIDAR, GPS, etc.) supports the integration of these systems into the vehicle. The authors in [Kukkala et al., 2018] classified the $ADAS$ systems to many categories based on their types, utilities, limitations, etc. In addition, many advanced driving assistance systems ($ADASs$) have been proposed and marketed, such as: Active Front Steering ($AFS$) basically to enhance vehicle's maneuverability and realize a lane keeping; Direct Yaw Control ($DYC$) or Electronic Stability Program ($ESP$) to improve vehicle's lateral stability; (Semi-) Active Suspensions

($AS$) to improve comfort, road holding and rollover avoidance [Chokor et al., 2019]. These systems influence the vehicle's behavior and enhance safety on the road. Moreover, many advanced studies are presented in the literature to deal with the development of these systems especially the Lane Keeping system. A Fuzzy Takagi-Sugeno control method is used in [Soualmi et al., 2011] to develop a lane keeping assistance system where a decision algorithm is integrated to manage the authority between the driver and the controller depending on the lateral deviation error. The authors in [Nguyen et al., 2015], [Nguyen et al., 2016] have developed a shared steering controller for lane keeping maneuver where the driver's activity and behavior are considered in the computation of the control input of assistance system, in order to manage conflict between both agents. An assistance steer-by-wire system is presented in [Perozzi et al., 2020], where the fusion of two steering inputs is done considering the driver's availability via monitoring system. The authors in [Sentouh et al., 2013] are applied the $H_2$ approach to calculate the assistance torque through a first order filter coordination variable. A weighting approach presented in [Borroni and Tanelli, 2018] is used to blend the two control inputs by using a fusion parameter $\alpha$ adjusted manually or automatically depending on the driving situations. A similar approach is developed in [Li et al., 2020] where the computation of $\alpha$ takes into consideration many factors: avoidance of lane departure, excessive steering, etc, to deal with lane following in case of tire blowout. Note that the main difference between the presented works cited above is how to determine the fusion parameter $\alpha$ in order to realize the assistance objective. All this interesting studies have motivated us to design an Advanced Driving Assistance System ($ADAS$). For that, this chapter deals with the development of $ADAS$ systems considering many control objectives for different driving situations. These systems aim to :

- Assist the driver in an intuitive way with high performance and efficiency.
- Guarantee safety while driving and realize an intuitive comfort for the driver in case of assistance.
- Keep stability of the switching when fusion of two control inputs.

Figure 4.1 summarizes the contributions of this chapter. It is composed of two sub-blocks, given as:

- Sub-block A: Design of an Advanced Driving Assistance System ($ADAS$) for lane keeping purpose through the Active Front Steering ($AFS$) in semi-autonomous vehicles, based on the $LPV/\mathcal{H}_\infty$ and the Super-Twisting Sliding Mode $STSM$ control techniques using steer-by-wire system. Then, a comparison is done between the two control approaches. However, this method can be adapted to overcome more complex maneuvers (following trajectories for overtaking, intersections, etc).
- Sub-block B: Development of centralized and decentralized multilayer Advanced Driving Assistance Systems ($ADASs$) involving Active Front Steering

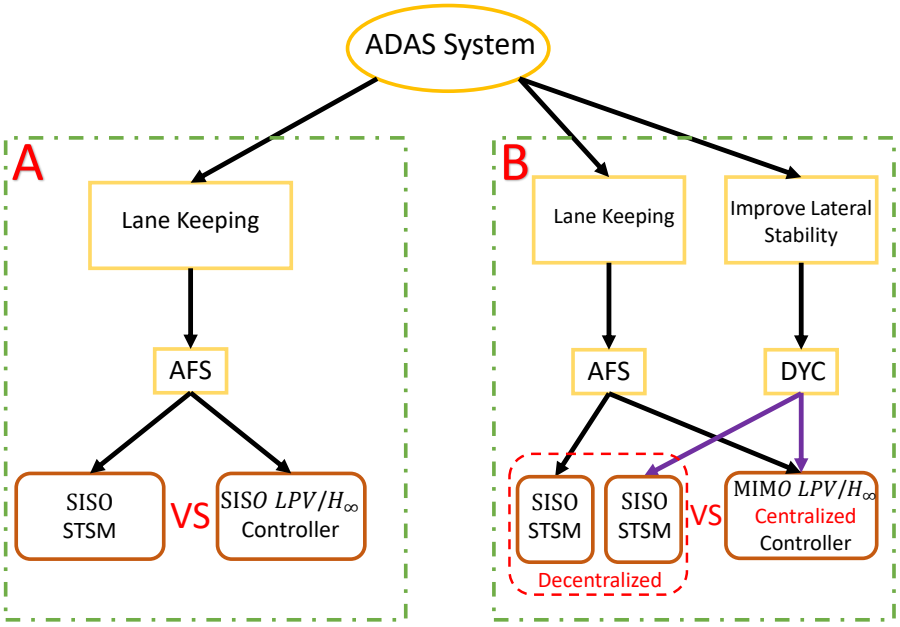


Figure 4.1 – General Architecture of the proposed Advanced Driving Assistance System.

($AFS$) for the lane keeping maneuver, and Direct Yaw Control ($DYC$) for the lateral stability improvement by using the $LPV/\mathcal{H}_\infty$ and the Super-Twisting Sliding Mode ($STSM$) control techniques respectively. Therefore, a comparison is done between the centralized and decentralized control architectures.

Finally, The proposed Sub-block A and B are validated by using Matlab/Simulink with a complete nonlinear model of the vehicle validated on "*SCANeR Studio*" (OKtal) professional simulator.

## 4.2 Control Synthesis Model

The vehicle bicycle model represented in the Section 1.2.2 is a linear vehicle model. For a road adherence coefficient $\mu = 1$ and side slip angle $\beta = \frac{\dot{y}}{\dot{x}}$, this model can be written as in the "Plant P" (equation 4.1). Note that this model is a $LPV$ model, with two variables being the vehicle side-slip angle and the yaw angle. It is usually used as reference model to suit the control problem of this work and it is given by the following system:

$$Plant\ P: \begin{cases} \dot{\beta} = -\frac{C_f+C_r}{mV_x}\beta - (1 + \frac{l_fC_f - l_rC_r}{mV_x^2})\dot{\psi} \\ \quad + \frac{C_f}{mV_x}\delta_{sw-c}, \\ \ddot{\psi} = -\frac{l_fC_f - l_rC_r}{I_z}\beta - \frac{l_f^2C_f + l_r^2C_r}{I_zV_x}\dot{\psi} \\ \quad + \frac{l_fC_f}{I_z}\delta_{sw-c} + \frac{1}{I_z}M_z, \end{cases} \tag{4.1}$$

where $\beta$ and $\dot{\psi}$ are respectively the vehicle side-slip angle and the vehicle yaw rate. $I_z$ is the vehicle yaw moment of inertia, $V_x$ is the vehicle longitudinal speed and

finally $\delta_{sw-c}$ and $M_z$ are the $AFS$ and the $DYC$ inputs respectively. The remaining notations of these equations and the vehicle parameters used for simulation are given in Tables 1 3. Even though these equations are valid when the vehicle operates in the stable region, they are sufficient and recommended to synthesize a robust controller. The state space representation of the *Plant* $P$ can be formalized as in (4.2), where $X = [\beta, \dot{\psi}]^T$ is the state vector, $U = [\delta_{sw-c}, M_z]^T$ is the control input. The elements of the state matrix $A \in IR^{2\times2}$ and the input matrix $B \in IR^{2\times2}$ are formalized in Appendix .2.

$$\dot{X} = \begin{bmatrix} \dot{\beta} \\ \ddot{\psi} \end{bmatrix} = \underbrace{\begin{pmatrix} a_{11} & a_{12} \\ a_{21} & a_{22} \end{pmatrix}}_{A} \begin{bmatrix} \beta \\ \dot{\psi} \end{bmatrix} + \underbrace{\begin{pmatrix} b_{11} & b_{12} \\ b_{21} & b_{22} \end{pmatrix}}_{B} \begin{bmatrix} \delta_{sw-c} \\ M_z \end{bmatrix} \tag{4.2}$$

## 4.3 Design of ADAS system (A)

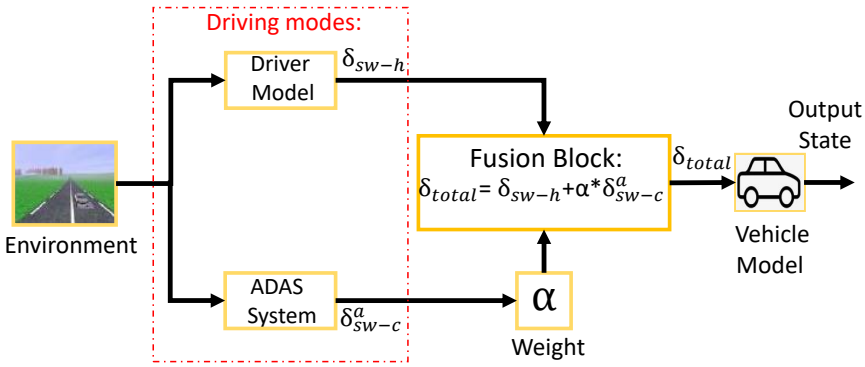


Figure 4.2 – Architecture of the Advanced Driving Assistance System.

Figure 4.2 shows the block diagram of the advanced driving assistance system ($ADAS$) developed in the following, to realize the lane keeping (sub-block A, see Figure 4.1). The main components are: the Fusion Block and the Driving Modes detailed in the following.

***Fusion block:***
The aim of the fusion block is to calculate the final steering wheel angle to the vehicle model. In the case of the development of $ADAS$ system using the Super-Twisting Sliding Mode ($STSM$) control approach, the total steering wheel angle is given as:

$$\delta_{total} = \delta_{sw-h} + \alpha * \delta^a_{sw-c}, \tag{4.3}$$

where $\delta_{total}$, $\delta_{sw-h}$ and $\delta^a_{sw-c}$ are the total steering wheel angle, steering wheel angles of human driver and $ADAS$ system respectively. $\alpha$ is an external parameter multiplied by the assistance steering wheel angle $\delta^a_{sw-c}$. It represents the percentage of assistance added by the driving assistance system to the driver's input. $\alpha$ is

bounded in [0,1], calculated depending on a decision layer developed in the following. $\alpha = 1$: for full assistance and $\alpha = 0$: for zero assistance.

In the case of the development of $ADAS$ system using the $LPV/\mathcal{H}_\infty$ control approach, the total steering wheel angle is given as:

$$\delta_{total} = \delta_{sw-h} + \delta^a_{sw-c}, \tag{4.4}$$

where $\alpha$ is an internal parameter implicitly expressed in $\delta^a_{sw-c}$ and figured by a time-varying scheduling gain $\rho$ discussed later in the decision layer.

***Driving Modes:***

a) Driver Model:
The Driver Model developed in Section 1.3.2.2 is used to represent the driver in the loop (human in-the-loop). His steering input will be noted as $\delta_{sw-h}$.

b) ADAS System:
The $ADAS$ system is a controller developed to assist the driver and help him during a lane keeping maneuver in order to avoid a dangerous situation. Two control approaches are detailed in the following to develop the $ADAS$ system:

- $LPV/\mathcal{H}_\infty$ control approach.
- Super-Twisting Sliding Mode ($STSM$) control approach.

### 4.3.1 $LPV/\mathcal{H}_\infty$ control approach

In this section, we present a detailed description of the development of the $ADAS$ system based on $LPV/\mathcal{H}_\infty$ approach. The optimal $\mathcal{H}_\infty$ theory based on offline Linear Matrix Inequality (LMI) optimal solutions, in the framework of $LPV$ systems is used to synthesis the controller of this $ADAS$ system. The global multilayer architecture is shown in the Figure 4.3. In the control layer, the output variable i.e the vehicle yaw rate $\dot{\psi}$ is fed-back from the nonlinear vehicle model and is controlled through an optimal $SISO\ LPV/\mathcal{H}_\infty$ controller, in order to realize a trajectory following. For that, a reference yaw rate generator is used to give the desired yaw rate $\dot{\psi}_{ref}$.

***Yaw rate generator at a look-ahead distance:***
The reference yaw rate generator is developed at a look-ahead distance $l_s$ in front of the vehicle, in order to generate a coherent yaw-rate reference $\dot{\psi}_{ref}$ to the $SISO\ LPV/\mathcal{H}_\infty$ controller for the trajectory following purpose. This controller aims that $\dot{\psi}$ follows $\dot{\psi}_{ref}$ in order to keep the lane with a high accuracy. For that, the yaw rate generator uses the current vehicle's speed $V_x$ and the information from the map matching $e_{y-l_s}$ to calculate the yaw rate reference $\dot{\psi}_{ref}$. Refer to [Tan and Huang, 2014], $\dot{\psi}_{ref}$ can be approximated as:

$$\dot{\psi}_{ref} = \frac{-2V_x e_{y-l_s}}{l_s^2} \tag{4.5}$$

where $e_{y-l_s}$ is the vehicle lateral error at a look-ahead distance $l_s$.

In addition, $\rho$ is a time-varying scheduling gain/parameter that schedules the assistance objective of the $SISO\ LPV/\mathcal{H}_\infty$ controller. $\rho$ is implicitly expressed in $\delta^a_{sw-c}$ which will be added to the $\delta_{sw-h}$ (see Figure 4.3). Then, a decision layer (the higher layer) is developed to monitor the driver's behavior. It sends the value of scheduling parameter $\rho$, based on the parameter $\lambda$ (discussed later). $\lambda$ is function of the lateral error ($e_y$) and driver's availability ($DA$) (see Figure 4.3). So, based on these information, the $SISO\ LPV/\mathcal{H}_\infty$ controller generates the control steering angle $\delta_{sw-c}$ as an assistance input, while considering actuators constraints (saturation and cut-off frequencies) in the actuator layer.

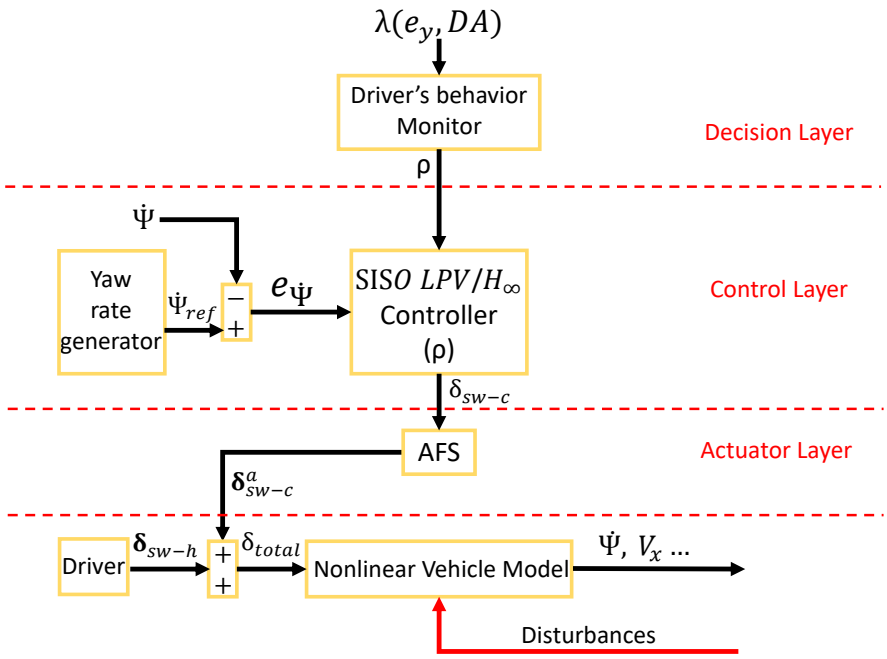


Figure 4.3 – $LPV/\mathcal{H}_\infty$ ADAS system Architecture.

#### 4.3.1.1 Overview on $LPV/\mathcal{H}_\infty$ control approach

The $LPV/\mathcal{H}_\infty$ control approach is a control technique used to add robustness on a system against disturbances. This control technique is applied to $LTI$ and $LPV$ systems. The aim is to find a stabilizing controller that minimizes the effect of an input disturbance $w(t)$ on a (weighted) controlled output $z(t)$. The General architecture of the $\mathcal{H}_\infty$ control technique is given in the Figure 4.4. Figure 4.4 shows the plant $P(S)$ to be controlled, the input $W_i(S)$ and output $W_o(S)$ weighting dynamic functions, and the $\mathcal{H}_\infty$ controller $K_{\mathcal{H}_\infty}(S)$ to be developed ($S$ is the Laplace transformation). The open-loop system formed by the interconnection of $P(S)$, $W_i(S)$, and $W_o(S)$ is called the generalized plant $\Sigma_g(S)$. In our present work, $P(S)$ represents an $LTI$ vehicle model, and $W_i(S)$ and $W_o(S)$ are scheduled $LPV$ filters. Thus, $\Sigma_g(S)$ is a $LPV$ system. The closed-loop system formed by the interconnection

of $\Sigma_g(S)$ and $K_{\mathcal{H}_\infty}(S)$ is called $C_l(S)$.

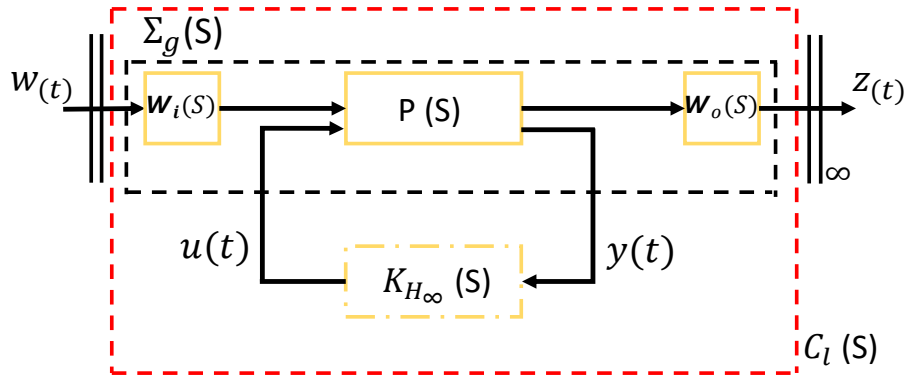


Figure 4.4 – $\mathcal{H}_\infty$ control Architecture (modified from [Shtessel et al., 2014])

Let's consider the generalized system $\sum_g$ and the controller $K_{\mathcal{H}_\infty}$ are Linear time-invariant $LTI$. The $\mathcal{H}_\infty$ control design consists to find the controller $K_{\mathcal{H}_\infty}$ that minimizes the $\mathcal{H}_\infty$ norm of the closed-loop system $C_l(S)$ as given in the following equation:

$$||C_l(S)||_\infty = sup_{\omega\in\Re}\bar{\sigma}(C_l(j\omega)) < \gamma, \tag{4.6}$$

where $\bar{\sigma}$ is the largest singular value, and $\gamma$ is the attenuation level. The $\mathcal{H}_\infty$ norm is the maximal gain of the frequency response of the system. It is also called the worst case attenuation level in the sense that it measures the maximum amplification that the system can deliver on the whole frequency set. For $SISO$ (respectively $MIMO$) systems, it represents the maximal peak value on the Bode magnitude (respectively singular value) plot of $C_l(j\omega)$; in other words, it is the largest gain if the system is fed by harmonic input signal [Sename et al., 2013]. More information about the $\mathcal{H}_\infty$ control are presented in [Zhou et al., 1996], [Apkarian et al., 1995], [Apkarian and Gahinet, 1995] and [Poussot-Vassal, 2008].

Now, let consider a $LPV$ system formulated by its generalized form $\sum_g$, such as:

$$\Sigma_g(\rho): \begin{bmatrix} \dot{x} \\ z \\ y \end{bmatrix} = \begin{bmatrix} A(\rho) & B_1(\rho) & B_2 \\ C_1(\rho) & D_{11}(\rho) & D_{12} \\ C_2 & D_{21} & 0 \end{bmatrix} \begin{bmatrix} x \\ w \\ u \end{bmatrix}, \tag{4.7}$$

where $x$ includes all the state variables of the system, $w$ is the exogenous input vector, $u$ represents the control inputs, $y$ is the measurement vector fed-back to the controller and $z$ is the weighted controlled output vector. $A$, $B_1$, $B_2$, $C_1$, $C_2$, $D_{11}$, $D_{12}$, and $D_{22}$ are known matrices with finite dimensions. $\rho$ is the vector of the varying parameters, it is known and bounded. Without loss of generality, we consider the case where $\rho = \{\rho_1, \rho_2\}$, since it is easy to understand and it will be used in the following section.
The $LPV/\mathcal{H}_\infty$ problem consists in finding the controller $K_{LPV/\mathcal{H}_\infty}(\rho_1, \rho_2)$, scheduled by the parameters $\rho_1$ and $\rho_2$, such that:

$$K_{LPV/\mathcal{H}_\infty}(\rho): \begin{bmatrix} \dot{x}_c \\ u \end{bmatrix} = \begin{bmatrix} A_c(\rho) & B_c(\rho) \\ C_c(\rho) & 0 \end{bmatrix} \begin{bmatrix} x_c \\ y \end{bmatrix}, \tag{4.8}$$

$$\begin{bmatrix} A(\rho)X + XA(\rho)^T + B_2\widetilde{C}(\rho) + \widetilde{C}(\rho)^T B_2^T & (*)^T & (*)^T & (*)^T \\ \widetilde{A}(\rho) + A(\rho)^T & YA(\rho) + A(\rho)^T Y + \widetilde{B}(\rho)C_2 + C_2^T\widetilde{B}(\rho)^T & (*)^T & (*)^T \\ B_1(\rho)^T & B_1(\rho)^T Y + D_{21}^T\widetilde{B}(\rho)^T & -\gamma I & (*)^T \\ C_1(\rho)X + D_{12}\widetilde{C}(\rho) & C_1(\rho) & D_{11}(\rho) & -\gamma I \end{bmatrix} < 0;$$

$$\begin{bmatrix} X(\rho) & I \\ I & Y(\rho) \end{bmatrix} > 0. \tag{4.9}$$

which minimizes the $\mathcal{H}_\infty$ norm of the closed-loop $LPV$ system formed by the interconnection of equations (4.7) and (4.8).

***Problem resolution:*** *$LMI$* ***based*** *$LPV/\mathcal{H}_\infty$:*
There are many approaches that exist in the literature to solve this problem such as: polytopic, gridding and Linear Fractional Transformation LFT [Zin, 2005]. In the present work, a polytopic approach (see [Scherer et al., 1997]) has been used for controller synthesis. Thanks to the Bounded Real Lemma ($BRL$) extended to $LPV$ systems, this controller can be found. According to the system 4.7 and after a change of basis presented in [Scherer et al., 1997], a non conservative $LMI$ that expresses the same problem as $BRL$ is formulated in (4.9) and a Semi-Definite Program ($SDP$) has been used to solve these inequalities equations (see [Doumiati et al., 2013]), while minimizing $\gamma$ for $\rho \in \Omega = [\underline{\rho_1}, \overline{\rho_1}]\ X\ [\underline{\rho_2}, \overline{\rho_2}]$.

The aim of the polytopic approach is to find the $\widetilde{A}$, $\widetilde{B}$ and $\widetilde{C}$ by using a common Lyapunov function, i.e common $X > 0$ and $Y > 0$ at each vertex of the polytope function of $\rho \in \Omega$. Noting that the number of vertex is 4 ($2^n$) where n is the number of parameters $\rho_i$. Thus, the solution can be obtained by the resolution of system (4.10) at each vertex of the convex hull $\{\omega_1 = (\underline{\rho_1}, \underline{\rho_2}), \omega_2 = (\overline{\rho_1}, \underline{\rho_2}), \omega_3 = (\underline{\rho_1}, \overline{\rho_2}), \omega_4 = (\overline{\rho_1}, \overline{\rho_2})\}$ of the convex hull $\Omega$:

$$\begin{cases} C_c(\rho) &= \widetilde{C}(\rho)M^{-T} \\ B_c(\rho) &= N^{-1}\widetilde{B}(\rho) \\ A_c(\rho) &= N^{-1}(\widetilde{A}(\rho) - YA(\rho)X - NB_c(\rho)C_2X \\ &- YB_2(\rho)C_c(\rho)M^{-T})M^{-T} \end{cases}, \tag{4.10}$$

where $M(\rho)$ and $N(\rho)$ are defined by the user so that $M(\rho)N(\rho)^T = I - X(\rho)Y(\rho)$. See [Scherer et al., 1997] for more details on the computation solution. Therefore, referring to the polytopic approach, the final controller, $K_{LPV/\mathcal{H}_\infty}(\rho)$, is the summation of each convex controller calculated on each vertex of the polytope [Apkarian et al., 1995] such as:

$$\begin{aligned} K_{LPV/\mathcal{H}_\infty}(\rho_1, \rho_2) = \alpha_1 K_{\mathcal{H}_\infty}(\omega_1) + \alpha_2 K_{\mathcal{H}_\infty}(\omega_2) \\ +\alpha_3 K_{\mathcal{H}_\infty}(\omega_3) + \alpha_4 K_{\mathcal{H}_\infty}(\omega_4), \end{aligned} \tag{4.11}$$

where $\sum_{i=1}^{i=4} \alpha_i(\rho_1, \rho_2) = 1$; $\alpha_i(\rho_1, \rho_2) > 0$. The polytopic coordinates $\alpha_i(\rho_1, \rho_2)$ weight the controllers on the vertices to construct the final controller (see Figure 4.5). $\alpha_i(\rho_1, \rho_2)$ are instantly evaluated by the following equations (the Matlab

function"*polydec*" (Robust Control Toolbox) is also useful to evaluate polytopes with more vertices):

$$\begin{aligned} \alpha_1 &= \frac{\overline{\rho_1}-\rho_1}{\overline{\rho_1}-\underline{\rho_1}}.\frac{\overline{\rho_2}-\rho_2}{\overline{\rho_2}-\underline{\rho_2}}; \quad & \alpha_3 &= \frac{\overline{\rho_1}-\rho_1}{\overline{\rho_1}-\underline{\rho_1}}.\frac{\rho_2-\underline{\rho_2}}{\overline{\rho_2}-\underline{\rho_2}}; \\ \alpha_2 &= \frac{\rho_1-\underline{\rho_1}}{\overline{\rho_1}-\underline{\rho_1}}.\frac{\overline{\rho_2}-\rho_2}{\overline{\rho_2}-\underline{\rho_2}}; \quad & \alpha_4 &= \frac{\rho_1-\underline{\rho_1}}{\overline{\rho_1}-\underline{\rho_1}}.\frac{\rho_2-\underline{\rho_2}}{\overline{\rho_2}-\underline{\rho_2}}. \end{aligned} \tag{4.12}$$

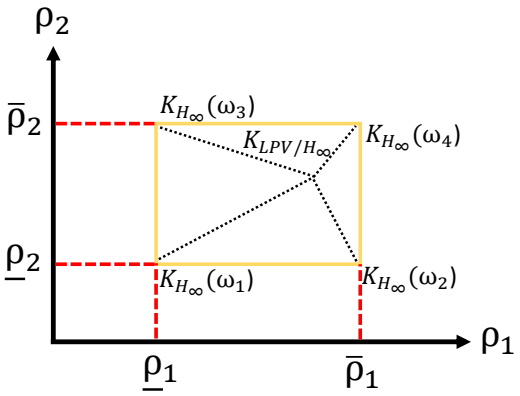


Figure 4.5 – Polytopic $\mathcal{H}_\infty$ controller

#### 4.3.1.2 Control Layer synthesis: $LPV/\mathcal{H}_\infty$ controller

The control layer architecture is drawn in Figure 4.6. As a standard $\mathcal{H}_\infty$ structure, it contains the controller $K_{LPV/\mathcal{H}_\infty}(\rho)$ to be synthesized, and the generalized plant $\sum_g$, where $\rho(\lambda)$ is a weighted parameter calculated by the decision making monitor to adapt the controller dynamics and performances according to the driving conditions.

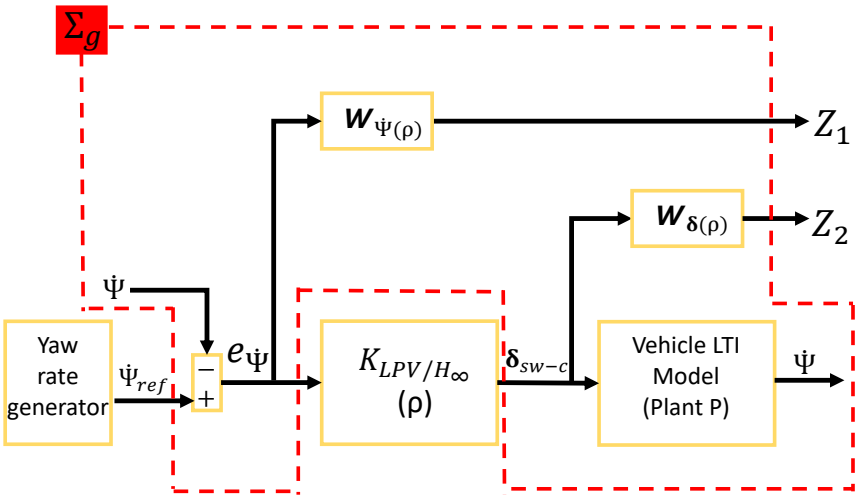


Figure 4.6 – Control layer Architecture.

The controller $K_{LPV/\mathcal{H}_\infty}(\rho)$ has as input, the error between the desired yaw rate on

trajectory (given by the reference yaw rate generator) and the actual yaw rate of the vehicle ($e_{\dot{\psi}}$=$\dot{\psi}_{ref}$-$\dot{\psi}$). Since the $\mathcal{H}_\infty$ approach is a model-based robust control technique, the actual yaw rate is calculated based on the $LTI$ vehicle model given in 4.2 (*Plant P*), while considering $M_z = 0$ and thus reducing $B$ to its first column $B_1$, because we aim to develop an assistance system through $\delta_{sw-c}$.
The state representation of the *Plant P* of the generalized plant $\sum_g$ is expressed in 4.13. It has $\delta_{sw-c}$ as control input; and the actual yaw rate $\dot{\psi}$, as output to be controlled. The elements of the state matrix $A \in IR^{2\times2}$ and the input matrix $B_1 \in IR^{2\times1}$ are formalized in Appendix .2.

$$\dot{X} = \begin{bmatrix} \dot{\beta} \\ \ddot{\psi} \end{bmatrix} = \underbrace{\begin{pmatrix} a_{11} & a_{12} \\ a_{21} & a_{22} \end{pmatrix}}_{A} \begin{bmatrix} \beta \\ \dot{\psi} \end{bmatrix} + \underbrace{\begin{pmatrix} b_{11} \\ b_{21} \end{pmatrix}}_{B_1} \delta_{sw-c} \tag{4.13}$$

The remaining subsystems of $\sum_g$ i.e. the weighting functions $W_{\dot{\psi}}(\rho)$ and $W_\delta(\rho)$ of Figure 4.6 are defined to characterize the performance objective $Z_1$ and the actuators' constraint $Z_2$ (the dynamics of the steering wheel actuator, given in Subsection 4.3.1.4, are neglected during the controller design process). The general form of these weights [Doumiati et al., 2014] is given by the following (numerical values are given in Section 4.3.3, since they depend on the simulated vehicle and integrated actuators):

- $W_{\dot{\psi}}(\rho)$ weights the yaw rate control objective:

$$W_{\dot{\psi}}(\rho) \;=\; \rho\frac{s/M_1 + 2\pi f_1}{s + 2\pi f_1 A_1}, \tag{4.14}$$

where $M_1$ is sufficiently high for a large robustness margin, and $A_1$ is the tolerated tracking error on $e_{\dot{\psi}}$. $W_{\dot{\psi}}(\rho)$ is shaped to reduce the yaw rate error in the range of frequencies below a roll-off frequency $f_1$ where the vehicle operates [Heißing and Ersoy, 2010]. $W_{\dot{\psi}}(\rho)$ is linearly parametrized by the varying parameter $\rho$, where $\rho \in \left\{\underline{\rho} \leq \rho \leq \overline{\rho}\right\}$ ($\underline{\rho}$ and $\overline{\rho}$ are constants representing the lower and higher values of $\rho$). When $\rho = \overline{\rho}$, the performance objective $e_{\dot{\psi}}$ is prioritized ($ADAS$ system is switched-on), on the contrary, when $\rho = \underline{\rho}$, $e_{\dot{\psi}}$ is relaxed (driver navigates correctly), and the assistance is deactivated.

- $W_\delta(\rho)$ weights the steering control input, $\delta_{sw-c}$:

$$W_\delta(\rho) \;=\; \frac{1}{\rho}\frac{s + 2\pi f_2/M_2}{\varepsilon_u s + 2\pi f_2}, \tag{4.15}$$

where $M_2$ is sufficiently high for a large robustness margin, $\varepsilon_u$ is concerned with the noise rejection at high frequencies and $f_2$ is the filter's frequency. This filter forces the steering system to act at this frequency in order to avoid driver annoyance. This filter design is inspired from [Atoui et al., 2021]. The novelty here is the dependency

of $W_\delta(\rho)$ on $\rho$, which allows to promote or penalize (relax) the steering depending on all possible situations. For instance, when $\rho = \overline{\rho}$, the driver's behaviors is not adequate, and the $AFS$ is promoted to maintain the lane keeping. When $\rho = \underline{\rho}$, that means the driver acts appropriately, and the $AFS$ is penalized (relaxed). In this case, the driver is the only responsible of driving.

After determining the subsystems of the Figure 4.6, the $\mathcal{H}_\infty$ control technique is applied in order to minimize the controlled outputs $Z_1$ and $Z_2$ for any exogenous input. $Z_1$ and $Z_2$ become the output of the plant $\sum_g$ to be controlled. For more information about the robust $LPV/\mathcal{H}_\infty$ theory, see [Sename et al., 2013] and [Gu et al., 2005].
Interconnection between $\sum_g$ subsystems is done using "*sysic*" Matlab function (Robust Control Toolbox). Since the generalized plant $\sum_g$ is $LPV$ [Apkarian et al., 1995], it can be formulated as:

$$\Sigma_g(\rho) : \begin{bmatrix} \dot{x} \\ z \\ y \end{bmatrix} = \begin{bmatrix} A(\rho) & B_1(\rho) & B_2(\rho) \\ C_1(\rho) & D_{11}(\rho) & D_{12}(\rho) \\ C_2 & D_{21} & 0 \end{bmatrix} \begin{bmatrix} x \\ w \\ U \end{bmatrix}, \tag{4.16}$$

where $\rho$ is time-varying scheduling parameter, $x$ includes the state variables of *Plant* $P$ and of the weighting functions, $w = [\dot{\psi}_{ref}]^T$ is the exogenous input vector that contains the reference state, $U = [\delta_{sw-c}]^T$ represents the control inputs, $y = [\dot{\psi}]^T$ is the measurement vector fed-back to the controller, and $z = [Z_1, Z_2]^T$ is the weighted controlled output vector of the generalized plant $\sum_g$.
Note that the matrices $B_2$, and $D_{12}$ depend on $\rho$, which is not compatible with $\mathcal{H}_\infty$ requirements for polytopic systems. However, this issue is relaxed using some filter on the control input [Apkarian and Gahinet, 1995].

***Problem resolution:** $LMI$ **based** $LPV/\mathcal{H}_\infty$**:***
The $LMI$ based $LPV/\mathcal{H}_\infty$ problem consists in finding the controller $K_{LPV/\mathcal{H}_\infty}(\rho)$, scheduled by the parameter $\rho$, such that:

$$K_{LPV/\mathcal{H}_\infty}(\rho) : \begin{bmatrix} \dot{x}_c \\ u \end{bmatrix} = \begin{bmatrix} A_c(\rho) & B_c(\rho) \\ C_c(\rho) & 0 \end{bmatrix} \begin{bmatrix} x_c \\ y \end{bmatrix}, \tag{4.17}$$

This controller aims to minimize the $\mathcal{H}_\infty$ norm of the closed-loop $LPV$ system formed by the equations (4.16) and (4.17). This controller can be found using the development in the Section 4.3.1.1. A Semi-Definite Program ($SDP$) (Yalmip/Sedumi solver) has been used to solve the inequalities equations given in (4.9) (see [Doumiati et al., 2013]), while minimizing $\gamma$ for $\rho = \{\underline{\rho}, \overline{\rho}\}$ ($\gamma_{optimal} = 1.15$).

According to the polytopic approach, the final controller, $K_{LPV/\mathcal{H}_\infty}(\rho)$, is the summation of each convex controller calculated at the vertices $\{\underline{\rho}, \overline{\rho}\}$ [Apkarian et al., 1995] such as:

$$K_{LPV/\mathcal{H}_\infty}(\rho) = \tfrac{(\overline{\rho}-\rho)}{(\overline{\rho}-\underline{\rho})} K_{\mathcal{H}_\infty}(\underline{\rho}) + \tfrac{(\rho-\underline{\rho})}{(\overline{\rho}-\underline{\rho})} K_{\mathcal{H}_\infty}(\overline{\rho}), \tag{4.18}$$

where $K_{\mathcal{H}_\infty}(\underline{\rho})$ and $K_{\mathcal{H}_\infty}(\overline{\rho})$ are the solutions of the polytopic problem at each vertex.

#### 4.3.1.3 Decision Layer: $\rho$ calculation

The decision layer is developed to adjust the controller according to the driver's behavior. This layer delivers the scheduling parameter $\rho$ depending on the parameter $\lambda$.
Let us introduce the parameter $\lambda$ function of the lateral error ($e_y$) with respect to the trajectory at the center of gravity of the vehicle ($CG$) and the driver's availability ($DA$). $DA$ is a dynamic variable related to the driver, and can be calculated based on different factors: driver's eyes analysis, driver's head position, level of driver's sleepiness, etc. Therefore, the calculation of diver's availability is not in the scope of this work and it is considered as an input to this layer. $\lambda$ is expressed as:

$$\lambda = |e_y| + (1 - DA) \tag{4.19}$$

As shown in the equation 4.19, $\lambda$ depends on $e_y$ and $DA$. Two rules for $\lambda$ are defined as follows:

- If the driver is in normal driving situation, $\lambda \leq \underline{\lambda}$, that means $|e_y| \leq \underline{e_y}$ and $DA$=1, then no need to assist the driver during this driving maneuver, and the assistance system should be switched-off. The driver is in normal driving situation and he is available.

- If the driver operates wrong, $\lambda \geq \overline{\lambda}$, that means $|e_y| \geq \overline{e_y}$ and/or $DA$ simply low, then the $ADAS$ System should be switched-on in order to compensate the driver's error and unavailability.

Referring to this analysis, the scheduled gain $\rho$ feeds the $LPV/\mathcal{H}_\infty$ controller with the sufficient information about the weights to be pushed or attenuated. The relation between $\rho$ and $\lambda$ is presented by a "*sigmoid*" function (4.20) (see Figure 4.7).

$$\rho = \underline{\rho} + \frac{\overline{\rho} - \underline{\rho}}{1 + e^{-\frac{8}{\overline{\lambda} - \underline{\lambda}}(\lambda - \frac{\overline{\lambda} + \underline{\lambda}}{2})}} \tag{4.20}$$

#### 4.3.1.4 Actuator Layer

The actuator layer includes the $AFS$ actuator used to generate the physical input of the system. The $AFS$ is an electrical motor which provides the added steering angle $\delta^a_{sw-c}$. In order to ensure that the $AFS$ actuator is able to provide the added steering angle demanded by the controller $\delta_{sw-c}$, the $AFS$ is modeled as follows:

$$\dot{\delta}^a_{sw-c} = 2\pi f_3(\delta_{sw-c} - \delta^a_{sw-c}) \tag{4.21}$$

where $\delta^a_{sw-c}$ follows $\delta_{sw-c}$, $f_3$ is the actuator cut-off frequency. This actuator is bounded between $\left[-\delta^a_{sw-c,max}, +\delta^a_{sw-c,max}\right]$, with $\delta^a_{sw-c,max}$ the maximum amount of steering angle that can be added by the $AFS$ actuator for assistance purpose.

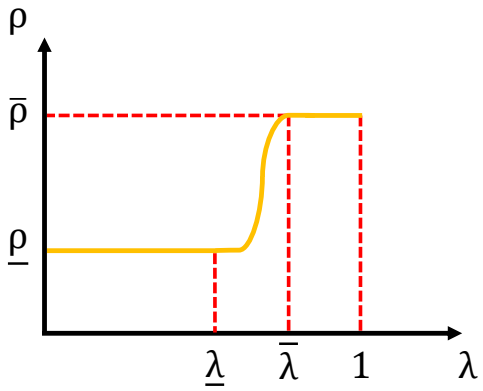


Figure 4.7 – Scheduling parameter $\rho$ function of the decision parameter $\lambda$

### 4.3.2 Super-Twisting Sliding Mode ($STSM$) control approach

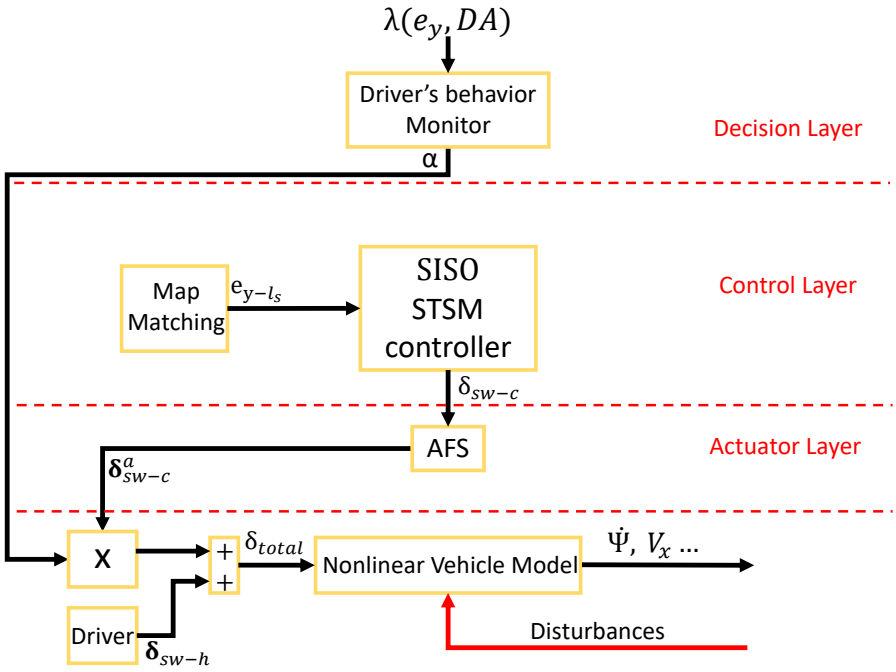


Figure 4.8 – Super-Twisting Sliding Mode ($STSM$) ADAS system Architecture.

In this section, the $ADAS$ system is developed based on the Super-Twisting Sliding Mode ($STSM$) control approach. By using this approach, we facilitate the controller development complexity and benefit from the robustness of the super-twisting algorithm. The global multilayer architecture is shown in the Figure 4.8. The main difference w.r.t the above approach is in the control layer, where the $AFS$ control input $\delta_{sw-c}$ is dedicated to control the lateral error at a look-ahead distance in order to realize a lane following. The decision layer is similar to the one of the first approach, where this layer generates the percentage of assistance figured by the parameter $\alpha$ based on $\lambda$. $\lambda$ depends on two criteria: lateral error ($e_y$) and driver's availability ($DA$). Finally, the actuator layer is developed to consider the actuators constraints.

#### 4.3.2.1 Control Layer synthesis: Super-Twisting Sliding Mode controller

The control layer consists of a $SISO$ $STSM$ controller that controls the lateral error at a look-ahead distance $l_s$ to realize a lane keeping. Thus, the $AFS$ is responsible of the control of the lateral error $e_y$. For that, the $STSM$ control technique developed in Section 1.4.2 is used to develop this controller. The control input is the steering wheel angle $\delta_{sw-c}$ for the lateral dynamics, it has the same form as $\delta_{sw-as}$ given in Section 1.4.2. Note that the $STSM$ control technique is one of the most robust control techniques that suit our control problem. Finally, the Map Matching bloc aims to localize the vehicle position on the reference map by calculating the value of the lateral error on a look-ahead distance $l_s$, w.r.t the trajectory.

#### 4.3.2.2 Decision Layer: $\alpha$ calculation

Similar to the decision layer in Section 4.3.1.3, the decision layer of the $STSM$ control approach monitors the driver's behaviors through $\lambda$ (function of the lateral error ($e_y$) and the driver's availability ($DA$)). This layer calculates the value of $\alpha$ depending on the parameter $\lambda$ given in 4.3.1.3. It sends instantly the value of $\alpha$ to the actuator layer in order to promote/attenuate the intervention of $ADAS$ system in the driving maneuver.

- When $\lambda \geq \overline{\lambda}$, the driver is no more available and distracted, then an assistance input is needed to be switched-on to compensate the driver's error, and $\alpha$ is equal to 1.

- When $\lambda \leq \underline{\lambda}$, $\alpha$ is equal to 0 and the $ADAS$ System is attenuated because the driver operates without any errors.

A "*sigmoid*" function (4.22) (see Figure 4.9) governs the relation between $\alpha$ and $\lambda$, to ensure a smooth and continuous variation of $\alpha$.

$$\alpha = \frac{1}{1 + e^{-\frac{8}{\overline{\lambda}-\underline{\lambda}}(\lambda - \frac{\overline{\lambda}+\underline{\lambda}}{2})}} \tag{4.22}$$

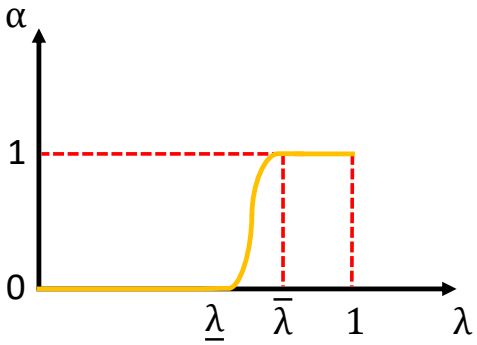


Figure 4.9 – Scheduling parameter $\alpha$

#### 4.3.2.3 Actuator Layer

The actuator layer developed in the Section 4.3.1.4, is used to generate the physical input $\delta^a_{sw-c}$ of the system.

### 4.3.3 Controllers' validation (A)

The proposed $SISO\ LPV/\mathcal{H}_\infty$ and $SISO$ Super-Twisting Sliding Mode ($STSM$) controllers are validated in this section. Validation is done by simulation using Matlab/Simulink with a complete nonlinear model of the vehicle, validated on "*SCANeR Studio*" (OKtal) simulator. Then, a comparison is done between the two controllers in order to show the difference in terms of performance and effectiveness of each control technique. The driver follows the track given in the Figure 4.10 trying to keep the lane. An $ADAS$ system is applied to assist and help the driver in the lane keeping process. The different parameters' numerical values of the two controllers used during the simulation are given in the Table 4.1.

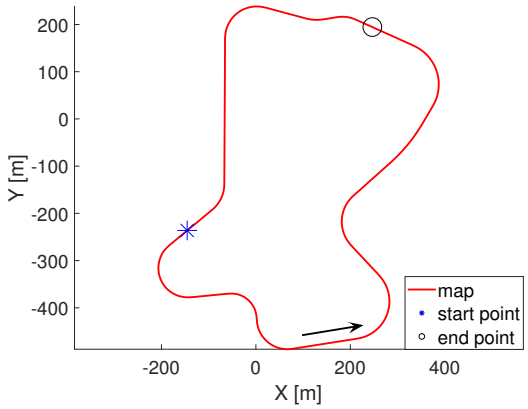


Figure 4.10 – Map of the tracked trajectory

Table 4.1 – Controller's Parameters for Simulation

| Parameters | Values |
|---|---|
| $M_1; M_2; A_1$ | $2; 1; 0.1 = 10\%$ |
| $f_1; f_2; f_3$ | $5\ Hz; 10\ Hz; 15\ Hz$ |
| $\underline{\rho}; \overline{\rho}$ | $0.01; 0.2$ |
| $\underline{e_y}; \overline{e_y}; \underline{\lambda}; \overline{\lambda}$ | $0.3; 0.5; 0.3; 0.5$ |
| $\delta^a_{sw-c,max}; \varepsilon_u; l_s$ | $5°; 0.01; 3$ |

#### 4.3.3.1 Simulation results

As mentioned before, this section is dedicated to validate and compare the proposed $SISO\ LPV/\mathcal{H}_\infty$ and the $SISO$ Super-Twisting Sliding Mode ($STSM$) controllers for a given scenario by using Matlab/Simulink. The scenario is defined in the way

that the driver realizes a path following maneuver at speed 60 $Km/h$ (see Figure 4.11) for the track given in the Figure 4.10. However, during this maneuver, sudden errors are injected on the driver's behavior between $35s$ and $50s$ and between $70s$ and $85s$ respectively, where the driver is no more available. The vehicle is deviated from the centerline of the road. Thus, an $ADAS$ system, represented by one of the two proposed controllers, is switched-on in order to compensate the driver's errors and avoid a dangerous situation. In this scenario, the comparison is done when the driver drives without $ADAS$ his vehicle (alone) and by integrating the proposed controllers i.e the $LPV/\mathcal{H}_\infty$ controller and the $STSM$ controller into the vehicle (driving with $ADAS$ system). This scenario shows the advantage of having an $ADAS$ system implemented in the vehicle for the lane keeping maneuver. The two proposed $ADAS$ system architectures monitor and supervise the vehicle situation and interact if necessary in order to compensate the inappropriate driver's action. The results are presented in the following to show the effectiveness of the developed $ADAS$ systems to help the driver during a lane keeping maneuver.

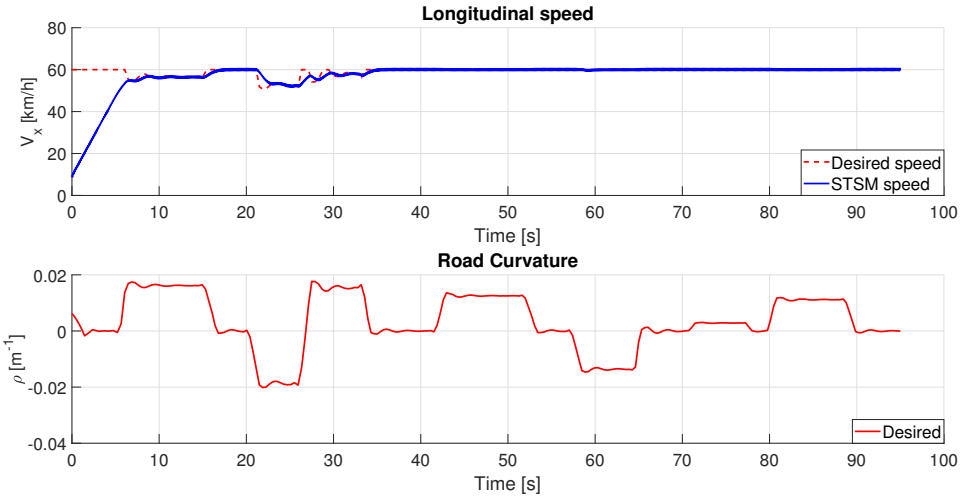


Figure 4.11 – The vehicle dynamic variables: speed and road curvature

The Figure 4.12 shows the lateral error w.r.t the trajectory of: driver without $ADAS$, driving with $ADAS$ $LPV/\mathcal{H}_\infty$ and driving with $ADAS$ $STSM$. As we can see, the error is injected at $35s$ on the driver's behavior and both $ADAS$ systems ($LPV/\mathcal{H}_\infty$ and $STSM$ controllers) diminish this error ($1m$) caused by the driver on the curvy road (see Figure 4.11). Thus, they have achieved the assistance goal with a high accuracy of lane keeping ($e_y$ between $-25cm$ and $20cm$, Figure 4.12). The two $ADAS$ systems are switched-on until t=$50s$, where $\lambda_i \geq \overline{\lambda}$ ($i = \{1 : ADAS{-}LPV/\mathcal{H}_\infty, 2 : ADAS{-}STSM\}$) because the driver is not available ($DA$=0) and the lateral error is more than $\overline{e_y}$ (see Figure 4.13). Remember that the $DA$ is assumed to be an input to our system that could be given by a diagnosis module in order to determine the driver's status with a delay of $0.5s$. Again at t=$70s$, an $ADAS$ system is still needed because there is a second error caused by the driver's behavior and $DA = 0$ again. The $ADAS$ systems assist the driver until

t=85$s$. At t=85$s$, the driver's behavior returned normal and he is available again to act on the vehicle's lateral control without any help.

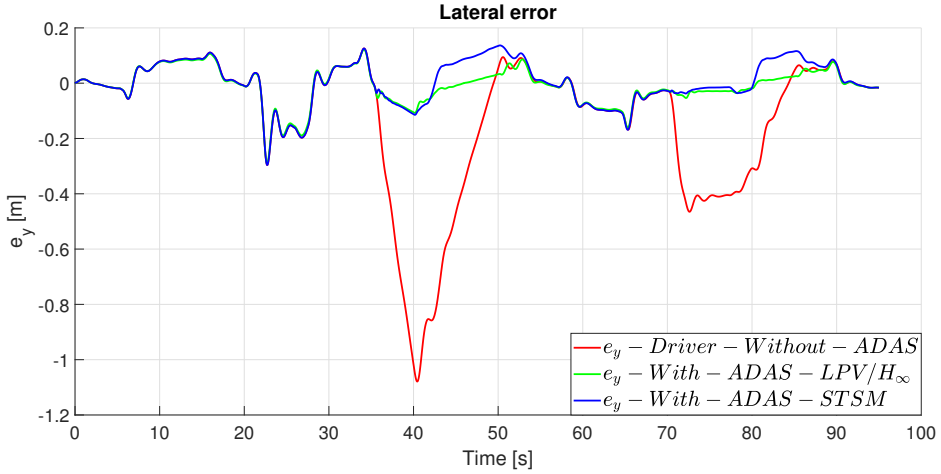


Figure 4.12 – The lateral error

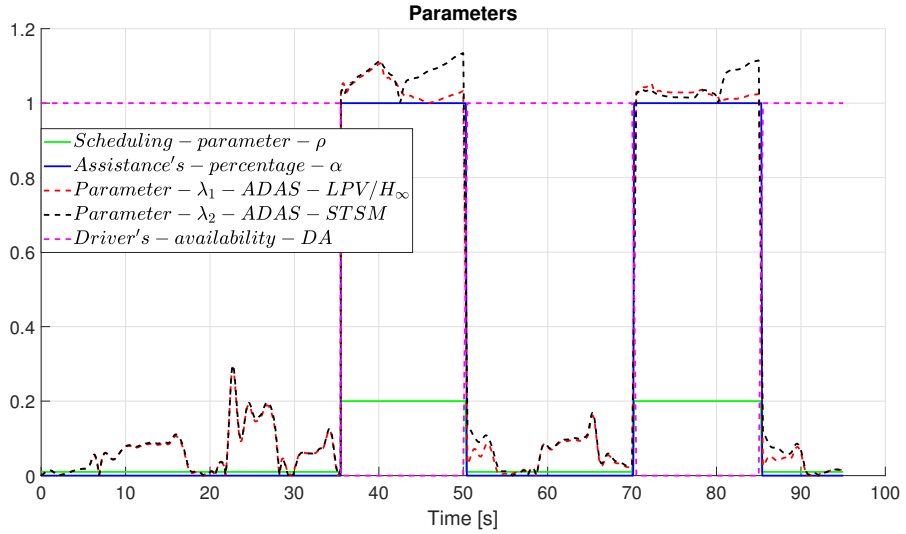


Figure 4.13 – The different parameters

These assistance systems can be explained by observing the decision layer of each $ADAS$ system architecture, in other words, the monitoring criterion $\lambda$ (function of $e_y$ and $DA$). Figures 4.13 and 4.14 show the two parameters $\lambda_1$ and $\lambda_2$, with the corresponding scheduling gain $\rho$ and the percentage of assistance $\alpha$ for the $LPV/\mathcal{H}_\infty$ and the $STSM$ $ADAS$ system architectures respectively, and, the driver's availability $DA$. For $\lambda_1 \geq \overline{\lambda}$ (resp. $\lambda_2 \geq \overline{\lambda}$), which means that the driver is not available and there is an error on his behavior, both $ADAS$ systems have switched-on to assist and help him, and remain the vehicle stable. When $\lambda_1 \geq \overline{\lambda}$, that means $DA = 0$ and $e_y$ is more than $\overline{e_y}$, (resp. $\lambda_2 \geq \overline{\lambda}$), especially between 35$s$ and 50$s$ and between 70$s$ and 85$s$, the scheduling gain $\rho$ of the $LPV/\mathcal{H}_\infty$ $ADAS$ system (resp. the percentage of assistance $\alpha$ of the $STSM$ $ADAS$ system) is set to $\rho = \overline{\rho}$

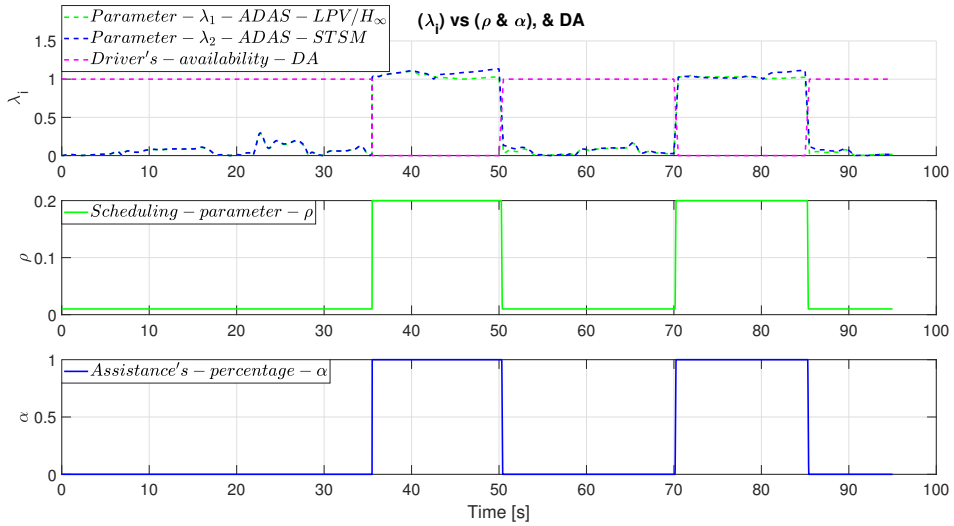


Figure 4.14 – $\lambda_i$ vs ($\rho$ & $\alpha$) & $DA$


Figure 4.15 – The different steering wheel angles

(resp. $\alpha = 1$), which activates the assistance. For the region, when $\lambda_1 \leq \underline{\lambda}$ (resp. $\lambda_2 \leq \underline{\lambda}$), the scheduling gain $\rho$ (resp. the percentage of assistance $\alpha$) is set to $\rho = \underline{\rho}$ (resp. $\alpha = 0$), which means the driver is available and acts correctly and the $ADAS$ system is Switched-off (see Fig. 4.14).
Based on this discussion, one can conclude that the $ADAS$ system is switched-on when it is needed in order to assist the driver depending on the driver's behavior. Refer to the Figures 4.12 and 4.14, the two $ADAS$ systems have almost the same behavior and they are able to help the driver by compensating his errors.

Figure 4.15 shows the driver steering angle $\delta_{sw-h}$ and the assistance $AFS$ steering angles $\delta_{sw-c}$ of both $ADAS$ system $LPV/\mathcal{H}_\infty$ and $STSM$ respectively on the steering wheels. Refer to this figure, both controllers are in conflict with the human

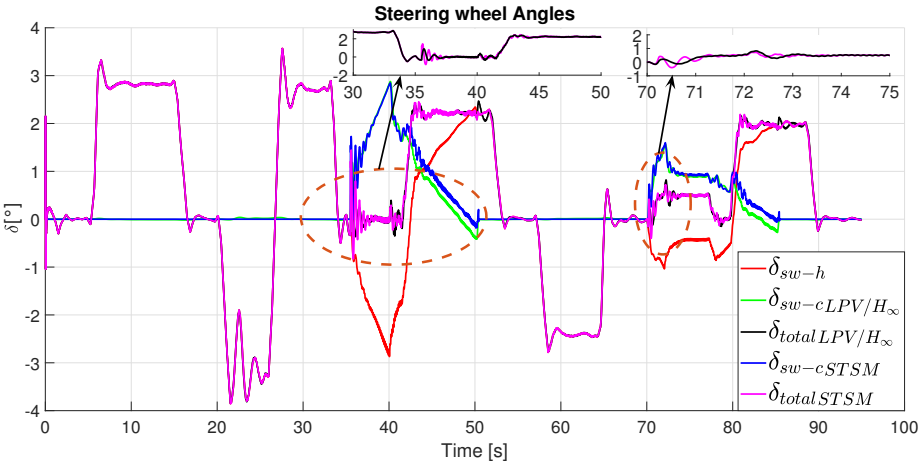


Figure 4.16 – The different total steering wheel angles

driver between $35s$ and $50s$ and between $70s$ and $85s$ in order to compensate his errors. In addition, we can notice that both controllers provide almost the similar steering angle (the green and blue curve have the same behavior), with some additional oscillations of $STSM$ controller compared to the $LPV/\mathcal{H}_\infty$ controller. However, $\delta_{sw-cLPV/H_\infty}$ and $\delta_{sw-cSTSM}$ have an opposite behavior w.r.t $\delta_{sw-h}$ (the red curve, Figure 4.15). To show the difference between the two controllers, both total steering angles, $\delta_{totalLPV/H_\infty}$ and $\delta_{totalSTSM}$, are presented in Figure 4.16. The oscillations appear more with the $STSM$ than the $LPV/\mathcal{H}_\infty$ controller, which correspond to the main known drawback of the $STSM$ approach. However, there are some oscillations in the $LPV/\mathcal{H}_\infty$ but with small peak values (see Figure 4.16). Figure 4.17 shows the different control inputs: the longitudinal $STSM$ motor torque in case of $ADAS$ $LPV/\mathcal{H}_\infty$ and $ADAS$ $STSM$; and the steering angle for the lateral $STSM$ and the $LPV/\mathcal{H}_\infty$ controllers for lateral displacement. Noting that the longitudinal displacement is achieved by a $STSM$ controller for both $ADAS$ system architectures. In addition, the $\delta_{totalLPV/H_\infty}$ and $\delta_{totalSTSM}$ are compared with the approximate steering angle $\delta_{approx}$ on the desired trajectory (Figure 4.17). $\delta_{approx}$ is given as:

$$\delta_{approx} = \rho^* * (l_f + l_r) \tag{4.23}$$

with $\rho^*$ the curvature of the desired trajectory, $l_f$ and $l_r$ the distances from the center of the vehicle to the front and rear wheels respectively. Finally, Figure 4.11 shows the longitudinal speed tracking of the desired one through the $STSM$ controller, the road curvature of the desired trajectory. Finally, Figure 4.18 shows the lateral and longitudinal accelerations. The lateral acceleration does not exceed the $\pm 4m/s^2$, which demonstrate a comfortable and stable driving zone, compared to the driving without $ADAS$. In addition, the actual longitudinal acceleration is pertinent ($< \pm 2m/s^2$) for a comfortable maneuver.

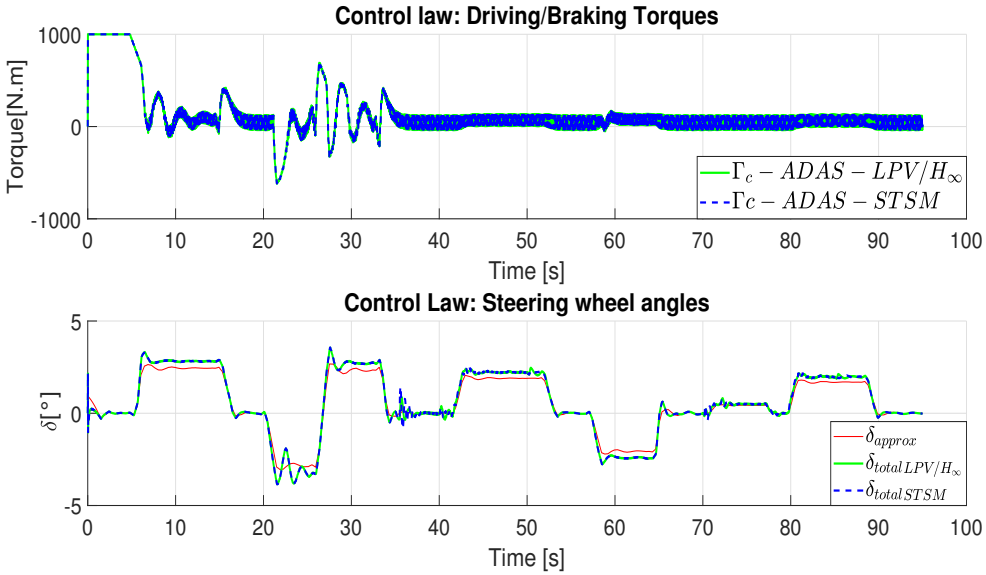


Figure 4.17 – The different control inputs

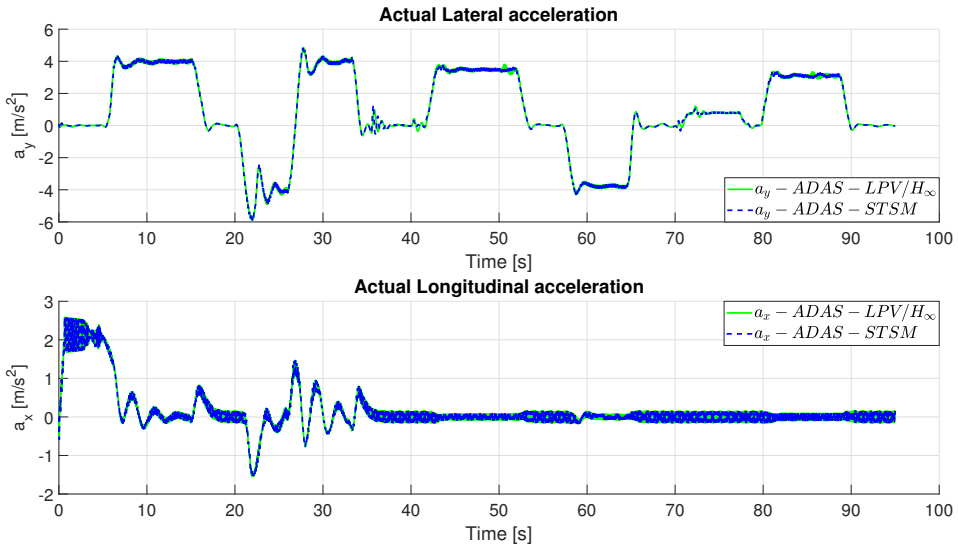


Figure 4.18 – The vehicle dynamic variables: lateral and longitudinal accelerations

## 4.4 Centralized vs Decentralized Advanced Driving Assistance (ADAS) System (B)

This section deals with the development of Centralized and Decentralized Advanced Driving assistance ($ADAS$) system involving the Active Front Steering ($AFS$) and the Direct Yaw Control ($DYC$) to assist the driver and help him, while guaranteeing the vehicle's stability during a lane keeping driving situation. Two $ADAS$ systems architectures are presented where a centralized and decentralized controllers are

developed. These controllers aim to realize the path following and improve the vehicle's stability in different driving situations.

### 4.4.1 Centralized Approach

In the centralized approach, a multi-input multi-output ($MIMO$) optimal single controller is developed to realize the two objectives: trajectory tracking and vehicle's stability improvement. The optimal corrective steering angle provided by the $AFS$ and the optimal Active Differential Braking ($ADB$) provided by the Direct Yaw Control ($DYC$) are generated by the developed controller, to minimize the vehicle state errors (yaw rate and side slip angle). The optimal $LPV/\mathcal{H}_\infty$ control technique presented in 4.3.1.1, is used to develop our controller. The global centralized multilayer control architecture is given in the Figure 4.19. In the control layer, the output variables i.e the vehicle yaw rate $\dot{\psi}$ and the side-slip angle $\beta$ are fed-back from the nonlinear Vehicle Model and are controlled/optimized together through an optimal $MIMO\ LPV/\mathcal{H}_\infty$ controller, in order to realize a lane following trajectory while guaranteeing vehicle's lateral stability. A yaw rate generator is used to generate the desired yaw rate $\dot{\psi}_{ref}$, and the desired side slip angle is equal to 0 ($\beta_{ref} = 0$) to enhance the lateral stability of the vehicle. In addition, two time-varying scheduling gains/parameters $\rho_1$ and $\rho_2$ schedule the two objectives of the $MIMO\ LPV/\mathcal{H}_\infty$ controller. Then, a decision layer (the higher layer) is developed to monitor the driver's behavior and the lateral stability. It sends the value of the scheduling parameters, based on two criteria: 1) driver's behavior $\lambda$, function of the lateral error ($e_y$) and driver's availability ($DA$), and 2) the lateral stability index ($SI$) [Inagaki et al., 1994], [Rajamani, 2012]. $SI$ is an indicator chosen in this thesis to evaluate and monitor the lateral stability of the vehicle. So, Based on all these information, the $MIMO\ LPV/\mathcal{H}_\infty$ controller generates the corrective control steering angle $\delta_{sw-c}$ and the corrective yaw moment $M_z$ as the control inputs. Finally, the actuators constraints are considered in the actuator layer.

#### 4.4.1.1 Centralized Control Layer synthesis: $LPV/\mathcal{H}_\infty$ controller

Figure 4.20 shows the control layer architecture. The standard $\mathcal{H}_\infty$ structure contains the controller $K_{LPV/\mathcal{H}_\infty}(\rho_1, \rho_2)$ to be synthesized, and the generalized plant $\sum_g$, where $\rho_1(\lambda)$ and $\rho_2(SI)$ are two weighted parameters calculated in the decision making layer, to adapt the controller dynamics and performances according to the driving conditions.

The errors between the desired trajectories and the actual ones of the yaw rate $e_{\dot{\psi}}$ ($e_{\dot{\psi}}$=$\dot{\psi}_{ref}$-$\dot{\psi}$) and the side-slip angle $e_\beta$ ($e_\beta$=$\beta_{ref}$-$\beta$) are the inputs to the controller $K_{LPV/\mathcal{H}_\infty}(\rho_1, \rho_2)$. Note that the $\mathcal{H}_\infty$ approach is a model-based robust control technique, then the actual yaw rate and the side-slip angle are calculated based on the $LTI$ vehicle model given 4.2 (*Plant P*).
Remember that the state representation of the *Plant P* of the generalized plant $\sum_g$ can be formalized as in 4.24, where $X = [\beta, \dot{\psi}]^T$ is the state vector (the actual yaw rate $\dot{\psi}$ and the side-slip angle $\beta$ are the outputs to be controlled), $U = [\delta_{sw-c}, M_z]^T$

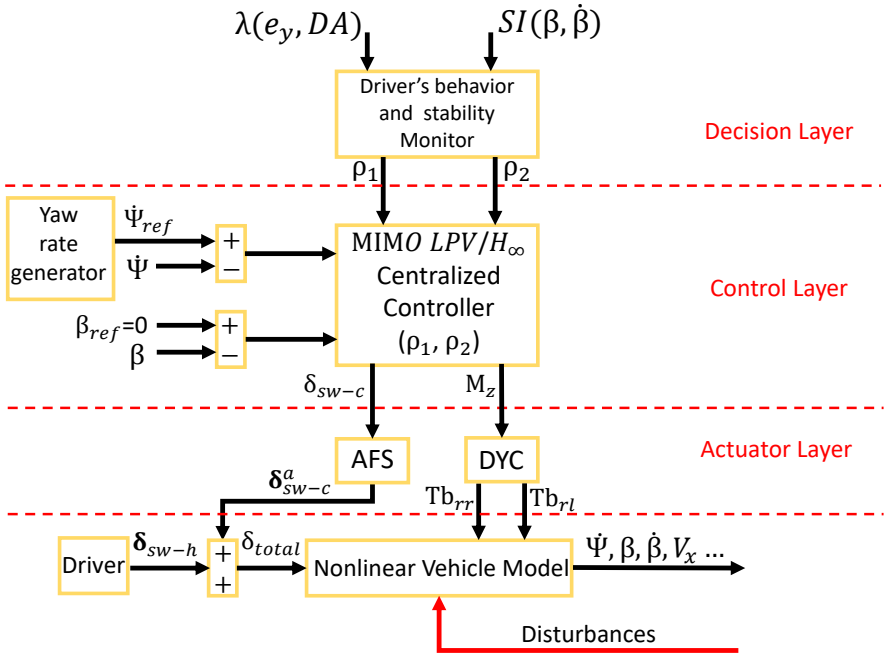


Figure 4.19 – Centralized $LPV/\mathcal{H}_\infty$ $ADAS$ system Architecture.

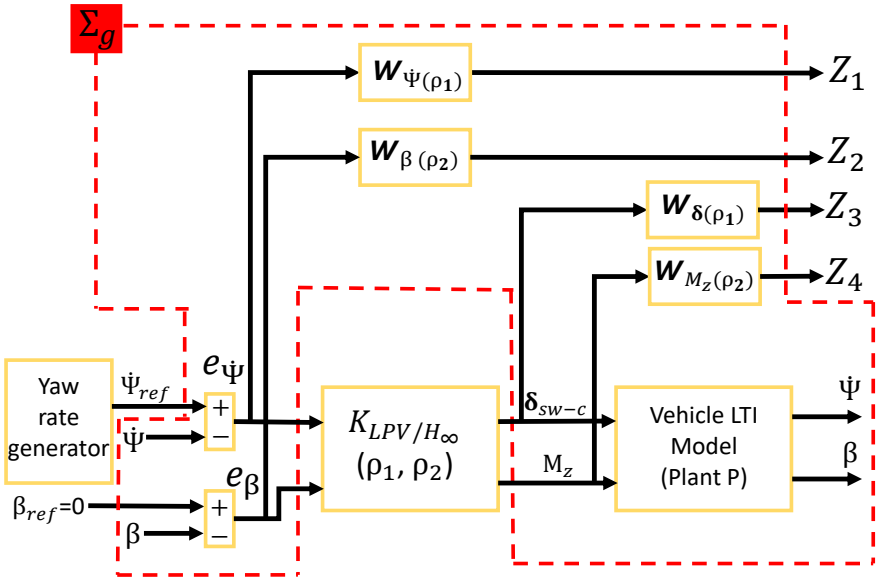


Figure 4.20 – Control layer Architecture.

is the vector of control inputs. The elements of the state matrix $A \in IR^{2\times2}$ and the input matrix $B \in IR^{2\times2}$ are formalized in Appendix .2.

The remaining subsystems of $\sum_g$ i.e. the weighting functions $W_{\dot{\psi}}(\rho_1)$, $W_\beta(\rho_2)$, $W_\delta(\rho_1)$, and $W_{M_z}(\rho_2)$ of Figure 4.20 are defined to characterize the performance

$$\dot{X} = \begin{bmatrix} \dot{\beta} \\ \ddot{\psi} \end{bmatrix} = \underbrace{\begin{pmatrix} a_{11} & a_{12} \\ a_{21} & a_{22} \end{pmatrix}}_{A} \begin{bmatrix} \beta \\ \dot{\psi} \end{bmatrix} + \underbrace{\begin{pmatrix} b_{11} & b_{12} \\ b_{21} & b_{22} \end{pmatrix}}_{B} \begin{bmatrix} \delta_{sw-c} \\ M_z \end{bmatrix} \tag{4.24}$$

objectives $Z_1$, $Z_2$, and the actuators' constraints $Z_3$ and $Z_4$. The general form of these weights [Doumiati et al., 2014] is given by the following (numerical values are given in Section 4.4.3):

- $W_{\dot{\psi}}(\rho_1)$ is similar to the filter in Section 4.3.1.2, it is used to weight the yaw rate control objective, :

$$W_{\dot{\psi}}(\rho_1) \quad = \quad \rho_1 \frac{s/M_1 + 2\pi f_1}{s + 2\pi f_1 A_1}, \tag{4.25}$$

where $M_1$ is sufficiently high for a large robustness margin, and $A_1$ is the tolerated tracking error on $e_{\dot{\psi}}$. $W_{\dot{\psi}}(\rho_1)$ is used to reduce the yaw rate error. $W_{\dot{\psi}}(\rho_1)$ is linearly parametrized by the varying parameter $\rho_1$, where $\rho_1 \in \left\{\underline{\rho_1} \leq \rho_1 \leq \overline{\rho_1}\right\}$ ($\underline{\rho_1}$ and $\overline{\rho_1}$ are constants representing the lower and higher values of $\rho_1$). When $\rho_1 = \overline{\rho_1}$, the performance objective $e_{\dot{\psi}}$ is prioritized ($ADAS$ system is switched-on), on the contrary, when $\rho_1 = \underline{\rho_1}$, $e_{\dot{\psi}}$ is relaxed (driver navigates correctly and the $ADAS$ system for trajectory following is switched-off).

- $W_\beta(\rho_2)$ weights the side-slip angle control objective:

$$W_\beta(\rho_2) \quad = \quad \frac{1}{\rho_2} \frac{s/M_2 + 2\pi f_2}{s + 2\pi f_2 A_2}. \tag{4.26}$$

$M_2$, $A_2$ and $f_2$ have similar meanings as $M_1$, $A_1$ and $f_1$. $W_\beta(\rho_2)$ is similar to $W_{\dot{\psi}}(\rho_1)$. The main difference is that $W_\beta(\rho_2)$ is inversely dependent on the varying parameter $\rho_2$. This is because $\rho_2$ is inversely related to the lateral stability $SI$, that means the lateral stability is prioritized when $\rho_2 = \underline{\rho_2}$ and vice-versa. This issue is explained later in the decision layer.

- $W_\delta(\rho_1)$ weights the steering control input, $\delta_{sw-c}$, $W_\delta(\rho_1)$ is similar to $W_\delta(\rho)$ used in Section 4.3.1.2:

$$W_\delta(\rho_1) \quad = \quad \frac{1}{\rho_1} \frac{s + 2\pi f_3/M_3}{\varepsilon_u s + 2\pi f_3}, \tag{4.27}$$

where $M_3$, $f_3$ and $\varepsilon_u$ have similar meanings as the filter's parameters presented in the section 4.3.1.2. $W_\delta(\rho_1)$ depends on $\rho_1$, which allows to promote or penalize the steering depending on all possible situations. For instance, when driver's behavior is wrong, $AFS$ is promoted to realize the lane keeping (When $\rho_1 = \overline{\rho_1}$) and if the driver acts appropriately, $AFS$ is penalized (relaxed) (when $\rho_1 = \underline{\rho_1}$) and in this case, the driver is the only responsible of driving action.

- $W_{M_z}(\rho_2)$ weights the braking control input, $M_z$:

$$W_{M_z}(\rho_2) \quad = \quad \rho_2 10^{-3} \frac{s/(2\pi f_4) + 1}{s/(\kappa 2\pi f_4) + 1}, \tag{4.28}$$

where $f_4$ is the braking actuator cut-off frequency and $\kappa$ to handle the braking actuator limitations (see [Doumiati et al., 2013]). When $\rho_2 = \underline{\rho_2}$, the braking control signal is promoted, on the contrary, when $\rho_2 = \overline{\rho_2}$, the braking input is penalized. This filter is designed depending on the vehicle's lateral stability.

Then, the $LPV/\mathcal{H}_\infty$ control technique described in the Section 4.3.1.1, where considering $\rho = \{\rho_1, \rho_2\}$, is applied in order to minimize the controlled outputs $Z_1$, $Z_2$, $Z_3$ and $Z_4$ of the generalized plant $\sum_g$ for any exogenous input. The Matlab function "*sysic*" interconnects the subsystems of $\sum_g$. Remember that $\sum_g$ is formulated as:

$$\Sigma_g(\rho) : \begin{bmatrix} \dot{x} \\ z \\ y \end{bmatrix} = \begin{bmatrix} A(\rho) & B_1(\rho) & B_2(\rho) \\ C_1(\rho) & D_{11}(\rho) & D_{12}(\rho) \\ C_2 & D_{21} & 0 \end{bmatrix} \begin{bmatrix} x \\ w \\ U \end{bmatrix}, \tag{4.29}$$

where $\rho = \{\rho_1, \rho_2\}$, $x$ includes the state variables of *Plant P* and the weighting functions, $w = [\dot{\psi}_{ref}, \beta_{ref}]^T$ is the exogenous reference input vector, $U = [\delta_{sw-c}, M_z]^T$ represents the control inputs, $y = [\dot{\psi}, \beta]^T$ is the measurement vector fed-back to the controller, and $z = [Z_1, Z_2, Z_3, Z_4]^T$ is the weighted controlled output vector.

***Problem resolution:** $LMI$ **based** $LPV/\mathcal{H}_\infty$**:***
According to the development in the Section 4.3.1.1, the controller$K_{LPV/\mathcal{H}_\infty}(\rho_1, \rho_2)$ can be found, in order to minimize the $\mathcal{H}_\infty$ norm of the closed-loop $LPV$ system formed by the equations (4.29) and (4.30). Note that, the controller $K_{LPV/\mathcal{H}_\infty}(\rho_1, \rho_2)$ is given as:

$$K_{LPV/\mathcal{H}_\infty}(\rho_1, \rho_2) : \begin{bmatrix} \dot{x}_c \\ u \end{bmatrix} = \begin{bmatrix} A_c(\rho) & B_c(\rho) \\ C_c(\rho) & 0 \end{bmatrix} \begin{bmatrix} x_c \\ y \end{bmatrix}, \tag{4.30}$$

Finally using the polytopic approach detailed in section 4.3.1.1 , the final controller, $K_{LPV/\mathcal{H}_\infty}(\rho_1, \rho_2)$, is the weighted summation of each convex controller calculated on each vertex of the polytope [Apkarian et al., 1995] such as:

$$\begin{aligned} K_{LPV/\mathcal{H}_\infty}(\rho_1, \rho_2) = \alpha_1 K_{\mathcal{H}_\infty}(\omega_1) + \alpha_2 K_{\mathcal{H}_\infty}(\omega_2) \\ +\alpha_3 K_{\mathcal{H}_\infty}(\omega_3) + \alpha_4 K_{\mathcal{H}_\infty}(\omega_4), \end{aligned} \tag{4.31}$$

as shown in Figure 4.21, where each vertex represents an objective.

#### 4.4.1.2 Decision Layer: $\rho_1$ and $\rho_2$ calculations

As said before, the decision layer is developed to monitor the controller according to the driving situations. This layer delivers the scheduling parameters $\rho_1$ and $\rho_2$ depending on the driver's behavior ($\lambda$) and the lateral stability index ($SI$) [Inagaki et al., 1994], [Rajamani, 2012]. $\rho_1$ is similar to $\rho$ given in Section 4.3.1.3. $\rho_1$ depends on the driver's behavior expressed by the parameter $\lambda$. Remember that $\lambda$ is function of $e_y$ and $DA$, given as:

$$\lambda = |e_y| + (1 - DA) \tag{4.32}$$

$\lambda$ has two rules, given as follows:

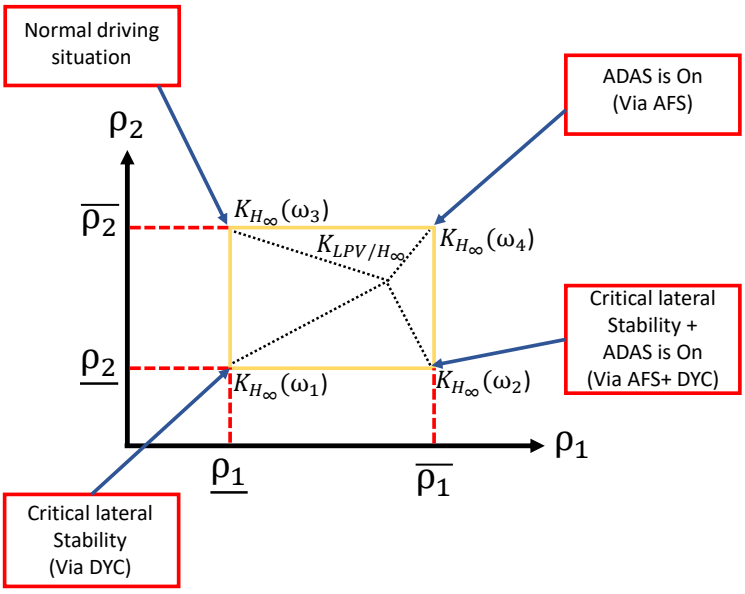


Figure 4.21 – Polytopic $\mathcal{H}_\infty$ controller

- When $\lambda \leq \underline{\lambda}$, that means $|e_y| \leq \underline{e_y}$ and $DA$=1, the $ADAS$ system ($AFS$) is switched-off.

- When $\lambda \geq \overline{\lambda}$, that means $|e_y| \geq \overline{e_y}$ and/or $DA$=0, so the $ADAS$ system ($AFS$) should be switched-on, in order to compensate the driver's errors and unavailability.

According to this analysis, the scheduled gain $\rho_1$ feeds the $LPV/\mathcal{H}_\infty$ controller the sufficient information about the weights to be pushed or attenuated. $\rho_1$ has the similar form of $\rho$, depending on $\lambda$ and presented by a "*sigmoid*" function (4.33) (see Figure 4.22).

$$\rho_1 = \underline{\rho_1} + \frac{\overline{\rho_1} - \underline{\rho_1}}{1 + e^{-\frac{8}{\overline{\lambda}-\underline{\lambda}}(\lambda - \frac{\overline{\lambda}+\underline{\lambda}}{2})}} \tag{4.33}$$

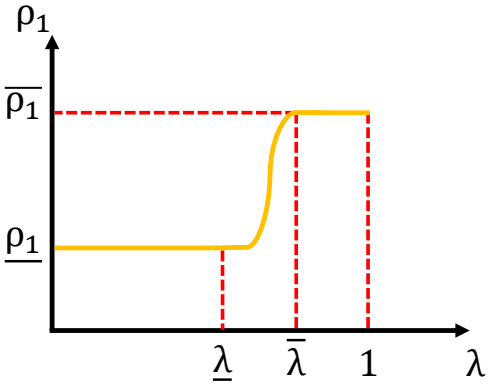


Figure 4.22 – Scheduling parameter $\rho_1$

For the $\rho_2$ calculation, $\rho_2$ depends on the lateral stability indicator $SI$. Let us introduce the definition of the lateral stability indicator $SI$.

***Lateral stability index*** $SI$***:***
The lateral stability index $SI$ reflects the orientation of the vehicle depending on the speed vector at the center of gravity ($CG$), and its rate of change. $SI$ is given as (see [Hamdan et al., 2020]):

$$SI = \left| c_1\beta + c_2\dot{\beta} \right|, \tag{4.34}$$

where $c_1$ and $c_2$ are estimated w.r.t the vehicle parameters and the shape of the road. $SI$ is between 0 and 1 in stable driving. $SI$ determines the driving situations. $SI$ has two rules:

- When $SI \leq \underline{SI}$ (a predefined lower threshold depending on the roads parameters and vehicle), the vehicle is in a normal driving situation (stable region) and $ADAS$ system for stability ($DYC$) is penalized .

- when $SI \geq \overline{SI}$ (a predefined higher threshold), the vehicle is in a critical lateral stability region (unstable region) and a stability $ADAS$ system ($DYC$) is needed to be triggered to reestablish the lateral stability of the vehicle.

According to this discussion, $\rho_2$ is calculated based on the $SI$ in order to provide the $LPV/\mathcal{H}_\infty$ controller information about the weights to be pushed or attenuated. The relation between $\rho_2$ and $SI$ is given through a "*sigmoid*" function (4.35) (see Fig. 4.23) that guarantees a continuous and smooth variation of $\rho_2$.

$$\rho_2 = \overline{\rho_2} - \frac{\overline{\rho_2} - \underline{\rho_2}}{1 + e^{-\frac{8}{\overline{SI} - \underline{SI}}\left(SI - \frac{\overline{SI} + \underline{SI}}{2}\right)}} \tag{4.35}$$

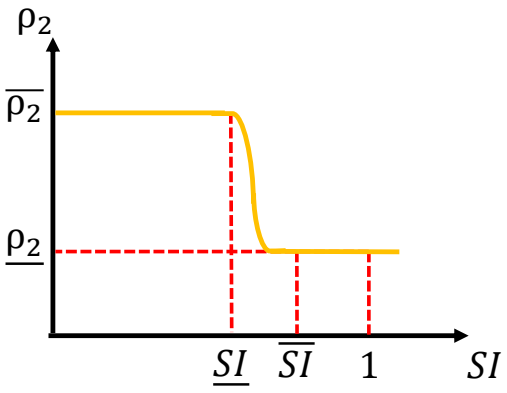


Figure 4.23 – Scheduling parameter $\rho_2$

#### 4.4.1.3 Actuator Layer:

The Actuator Layer contains the two actuators used to generate the physical control inputs of the system. In the present work, the $AFS$ and the $DYC$ have been used to provide these inputs. The $AFS$ model developed in the Section 4.3.1.4, is used to generate the corrective steering angle. Note that the total steering wheel angle is given as:

$$\delta_{total} = \delta_{sw-h} + \delta^a_{sw-c}, \tag{4.36}$$

where $\rho_1$ is implicitly expressed in $\delta^a_{sw-c}$.

Concerning the $DYC$ actuator, the $DYC$ moment $M_z$ can be realized by applying on the low-level a differential braking torque on one rear wheel (left of right) of radius r [Hamdan et al., 2020]. The applied braking torque is given as follows:

$$\begin{cases} \begin{cases} Tb_{rr} = -\frac{2*M_z*r}{t_r}, \\ Tb_{lr} = 0, \end{cases} & if\ M_z \leq 0, \\ \begin{cases} Tb_{lr} = \frac{2*M_z*r}{t_r}, \\ Tb_{rr} = 0, \end{cases} & if\ M_z > 0, \end{cases} \tag{4.37}$$

where $Tb_{lr}$ and $Tb_{rr}$ are the left and right differential braking torques respectively. A simple model for the electro mechanical braking ($EMB$) actuator is used. The $EMB$ actuator is modeled as:

$$\dot{T}^a_{b,rj} = 2\pi f_5 (T_{b,rj} - T^a_{b,rj}), \tag{4.38}$$

where $T^a_{b,rj}$ follows $T_{b,rj}$, $f_5$ is the actuator cut-off frequency. This actuator control is bounded between $[0, T^a_{b,max}]$, where $T^a_{b,max}$ is the saturation of the $EMB$ actuator.

### 4.4.2 Decentralized Approach

In the decentralized approach, we decoupled the two objectives (trajectory tracking and vehicle's stability improvement) into two sub-control problems. The $STSM$ control technique is applied to provide the control inputs, such as: $AFS$ is responsible on the control of the lateral error ($e_y$); $DYC$ is responsible on the control of side slip angle ($\beta$) to enhance stability. The global decentralized multilayer control architecture is shown in Figure 4.24. The main difference w.r.t the centralized one is in the control layer, where each controller generates his input by neglecting the other. The inputs are: $AFS$ control input $\delta_{sw-c}$ dedicated to minimize the lateral error ($e_y$) in order to follow the trajectory, and $DYC$ control input $M_z$ is devoted to control the side slip angle $\beta$ to improve vehicle's stability. However, the decision and actuator layers are similar to the ones of the centralized approach, where the decision layer generates the two weights: $\alpha$ and $\gamma$ function of $\lambda$ and $SI$ respectively. The aim of these gains is to promote/attenuate both $STSM$ controllers depending on driver's behavior ($\lambda$) and the lateral stability indicator ($SI$).

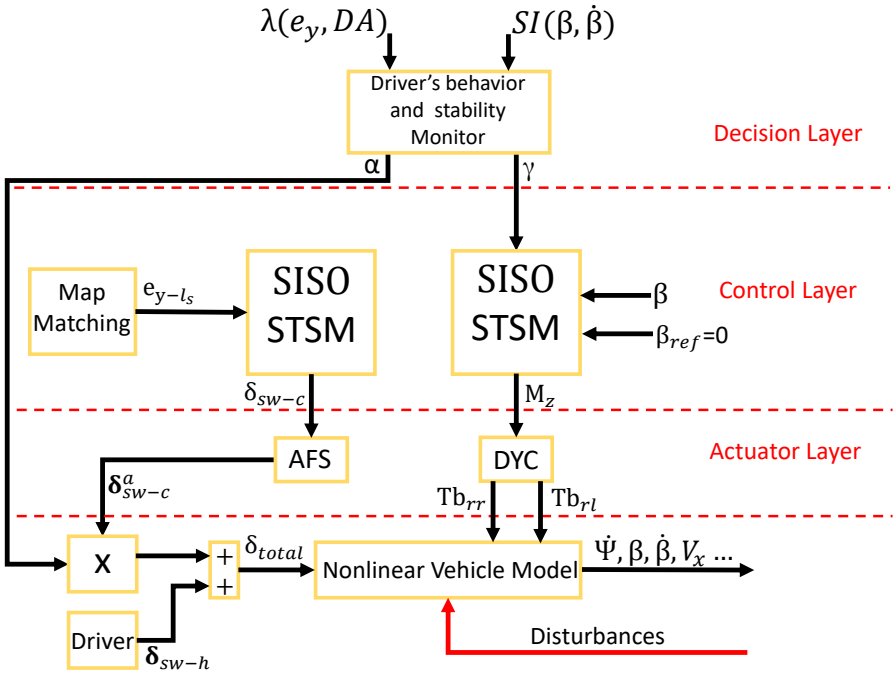


Figure 4.24 – Decentralized *STSM ADAS* system Architecture.

$$\dot{X} = \begin{bmatrix} \dot{\beta} \\ \ddot{\psi} \end{bmatrix} = \underbrace{\begin{pmatrix} a_{11} & a_{12} \\ a_{21} & a_{22} \end{pmatrix}}_{A} \begin{bmatrix} \beta \\ \dot{\psi} \end{bmatrix} + \underbrace{\begin{pmatrix} b_{11} \\ b_{21} \end{pmatrix}}_{B_1} \begin{bmatrix} \delta_{sw-c} \end{bmatrix} \tag{4.39}$$

#### 4.4.2.1 Decentralized Control Layer synthesis: Super-twisting sliding mode controllers

The control layer consists of two *SISO STSM* controllers generating the control inputs. For that, the detailed *STSM* control technique given in Section 1.4.2, is recalled here to find the control inputs: $\delta_{sw-c}$ and $M_z$. The *AFS* provides the $\delta_{sw-c}$ to minimize the lateral error $e_y$ and realize the path following. Note that, $\delta_{sw-c}$ is similar to $\delta_{sw-as}$ given in Section 1.4.2. The DYC generates the yaw moment $M_z$ to control the side slip angle $\beta$ and enhance the vehicle's lateral stability.
The *STSM*-based *AFS* control synthesis model (4.39) is similar to (4.24), while considering $M_z = 0$, and thus, reducing $B$ to its first column $B_1$. The driver steering input $\delta_{sw-h}$ is neglected in the synthesis model and it is fed-forward to the system.
The *STSM*-based *DYC* control synthesis model (4.40) is similar to (4.24), while considering $\delta_{sw-c} = 0$, and thus, reducing $B$ to its second column $B_2$. The driver steering input $\delta_{sw-h}$ is also neglected in the synthesis model.

$$\dot{X} = \begin{bmatrix} \dot{\beta} \\ \ddot{\psi} \end{bmatrix} = \underbrace{\begin{pmatrix} a_{11} & a_{12} \\ a_{21} & a_{22} \end{pmatrix}}_{A} \begin{bmatrix} \beta \\ \dot{\psi} \end{bmatrix} + \underbrace{\begin{pmatrix} b_{12} \\ b_{22} \end{pmatrix}}_{B_2} \begin{bmatrix} M_z \end{bmatrix} \tag{4.40}$$

Let's recall the second order system given as:

$$\dot{X} = f(X,t) + g(X,t)u(t) \tag{4.41}$$

where $X = [e_y, \beta]^T$, and $f(X,t) = AX$. In the case of the $AFS$ controller synthesis $g(X,t) = B_1$ and $u = \delta_{sw-c}$ as can be seen from (4.39). In the case of the $DYC$ controller synthesis $g(X,t) = B_2$ and $u = M_z$ as can be seen from (4.40).
Let's define $E = [e_y, e_\beta] = [y - y^*, \beta_{ref} - \beta]^T$ the error vector between the actual and the desired states. $y^*$ and $\beta_{ref} = 0$ are the desired lateral coordinate of the road and the desired side slip angle respectively. $e_y$ is calculated by a Map Matching block at a look-ahead distance $l_s$ (see Figure 4.24), that localizes the vehicle on the reference map.
Let's define the two sliding variables for the two controllers as follows:

$$\begin{array}{ll} s_{e_y} = \dot{e_y} + \lambda_y e_y, & \lambda_y > 0 \\ s_\beta = \gamma(e_\beta + \lambda_\beta \dot{e_\beta}) & \lambda_\beta > 0 \end{array} \tag{4.42}$$

where $\lambda_y$ and $\lambda_\beta$ are positive constants. The sliding variable $s_{e_y}$ has a relative degree equal to one w.r.t the control input $\delta_{sw-c}$ (for the lateral dynamics) since $b_{11}$ and $b_{21}$ are not zero as can be seen in the $AFS$ synthesis model of (4.39). Similarly, $s_\beta$ has a relative degree of one w.r.t the control input $M_z$ since $b_{22}$ is not zero as can be seen in the $DYC$ synthesis model of (4.40). $\gamma_{(SI)}$ is a scheduling gain which varies between 0 and 1, provided by the decision layer discussed later. When $\gamma_{(SI)}$ is equal to 1, the $DYC$ controller is promoted. When $\gamma_{(SI)}$ is equal to 0, the $DYC$ controller is attenuated.

Thus, in order to achieve the convergence of the sliding variables to the sliding surface defined by $s = 0$ and based on the Section 1.4.2, the $STSM$ control inputs of the $AFS$ and the $DYC$ are respectively given by:

$$\begin{array}{l} \delta_{sw-c} = -\alpha_{\delta,1} |s_{\dot{\psi},\theta}|^{\tau_\delta} sign(s_{\dot{\psi},\theta}) - \alpha_{\delta,2} \int_0^t sign(s_{\dot{\psi},\theta}) d\tau, \\ M_z = -\alpha_{M_z,1} |s_\beta|^{\tau_{M_z}} sign(s_\beta) - \alpha_{M_z,2} \int_0^t sign(s_\beta) d\tau, \end{array} \tag{4.43}$$

where $\alpha_{\delta,1}$ and $\alpha_{\delta,2}$ (resp. $\alpha_{M_z,1}$ and $\alpha_{M_z,2}$) are positive gains satisfying the conditions of (1.46). $\tau_\delta$ and $\tau_{M_z}$ are constants in ]0, 0.5]. The function $sign$ is smoothed by the approximation $sign(s) = \frac{s}{|s|+\varepsilon}$, where $\varepsilon$ is a positive small value.
The $STSM$ control inputs guarantee the convergence of $s_{e_y}$ and $s_\beta$ in a finite time to zero. Once $s_{e_y} = 0$ and $s_\beta = 0$ , this means that $y$ will converge to $y^*$ and the side-slip angle $\beta$ will converge to $\beta_{ref}$ respectively.

#### 4.4.2.2 Decision Layer: $\alpha$ and $\gamma$ calculation

Similar to the decision layer of the centralized approach, the decision layer of the decentralized approach monitors all the control objectives based on some monitoring criteria: the driver's behavior ($\lambda$) and the lateral stability index ($SI$). Then, it calculates and sends instantly the values of $\alpha$ and $\gamma$ to relax/promote the corresponding control objective depending on the vehicle situation.

$\alpha$ is similar to the one given in 4.3.2.2. $\alpha$ depends on the driver's behavior $\lambda$.

- When $\lambda \leq \underline{\lambda}$, that means $|e_y| \leq \underline{e_y}$ and $DA$=1, $\alpha$ approaches to 0 and the $ADAS$ system ($AFS$) is attenuated.

- When $\lambda \geq \overline{\lambda}$, that means $|e_y| \geq \overline{e_y}$ and/or $DA$=0, $\alpha$ approaches to 1 so the $ADAS$ system ($AFS$) should be promoted.

A "*sigmoid*" function (4.44) (see Figure 4.25) governs the relation between $\alpha$ and $\lambda$, to ensure a continuous and smooth variation of $\alpha$.

$$\alpha = \frac{1}{1 + e^{-\frac{8}{\overline{\lambda} - \underline{\lambda}}(\lambda - \frac{\overline{\lambda} + \underline{\lambda}}{2})}} \tag{4.44}$$

By the same way, $\gamma$ depends on the lateral stability index $SI$.

- When $SI \leq \underline{SI}$, $\gamma$ approaches to 0 since no lateral stability risk and the $ADAS$ system ($DYC$) is penalized .

- When $SI \geq \overline{SI}$, $\gamma$ approaches to 1 since the lateral stability risk is high and the $ADAS$ system ($DYC$) is promoted (activated).

A "*sigmoid*" function (4.45) (see Figure 4.25) governs the relation between $\gamma$ and $SI$, to ensure a continuous and smooth variation of $\gamma$.

$$\gamma = \frac{1}{1 + e^{-\frac{8}{\overline{SI} - \underline{SI}}(SI - \frac{\overline{SI} + \underline{SI}}{2})}} \tag{4.45}$$

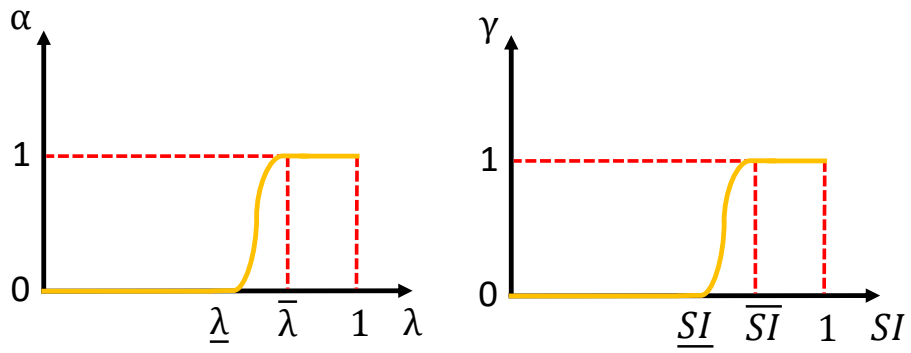


Figure 4.25 – Scheduling gains $\alpha$ and $\gamma$

#### 4.4.2.3 Actuator Layer:

Similar to the actuator layer of the centralized approach, actuator layer is used in the decentralized approach to generate the physical inputs $\delta_{sw-c}$ and $M_z$ of the system (see Section 4.4.1.3). Remember that the final steering wheel angle is given in the Equation 4.3.

### 4.4.3 Centralized and decentralized architectures validation and comparison (B)

This section is dedicated to validate and compare the centralized and decentralized control architectures for two different scenarios, using Matlab/Simulink. The simulation model of the full vehicle is developed and validated on "*SCANeR Studio*" (OKtal) simulator. Both scenarios are defined later to solicit the two objectives: the lane keeping and the lateral stability using the test track given in Figure 4.10. For both scenarios, a comparison is done by integrating the proposed $MIMO\ LPV/\mathcal{H}_\infty$ (centralized) and the $SISO$ Super-Twisting Sliding Mode ($STSM$)(decentralized) controllers into the vehicle, and comparing it to a vehicle without $ADAS$, where the controllers are not implemented (human driver without $ADAS$). Numerical values of the controller parameters used in the simulation are provided in Table 4.2.

Table 4.2 – Controllers' Parameters for Simulation

| Parameters | Values |
|---|---|
| $M_1 = M_2; M_3; A_1 = A_2; \varepsilon_u; \kappa$ | $2; 1; 0.1 = 10\%; 0.01; 100$ |
| $f_1 = f_2; f_3 = f_4 = f_5;$ | $11.15\ Hz; 10\ Hz$ |
| $c_1; c_2;$ | 9.55;2.49 |
| $\underline{e_y}; \overline{e_y}; \underline{\lambda}; \overline{\lambda}; \underline{SI}; \overline{SI}$ | $0.5; 0.7; 0.5; 0.7; 0.6; 0.7$ |
| $\lambda_y; \lambda_\beta; \varepsilon;$ | $8; 0.1; 1$ |
| $\alpha_{\delta,1}; \tau_\delta; \alpha_{\delta,2}$ | 0.1;0.5;0.01 |
| $\alpha_{M_z,1}; \tau_{M_z}; \alpha_{M_z,2}$ | 1000;0.5;0.1 |
| $\underline{\rho_1}; \overline{\rho_1}; \underline{\rho_2}; \overline{\rho_2}$ | $0.01; 1; 0.45; 10$ |
| $\delta^a_{sw-c,max}; T^a_{b,max}$ | $5°; 1200\ N.m$ |
| $l_s; r; t_r$ | $3; 0.3076; 0.75$ |

#### 4.4.3.1 Scenario 1:

This scenario is defined to test and validate the proposed controllers which aim to assist the driver in the lane keeping maneuver and improve the vehicle's stability, when needed, based on the decision monitoring. To do that, two errors are injected between $35s$ and $50s$ and between $70s$ and $85s$ on the driver's behavior at speed 60 $km/h$ (see Figure 4.26), when he is no more available. The vehicle is deviated from the lane and the $ADAS$ system represented by the centralized or decentralized controller, is activated to diminish the driver's error (through $AFS$) and retain the lateral stability of the vehicle (through $DYC$). The simulation results show the importance of having an $ADAS$ system in the vehicle, compensating driver's error and enhancing vehicle's stability. During this scenario, a comparison is done between the vehicle without $ADAS$ (where driver is alone), and with the proposed

controllers i.e the driving with $ADAS\ LPV/\mathcal{H}_\infty$ centralized and the driving with $ADAS\ STSM$ decentralized controllers.

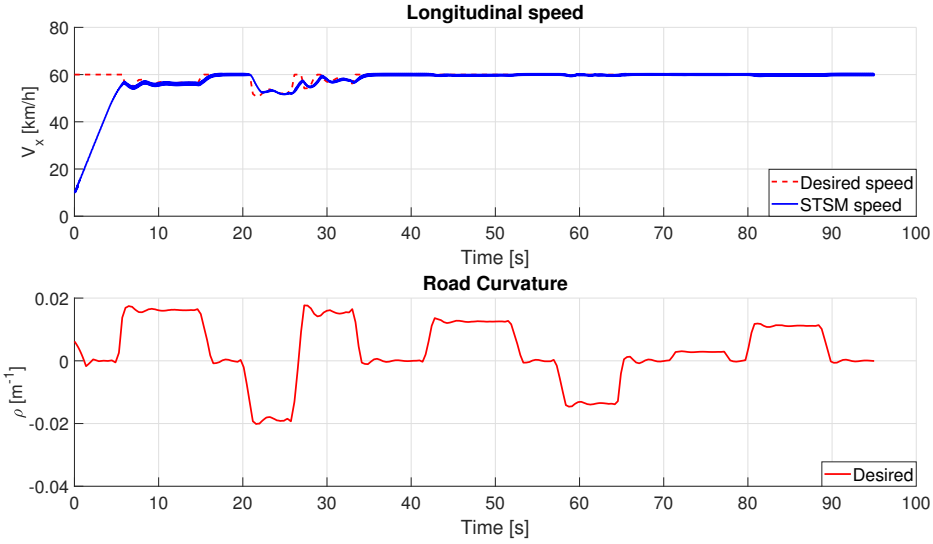


Figure 4.26 – The vehicle dynamic variables: speed and road curvature - Scenario 1

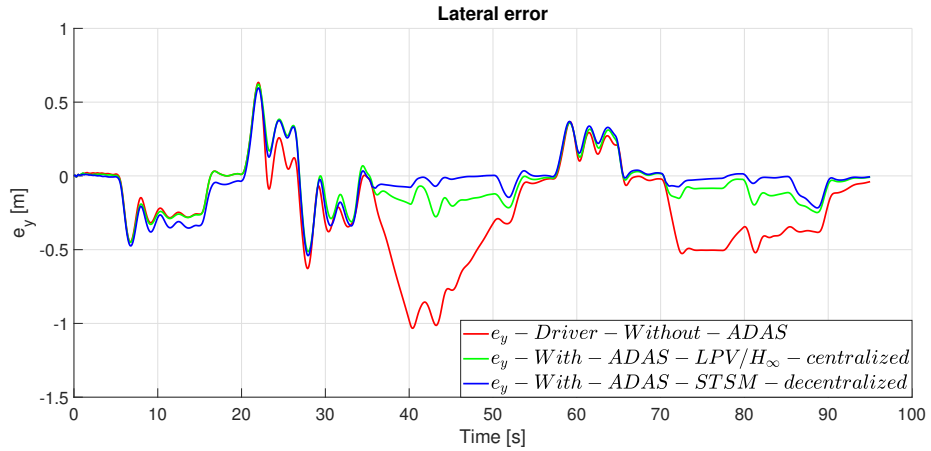


Figure 4.27 – The lateral error - Scenario 1

The Figure 4.27 shows the lateral error of: driver without $ADAS$, driving with $ADAS$-$LPV/\mathcal{H}_\infty$-centralized and driving with $ADAS$-$STSM$-decentralized. As we can see, the errors are injected on the driver's behavior between $35s$ and $50s$ and between $70s$ and $85s$. Both $ADAS$ systems ($LPV/\mathcal{H}_\infty$ and $STSM$ controllers) diminish this error ($1m$) caused by the driver on the curvy road (see Figure 4.26). Thus, the two controllers have achieved the assistance goal with acceptable accuracy of lane keeping ($e_y$ between $-60cm$ and $60cm$, Figure 4.27). However, Figure 4.27 shows that the $ADAS$-$STSM$-decentralized controller is capable to diminish more the lateral error $e_y$ to zero compared to the $ADAS$-$LPV/\mathcal{H}_\infty$-centralized controller that is less performant. Noting that the $SISO\ STSM$-$AFS$ controller realizes the

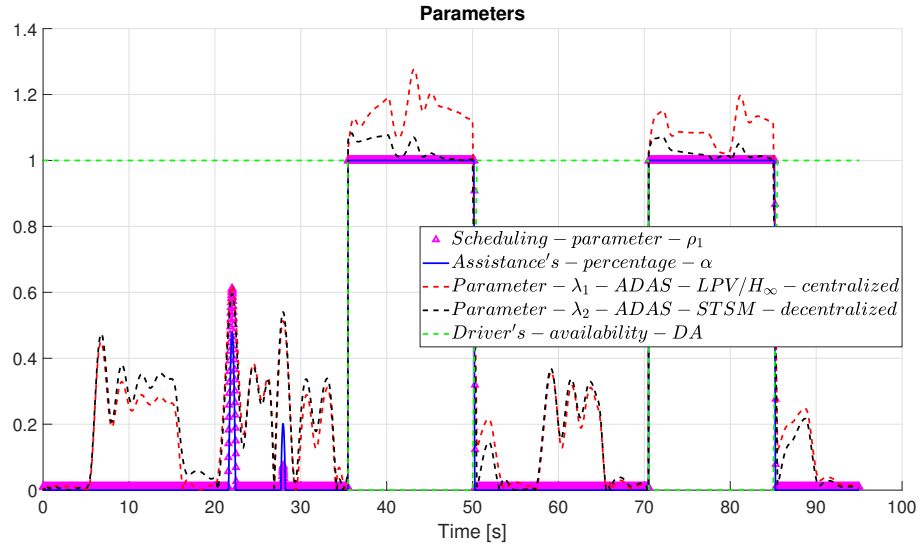


Figure 4.28 – The different parameters - Scenario 1

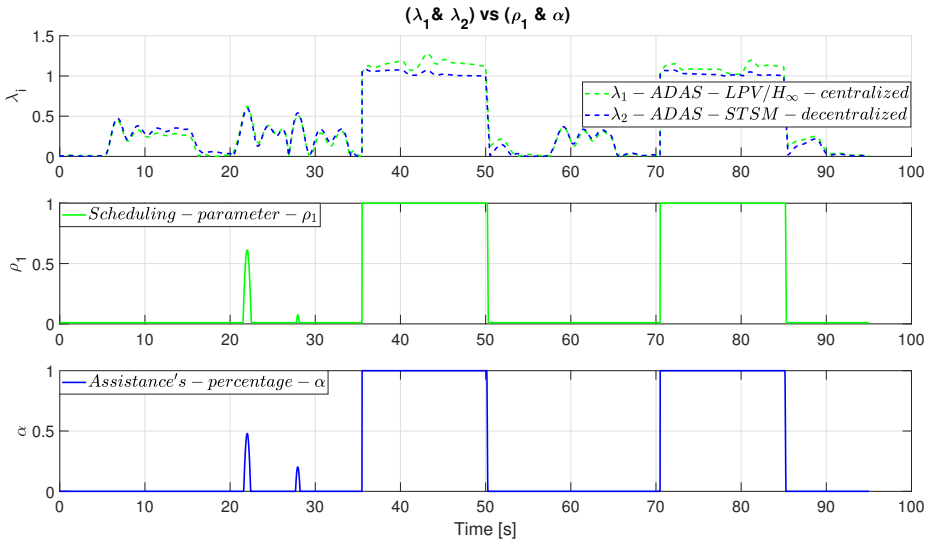


Figure 4.29 – $\lambda_i$ vs $\rho$ and $\alpha$ - Scenario 1

lane keeping objective independently of *SISO STSM-DYC* controller that aims to retain vehicle's lateral stability (see Figure 4.24), for this reason the *ADAS-STSM*-decentralized controller is more performant w.r.t the *ADAS-LPV/*$\mathcal{H}_\infty$-centralized controller, because in the *ADAS-STSM*-decentralized controller, there is a separation between the actuators and the control objectives.

The two *ADAS* controllers are switched-on until t=50$s$, where $\lambda_i \geq \overline{\lambda}$ ($i = \{1 : ADAS - LPV/\mathcal{H}_\infty - centralized, 2 : ADAS - STSM - decentralized\}$) because the driver's availability $DA$ is equal to 0 and the lateral error is more than $\overline{e_y}$ (see Figure 4.28). Remember that $DA$ reflects the driver's status (1 for available or 0 for not available). Again at t=70$s$, an *ADAS* controller is still needed because there is

a second error caused by the driver's behavior and $DA$=0. The ADAS controllers assist the driver until t=85$s$. At t=85$s$, the driver's behavior returns normal and $DA$=1, then the two $ADAS$ controllers are switched-off.
The switching-on of the two $ADAS-AFS$ controllers can be explained by observing the decision layer of each $ADAS$ system architecture, in other words, the monitoring criterion $\lambda_1$ and $\lambda_2$. Figure 4.29 shows the two parameters $\lambda_1$ and $\lambda_2$, with the corresponding scheduling parameter $\rho_1$ and the percentage of assistance $\alpha$ for the $LPV/\mathcal{H}_\infty$-centralized and the $STSM$-decentralized $ADAS$ system architectures respectively. For $\lambda_1 \geq \overline{\lambda}$ (resp. $\lambda_2 \geq \overline{\lambda}$), which means that the driver lost control and the two $ADAS - AFS$ controllers have switched-on to assist and help him. When $\lambda_1 \geq \overline{\lambda}$, that means $DA = 0$ and/or $e_y$ is more than $\overline{e_y}$, (resp. $\lambda_2 \geq \overline{\lambda}$), especially between 35$s$ and 50$s$ and between 70$s$ and 85$s$, the scheduling gain $\rho_1$ of the $LPV/\mathcal{H}_\infty$-centralized controller (resp. the percentage of assistance $\alpha$ of the $STSM$-decentralized controller) is set to $\rho_1 = \overline{\rho_1}$ (resp. $\alpha = 1$), which activates the assistance. For the region, when $\lambda_1 \leq \underline{\lambda}$ (resp. $\lambda_2 \leq \underline{\lambda}$), the scheduling gain $\rho_1$ (resp. the percentage of assistance $\alpha$) is set to $\rho_1 = \underline{\rho_1}$ (resp. $\alpha = 0$), which means the driver acts correctly and the $ADAS - AFS$ controllers are switched-off.
Based on this discussion, one can conclude that the $ADAS - AFS$ controllers are switched-on when needed in order to assist the driver. Refer to the Figure 4.29, the two $ADAS - AFS$ controllers have almost the same behavior and they are able to help the driver by compensating his errors.

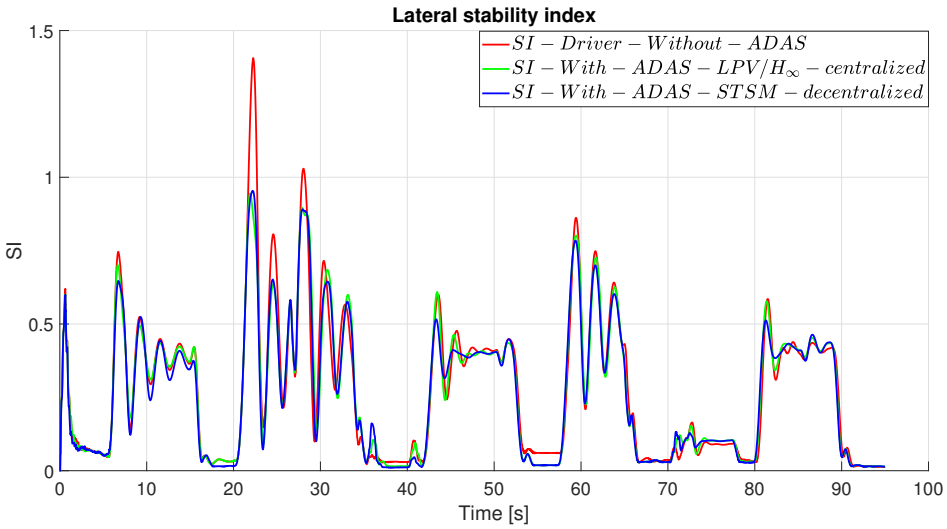


Figure 4.30 – The lateral stability $SI$ - Scenario 1

On the other hand, both control architectures have similar influence on the lateral stability index $SI$ as shown in the Figure 4.30. The vehicle's lateral stability objective is achieved by the two controllers in order to prevent an undesirable driving situation ($SI > 1$). Noting that ($SI_{without-ADAS} > 1$) at t=22$s$ for example, because the actual longitudinal speed is higher than the desired one (see Figure 4.26).
However, refer to the Figures 4.30 and 4.27, the $SI$ with $ADAS$-$LPV/\mathcal{H}_\infty$-centralized is less than $SI$ with $ADAS$-$STSM$-decentralized at t=22$s$ ($SI_{LPV/\mathcal{H}_\infty} <$

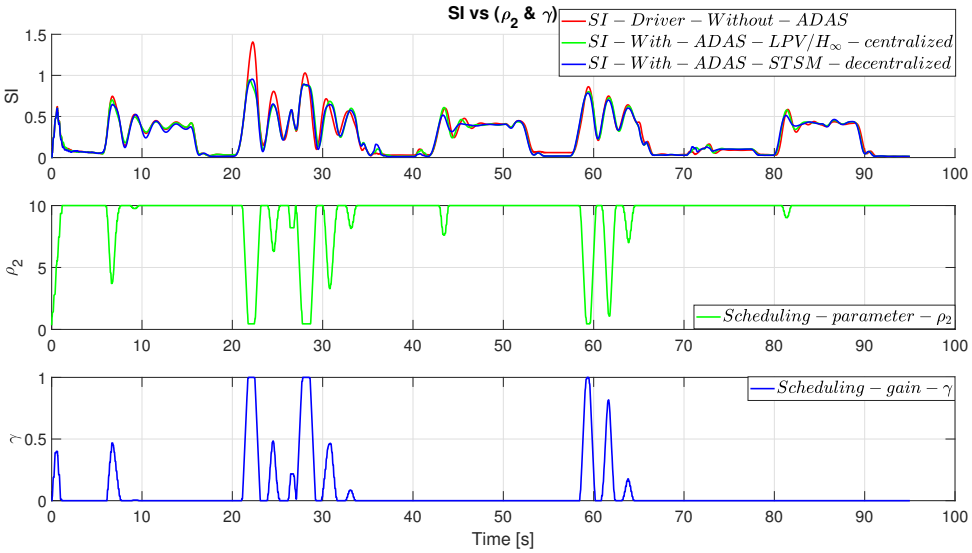


Figure 4.31 – $SI$ vs $\rho_2$ and $\gamma$ - Scenario 1

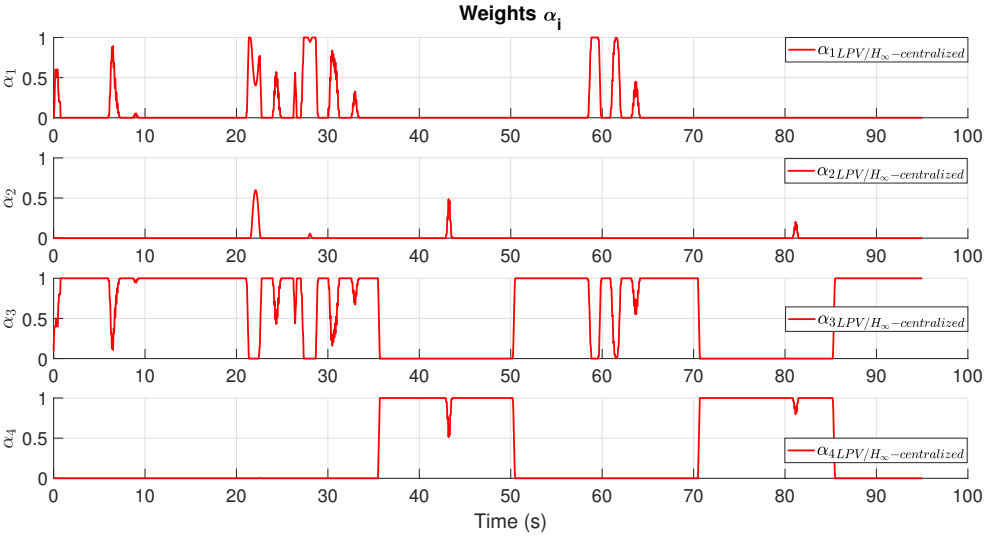


Figure 4.32 – Weights $\alpha_i$-vertices controllers - Scenario 1

$SI_{STSM}$), but the lateral error with $ADAS$-$LPV/\mathcal{H}_\infty$-centralized is bigger than the lateral error with $ADAS$-$STSM$-decentralized ($e_{y-LPV/\mathcal{H}_\infty} > e_{y-STSM}$ at t=22$s$). The reason is that the $LPV/\mathcal{H}_\infty$ controller is a centralized controller which compromises between the two objectives (lane keeping and stability enhancing), but the decentralized controllers (Figure 4.24) accomplish their role independently. Another example, at t=60$s$, $SI_{LPV/\mathcal{H}_\infty} > SI_{STSM}$ due to the driving on a curvy road (see Figure 4.26).

Figure 4.31 shows the lateral $SI$ with the corresponding scheduling parameter $\rho_2$ and the scheduling gain $\gamma$ of both control architectures. The lateral $SI$ of the vehicle without $ADAS$ (driver without $ADAS$) exceeds $SI = 1$, which means that the vehicle has lost its stability, while both control architectures have covered back the

$SI$ under $SI = \underline{SI}$, and thus, they have succeeded to remain the vehicle stable during the overall trajectory. Therefore, $\rho_2$ is chosen as $\rho_2 = \underline{\rho_2}$ (resp. $\gamma$ is chosen as $\gamma = 1$) when $SI \geq \overline{SI}$ for the lateral stability enhancement through the activation of differential braking actuator ($DYC$). When $SI \leq \underline{SI}$, $\rho_2$ (resp. $\gamma$) deviates to $\rho_2 = \overline{\rho_2}$ (resp $\gamma = 0$) which means the deactivation of the differential braking actuator ($DYC$), and there is no risk of lateral stability.

Concerning the centralized $LPV/\mathcal{H}_\infty$ $ADAS$ system control architecture, the choice and the tuning of the parameters $\rho_1$ and $\rho_2$ (Figure 4.19) is not obvious since the $LPV/\mathcal{H}_\infty$ controller aims to compromise between the different control objectives in order to give an optimal result. Many simulations with tuning of these parameters are done to get the optimal ones. The different weights $\alpha_i$ (Equation 4.31) are given in the Figure 4.32. They correspond to the controllers vertices of Figure 4.21.

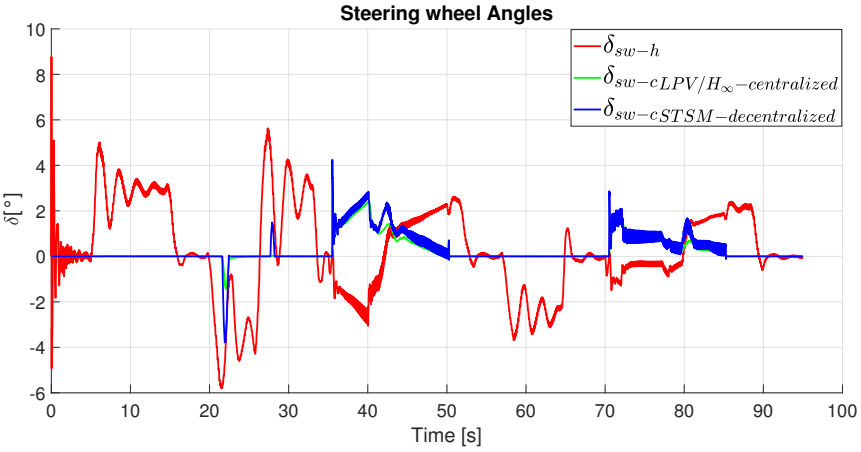


Figure 4.33 – The different steering wheel angles - Scenario 1

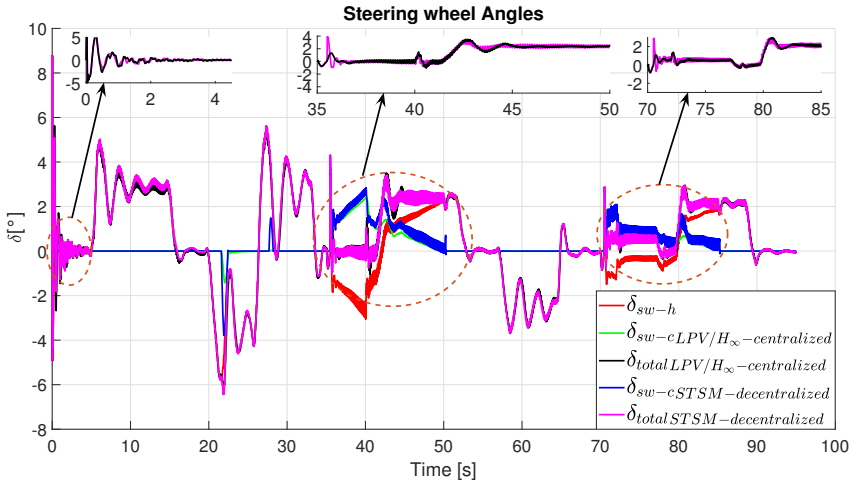


Figure 4.34 – The different total steering wheel angles - Scenario 1

Figure 4.33 shows the human driver steering angle $\delta_{sw-h}$ and the $AFS$ steering angle

$\delta_{sw-c}$ of both controllers: the $LPV/\mathcal{H}_\infty$-centralized and the $STSM$-decentralized respectively on the steering wheels. One can notice that, the both controllers provide almost the similar steering angle, with some additional oscillations of $STSM$-decentralized controller. The two controllers are in conflict with the driver between $35s$ and $50s$ and between $70s$ and $85s$ in order to compensate his errors. The different total steering angles: $\delta_{totalLPV/H_\infty-centralized}$ and $\delta_{totalSTSM-decentralized}$ are given in the Figure 4.34. As we can notice, oscillations appear more with the $STSM$-decentralized than the $LPV/\mathcal{H}_\infty$-centralized controller. Moreover, the advantage of using $STSM$ control technique is that it is simple and easy to implement with a low cost. However, the point of weakness of this technique is the oscillation and chattering. Figure 4.35 shows the braking of the $EMB$ at the left and right rear wheels. The $LPV/\mathcal{H}_\infty$-centralized controller activates a little bit more the braking to compromise between the different objectives of the centralized controller, on contrary to the $STSM$-decentralized controller which activates the braking only to cover back the lateral stability when necessary. Finally, Figure 4.26 shows the longitudinal speed tracking to the desired one through the $STSM$ longitudinal controller, the road curvature of the desired trajectory. The lateral and longitudinal accelerations are given in the Figure 4.36 . The lateral acceleration does not exceed the $\pm 5m/s^2$, and the actual longitudinal acceleration is pertinent ($< \pm 2m/s^2$) which demonstrate a comfortable and stable driving maneuver.

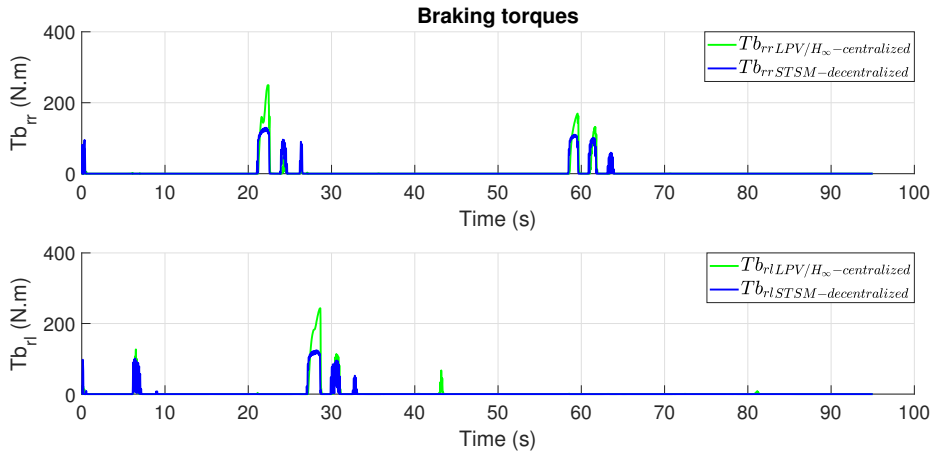


Figure 4.35 – The braking torques - Scenario 1

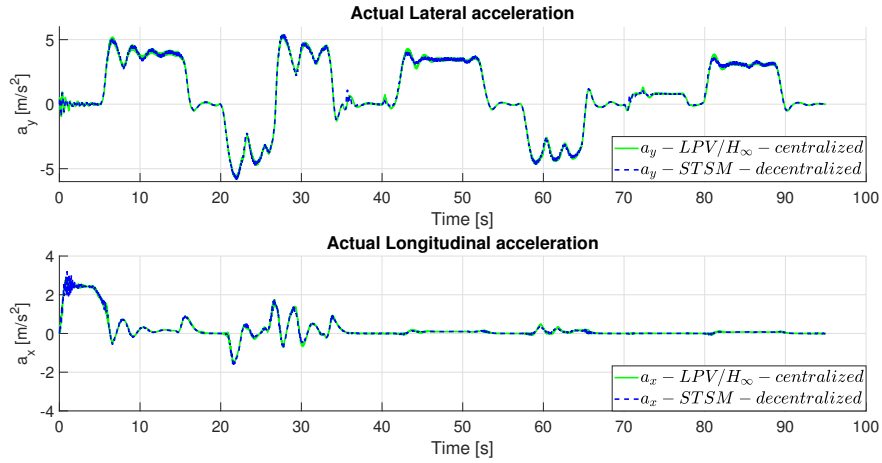


Figure 4.36 – The vehicle dynamic variables: lateral and longitudinal accelerations - Scenario 1

#### 4.4.3.2 Scenario 2:

Similar to the scenario 1, a second scenario is defined to treat the case of inappropriate behavior of the human driver when he is destroyed on a curvy road, where the lateral stability is more solicited. For that, the errors are injected on the driver's behavior between $9s$ and $23s$ and between $40s$ and $70s$ where the road is curvy at a speed 60 $Km/h$ (see Figure 4.37). The different lateral errors of: driver without $ADAS$, driving with $ADAS$-$LPV/\mathcal{H}_\infty$-centralized and driving with $ADAS$-$STSM$-decentralized are shown in the Figure 4.38. $e_y$ is between $-45cm$ and $45cm$ for the two $ADAS$ systems (centralized and decentralized), that means both controllers are capable to diminish the error ($1.1m$, without $ADAS$) caused by the driver on the curvy road. However, the results show that the $ADAS$-$STSM$-decentralized controller is more performant to follow the trajectory compared to the $LPV/\mathcal{H}_\infty$-centralized controller ($e_{y-STSM} < e_{y-LPV/\mathcal{H}_\infty}$ for the intervals $[9s; 23s]$ and $[40s; 70s]$).

For the region of errors of the driver ($[9s; 23s]$ and $[40s; 70s]$), the two $ADAS$ controllers are activated because $\lambda_{1,2} \geq \overline{\lambda}$ as given in the Figure 4.39. Figure 4.39 shows the different parameters related to the activation of both $ADAS$ controllers. This activation can be decided through the decision layer of the $ADAS$ system architectures, that monitors the driver's behavior $\lambda_1$ and $\lambda_2$ (function of $e_y$ and $DA$), and calculates the corresponding scheduling parameter $\rho_1$ (centralized) and the percentage of assistance $\alpha$ (decentralized)(see Figure 4.40).
For the intervals $[9s; 23s]$ and $[40s; 70s]$, where $\lambda_1 \geq \overline{\lambda}$ (resp. $\lambda_2 \geq \overline{\lambda}$), the scheduling gain $\rho_1$ of the $LPV/\mathcal{H}_\infty$-centralized controller (resp. the percentage of assistance $\alpha$ of the $STSM$-decentralized controller) is chosen as $\rho_1 = \overline{\rho_1}$ (resp. $\alpha$ is chosen as $\alpha = 1$), in order to promote the lane keeping assistance objective (Figure 4.40). For the region, when $\lambda_1 \leq \underline{\lambda}$ (resp. $\lambda_2 \leq \underline{\lambda}$), the scheduling gain $\rho_1$ (resp. the percentage of assistance $\alpha$) is chosen as $\rho_1 = \underline{\rho_1}$ (resp. $\alpha$ is chosen as $\alpha = 0$), which means the lane keeping assistance objective is attenuated and the $ADAS - AFS$ controllers

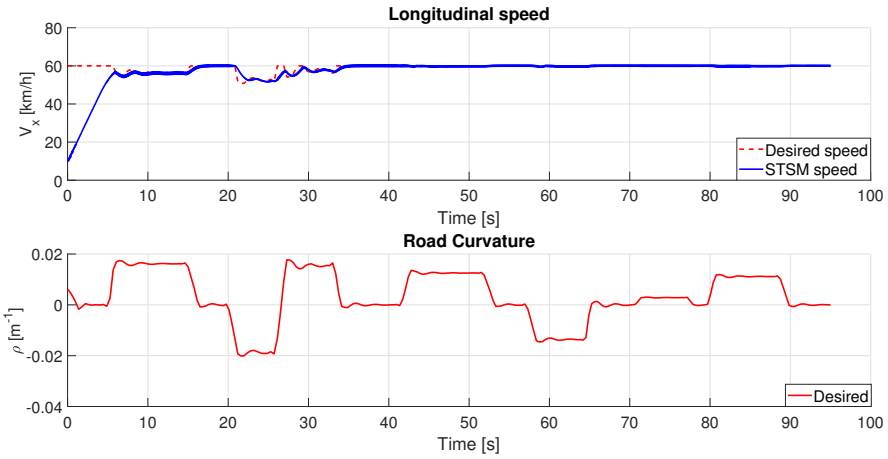


Figure 4.37 – The vehicle dynamic variables: speed and road curvature - Scenario 2

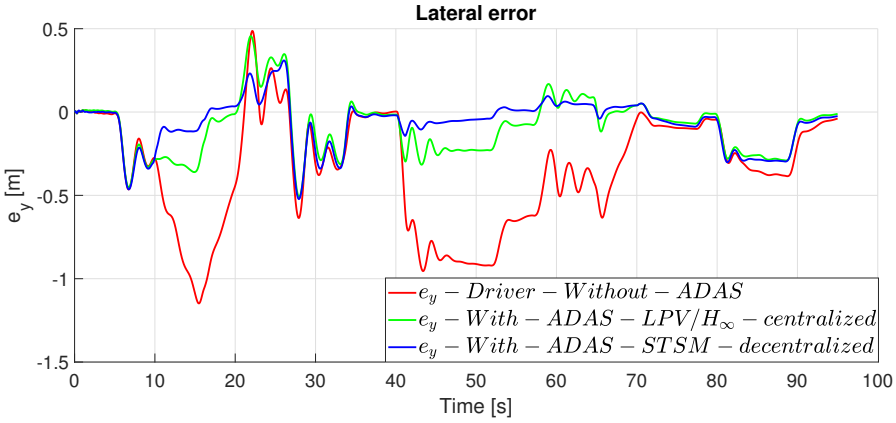


Figure 4.38 – The lateral error - Scenario 2

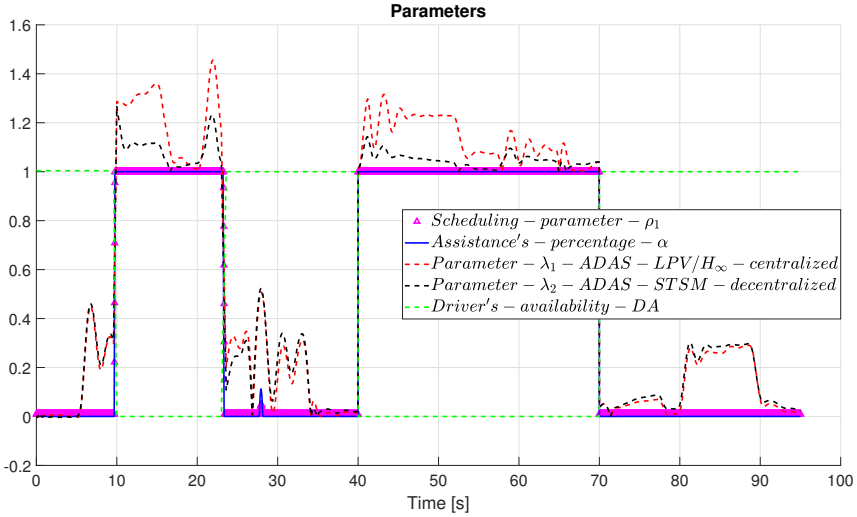


Figure 4.39 – The different parameters - Scenario 2

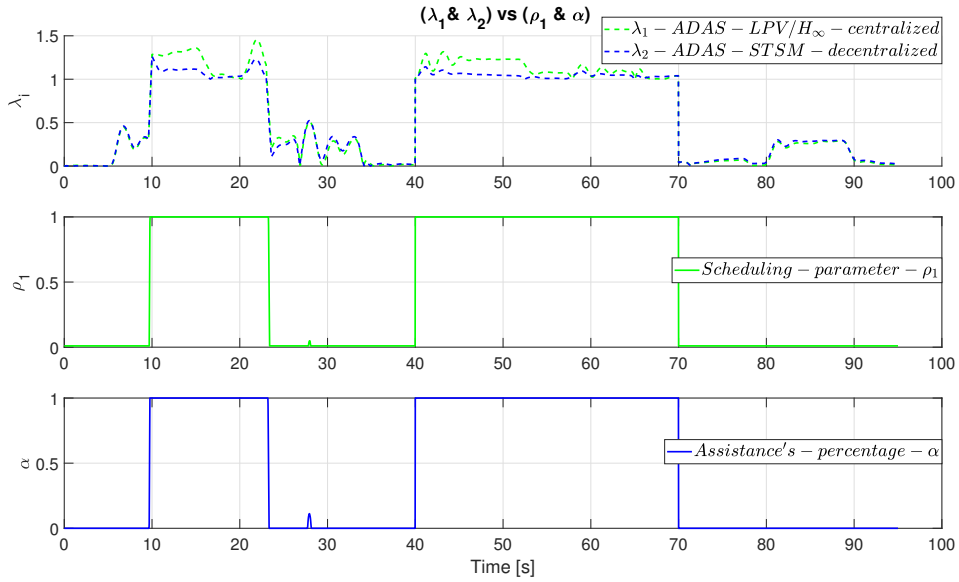


Figure 4.40 – $\lambda_i$ vs $\rho$ and $\alpha$ - Scenario 2

are deactivated. Based on the Figure 4.40, the two $ADAS - AFS$ controllers have the same behavior w.r.t the time of activation and deactivation.
Figures 4.41 and 4.42 show the lateral stability index $SI$ with the corresponding scheduling parameter $\rho_2$ and the scheduling gain $\gamma$ of both control architectures. The lateral $SI$ is covered back to $SI = \underline{SI}$ by the act of using $ADAS - DYC$ controllers in both control architectures. Both controllers have almost similar influence on the $SI$. However, at t=60$s$, the $SI$ with $ADAS$-$LPV/\mathcal{H}_\infty$-centralized is higher than $SI$ with $ADAS$-$STSM$-decentralized ($SI_{LPV/\mathcal{H}_\infty} > SI_{STSM}$), because the $LPV/\mathcal{H}_\infty$ controller is a centralized controller that compromises between control objectives on a curvy road (see Figure 4.37) to find the optimal solution. Therefore, when $SI \geq \overline{SI}$, $\rho_2$ is set to $\rho_2 = \underline{\rho_2}$ (resp. $\gamma = 1$) in order to promote the lateral stability through the activation of differential braking actuators ($DYC$). When $SI \leq \underline{SI}$, $\rho_2$ (resp. $\gamma$) deviates to $\rho_2 = \overline{\rho_2}$ (resp $\gamma = 0$) which means the differential braking actuators ($DYC$) are switched-off, and the lateral stability objective is relaxed. The fluctuations of the different weights $\alpha_i$ are given in the Figure 4.43.

Figure 4.44 shows the driver steering angle $\delta_{sw-h}$ and the $AFS$ steering angle $\delta_{sw-c}$ of both controllers: the $LPV/\mathcal{H}_\infty$-centralized and the $STSM$-decentralized respectively on the steering wheels. One can notice that the both controllers provide almost the similar steering angle, with some additional chattering of $STSM$-decentralized controller. The two controllers are in conflict with the human driver between 9$s$ and 23$s$ and between 40$s$ and 70$s$ in order to compensate his errors. The different total steering angles $\delta_{totalLPV/H_\infty - centralized}$ and $\delta_{totalSTSM - decentralized}$ are given in the Figure 4.45. As we can notice, oscillations and some chattering appear more with the $STSM$-decentralized than the $LPV/\mathcal{H}_\infty$-centralized controller. Thus, that is a drawback of using $STSM$ control technique. Figure 4.46 shows the braking of the $EMB$ at the left and right rear wheels. The $LPV/\mathcal{H}_\infty$-centralized

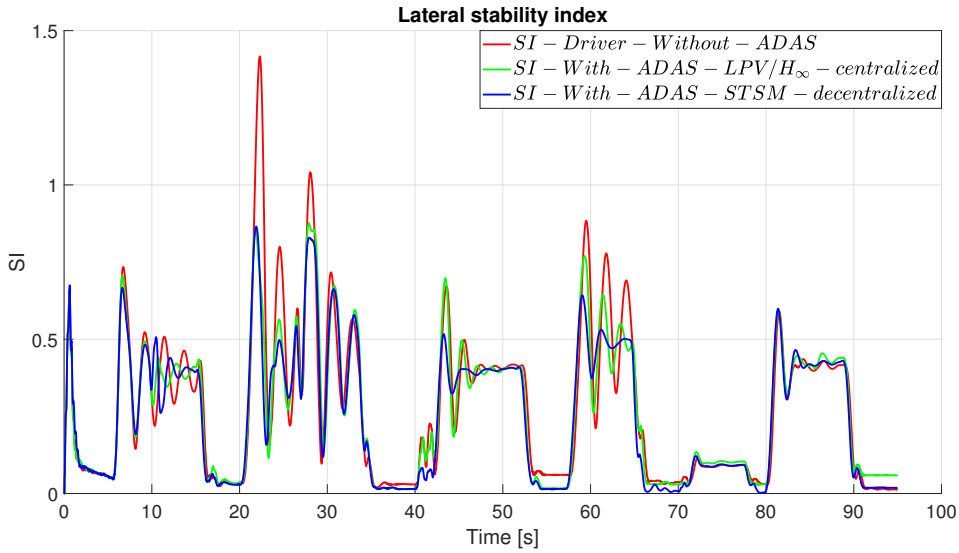


Figure 4.41 – The lateral stability $SI$ - Scenario 2

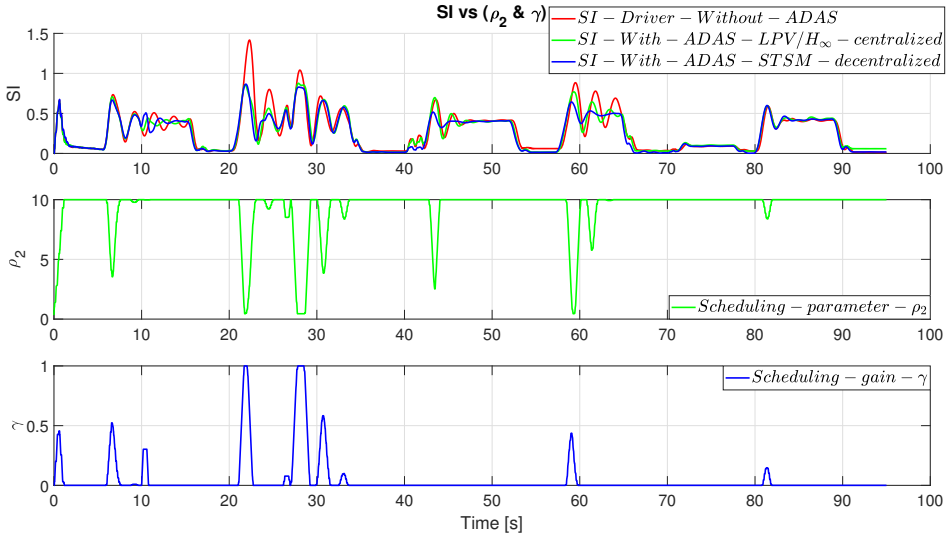


Figure 4.42 – $SI$ vs $\rho_2$ and $\gamma$ - Scenario 2

controller activates a little bit more the braking to compromise between the different objectives of centralized controller, compared to the $STSM$-decentralized controller which activates the braking only when necessary. Finally, Figure 4.37 shows the longitudinal speed tracking to the desired one through the $STSM$ longitudinal controller, the road curvature of the desired trajectory and the lateral and longitudinal accelerations are given in the Figure 4.47. The lateral acceleration does not exceed the $\pm 5m/s^2$, and the actual longitudinal acceleration is pertinent ($< \pm 2m/s^2$) which guarantee a comfortable and safe driving maneuver.

We can conclude from the results of the two scenarios discussed above that the sliding mode control technique is a promising, simple, intuitive, robust and practical control

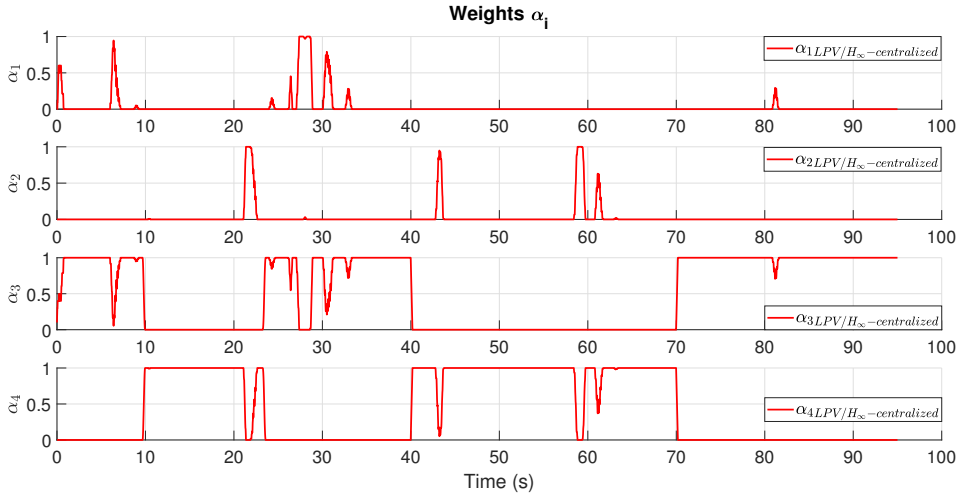


Figure 4.43 – Weights $\alpha_i$-vertices controllers - Scenario 2

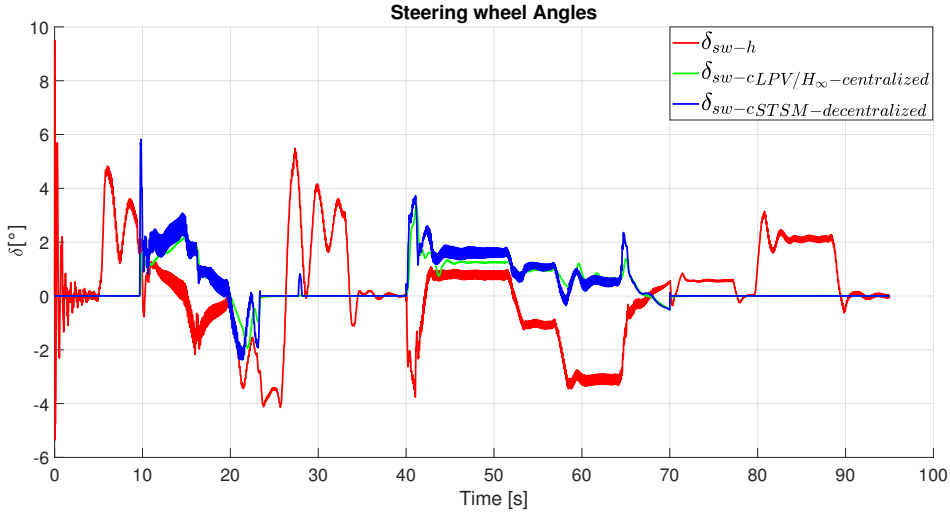


Figure 4.44 – The different steering wheel angles - Scenario 2

technique, with high quality of performance, quick computational time and low cost. However, its main drawback is the chattering and oscillations while guaranteeing only the local sub-systems closed-loop stability. Concerning the $LPV/\mathcal{H}_\infty$ control technique, it is complex, optimal, applicable to problems with multivariable systems and robust technique with very high quality of performance, slower computational time, and high cost. Moreover, this technique is more performant in terms of reducing chattering and oscillations, and more relevant to handle a complex system while guaranteeing the global system closed-loop stability. However, the choice and the tuning of the parameters $\rho_1$ and $\rho_2$ (Figure 4.19) is not obvious in order to give optimal results, since the $LPV/\mathcal{H}_\infty$ controller aims to compromise between the different control objectives, using multi-inputs. For that, many different performed tests and scenarios are done during the tuning of these parameters for scenarios 1 and 2 treated above. Thus, the optimal and performant results for scenarios 1 and 2 are integrated and discussed in this work.

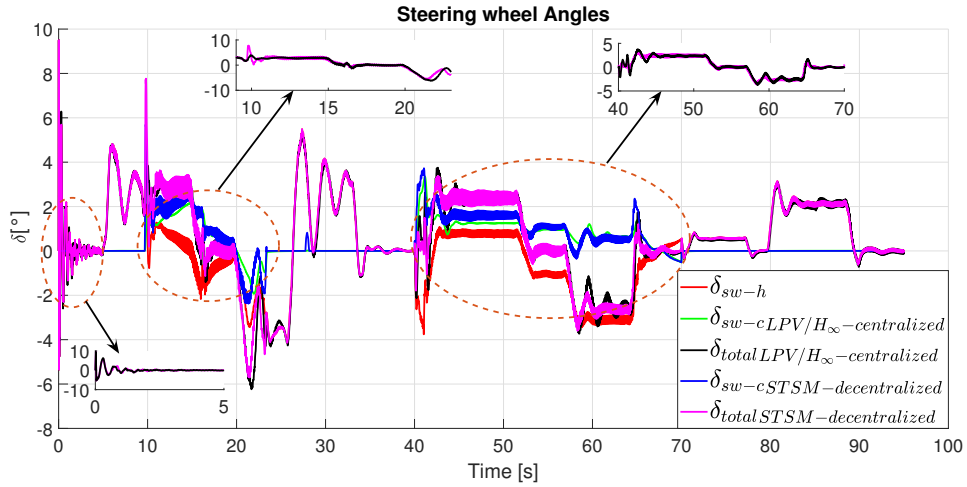


Figure 4.45 – The different total steering wheel angles - Scenario 2

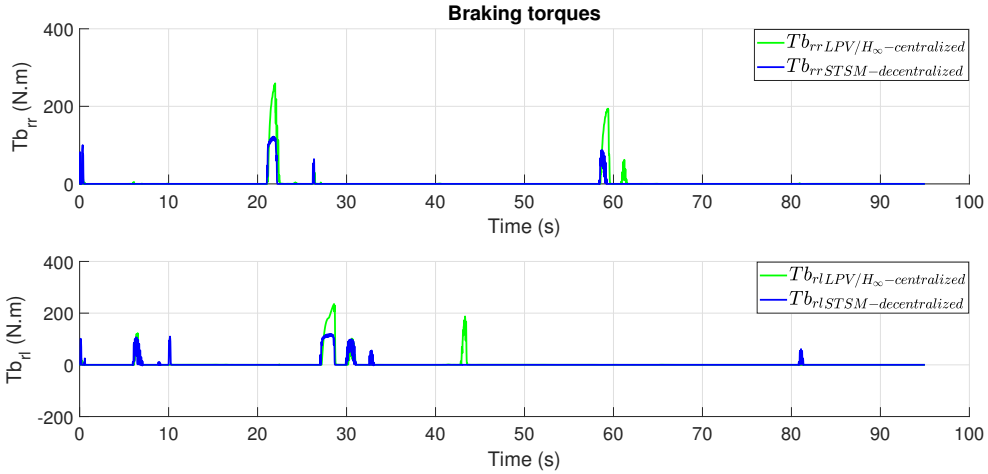


Figure 4.46 – The braking torques - Scenario 2

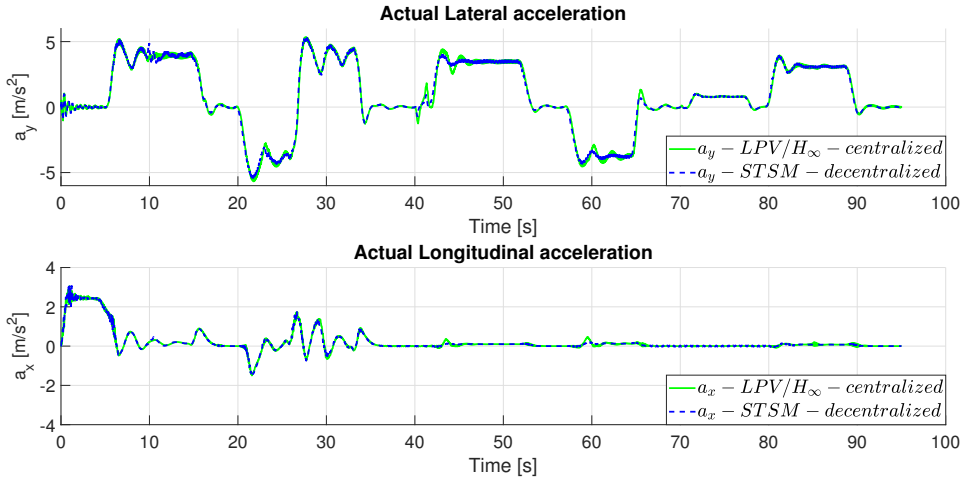


Figure 4.47 – The vehicle dynamic variables: lateral and longitudinal accelerations - Scenario 2

## 4.5 Simulation-based evaluation and discussion

In order to discuss the evaluation of the proposed control architectures with respect to the choosing of thresholds for the activation of $ADAS$ systems (Active Front Steering ($AFS$)), the scenario 1 used in the Section 4.4.3.1 is conducted here with the different values of $\underline{\lambda}$ and $\overline{\lambda}$ (Equation 4.32). Let's define three cases: $a$, $b$ and $c$ to analyze the evaluation of the controllers w.r.t the variable $\lambda$. Each case corresponds to some defined values of $\underline{\lambda}$ and $\overline{\lambda}$ given as: $a)\{0.25m; 0.45m\}$, $b)\{0.4m; 0.6m\}$ and $c)\{0.5m; 0.7m\}$. Our hypotheses are:

- Hypothesis 1: the decrease of the lower threshold $\underline{\lambda}$ of $\lambda$ for the activation of the $ADA$S system leads to an increase in the performance of the lane keeping system.
- Hypothesis 2: the lane keeping objective and the lateral stability enhancement are inversely dependent, that means more we increase the weight on the lane keeping objective, the lateral stability enhancement is penalized.

The hypothesis 1 is verified for both control architectures (centralized and decentralized). As we can see, in the Figures 4.48 and 4.50, $e_y(a) < e_y(b) < e_y(c)$ for both architectures because $\underline{e_y}(a) < \underline{e_y}(b) < \underline{e_y}(c)$. Thus, more the value of $\underline{\lambda}$ is small (lower threshold of activation of the $ADAS$ system), more the performance of the $ADAS$ lane keeping system is improved.
By observing the Figures 4.48 & 4.49, and Figures 4.50 & 4.51 respectively, we can notice for the regions where $e_y$ is smaller, the value of $SI$ is higher for both centralized and decentralized architectures. For example, around t=$10s; 30s; 60s$, when $e_y(a) < e_y(b) < e_y(c)$, thus $SI(a) > SI(b) > SI(c)$. This observation confirms the hypothesis 2 which describes the evaluation of $e_y$ w.r.t $SI$ in critical situations.

To summarize, many different performed tests and scenarios are done during the

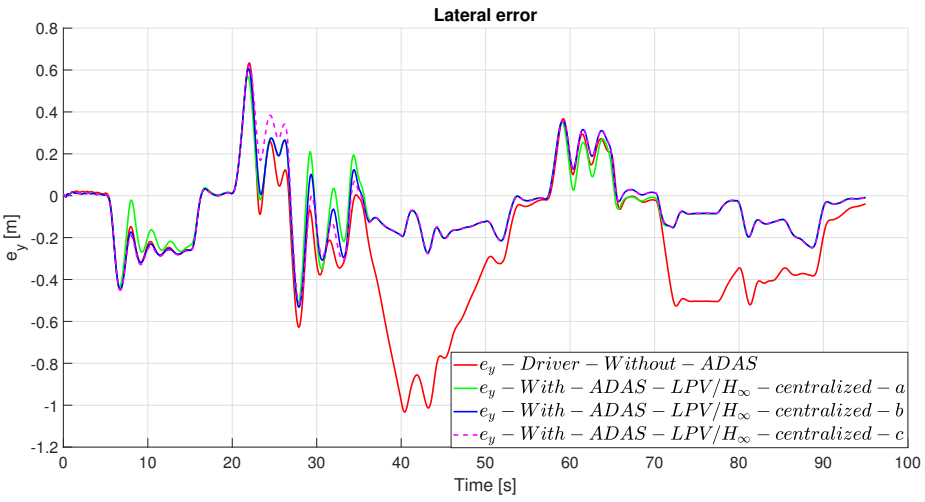


Figure 4.48 – Centralized $LPV/\mathcal{H}_\infty$ architecture - $e_y$ comparison

tuning of $\underline{\lambda}$ and $\overline{\lambda}$ in order to obtain the optimal results. Noting that the optimal results of scenarios 1 and 2 are illustrated and represented in the Section 4.4.3, corresponding to the case $c)\{\underline{\lambda} = 0.5m; \overline{\lambda} = 0.7m\}$.

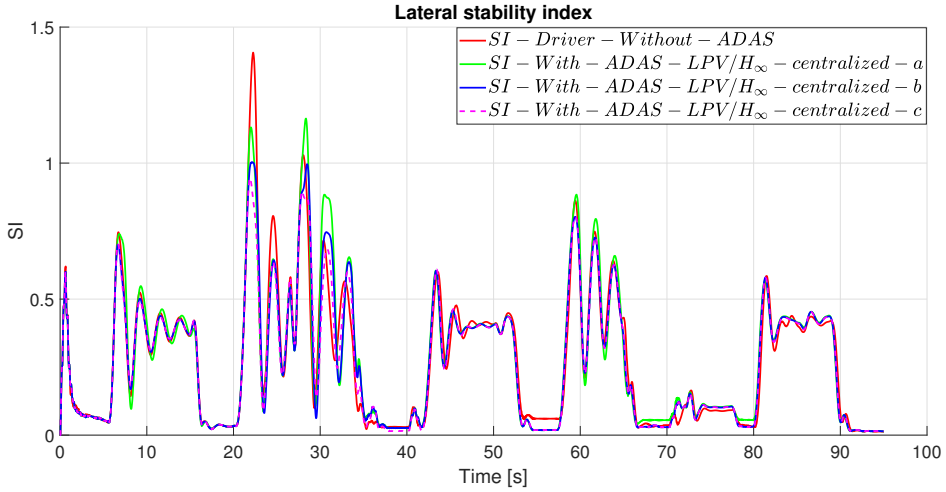


Figure 4.49 – Centralized $LPV/\mathcal{H}_\infty$ architecture - $SI$ comparison

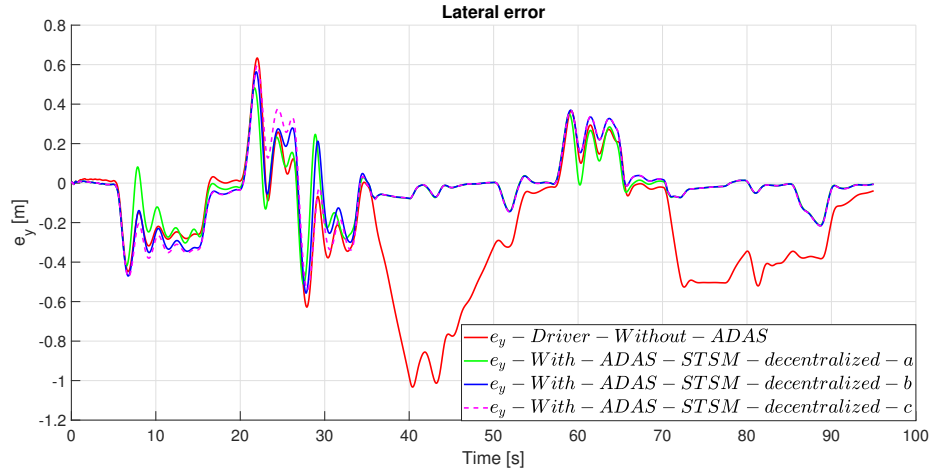


Figure 4.50 – Decentralized $STSM$ architecture - $e_y$ comparison

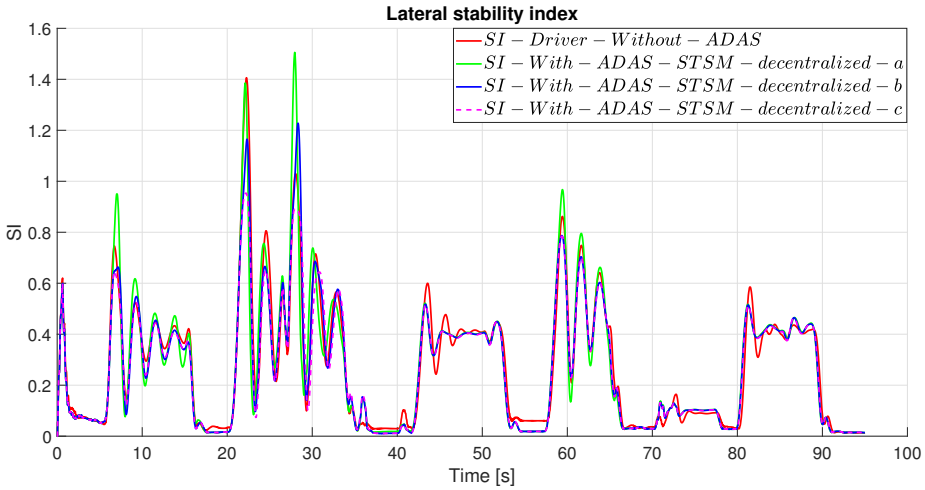


Figure 4.51 – Decentralized $STSM$ architecture - $SI$ comparison

## 4.6 Controllers performance comparison

In order to address the advantage of having a Direct Yaw Controller ($DYC$) in the $ADAS$ system that enhances the vehicle's lateral stability, a comparison is carried on in this work. The comparison is done between the $SISO\ LPV/\mathcal{H}_\infty$ controller (see Figure 4.3) and the $MIMO\ LPV/\mathcal{H}_\infty$ centralized controller involving $AFS$ and $DYC$ (see Figure 4.19) by using the same scenario 1 of Section 4.4.3. During this study, the values of the scheduling gains (given in Tables 4.1 and 4.2) remain the same. $\underline{\lambda}$ and $\overline{\lambda}$ are equal to $0.5m$ and $0.7m$ respectively. The results show that the $SISO\ LPV/\mathcal{H}_\infty$ controller is more performant in terms of diminishing $e_y$ compared to the second controller, despite the weak lateral stability. However, the $MIMO\ LPV/\mathcal{H}_\infty$ centralized controller is the optimal one because he compromises between two control objectives and realizes a lane keeping maneuver while guaranteeing the lateral stability of the vehicle. Figure 4.52 and Figure 4.53 show the lateral error $ey$ and the lateral stability $SI$ of: driver without $ADAS$, driving with $ADAS$-$SISO\ LPV/\mathcal{H}_\infty$ and driving with $ADAS$-$MIMO\ LPV/\mathcal{H}_\infty$-centralized. As shown in these figures, around t=$22s$, the lateral error of the $SISO\ LPV/\mathcal{H}_\infty$ controller is less than the lateral error of the $MIMO\ LPV/\mathcal{H}_\infty$ controller, and $e_{y-LPV/\mathcal{H}_\infty} < e_{y-LPV/\mathcal{H}_\infty-centralized}$. However, the lateral stability index $SI$ of the $SISO\ LPV/\mathcal{H}_\infty$ controller is higher than the $SI$ of the $MIMO\ LPV/\mathcal{H}_\infty$ controller around t=$22s$ (thanks to the $DYC$ in the $ADAS$-$MIMO\ LPV/\mathcal{H}_\infty$-centralized architecture) and $SI_{LPV/\mathcal{H}_\infty} > SI_{LPV/\mathcal{H}_\infty-centralized}$ and again the hypothesis 2 of the Section 4.5 is justified.

A similar comparison is also done between the $SISO$ Super-Twisting Sliding Mode ($STSM$) controller (see Figure 4.8) and the two $SISO\ STSM$ controllers in the decentralized approach involving $AFS$ and $DYC$ (see Figure 4.24) by using the same scenario 1 of Section 4.4.3. This comparison shows the advantage of having a Direct Yaw Controller ($DYC$) in the $ADAS$ system architecture that stabilizes

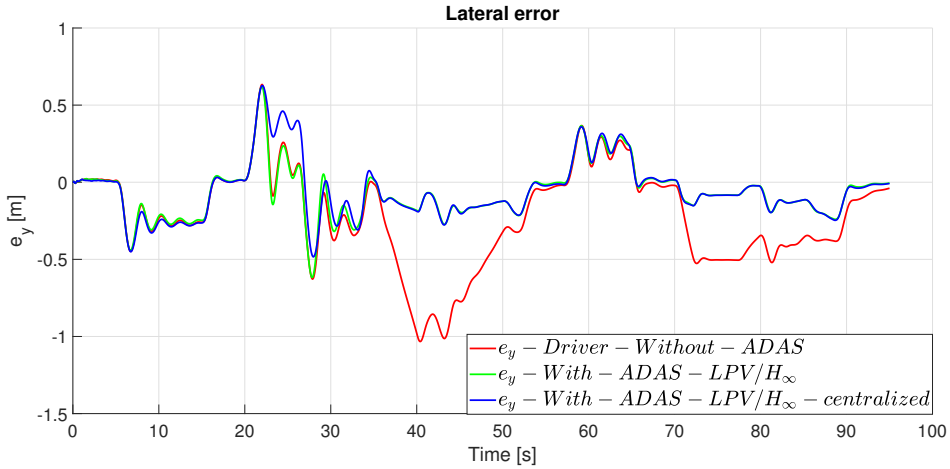


Figure 4.52 – $LPV/\mathcal{H}_\infty$ controllers - $e_y$ comparison

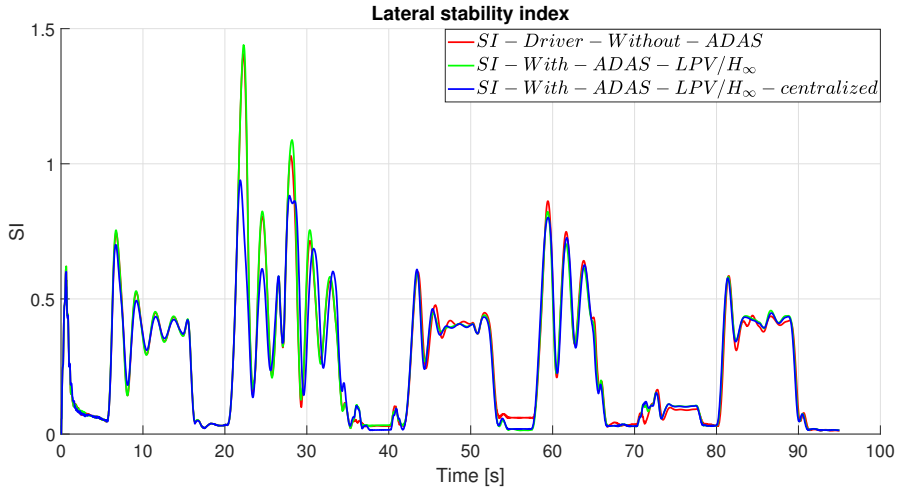


Figure 4.53 – $LPV/\mathcal{H}_\infty$ controllers - $SI$ comparison

the vehicle. The values of the different parameters of the controllers are given in the Table 4.2. The results show that the $SISO$ Super-Twisting Sliding Mode ($STSM$) controller is more able to diminish the lateral error $e_y$ compared to the decentralized approach without guaranteeing of the vehicle's lateral stability. However, the two $SISO$ $STSM$ controllers ($ADAS$-$STSM$ decentralized approach) are more performant where the lane keeping is done with an enhancement of the lateral stability of the vehicle. The lateral error $ey$ and the lateral stability $SI$ of: driver without $ADAS$, driving with $ADAS$-$STSM$ and driving with $ADAS$-$STSM$-decentralized are given Figure 4.54 and Figure 4.55. Refer to these figures, around t=$25s; 30s$, $e_{y-ADAS-STSM} < e_{y-ADAS-STSM-decentralized}$ and the $ADAS$ $SISO$ Super-Twisting Sliding Mode ($STSM$) controller is more performant compared to the $ADAS$-$STSM$-decentralized. However, the $ADAS$-$STSM$-decentralized is more performant in terms diminishing $SI$ compared to the $ADAS$ $SISO$ $STSM$ controller and $SI_{ADAS-STSM} > SI_{ADAS-STSM-decentralized}$ around t=$25s; 30s$. Again the results confirm the advantage of using a $DYC$ $ADAS$ system to stabilize thee vehicle.

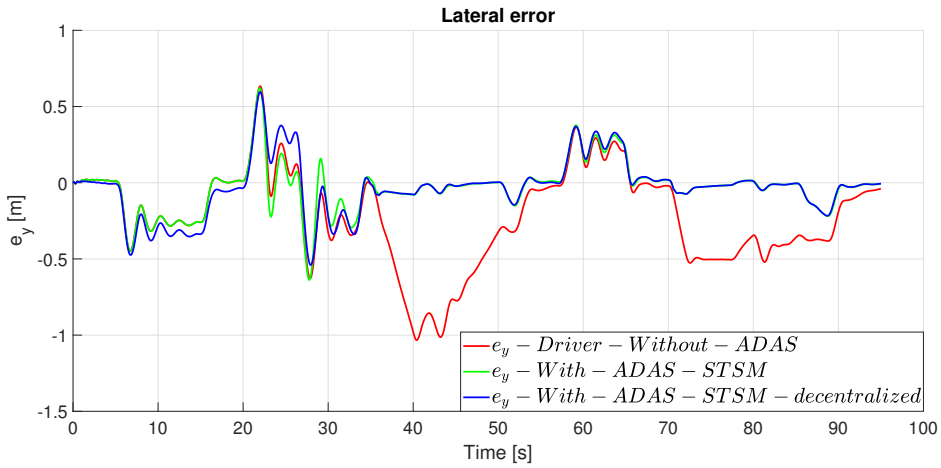


Figure 4.54 – $STSM$ controllers - $e_y$ comparison

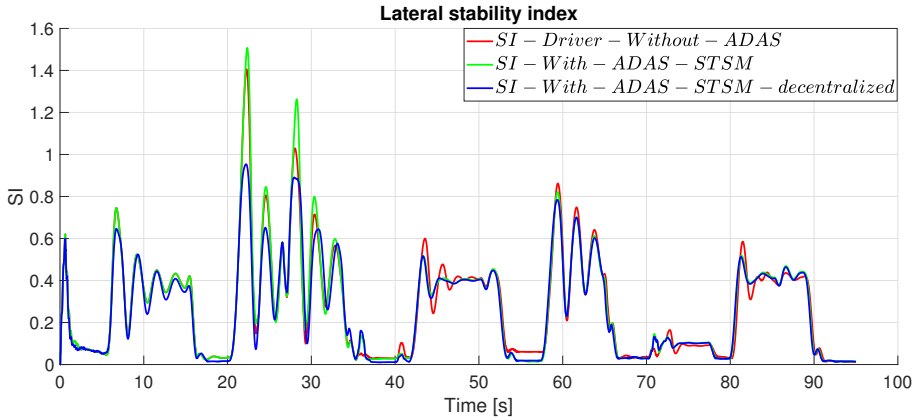


Figure 4.55 – $STSM$ controllers - $SI$ comparison

## 4.7 Conclusion and perspectives

To conclude, a development of Advanced Driving Assistance Systems is detailed in this chapter for the lane keeping maneuver and the vehicle's lateral stability enhancement. The different driving modes including the $ADAS$ systems have been developed in this work. Two control approaches: the $LPV/\mathcal{H}_\infty$ and the Super-Twisting Sliding Mode ($STSM$) control approaches are detailed to develop the controllers of the lane keeping $ADAS$ systems. Then a centralized and decentralized Advanced Driving Assistance System ($ADAS$) architectures have been proposed involving Active Front Steering ($AFS$) and Direct Yaw Control ($DYC$), to deal with two control objectives: the lane keeping and the vehicle's lateral stability. The proposed controllers are validated by using Matlab/Simulink with a complete nonlinear model of the vehicle validated on "*SCANeR Studio*" (OKtal) professional simulator, and a comparison is done between them. Results show the effectiveness and the performance of the proposed $ADAS$ systems, and an almost similar performance of the centralized architecture with its decentralized equivalent. However, decentralized architecture

is simpler and easier to tune and implement than centralized controller. Hence, the decentralized architecture could be much more interesting from an engineering point of view.

# *Conclusion and Perspectives*

In this final chapter, we summarize the main contributions done during the thesis. We then suggest some ideas for our future work and studies.

## Conclusion

After reviewing the state of the art about the levels of autonomy, the shared control and the advanced driving assistance systems (*ADAS*), a new shared lateral control for lane keeping maneuver is treated in this thesis to deal with the transition management and authority between the driver and the autonomous system (level 3) (part I). Moreover, we have developed many *ADAS* systems considering many control objectives to help and assist the driver when keeping the lane (level 2)(part II).

In this thesis, the main contributions are:

- Development of the global shared lateral control architecture in order to prepare the environment work. The driver model and the autonomous system are developed and validated on Matlab/Simulink with a complete nonlinear vehicle model validated on the "*SCANeR Studio*" simulator. This shared control aims to blend the inputs of both agents (human driver and autonomous system).

- Development of two shared lateral control architectures. Different criteria have been defined to be integrated in the decision-making process, such as: the degree of confidence of each input, the lateral error, the driver's availability, the driver's behavior and the take over request (*TOR*). Then, development of many decision-making algorithms to determine the control authority and shifting between the two agents, and finally to calculate the fusion parameter. Definition of different cases studies and scenarios to test and validate our proposed shared control approaches. The two architectures are:

    - A shared lateral control architecture based on a Fuzzy Logic Controller (*FLC*) and a situation-based analysis block for decision making and control authority allocation between the human driver and the autonomous system. The aim of this shared control is to manage the control authority in an autonomous system failure context.

  - ◇ A shared lateral control architecture based on a transition system and a coordinator-based block for decision making and transition management between both agents in a take over request ($TOR$) context.

- Validation and implementation of the proposed shared lateral control architectures on Matlab/Simulink and on the "*SCANeR Studio*" vehicle's simulator (OKTAL) interacted with the human in-the-loop through the "*Logitech G29*" steering wheel for the different driving situations.

- Development of many Advanced Driving Assistance System ($ADAS$) (level 2) involving the Active Front Steering ($AFS$) and Direct Yaw Control ($DYC$) based on many control techniques: the $LPV/\mathcal{H}_\infty$ and the Super-Twisting Sliding Mode $STSM$. These systems aim to help the driver during lane keeping, keep the vehicle's lateral stability and guarantee safety and driving comfort. Moreover, validation and implementation of these systems on Matlab/Simulink with a complete nonlinear vehicle model validated on the "*SCANeR Studio*" simulator where a comparison is done between the different proposed $ADAS$ systems and architectures.

To conclude, the transition and the control authority between the two agents in the framework of shared lateral control is carried out in this thesis. The developed decision-making algorithms proved a smooth and safe transitions between both agents, when switching during a lane keeping maneuver. The simulation and experiment results illustrate the safe and good performance of the different proposed methods for shared lateral control. Finally, the lane keeping objective while guaranteeing the vehicle's stability is done through the different developed $ADAS$ systems where many comparisons are done to show the effectiveness in terms of performance and robustness of each proposed architecture.

# Perspectives

In the future works, we will:

- Consider other criteria to prove the effectiveness of the decision making process especially during the transition phase.

- Develop a learning-based decision layer for $ADAS$ architectures to cover more driving situations. The learning process can be done by simulations and experiments, what is more precise than tuned parameters.

- Consider more complex maneuvers to assist and help the driver, like overtaking, collision avoidance, etc.

- Validate the different architectures of $ADAS$ systems on the "*SCANeR Studio*" simulator which help the driver acting on the vehicle's control through the "*Logitech G29*" steering wheel.

- Integrate a Human-machine interface that permits a direct interaction between the system and the human driver and facilitates the exchange of information between them.
- Develop a Model Predictive Control ($MPC$) to predict the driver's behavior for some horizon. It could be useful in the shared control framework.

# *Appendices*

## .1 Robotic Formalism Model

The vehicle model is based on a robotic formalism model presented in [Chebly et al., 2019], [Chebly, 2017]. However, to simplify the controller design, some assumptions are given in [Chebly et al., 2019]. With all assumptions, the reduced vehicle model used to establish control laws, can be written as:

$$\begin{aligned}
&m_e\ddot{x} - m\dot{y}\dot{\psi} + L_3\dot{\psi}^2 + F_{aero} \\
&+ \delta(2C_{\alpha_f}\delta - 2C_{\alpha_f}\frac{\dot{x}(\dot{y} + L_f\dot{\psi})}{\dot{x}^2 - (\frac{E}{2}\dot{\psi})^2}) = g_1 \\
&m\ddot{y} + m\dot{x}\dot{\psi} - L_3\ddot{\psi} \\
&+ 2C_{\alpha_f}\frac{\dot{x}(\dot{y} + L_f\dot{\psi})}{\dot{x}^2 - (\frac{E}{2}\dot{\psi})^2} + 2C_{\alpha_r}\frac{\dot{x}(\dot{y} - L_r\dot{\psi})}{\dot{x}^2 - (\frac{E}{2}\dot{\psi})^2} = g_2 \\
&I_3\ddot{\psi} + 2L_fC_{\alpha_f}\frac{\dot{x}(\dot{y} + L_f\dot{\psi})}{\dot{x}^2 - (\frac{E}{2}\dot{\psi})^2} \\
&- 2L_rC_{\alpha_r}\frac{\dot{x}(\dot{y} - L_r\dot{\psi}))}{\dot{x}^2 - (\frac{E}{2}\dot{\psi})^2} - L_3(\ddot{y} + \dot{x}\dot{\psi}) = g_3
\end{aligned} \tag{46}$$

where $x$ and $y$ are the longitudinal and the lateral positions of the vehicle at its center of gravity (COG). $\psi$ is the yaw angle. $F_{aero}$ is the longitudinal aerodynamic force. $m_e, g_1, g_2$ and $g_3$ are given by:

$$\begin{aligned}
&m_e = m + 4\tfrac{I_w}{R_{eff}^2}, \\
&g_1 = \tfrac{\tau_w}{R_{eff}}, \\
&g_2 = (2C_{\alpha_f} - 2\tfrac{I_w}{R_{eff}^2}\ddot{x})\delta, \\
&g_3 = L_fg_2 + (-\tfrac{E}{2}C_{\alpha_f}\tfrac{E\dot{\psi}(\dot{y}+L_f\dot{\psi})}{\dot{x}^2-(\frac{E}{2}\dot{\psi})^2})\delta.
\end{aligned}$$

The control inputs to the vehicle are the steering wheel angle, $\delta$, and the Driving/Braking wheels torque $\tau_w$. More details about the vehicle parameters are given in [Chebly et al., 2019].

## .2 Bicycle Model

$$\begin{aligned} a_{11} &= -(C_f + C_r)/(m * V_x), \\ a_{12} &= -(1 + (l_f * C_f - l_r * C_r))/(m * V_x^2), \\ a_{21} &= -(l_f * C_f - l_r * C_r)/I_z, \\ a_{22} &= -(l_f^2 * C_f + l_r^2 * C_r)/(I_z * V_x), \end{aligned} \tag{47}$$

$$\begin{aligned} b_{11} &= C_f/(m * V_x), \\ b_{21} &= (l_f * C_f)/I_z, \\ b_{12} &= 0, \\ b_{22} &= 1/I_z, \end{aligned} \tag{48}$$

# *Bibliography*


[Abbink and Mulder, 2010] Abbink, D. A. and Mulder, M. (2010). Neuromuscular analysis as a guideline in designing shared control. *Advances in Haptics, Mehrdad Hosseini Zadeh (Ed.), ISBN: 9789533070933.*

[Ackermann et al., 1995] Ackermann, J., Guldner, J., Sienel, W., Steinhauser, R., and Utkin, V. I. (1995). Linear and nonlinear controller design for robust automatic steering. *IEEE Transactions on Control Systems Technology*, 3(1):132–143.

[Administration et al., 2013] Administration, N. H. T. S. et al. (2013). Preliminary statement of policy concerning automated vehicles. *Washington, DC*, 1:14.

[Apkarian and Gahinet, 1995] Apkarian, P. and Gahinet, P. (1995). A convex characterization of gain-scheduled $h\infty$ controllers. *IEEE Transactions on Automatic Control*, 40(5):853–864.

[Apkarian et al., 1995] Apkarian, P., Gahinet, P., and Becker, G. (1995). Self-scheduled $h\infty$ control of linear parameter-varying systems: a design example. *Automatica*, 31(9):1251–1261.

[Atoui et al., 2021] Atoui, H., Milanés, V., Sename, O., and Martinez, J. J. (2021). Real-time look-ahead distance optimization for smooth and robust steering control of autonomous vehicles. In *2021 29th Mediterranean Conference on Control and Automation (MED)*, pages 924–929. IEEE.

[Ayoub et al., 2019] Ayoub, J., Zhou, F., Bao, S., and Yang, X. J. (2019). From manual driving to automated driving: A review of 10 years of autoui. In *Proceedings of the 11th international conference on automotive user interfaces and interactive vehicular applications*, pages 70–90.

[Benloucif et al., 2016a] Benloucif, M., Sentouh, C., Floris, J., Simon, P., Boverie, S., and Popieul, J. (2016a). Cooperation between the driver and an automated driving system taking into account the driverâĂŹs state. In *Driving Simulation and Virtual Reality, 15th International Conference.*

[Benloucif et al., 2017] Benloucif, M. A., Nguyen, A.-T., Sentouh, C., and Popieul, J.-C. (2017). A new scheme for haptic shared lateral control in highway driving using trajectory planning. *IFAC-PapersOnLine*, 50(1):13834–13840.

[Benloucif et al., 2016b] Benloucif, M. A., Popieul, J.-C., and Sentouh, C. (2016b). Architecture for multi-level cooperation and dynamic authority management in an automated driving system-a case study on lane change cooperation. *IFAC-PapersOnLine*, 49(19):615–620.

[Benloucif et al., 2016c] Benloucif, M. A., Popieul, J.-C., and Sentouh, C. (2016c). Multi-level cooperation between the driver and an automated driving system during lane change maneuver. In *2016 IEEE Intelligent Vehicles Symposium (IV)*, pages 1224–1229. IEEE.

[Blaschke et al., 2009] Blaschke, C., Breyer, F., Färber, B., Freyer, J., and Limbacher, R. (2009). Driver distraction based lane-keeping assistance. *Transportation research part F: traffic psychology and behaviour*, 12(4):288–299.

[Boink et al., 2014] Boink, R., Van Paassen, M. M., Mulder, M., and Abbink, D. A. (2014). Understanding and reducing conflicts between driver and haptic shared control. In *2014 IEEE International Conference on Systems, Man, and Cybernetics (SMC)*, pages 1510–1515. IEEE.

[Borojeni et al., 2016] Borojeni, S. S., Chuang, L., Heuten, W., and Boll, S. (2016). Assisting drivers with ambient take-over requests in highly automated driving. In *Proceedings of the 8th International Conference on Automotive User Interfaces and Interactive Vehicular Applications*, pages 237–244.

[Borroni and Tanelli, 2018] Borroni, F. and Tanelli, M. (2018). A weighting approach to the shared-control of lateral vehicle dynamics. *IFAC-PapersOnLine*, 51(9):305–310.

[Bueno et al., 2016] Bueno, M., Dogan, E., Selem, F. H., Monacelli, E., Boverie, S., and Guillaume, A. (2016). How different mental workload levels affect the take-over control after automated driving. In *2016 IEEE 19th International Conference on Intelligent Transportation Systems (ITSC)*, pages 2040–2045. IEEE.

[Canudas-de Wit et al., 2003] Canudas-de Wit, C., Tsiotras, P., Velenis, E., Basset, M., and Gissinger, G. (2003). Dynamic friction models for road/tire longitudinal interaction. *Vehicle System Dynamics*, 39(3):189–226.

[Chandrasekaran and Conrad, 2015] Chandrasekaran, B. and Conrad, J. M. (2015). Human-robot collaboration: A survey. In *SoutheastCon 2015*, pages 1–8. IEEE.

[Chebly, 2017] Chebly, A. (2017). *Trajectory planning and tracking for autonomous vehicles navigation*. PhD thesis, Université de Technologie de Compiègne.

[Chebly et al., 2019] Chebly, A., Talj, R., and Charara, A. (2019). Coupled longitudinal/lateral controllers for autonomous vehicles navigation, with experimental validation. *Control Engineering Practice*, 88:79–96.

[Chokor, 2019] Chokor, A. (2019). *Design of several centralized and decentralized multilayer robust control architectures for global chassis control.* PhD thesis, Compiègne.

[Chokor et al., 2019] Chokor, A., Talj, R., Doumiati, M., and Charara, A. (2019). A global chassis control system involving active suspensions, direct yaw control and active front steering. *IFAC-PapersOnLine*, 52(5):444–451.

[Chu et al., 2022] Chu, D., Li, H., Zhao, C., and Zhou, T. (2022). Trajectory tracking of autonomous vehicle based on model predictive control with pid feedback. *IEEE Transactions on Intelligent Transportation Systems.*

[de Winter and Dodou, 2011] de Winter, J. C. and Dodou, D. (2011). Preparing drivers for dangerous situations: A critical reflection on continuous shared control. In *2011 IEEE International conference on systems, man, and cybernetics*, pages 1050–1056. IEEE.

[Doumiati et al., 2013] Doumiati, M., Sename, O., Dugard, L., Martinez-Molina, J.-J., Gaspar, P., and Szabo, Z. (2013). Integrated vehicle dynamics control via coordination of active front steering and rear braking. *European Journal of Control*, 19(2):121–143.

[Doumiati et al., 2014] Doumiati, M., Victorino, A., Talj, R., and Charara, A. (2014). Robust lpv control for vehicle steerability and lateral stability. In *53rd IEEE Conference on Decision and Control, pp. 4113–4118.*

[Dugoff et al., 1970] Dugoff, H., Fancher, P., and Segel, L. (1970). An analysis of tire traction properties and their influence on vehicle dynamic performance. *SAE transactions*, pages 1219–1243.

[Edelmann et al., 2007] Edelmann, J., Plöchl, M., Reinalter, W., and Tieber, W. (2007). A passenger car driver model for higher lateral accelerations. *Vehicle System Dynamics*, 45(12):1117–1129.

[Falcone et al., 2008] Falcone, P., Borrelli, F., Tseng, H. E., Asgari, J., and Hrovat, D. (2008). Linear time-varying model predictive control and its application to active steering systems: Stability analysis and experimental validation. *International Journal of Robust and Nonlinear Control: IFAC-Affiliated Journal*, 18(8):862–875.

[Favarò et al., 2017] Favarò, F. M., Nader, N., Eurich, S. O., Tripp, M., and Varadaraju, N. (2017). Examining accident reports involving autonomous vehicles in california. *PLoS one*, 12(9):e0184952.

[Ferrara and Vecchio, 2009] Ferrara, A. and Vecchio, C. (2009). Second order sliding mode control of vehicles with distributed collision avoidance capabilities. *Mechatronics*, 19(4):471–477.

[Flemisch et al., 2010] Flemisch, F., Nashashibi, F., Rauch, N., Schieben, A., Glaser, S., Temme, G., Resende, P., Vanholme, B., Löper, C., Thomaidis, G., et al. (2010). Towards highly automated driving: Intermediate report on the haveit-joint system.

[Flemisch et al., 2003] Flemisch, F. O., Adams, C. A., Conway, S. R., Goodrich, K. H., Palmer, M. T., and Schutte, P. C. (2003). The h-metaphor as a guideline for vehicle automation and interaction.

[Gasser et al., 2012] Gasser, T., Arzt, C., Ayoubi, M., Bartels, A., Eier, J., Flemisch, F., Häcker, D., Hesse, T., Huber, W., Lotz, C., et al. (2012). Legal consequences of an increase in vehicle automation: Consolidated final report of the project group. *Bundesanstalt für Straßenwesen*.

[Gu et al., 2005] Gu, D.-W., Petkov, P., and Konstantinov, M. M. (2005). *Robust control design with MATLAB®*. Springer Science & Business Media.

[Guo, 2017] Guo, C. (2017). *Designing driver-vehicle cooperation principles for automated driving systems*. PhD thesis.

[Hamdan et al., 2020] Hamdan, A., Chokor, A., Talj, R., and Doumiati, M. (2020). A centralized multilayer lpv/h-infinity control architecture for vehicleâĂŹs global chassis control, and comparison with a decentralized architecture. In *21rst IFAC (International Federation of Automatic Control)*.

[Heißing and Ersoy, 2010] Heißing, B. and Ersoy, M. (2010). *Chassis handbook: fundamentals, driving dynamics, components, mechatronics, perspectives*. Springer Science & Business Media.

[Hima et al., 2011] Hima, S., Lusseti, B., Vanholme, B., Glaser, S., and Mammar, S. (2011). Trajectory tracking for highly automated passenger vehicles. *IFAC Proceedings Volumes*, 44(1):12958–12963.

[Hingwe and Tomizuka, 1997] Hingwe, P. and Tomizuka, M. (1997). Experimental evaluation of a chatter free sliding mode control for lateral control in ahs. In *Proceedings of the 1997 American Control Conference (Cat. No. 97CH36041)*, volume 5, pages 3365–3369. IEEE.

[Hogan, 1985] Hogan, N. (1985). Impedance control: An approach to manipulation: Part iiâĂŤimplementation.

[Holländer and Pfleging, 2018] Holländer, K. and Pfleging, B. (2018). Preparing drivers for planned control transitions in automated cars. In *Proceedings of the 17th International Conference on Mobile and Ubiquitous Multimedia*, pages 83–92.

[Hoult and Cole, 2008] Hoult, W. and Cole, D. J. (2008). A neuromuscular model featuring co-activation for use in driver simulation. *Vehicle System Dynamics*, 46(S1):175–189.

[Inagaki et al., 1994] Inagaki, S., Kshiro, I., and Yamamoto, M. (1994). Analysis on vehicle stability in critical cornering using phase-plane method. In *International Symposium on Advanced Vehicle Control 1994*.

[Iwano et al., 2014] Iwano, K., Raksincharoensak, P., and Nagai, M. (2014). A study on shared control between the driver and an active steering control system in emergency obstacle avoidance situations. *IFAC Proceedings Volumes*, 47(3):6338–6343.

[Jensen et al., 2011] Jensen, M. J., Tolbert, A. M., Wagner, J. R., Switzer, F. S., and Finn, J. W. (2011). A customizable automotive steering system with a haptic feedback control strategy for obstacle avoidance notification. *IEEE transactions on vehicular technology*, 60(9):4208–4216.

[Johns et al., 2016] Johns, M., Mok, B., Sirkin, D., Gowda, N., Smith, C., Talamonti, W., and Ju, W. (2016). Exploring shared control in automated driving. In *2016 11th ACM/IEEE International Conference on Human-Robot Interaction (HRI)*, pages 91–98. IEEE.

[Jugade, 2019] Jugade, S. (2019). *Shared control authority between human and autonomous driving system for intelligent vehicles*. PhD thesis, Université de Technologie de Compiègne.

[Kerschbaum et al., 2015] Kerschbaum, P., Lorenz, L., and Bengler, K. (2015). A transforming steering wheel for highly automated cars. In *2015 ieee intelligent vehicles symposium (iv)*, pages 1287–1292. IEEE.

[Khalil and Kleinfinger, 1986] Khalil, W. and Kleinfinger, J. (1986). A new geometric notation for open and closed-loop robots. In *Proceedings. 1986 IEEE International Conference on Robotics and Automation*, volume 3, pages 1174–1179. IEEE.

[Khalil and Kleinfinger, 1987] Khalil, W. and Kleinfinger, J.-F. (1987). Minimum operations and minimum parameters of the dynamic models of tree structure robots. *IEEE Journal on Robotics and Automation*, 3(6):517–526.

[Kiencke, 1993] Kiencke, U. (1993). Realtime estimation of adhesion characteristic between tyres and road. *IFAC Proceedings Volumes*, 26(2):15–18.

[Kiencke and Nielsen, 2000] Kiencke, U. and Nielsen, L. (2000). Automotive control systems: for engine, driveline, and vehicle.

[Kim and Yang, 2017] Kim, H. J. and Yang, J. H. (2017). Takeover requests in simulated partially autonomous vehicles considering human factors. *IEEE Transactions on Human-Machine Systems*, 47(5):735–740.

[Kim et al., 2018] Kim, W., Kim, H.-S., Lee, S.-J., Kim, J., and Yoon, D. (2018). Transitions from autopilot to manual control in highly automated driving: Cognitive simulations. In *2018 IEEE 88th Vehicular Technology Conference (VTC-Fall)*, pages 1–5. IEEE.

[Kukkala et al., 2018] Kukkala, V. K., Tunnell, J., Pasricha, S., and Bradley, T. (2018). Advanced driver-assistance systems: A path toward autonomous vehicles. *IEEE Consumer Electronics Magazine*, 7(5):18–25.

[Land and Horwood, 1995] Land, M. and Horwood, J. (1995). Which parts of the road guide steering? *Nature*, 377(6547):339–340.

[Li et al., 2020] Li, A., Chen, Y., Lin, W.-C., and Du, X. (2020). Shared steering control of tire blowout for ground vehicles. In *2020 American Control Conference (ACC)*, pages 4862–4867. IEEE.

[Li and Wang, 2007] Li, L. and Wang, F.-Y. (2007). *Advanced motion control and sensing for intelligent vehicles*. Springer Science & Business Media.

[Li et al., 2018] Li, M., Cao, H., Song, X., Huang, Y., Wang, J., and Huang, Z. (2018). Shared control driver assistance system based on driving intention and situation assessment. *IEEE Transactions on Industrial Informatics*, 14(11):4982–4994.

[Lim, 1998] Lim, E. M. (1998). Lateral and longitudinal vehicle coupling in the automated highway system, master of science thesis. *University of California, Berkeley*.

[Lin et al., 2021] Lin, F., Wang, S., Zhao, Y., and Cai, Y. (2021). Research on autonomous vehicle path tracking control considering roll stability. *Proceedings of the Institution of Mechanical Engineers, Part D: Journal of Automobile Engineering*, 235(1):199–210.

[Lv et al., 2021] Lv, C., Li, Y., Xing, Y., Huang, C., Cao, D., Zhao, Y., and Liu, Y. (2021). Human–machine collaboration for automated driving using an intelligent two-phase haptic interface. *Advanced Intelligent Systems*, 3(4):2000229.

[MacAdam, 1980] MacAdam, C. C. (1980). An optimal preview control for linear systems.

[Marino et al., 2011] Marino, R., Scalzi, S., and Netto, M. (2011). Nested pid steering control for lane keeping in autonomous vehicles. *Control Engineering Practice*, 19(12):1459–1467.

[Markkula et al., 2005] Markkula, G., Kutila, M., Engstroem, J., Victor, T., and Larsson, P. (2005). Online detection of driver distraction: preliminary results from the aide project. In *International Truck and Bus Safety and Security Symposium, 2005, Alexandria, Virginia, USA*.

[Mars et al., 2011] Mars, F., Saleh, L., Chevrel, P., Claveau, F., and Lafay, J.-F. (2011). Modeling the visual and motor control of steering with an eye to shared-control automation. In *Proceedings of the human factors and ergonomics society annual meeting*, volume 55, pages 1422–1426. SAGE Publications Sage CA: Los Angeles, CA.

[Melcher et al., 2015] Melcher, V., Rauh, S., Diederichs, F., Widlroither, H., and Bauer, W. (2015). Take-over requests for automated driving. *Procedia Manufacturing*, 3:2867–2873.

[Miller et al., 2014] Miller, D., Sun, A., and Ju, W. (2014). Situation awareness with different levels of automation. In *2014 IEEE International Conference on Systems, Man, and Cybernetics (SMC)*, pages 688–693. IEEE.

[Mirnig et al., 2017] Mirnig, A. G., Gärtner, M., Laminger, A., Meschtscherjakov, A., Trösterer, S., Tscheligi, M., McCall, R., and McGee, F. (2017). Control transition interfaces in semiautonomous vehicles: A categorization framework and literature analysis. In *Proceedings of the 9th international conference on automotive user interfaces and interactive vehicular applications*, pages 209–220.

[Miyata and Norman, 1986] Miyata, Y. and Norman, D. A. (1986). Psychological issues in support of multiple activities. *User centered system design: New perspectives on human-computer interaction*, pages 265–284.

[Muzet, 2006] Muzet, A. (2006). Bruit et sommeil: répercussions sur la santé. *médecine/sciences*, 22(11):973–978.

[Nehaoua and Nouvelière, 2012] Nehaoua, L. and Nouvelière, L. (2012). Backstepping based approach for the combined longitudinal-lateral vehicle control. In *2012 IEEE intelligent vehicles symposium*, pages 395–400. IEEE.

[Nguyen et al., 2015] Nguyen, A., Sentouh, C., and Popieul, J.-C. (2015). Online adaptation of the authority level for shared lateral control of driver steering assist system using dynamic output feedback controller. In *IECON 2015-41st Annual Conference of the IEEE Industrial Electronics Society*, pages 003767–003772. IEEE.

[Nguyen et al., 2016] Nguyen, A.-T., Sentouh, C., and Popieul, J.-C. (2016). Driver-automation cooperative approach for shared steering control under multiple system constraints: Design and experiments. *IEEE Transactions on Industrial Electronics*, 64(5):3819–3830.

[Pacejka and Besselink, 1997] Pacejka, H. and Besselink, I. (1997). Magic formula tyre model with transient properties. *Vehicle system dynamics*, 27(S1):234–249.

[Perozzi et al., 2020] Perozzi, G., Sentouh, C., Floris, J., and Popieul, J.-C. (2020). On nonlinear control for lane keeping assist system in steer-by-wire road wheeled vehicles.

[Politis et al., 2015] Politis, I., Brewster, S., and Pollick, F. (2015). Language-based multimodal displays for the handover of control in autonomous cars. In *Proceedings of the 7th international conference on automotive user interfaces and interactive vehicular applications*, pages 3–10.

[Popieul et al., 2002] Popieul, J., Simon, P., and Losleveur, P. (2002). Using failure detection and diagnosis methods to detect dangerous evolutions of the driver behaviour. *Control Engineering Practice*, 10(5):577–583.

[Poussot-Vassal, 2008] Poussot-Vassal, C. (2008). *Commande robuste LPV multi-variable de chassis automobile*. PhD thesis, Grenoble INPG.

[Rajamani, 2011] Rajamani, R. (2011). *Vehicle dynamics and control*. Springer Science & Business Media.

[Rajamani, 2012] Rajamani, R. (2012). *Vehicle Dynamics and Control*. Springer.

[Rath et al., 2018] Rath, J. J., Sentouh, C., and Popieul, J.-C. (2018). Robust lane keeping control in automated vehicles: A driver-in-the loop approach. In *2018 21st International Conference on Intelligent Transportation Systems (ITSC)*, pages 3327–3332. IEEE.

[Regan et al., 2011] Regan, M. A., Hallett, C., and Gordon, C. P. (2011). Driver distraction and driver inattention: Definition, relationship and taxonomy. *Accident Analysis & Prevention*, 43(5):1771–1781.

[Reimer et al., 2016] Reimer, B., Pettinato, A., Fridman, L., Lee, J., Mehler, B., Seppelt, B., Park, J., and Iagnemma, K. (2016). Behavioral impact of drivers' roles in automated driving. In *Proceedings of the 8th international conference on automotive user interfaces and interactive vehicular applications*, pages 217–224.

[Reznik, 1997] Reznik, L. (1997). *Fuzzy controllers handbook: how to design them, how they work*. Elsevier.

[Rivera et al., 2011] Rivera, J., Garcia, L., Mora, C., Raygoza, J. J., and Ortega, S. (2011). Super-twisting sliding mode in motion control systems. *Sliding mode control*, pages 237–254.

[SAE, 2016] SAE, S. (2016). J3016-taxonomy and definitions for terms related to on-road motor vehicle automated driving systems. *Surface Vehicle Recommended Practive*.

[Saleh et al., 2013] Saleh, L., Chevrel, P., Claveau, F., Lafay, J.-F., and Mars, F. (2013). Shared steering control between a driver and an automation: Stability in the presence of driver behavior uncertainty. *IEEE Transactions on Intelligent Transportation Systems*, 14(2):974–983.

[Saleh et al., 2011] Saleh, L., Chevrel, P., Mars, F., Lafay, J.-F., and Claveau, F. (2011). Human-like cybernetic driver model for lane keeping. *IFAC Proceedings Volumes*, 44(1):4368–4373.

[Salvucci and Gray, 2004] Salvucci, D. D. and Gray, R. (2004). A two-point visual control model of steering. *Perception*, 33(10):1233–1248.

[Schaap et al., 2017] Schaap, N., van der Horst, R., van Arem, B., and Brookhuis, K. (2017). The relationship between driver distraction and mental workload. In *Driver Distraction and Inattention*, pages 63–80. CRC Press.

[Scherer et al., 1997] Scherer, C., Gahinet, P., and Chilali, M. (1997). Multiobjective output-feedback control via lmi optimization. *IEEE Transactions on automatic control*, 42(7):896–911.

[Sename et al., 2013] Sename, O., Gaspar, P., and Bokor, J. (2013). *Robust control and linear parameter varying approaches: application to vehicle dynamics*. Springer, vol. 437.

[Sentouh et al., 2009] Sentouh, C., Chevrel, P., Mars, F., and Claveau, F. (2009). A sensorimotor driver model for steering control. In *2009 IEEE International Conference on Systems, Man and Cybernetics*, pages 2462–2467. IEEE.

[Sentouh et al., 2010] Sentouh, C., Debernard, S., Popieul, J.-C., and Vanderhaegen, F. (2010). Toward a shared lateral control between driver and steering assist controller. *IFAC Proceedings Volumes*, 43(13):404–409.

[Sentouh et al., 2013] Sentouh, C., Soualmi, B., Popieul, J.-C., and Debernard, S. (2013). Cooperative steering assist control system. In *2013 IEEE international conference on systems, man, and cybernetics*, pages 941–946. IEEE.

[Shtessel et al., 2014] Shtessel, Y., Edwards, C., Fridman, L., and Levant, A. (2014). *Sliding mode control and observation*. Springer.

[Soualmi, 2014] Soualmi, B. (2014). *Coopération Homme Machine pour la conduite automatisée: une approche par partage haptique du contrôle*. PhD thesis.

[Soualmi et al., 2011] Soualmi, B., Sentouh, C., Popieul, J.-C., and Debernard, S. (2011). Fuzzy takagi-sugeno lq controller for a shared control of vehicle. In *2011 14th International IEEE Conference on Intelligent Transportation Systems (ITSC)*, pages 956–961. IEEE.

[Stevens et al., 2019] Stevens, G., Meurer, J., Pakusch, C., and Bossauer, P. (2019). Investigating car futures from different angles. *Mensch und Computer 2019-Workshopband*.

[Tan and Huang, 2014] Tan, H.-S. and Huang, J. (2014). Design of a high-performance automatic steering controller for bus revenue service based on how drivers steer. *IEEE Transactions on Robotics*, 30(5):1137–1147.

[Ungoren and Peng, 2005] Ungoren, A. Y. and Peng, H. (2005). An adaptive lateral preview driver model. *Vehicle system dynamics*, 43(4):245–259.

[Utkin, 2013] Utkin, V. (2013). On convergence time and disturbance rejection of super-twisting control. *IEEE Transactions on Automatic Control*, 58(8).

[van der Heiden et al., 2017] van der Heiden, R. M., Iqbal, S. T., and Janssen, C. P. (2017). Priming drivers before handover in semi-autonomous cars. In *Proceedings of the 2017 CHI conference on human factors in computing systems*, pages 392–404.

[van der Meulen et al., 2016] van der Meulen, H., Kun, A. L., and Janssen, C. P. (2016). Switching back to manual driving: How does it compare to simply driving away after parking? In *Proceedings of the 8th international conference on automotive user interfaces and interactive vehicular applications*, pages 229–236.

[Villagra et al., 2007] Villagra, J., d'Andréa Novel, B., Pengov, M., Bösiger, M., and Devouge, Q. (2007). A realistic vehicle model for esp-like control laws synthesis. In *2007 European Control Conference (ECC)*, pages 644–651. IEEE.

[Wada et al., 2016] Wada, T., Sonoda, K., Okasaka, T., and Saito, T. (2016). Authority transfer method from automated to manual driving via haptic shared control. In *2016 IEEE International Conference on Systems, Man, and Cybernetics (SMC)*, pages 002659–002664. IEEE.

[Walch et al., 2015] Walch, M., Lange, K., Baumann, M., and Weber, M. (2015). Autonomous driving: investigating the feasibility of car-driver handover assistance. In *Proceedings of the 7th international conference on automotive user interfaces and interactive vehicular applications*, pages 11–18.

[Walch et al., 2016] Walch, M., Sieber, T., Hock, P., Baumann, M., and Weber, M. (2016). Towards cooperative driving: Involving the driver in an autonomous vehicle's decision making. In *Proceedings of the 8th international conference on automotive user interfaces and interactive vehicular applications*, pages 261–268.

[White et al., 2013] White, A. P., Zhu, G., and Choi, J. (2013). *Linear parameter-varying control for engineering applications*. Springer.

[Wulf et al., 2014] Wulf, F., Rimini-Döring, M., Arnon, M., and Gauterin, F. (2014). Recommendations supporting situation awareness in partially automated driver assistance systems. *IEEE Transactions on Intelligent Transportation Systems*, 16(4):2290–2296.

[Zhao et al., 2012] Zhao, P., Chen, J., Song, Y., Tao, X., Xu, T., and Mei, T. (2012). Design of a control system for an autonomous vehicle based on adaptive-pid. *International Journal of Advanced Robotic Systems*, 9(2):44.

[Zhou et al., 1996] Zhou, K., Doyle, J. C., Glover, K., et al. (1996). *Robust and optimal control*, volume 40. Prentice hall New Jersey.

[Zin, 2005] Zin, A. (2005). *Sur la commande robuste de suspensions automobiles en vue du contrôle global de châssis*. PhD thesis, Institut National Polytechnique de Grenoble-INPG.

[Zou et al., 2018] Zou, Q., Li, H., Zhang, R., and Pei, T. (2018). A survey of cooperative driving between auxiliary autonomous system and human driver. In *MATEC Web of Conferences*, volume 160, page 05001. EDP Sciences.